frontiers | Research Topics

Exploiting biomarkers of CNS disorders: targets for therapeutics and non-invasive tools for diagnosis, prognosis, monitoring

Edited by
Ana Semeano, Hai Sun and Gal Bitan

Published in
Frontiers in Molecular Neuroscience
Frontiers in Neuroscience

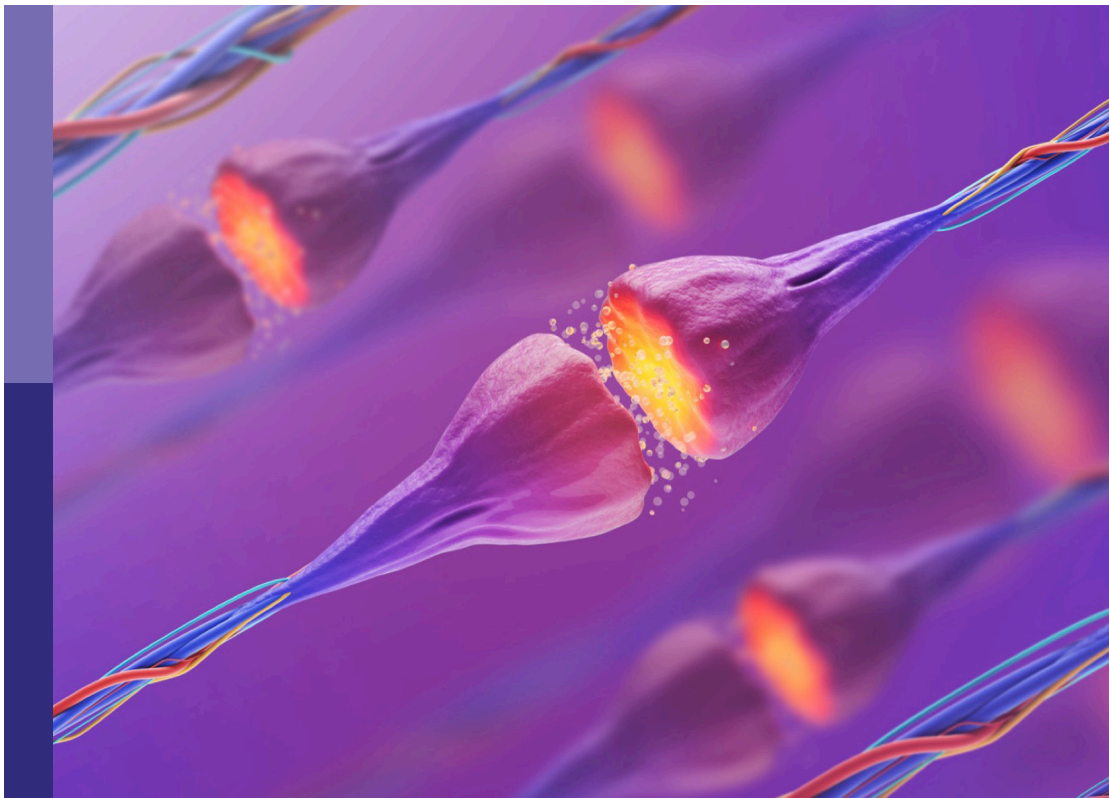

ISSN 1664-8714
ISBN 978-2-8325-6209-3
DOI 10.3389/978-2-8325-6209-3

About Frontiers

Frontiers is more than just an open access publisher of scholarly articles: it is a pioneering approach to the world of academia, radically improving the way scholarly research is managed. The grand vision of Frontiers is a world where all people have an equal opportunity to seek, share and generate knowledge. Frontiers provides immediate and permanent online open access to all its publications, but this alone is not enough to realize our grand goals.

Frontiers journal series

The Frontiers journal series is a multi-tier and interdisciplinary set of open-access, online journals, promising a paradigm shift from the current review, selection and dissemination processes in academic publishing. All Frontiers journals are driven by researchers for researchers; therefore, they constitute a service to the scholarly community. At the same time, the *Frontiers journal series* operates on a revolutionary invention, the tiered publishing system, initially addressing specific communities of scholars, and gradually climbing up to broader public understanding, thus serving the interests of the lay society, too.

Dedication to quality

Each Frontiers article is a landmark of the highest quality, thanks to genuinely collaborative interactions between authors and review editors, who include some of the world's best academicians. Research must be certified by peers before entering a stream of knowledge that may eventually reach the public - and shape society; therefore, Frontiers only applies the most rigorous and unbiased reviews. Frontiers revolutionizes research publishing by freely delivering the most outstanding research, evaluated with no bias from both the academic and social point of view. By applying the most advanced information technologies, Frontiers is catapulting scholarly publishing into a new generation.

What are Frontiers Research Topics?

Frontiers Research Topics are very popular trademarks of the *Frontiers journals series*: they are collections of at least ten articles, all centered on a particular subject. With their unique mix of varied contributions from Original Research to Review Articles, Frontiers Research Topics unify the most influential researchers, the latest key findings and historical advances in a hot research area.

Find out more on how to host your own Frontiers Research Topic or contribute to one as an author by contacting the Frontiers editorial office: frontiersin.org/about/contact

Exploiting biomarkers of CNS disorders: targets for therapeutics and non-invasive tools for diagnosis, prognosis, monitoring

Topic editors

Ana Semeano — Northeastern University, United States

Hai Sun — Rutgers, The State University of New Jersey, United States

Gal Bitan — University of California, Los Angeles, United States

Citation

Semeano, A., Sun, H., Bitan, G., eds. (2025). *Exploiting biomarkers of CNS disorders: targets for therapeutics and non-invasive tools for diagnosis, prognosis, monitoring*. Lausanne: Frontiers Media SA. doi: 10.3389/978-2-8325-6209-3

Table of contents

frontiers | Frontiers in Molecular Neuroscience

TYPE Original Research
PUBLISHED 16 October 2023
DOI 10.3389/fnmol.2023.1222506

OPEN ACCESS

EDITED BY
Gal Bitan,
University of California, Los Angeles,
United States

REVIEWED BY
Evgeny Ermakov,
Institute of Chemical Biology and Fundamental Medicine (RAS), Russia
Christopher Bartley,
National Institute of Mental Health (NIH),
United States

*CORRESPONDENCE
Omar M. A. El-Agnaf
✉ oelagnaf@hbku.edu.qa

RECEIVED 14 May 2023
ACCEPTED 22 September 2023
PUBLISHED 16 October 2023

CITATION
Mesleh A, Ehtewish H, Lennard K, Abdesselem HB, Al-Shaban F, Decock J, Alajez NM, Arredouani A, Emara MM, Albagha O, Stanton LW, Abdulla SA, Blackburnand JM and El-Agnaf OMA (2023) High-throughput autoantibody screening identifies differentially abundant autoantibodies in autism spectrum disorder. *Front. Mol. Neurosci.* 16:1222506. doi: 10.3389/fnmol.2023.1222506

High-throughput autoantibody screening identifies differentially abundant autoantibodies in autism spectrum disorder

Areej Mesleh[1,2], Hanan Ehtewish[1,2], Katie Lennard[3], Houari B. Abdesselem[1,4], Fouad Al-Shaban[1,2], Julie Decock[1,5], Nehad M. Alajez[1,5], Abdelilah Arredouani[1,6], Mohamed M. Emara[7], Omar Albagha[1], Lawrence W. Stanton[1,2], Sara A. Abdulla[2], Jonathan M. Blackburnand[3,8,9] and Omar M. A. El-Agnaf[1,2]*

[1]College of Health and Life Sciences, Hamad Bin Khalifa University, Qatar Foundation, Doha, Qatar, [2]Neurological Disorders Research Center, Qatar Biomedical Research Institute, Hamad Bin Khalifa University, Qatar Foundation, Doha, Qatar, [3]Sengenics Corporation, Level M, Plaza Zurich, Damansara Heights, Kuala Lumpur, Malaysia, [4]Proteomics Core Facility, Qatar Biomedical Research Institute, Hamad Bin Khalifa University, Qatar Foundation, Doha, Qatar, [5]Translational Cancer and Immunity Center, Qatar Biomedical Research Institute, Hamad Bin Khalifa University, Qatar Foundation, Doha, Qatar, [6]Diabetes Research Center, Qatar Biomedical Research Institute, Hamad Bin Khalifa University, Doha, Qatar, [7]Basic Medical Sciences Department, College of Medicine, Qatar University Health, Qatar University, Doha, Qatar, [8]Department of Integrative Biomedical Sciences, Faculty of Health Sciences, University of Cape Town, Cape Town, South Africa, [9]Institute of Infectious Disease and Molecular Medicine, Faculty of Health Sciences, University of Cape Town, Cape Town, South Africa

Introduction: Autism spectrum disorder (ASD) is a neurodevelopmental condition characterized by defects in two core domains, social/communication skills and restricted/repetitive behaviors or interests. There is no approved biomarker for ASD diagnosis, and the current diagnostic method is based on clinical manifestation, which tends to vary vastly between the affected individuals due to the heterogeneous nature of ASD. There is emerging evidence that supports the implication of the immune system in ASD, specifically autoimmunity; however, the role of autoantibodies in ASD children is not yet fully understood.

Materials and methods: In this study, we screened serum samples from 93 cases with ASD and 28 healthy controls utilizing high-throughput KoRectly Expressed (KREX) i-Ome protein-array technology. Our goal was to identify autoantibodies with differential expressions in ASD and to gain insights into the biological significance of these autoantibodies in the context of ASD pathogenesis.

Result: Our autoantibody expression analysis identified 29 differential autoantibodies in ASD, 4 of which were upregulated and 25 downregulated. Subsequently, gene ontology (GO) and network analysis showed that the proteins of these autoantibodies are expressed in the brain and involved in axonal guidance, chromatin binding, and multiple metabolic pathways. Correlation analysis revealed that these autoantibodies negatively correlate with the age of ASD subjects.

Conclusion: This study explored autoantibody reactivity against self-antigens in ASD individuals' serum using a high-throughput assay. The identified autoantibodies were reactive against proteins involved in axonal guidance, synaptic function, amino acid metabolism, fatty acid metabolism, and chromatin binding.

KEYWORDS

autism spectrum disorder, autoantibodies, profiling, pathways, biomarker

1. Introduction

Autism spectrum disorder (ASD) is a term that encompasses a group of neurodevelopmental conditions. The common dominator of these conditions is a defect in two core domains, social/communication skills and restricted or repetitive behaviors (American Psychiatric Association, 2013). There is no approved biomarker for ASD diagnosis, and the current diagnostic method is based on clinical evaluation, which tends to vary greatly between the affected individuals. The advancement in high-throughput proteomics techniques, which made measuring multiple proteins simultaneously a reality, motivated scientists to undertake proteomics discovery studies using body fluids of ASD subjects in an effort to identify biomarkers for diagnosis and understanding of ASD pathogenesis (Voineagu et al., 2011; Saghazadeh et al., 2019; Hewitson et al., 2021). Many of these studies have identified dysregulation in various components of the immune system as they observed upregulation in pro-inflammatory markers, such as IFN-γ, TNF-α, IL-6, and IL-8, in the brain of ASD individuals at both the protein and mRNA levels (Voineagu et al., 2011; Saghazadeh et al., 2019), thus suggesting that pro-inflammation may play a pivotal role in ASD pathogenesis.

In addition, autoimmune abnormalities have been observed in ASD (reviewed by Edmiston et al., 2017). The notion that maternal autoantibodies may play a role in children's neurodevelopment arose when maternal IgG antibodies were found in the cerebrospinal fluid of fetuses and newborns, suggesting that maternal autoantibodies can pass through the blood–brain barrier (Adinolfi et al., 1976). Several studies further observed that maternal autoantibodies of ASD subjects are reactive toward fetal brain proteins (Braunschweig et al., 2008, 2013). Moreover, studies on the blood of ASD children found a significant increase of autoantibodies in ASD compared to healthy controls; these autoantibodies were specific for myelin basic protein (MBP), ribosomal P protein, and nuclear antigens (Singh et al., 1993; Mostafa et al., 2014, 2016). The majority of published studies have tested a limited number of autoantibodies in ASD, and, there is yet to be a study that utilizes high-throughput technology to test a large number of autoantibodies in ASD cases. Therefore, the overall landscape of ASD's autoantibody reactivity across a large spectrum of self-antigens is still unknown.

Autoantibodies originate from autoreactive B-cells. In a normal scenario, B-cells producing antibodies that bind with a high affinity to self-antigens are eliminated, while B-cells producing antibodies with medium-/low-binding affinity are more likely to escape the elimination processes (Ludwig et al., 2017). Many low-affinity autoantibodies have anti-inflammatory features depending on the antibody subclass (IgM) and the post-translational modifications it has undergone (glycosylation/sialylation) (Karsten et al., 2012; Mannoor et al., 2013). However, in many cases, autoantibodies against self-antigens can interfere with physiological processes and induce devastating life-long illnesses. For instance, autoantibodies may disrupt the physiological function of the cells by different mechanisms such as mimicking receptor function, inducing cell signaling and inflammatory processes, blocking neurotransmission, and inducing cell lysis (Ludwig et al., 2017).

Collectively, the studies mentioned above have presented emerging evidence linking immune system dysregulation to ASD. Nevertheless, the comprehensive autoantibody profile of individuals with ASD and the potential mechanisms through which these autoantibodies might influence ASD remain to be fully elucidated. Therefore, investigating the autoantibody profile of ASD individuals might provide insights into the autoimmune status of ASD. Herein, we screen for 1,623 autoantibodies using the serum of 93 ASD individuals and 28 healthy controls between the ages of 6 and 15 years. To the best of our knowledge, this is the first study that screens serum autoantibodies of ASD using high-throughput KoRectly Expressed (KREX) technology. The study aims to explore the autoreactivity of IgG antibodies against self-antigens in ASD individuals to identify potential autoantibodies that could underly ASD pathology.

2. Materials and methods

2.1. Study design and samples collection

A total of 121 serum samples were used in this study, comprising 93 samples from individuals with ASD and 28 samples from healthy controls (HCs). Non-fasting peripheral blood was collected on the day of the interview and processed to obtain serum, which was subsequently stored at −80°C until further analysis. All sample processing and storage procedures were conducted at Qatar Biomedical Research Institute (QBRI). The study was performed in accordance with the guidelines of the Declaration of Helsinki and was ethically approved (QBRI-IRB 2018-024). Written informed consent and assent were given to both parents and children, respectively, for all ASD individuals and HCs. ASD individuals were clinically diagnosed using the Diagnostic and Statistical Manual of Mental Disorders, Fifth Edition (DSM-5). The severity levels of ASD individuals were evaluated using the second edition of the Autism Diagnostic Observation Schedule (ADOS-2) test. In addition, the social and communication skills of HCs were evaluated using the Social Communication Questionnaire (SCQ). Table 1 summarizes the demographic information obtained from the participants.

TABLE 1 Study participant summary statistics.

	ASD cases	Healthy controls	Statistical test
Number of participants	$N = 93$	$N = 28$	-
Age (mean ± SD)	8.26 ± 2.29	11.29 ± 2.05	3.537×10^{-8}
Gender (F/M)	20/73	14/14	0.008
DSM-5	3.78 ± 1.72	-	-
ADOS-2 scores (mean ± SD)	6.39 ± 1.47	-	-
SCQ	-	5.71 ± 3.35	-

2.2. Samples processing, assay description, and normalization

ASD cohort samples were processed at Qatar Biomedical Research Institute (QBRI). Samples were analyzed for antigen-specific autoantibodies using i-Ome protein arrays (Sengenics, Singapore), developed using KREX technology to provide a high-throughput immunoassay based on correctly folded, full-length, and functional recombinant human proteins (Blackburn et al., 2012; Adeola et al., 2016). The i-Ome arrays contain more than 1,600 human antigens, enriched for kinases, signaling molecules, cytokines, interleukins, chemokines, as well as known autoimmune antigens; the full list of proteins is provided in Supplementary Table S1. In addition, the array content is curated to represent the characteristics of protein subsets including both known and possible autoantigenic proteins across a range of disease areas (including immune-mediated diseases, malignancy, neurological disorders, endocrine disorders, and immunodeficiency). All proteins are of full length, with the exception of receptor tyrosine kinases, which are depicted as distinct cytosolic and extracellular domains.

The antigens were expressed in Sf9 insect cells, serving as fusions to a biotin carboxyl carrier protein (BCCP) domain through the utilization of a baculoviral system, a methodology previously described (Beeton-Kempen et al., 2014). The BCCP tag is endowed with biotinylation *in vivo* by host cell biotin ligase, onto a single specific lysine residue, positioned ∼50 Angstroms away from the N- and C-termini of the tag. The biotin moiety serves as a site for connecting each recombinant protein to a streptavidin-coated microarray surface, as previously described (Beeton-Kempen et al., 2014). It is important to note that insect cells are well known for their capacity to bestow mammalian-like glycosylation as well as other PTMs onto recombinant proteins.

Samples were diluted in Serum Albumin Buffer (SAB) at optimized dilution 1:200. Samples and controls were randomized and added to the microarray slides for 1 h, and each slide contained antigens that were spotted in technical quadruplicate, and then IgG levels were then detected by a secondary Cy3-labeled anti-human IgG antibody. Slides were scanned at a fixed setting using an Agilent G4600AD fluorescence microarray scanner, generating a 16-bit TIFF file. A visual quality control check was conducted, and arrays showing spot merging or other artifacts were re-assayed. A GenePix Array List (GAL) file containing information regarding the location and identity of all probed spots was used to aid with image analysis. Automatic extraction and quantification of each spot were performed using GenePix Pro 7 software (Molecular Devices), generating the mean foreground and local background pixel intensities for each spot. Raw data were imported in R (version 4.0.5) and were analyzed using a Sengenics in-house normalization pipeline.

The data were log2 transformed and normalized by subtracting the mean background intensity from the mean foreground intensity to get the net intensity per spot in the relative fluorescence unit (RFU). Subsequently, antigen replicas with coefficient variation (CV%) > 20% were flagged and excluded. Thereafter, the generated dataset underwent negative control filtration (NCF), an approach for excluding non-specific autoantibody signals. In brief, NCF identifies a baseline low-level net intensity for the array using quadruplicate technical replicates of a negative control protein that does not react with sera. Individual antigens with intensity values that correlate closely with the negative control spots across all the samples possess no meaningful information related to the disease being studied and, therefore, are excluded from downstream analyses. No arbitrary cutoff value was used to eliminate non-reactive signals. Furthermore, Loess normalization was applied to the dataset using the normalizeCyclicLoess function in R, which normalizes each pair of columns in a matrix to each other. Then, combat correction, which utilizes the empirical Bayesian approach, was applied to adjust for batch effect when the potential cause of variation is known, as samples were processed in two different batches across 2021 and 2022. A *t*-distributed stochastic neighbor embedding (t-SNE) plot of the data before and after normalization is displayed in Supplementary Figure S1.

2.3. Autoantibody identification and pathway prediction

Differentially expressed autoantibodies were identified using the *Limma* (Linear Models for Microarray Data) package (version 3.46.0) in R. Age and sex were weighted as covariates in the model because they showed a significant difference between ASD cases and HC (Table 1). Supplementary Figure S2 illustrates that the dataset does not exhibit age- or sex-dependent clustering. Differentially expressed autoantibodies were considered significant if their unadjusted p-value ≤ 0.05, given that none of the autoantibodies withstood Benjamini–Hochberg (BH) multiple correction. Correlation analysis with the ADOS-2 score and age was performed using the cor.test function, and all the heatmaps were generated using the Heatmap function from the ComplexHeatmap package. All the analyses were conducted using R software (version 4.0.5).

Protein enrichment analysis was performed on the corresponding proteins of the differentially expressed autoantibodies using ShinyGO (version 0.77) (http://bioinformatics.sdstate.edu/go/) to detect overrepresentation in cellular components, molecular functions, and biological processes in addition to the KEGG database. All the enriched terms were tested using a Fisher exact test with an adjusted p-value (FDR < 0.05), and a minimum of two proteins were required in each enriched pathway. Protein–protein interactions (PPIs) and hub proteins of the differential autoantibodies were identified using STRING (version 11.5), and then the network files were uploaded to Cytoscape (version 3.9.1) for network visualization and hub proteins identification.

2.4. Sequence identity analysis

To assess cross-reactivity among proteins that express similar antigen epitopes and are highly correlated, we checked the correlation between the differentially expressed autoantibodies. The corresponding proteins of highly correlated autoantibodies

($R^2 > 0.7$) were then aligned using the Uniport alignment tool. In addition, we used the BLAST tool to check protein isoforms with >50% identity and then performed correlation to rule out the possibility of cross-reactivity between the detected autoantibodies and the antigens available in the panel.

3. Results

3.1. Cohort characteristics

An overview of the study design is illustrated in Figure 1. This study tested a total of 121 participants, i.e., ASD cases ($n = 93$) and HCs ($n = 28$), who ranged from 6 to 15 years of age. The average ages for ASD cases and HCs were 8.26 ± 2.29 and 11.29 ± 2.05, respectively. The male-to-female ratio in the HCs group was equal (50%); however, the majority of ASD cases (78.5%) were male subjects because the prevalence of ASD is higher in male subjects compared to female subjects, and it can reach up to 4:1 (Maenner et al., 2021), which is consistent with the male-to-female ratio in the ASD group. Both age and sex exhibited statistically significant differences between the groups (Table 1). All ASD cases were clinically diagnosed with ASD using DSM-5. Subsequently, the severity level of 50 ASD cases was assessed using the ADOS-2 score. The demographic information of ASD cases and HCs is summarized in Table 1. Upon visualizing the screened samples and autoantibodies on a heatmap, we identified a pattern of self-reactive polyspecific antibodies (PSA) in nine samples, as shown in Figure 2. This pattern occurs when the antibodies retain low-affinity characteristics with a spectrum of antigens, including self-antigens. This phenomenon happens because of some types of infections and autoimmune conditions (Wang et al., 1999).

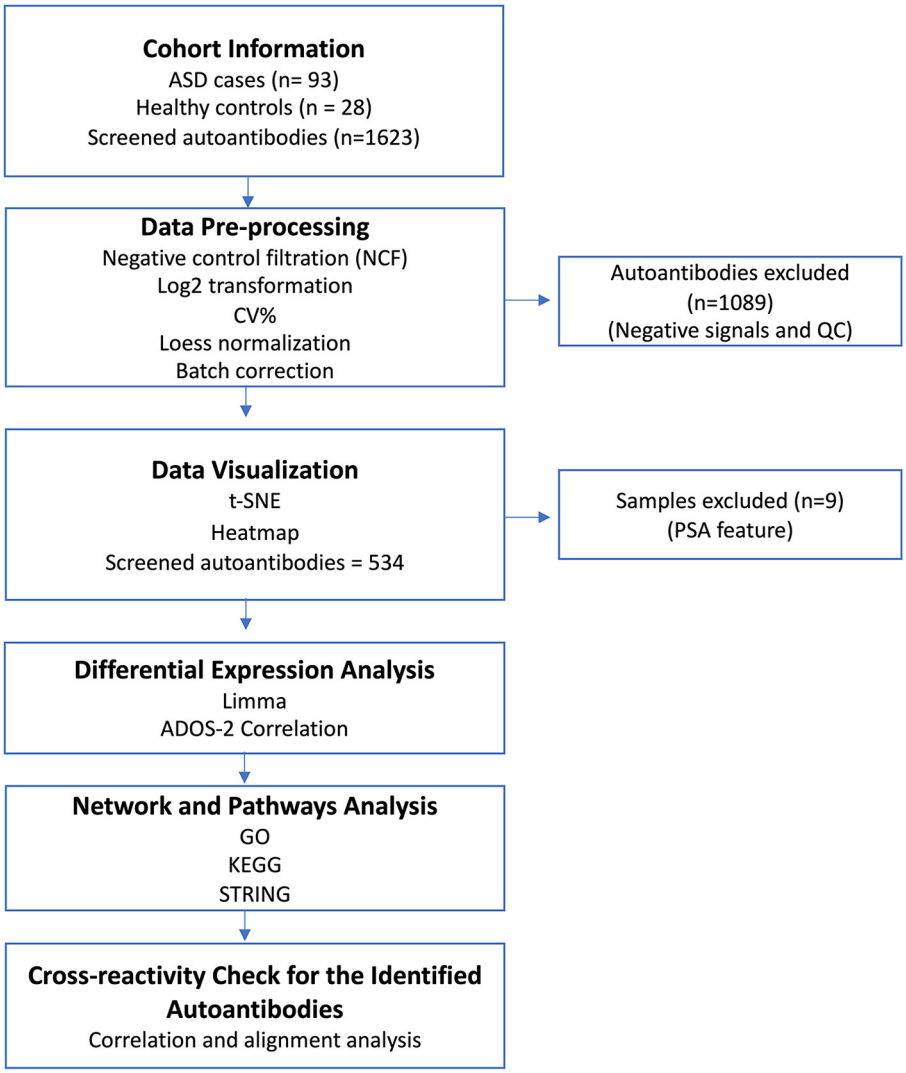

FIGURE 1
Study overview. Serum samples from ASD cases ($n = 93$) and healthy controls (HCs; $n = 28$) were collected along with the participants' demographic information. The serum samples were screened using Sengenics iOme arrays. Data pre-processing and QC analysis were performed on the generated data. Then, the generated data were visualized to detect sample outliers and batch effects. Different bioinformatic and statistical analysis approaches were deployed to analyze the dataset. Finally, a cross-reactivity check was performed on the potential autoantibodies to confirm the validity of their signals.

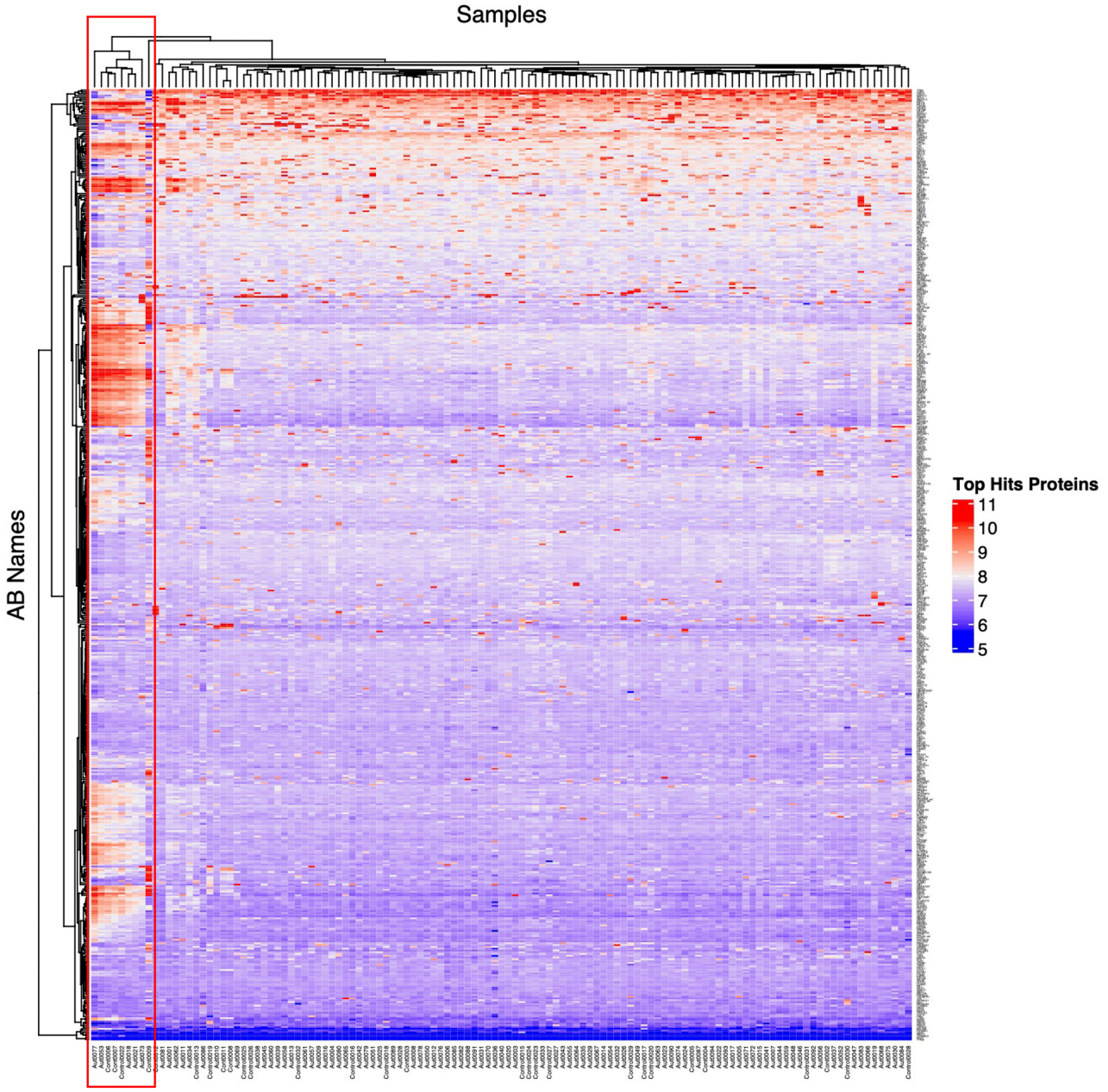

FIGURE 2
Unsupervised heatmap of ASD cases and HCs. This unsupervised heatmap was generated from all screened samples and autoantibodies (AB); the red box highlights the self-reactive polyspecific antibody (PSA) response in the samples. Any sample that exhibits this phenotype was excluded from downstream analysis.

All samples that displayed PSA features were removed from downstream analysis.

3.2. Autoantibodies profiling identified up and downregulated humoral response to self-antigens in ASD

Autoantibody screening was performed against a total of 1,623 antigens, 534 of which were retained after filtration of antigens whose signals highly correlated across the cohort with the negative control probes (as described in Section 2). Blood profiling of the humoral response to self-antigens identified 29 autoantibodies with differential expression (unadjusted *p-value* $\leq$ 0.05) in ASD individuals compared to HCs (Table 2). The significant autoantibody expression levels are depicted on the heatmap (Figure 3A). The signals of four autoantibodies were increased (PSIP1, NAP1L3, GNB3, and ZMYM2), while those of 25 autoantibodies were decreased in ASD (CTNNB1, MAPK1, SSNA1, LDHB, GOT1, etc.; Figure 3B; Table 2). The top upregulated and downregulated autoantibodies are shown

in boxplots (Supplementary Figures S3A, B). Furthermore, correlation analysis was performed on all detected autoantibodies and the ASD severity score (ADOS-2), a tool used to assess the severity level of ASD at different developmental stages. Out of all autoantibodies, 22 exhibited a significant weak correlation with the ADOS-2 score (Supplementary Table S2). However, only one protein (GOT1) from the differentially expressed autoantibodies list exhibited a significant weak positive correlation with the ADOS-2 score (Supplementary Figure S3C; Table 2). Moreover, correlation analysis was performed on the differential autoantibodies to examine the dynamic changes between the significant autoantibodies' concentration and age. Interestingly, 25 out of 29 autoantibodies negatively correlated with age, 9 of which were significantly correlated (Figure 4; Supplementary Table S2).

3.3. Gene ontology and network analysis revealed enrichment in autoantibodies against metabolic pathways and neuronal proteins

To better understand the biological relevance between the identified autoantibodies, gene ontology (GO) enrichment analysis was performed on the corresponding proteins of those autoantibodies listed in Table 2. The results revealed that the majority of the autoantibodies were raised against proteins expressed in metabolic pathways. The KEGG database showed enrichment in multiple metabolic pathways, including carbon metabolism, glycolysis and gluconeogenesis, and fructose/mannose metabolism, in addition to pathways involved in amino acid metabolisms such as cysteine and methionine pathways. Nine corresponding proteins were involved in the metabolic pathways, and those proteins are NME4, TPI1, LDHB, GOT1, ACAT2, SORD, GGPS1, TK1, and RBKS. Another enriched category was signaling pathways such as Ras, Rap1, ErbB, and MAPK as autoantibodies against MAPK1, GNB3, VEGFB, PARK2, CTNNB2, and PRKD2 were differentially expressed in ASD. Furthermore, autoantibodies against neuronal processes such as axonal guidance were enriched, and included three corresponding proteins, EPHA3, MAPK1, and PAK2, as well as glutamatergic and cholinergic synapses, which included MAPK1 and GNB3 proteins. No enrichment was found at the specific cell component. However, enrichment in molecular functions was evident in adenyl nucleotide binding, kinases, phosphate group transfer, and chromatin binding. Biological processes included enrichment in enzyme-linked receptor protein signaling pathway, organophosphate metabolic process, cell motility, migration, and positive regulation of transcription (Figure 5A; Supplementary Table S3). Moreover, autistic disorder was among disease alliance enriched terms, and included MAPK1 and CTNNB1 proteins (FDR = 0.044). Protein–protein interaction (PPIs) network of the corresponding proteins is displayed in Figure 5B, along with the hub proteins.

3.4. Autoantibodies cross-reactivity check to ensure specific epitope recognition of the identified autoantibodies

In order to check the cross-reactivity, correlation analysis was performed on the 29 autoantibodies identified by Limma analysis. Subsequently, sequence alignment and identity analysis were performed on the highly correlated autoantibodies ($R^2 >$ 0.7). The correlation matrix (Figure 6A) showed that ACAT2 correlated with TPI1, GOT1, and LDHB; SSNA1 correlated with GOT1, ACAT2, and GGPS1; LDHB correlated with GOT1 only; and GOT1 correlated with TPI1 only. Alignments and identity analysis of those protein sequences revealed that all proteins are <25% identical, and the fact that those proteins are not even isoforms indicates a low chance of cross-reactivity (Figure 6B; Supplementary Figure S4). Thus, this observed correlation might stem from a biological/functional relevance rather than antibody cross-reactivity *per-se*.

Another source of possible cross-reactivity is sequence homology between protein isoforms. Therefore, the Uniprot protein database was used to check sequence homology between the differential autoantibodies proteins ($n = 29$) and their isoforms that were also tested in the same iOme panel. Three proteins showed > 50% homology with their isoforms in the iOme panel: MAPK1 and MAPK3 were 83% identical, and PAK2 and PAK4 and also YWHAE and YWHAG were ~64% identical. However, proteins with high homology were not found to be differentially expressed, and they exhibited a low correlation with their significant counterparts except for MAPK1 and MAPK3, which were highly correlated ($R^2 = 0.95$), see Figure 6C. Therefore, based on the correlation and homology analysis findings, cross-reactivity cannot be ruled out for MAPK1 and MAPK3; however, protein co-expression might explain the high correlation. Overall, most of the identified autoantibodies are less likely to exhibit cross-reactivity except for MAPK1's autoantibody, which might cross-react with MAPK3. Although sequence similarity was excluded among the candidate antigens, conformational molecular mimicry cannot be excluded.

4. Discussion

Several studies have identified the presence of autoantibodies against fetal brain and neuronal proteins in ASD children and their mothers (Piras et al., 2014; Abou-Donia et al., 2019; Mazón-Cabrera et al., 2019; Ramirez-Celis et al., 2021). The implication of those autoantibodies and whether or not they interfere with normal developmental and biological processes are still unknown. In our study, we performed quantitative autoantibody profiling using 1,623 antigens for ASD subjects and healthy controls in an effort to identify differentially expressed autoantibodies and to elucidate the biological relevance of those autoantibodies in ASD. An aggregate of 534 autoantibodies were identified across the screened samples, 29 of which were differentially expressed in ASD (Figure 3; Table 2). The highest FC differences between ASD cases and HCs were observed in two proteins, PSIP1 (FC ~ 1.7) and NAP1L3 (FC ~ 1.6), which were upregulated in ASD. PSIP1 is a nuclear protein and a transcription coactivator that is involved in neurogenesis processes such as neuroepithelial cell

TABLE 2 Differentially expressed autoantibodies list.

Protein symbol	Protein name	Fold change (FC)	*Limma* *p*-value	Protein expression in the brain	*p*-value, correlation coefficient
ACAT2	Acetyl-CoA acetyltransferase 2	0.84	0.011	(+)	0.50, 0.096
APPL1	Adaptor protein, phosphotyrosine interacting with PH domain and leucine zipper 1	0.88	0.026	(+)	0.08, −0.24
CARHSP1	Calcium-regulated heat-stable protein 1	0.84	0.010	(+)	0.13, 0.21
CTNNB1	Catenin beta 1	0.78	0.056	Highest expression in Cereb*	0.82, 0.03
ECI2	Enoyl-CoA delta isomerase 2	0.89	0.015	(+)	0.93, 0.01
EPHA3_ext	EPH receptor A3	0.92	0.042	(+)	0.56, −0.08
GGPS1	Geranylgeranyl diphosphate synthase 1	0.83	0.025	Low expression in BG, Hipp, and CC*	0.53, −0.08
GIPC1	GAIP interacting protein C-terminus	0.88	0.005	(+)	0.95, −0.008
GNB3	Guanine nucleotide-binding protein G	1.05	0.037	(+)	0.62, −0.07
GOT1	Glutamic-oxaloacetic transaminase 1	0.85	0.017	(+)	0.04, 0.288
HDAC4	Histone deacetylase 4	0.85	0.026	(+)	0.07, −0.25
ILF2	Interleukin enhancer binding factor 2	0.86	0.042	(+)	0.97, 0.004
KRT8	Keratin 8	0.81	0.018	NA	0.84, −0.028
LDHB	Lactate dehydrogenase B	0.87	0.012	(+)	0.25, 0.165
MAPK1	Mitogen-activated protein kinase 1	0.73	0.045	(+)	0.28, −0.15
NAP1L3	Nucleosome assembly protein 1 like 3	1.61	0.057	RNA levels are high in the brain	0.39, −0.12
NME4	NME/NM23 nucleoside diphosphate kinase 4	0.92	0.020	(+)	0.21, 0.17
PAK2	P21 (RAC1)-activated kinase 2	0.91	0.017	Low expression in CC and Endoth*	0.99, −0.0005
PRKD2	Protein kinase D2	0.88	0.025	(+)	0.17, −0.19
PSIP1	PC4 and SRSF1 interacting protein 1	1.68	0.045	(+)	0.33, 0.13
RBKS	Ribokinase	0.89	0.019	Low expression in Cereb, BG, and Hipp*	0.31, 0.14
SORD	Sorbitol dehydrogenase	0.89	0.011	NA	0.44, 0.11
SSNA1	SS nuclear autoantigen 1	0.79	0.027	NA	0.88, 0.020
TK1	Thymidine kinase 1	0.91	0.047	Low expression in Hipp and CC*	0.66, 0.062
TPI1	Triosephosphate isomerase 1	0.92	0.044	(+)	0.75, 0.045
VEGFB	Vascular endothelial growth factor B	0.843	0.043	NA	0.23, −0.17
YWHAE	Tyrosine 3-monooxygenase/tryptophan 5-monooxygenase activation protein epsilon	0.88	0.052	(+)	0.30, 0.14
ZKSCAN3	Zinc finger with KRAB and SCAN domains 3	0.84	0.04	(+)	0.73, 0.048
ZMYM2	Zinc finger MYM-type containing 2	1.05	0.04	(+)	0.38, 0.12

*Cereb, cerebellum; BG, basal ganglia; Hippo, hippocampus; CC, cerebral cortex; Endoth., endothelium.

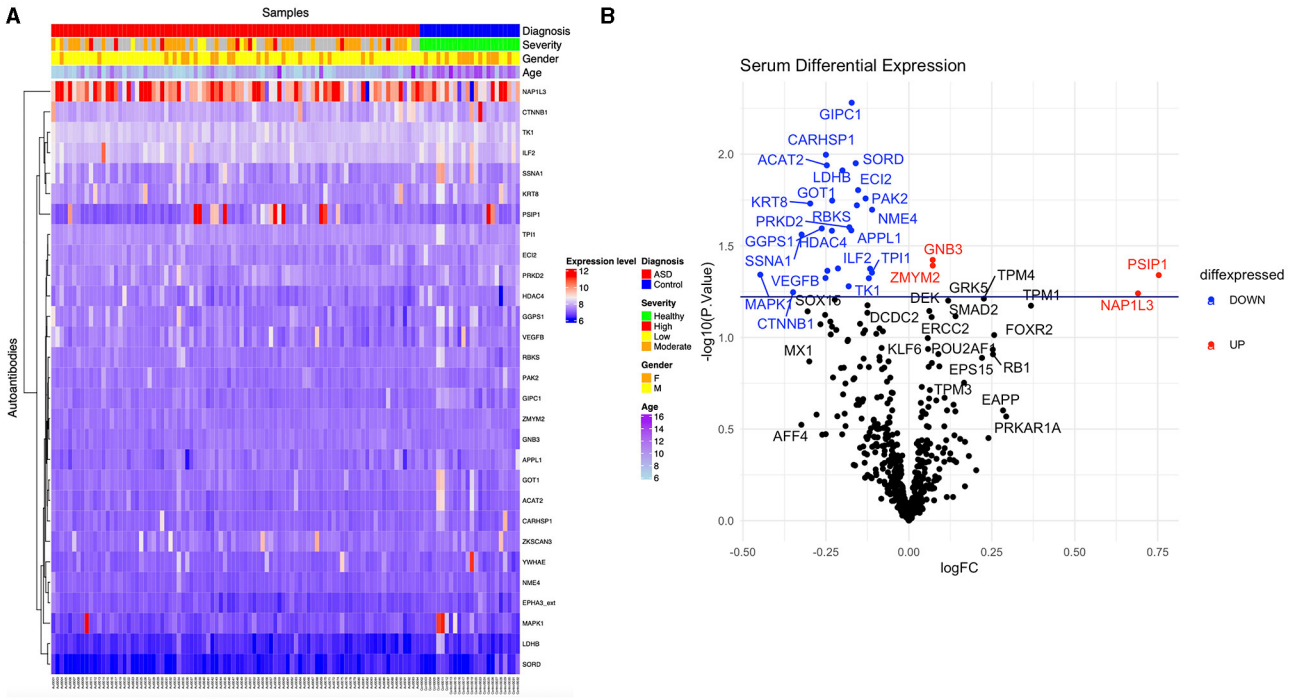

FIGURE 3
Differential expression of ASD autoantibodies. **(A)** Supervised heatmap of ASD cases and HCs using the differential autoantibodies (p-value ≤ 0.05), gender (male = yellow, female = orange), diagnosis (ASD = red, HCs = blue), severity (healthy = green, high = red, low = yellow, moderate = orange), and expression level (high = red, low=blue). **(B)** The volcano plot shows log2 fold change (x-axis) against Limma −log10 p-value (y-axis) for all the autoantibodies differentially expressed between HCs and ASD cases. The top significantly upregulated and downregulated proteins are labeled in red and blue, respectively.

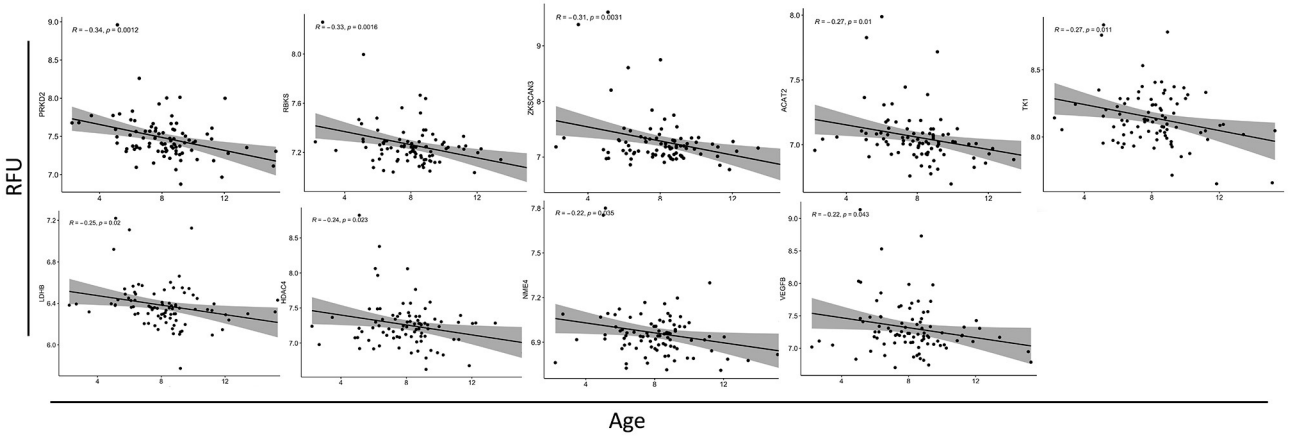

FIGURE 4
Correlation analysis between autoantibodies relative fluorescence unit (RFU) values and the age of ASD subjects. Scatterplots of all the significantly correlated autoantibodies. The correlation coefficients (R^2) and associated p-values are shown in each figure (top left).

differentiation (Chylack et al., 2004). Furthermore, NAP1L3 is also a nucleosome protein and a histone chaperone that plays a crucial role in epigenetic transcription regulation (Heshmati et al., 2018). Interestingly, both proteins have chromatin-binding abilities and were enriched in the chromatin-binding term in GO analysis. Moreover, other corresponding proteins also enriched in chromatin binding GO term are HDAC4, CTNNB1, and ZKSCAN3; however, unlike PSIP1 and NAP1L3, these proteins exhibited reduced expression in ASD compared to HCs. HDAC4 encodes for histone deacetylase 4, a protein involved in the deacetylation of the core histones, thus regulating transcription (Wang et al., 2014). Deletion in HDAC4 has been reported in ASD (Williams et al., 2010). CTNNB1 is a beta-catenin protein involved in the Wnt pathway in the neurons. Interestingly, according to the

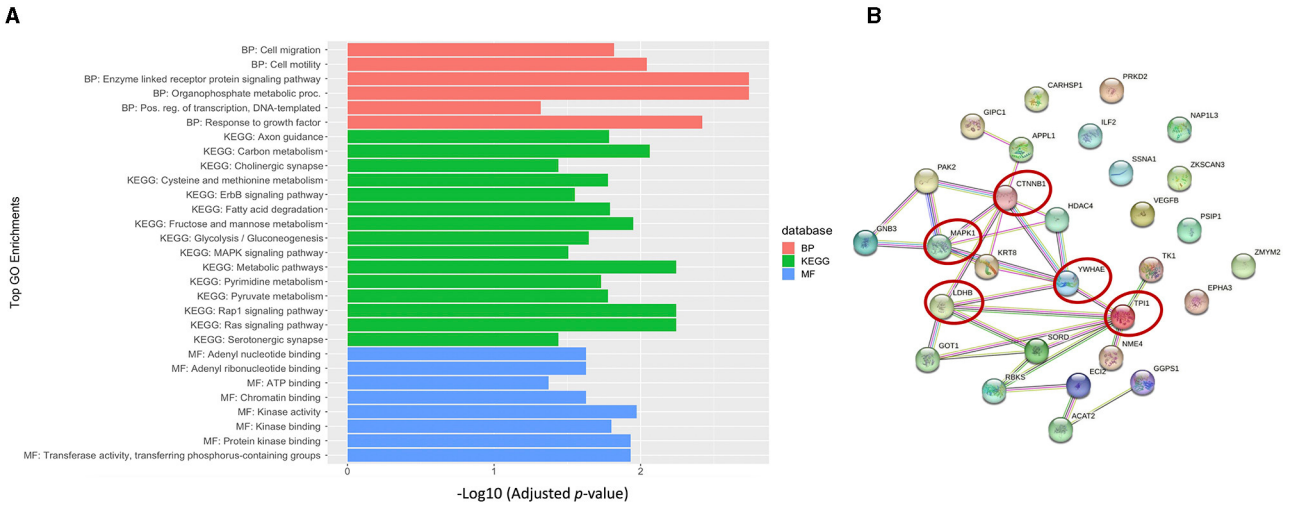

FIGURE 5
Biological relevance of the differential autoantibodies. **(A)** Top GO terms of the differential autoantibody's proteins; BP, biological process; MF, molecular function. **(B)** STRING protein-protein interaction (PPI) network and hub proteins list are highlighted with red circles.

Simons Foundation Autism Research Initiative (SFARI) database, CTNNB1 nonsense and missense mutations have been reported in ASD subjects (O'Roak et al., 2012). No evidence has been reported on the relationship between ASD pathogenesis and ZKSCAN3.

Interestingly, differential levels of autoantibodies against proteins with neuronal-related function were also detected in our cohort. For instance, EPHA3, MAPK1, PAK2, and SSNA1 are important for the axonal guidance process during neurogenesis (Brown et al., 2000; Hammarlund et al., 2009; Ding et al., 2015; Lawrence et al., 2021). Moreover, MAPK1 is also involved in cholinergic and serotonergic synapse (as shown in our GO analysis). MAPK1 is highly expressed in the human brain and is involved in various processes such as synaptic plasticity, learning, and memory (Thomas and Huganir, 2004). Although we were not able to rule out the cross-reactivity between MAPK1 and MAPK3 due to their high correlation and homology, MAPK1 and MAPK3 are both as important in the MAPK/ERK cascade and participate in the same biological processes; thus, they might both correlate due to their biological relevance. Moreover, recent studies showed that MAPK1 and MAPK3 can generally compensate for each other in most tissues and have a very similar expression pattern (Upadhya et al., 2013; Frémin et al., 2015). MAPK1 has a critical role in multiple signaling pathways such as MAPK, ErbB, Ras, and Rap1 pathways, as shown in GO enrichment analysis (Figure 5A; Upadhya et al., 2013).

Another pathway of autoantibodies that was found to be differentially expressed in nine of its proteins is the metabolic pathway, which includes amino acids and fatty acid metabolism, gluconeogenesis, and glycolysis. Amongst these autoantibodies is one that corresponds to the LDHB protein. Autoantibodies against this protein have been reported to be upregulated in ASD children and their mothers (Braunschweig et al., 2013; Ramirez-Celis et al., 2021) contrary to our cohort, where it was found downregulated. This discrepancy could potentially stem from technical differences as the aforementioned studies utilized western blotting for detection, while our study employed iOme microarray. In addition, both western blotting and iOme microarray entail different normalization approaches. LDHB is an enzyme that catalyzes the conversion of lactate to pyruvate, a critical energy substrate. A recent study using an LDHB knock-out mouse model showed that LDHB deficiency triggers gliosis, neuroinflammation, and neurodegeneration in the brain (Park et al., 2022). Only one autoantibody, corresponding to GOT1 protein, exhibited a significant but weak correlation with the ADOS-2 scores. Our GO analysis revealed that GOT1 is involved in multiple metabolic processes, such as cysteine and methionine metabolism pathways. Paradoxically, our findings revealed a negative correlation between age and the majority of the identified autoantibodies. This finding suggests that there is an overall reduction in autoantibody signal as ASD children age increases. Moreover, our study could not confirm the source of the identified autoantibodies; therefore, more longitudinal studies are needed to validate and properly curate the origins and the dynamic changes of these autoantibodies.

Considering the existing reports on ASD, autoantibodies against glyceraldehyde-3phosphate dehydrogenase (GAPDH) have previously been identified (Mazón-Cabrera et al., 2023). Unfortunately, this specific autoantigen is not included in the Sengenics autoantigen panel. On the other hand, autoantibodies against stress-induced phosphoprotein 1 (STIP1) have been previously identified in ASD (Braunschweig et al., 2013), and the autoantigen is present in the Sengenics panel; however, our results revealed no statistically significant difference in its expression. It is crucial to highlight that autoantibodies targeting these proteins were primarily identified in mothers of ASD children rather than the children themselves. Another study highlighted the significance of GFAP and SNCA autoantibodies in ASD subjects (Abou-Donia et al., 2019). However, our study indicated that GFAP did not yield

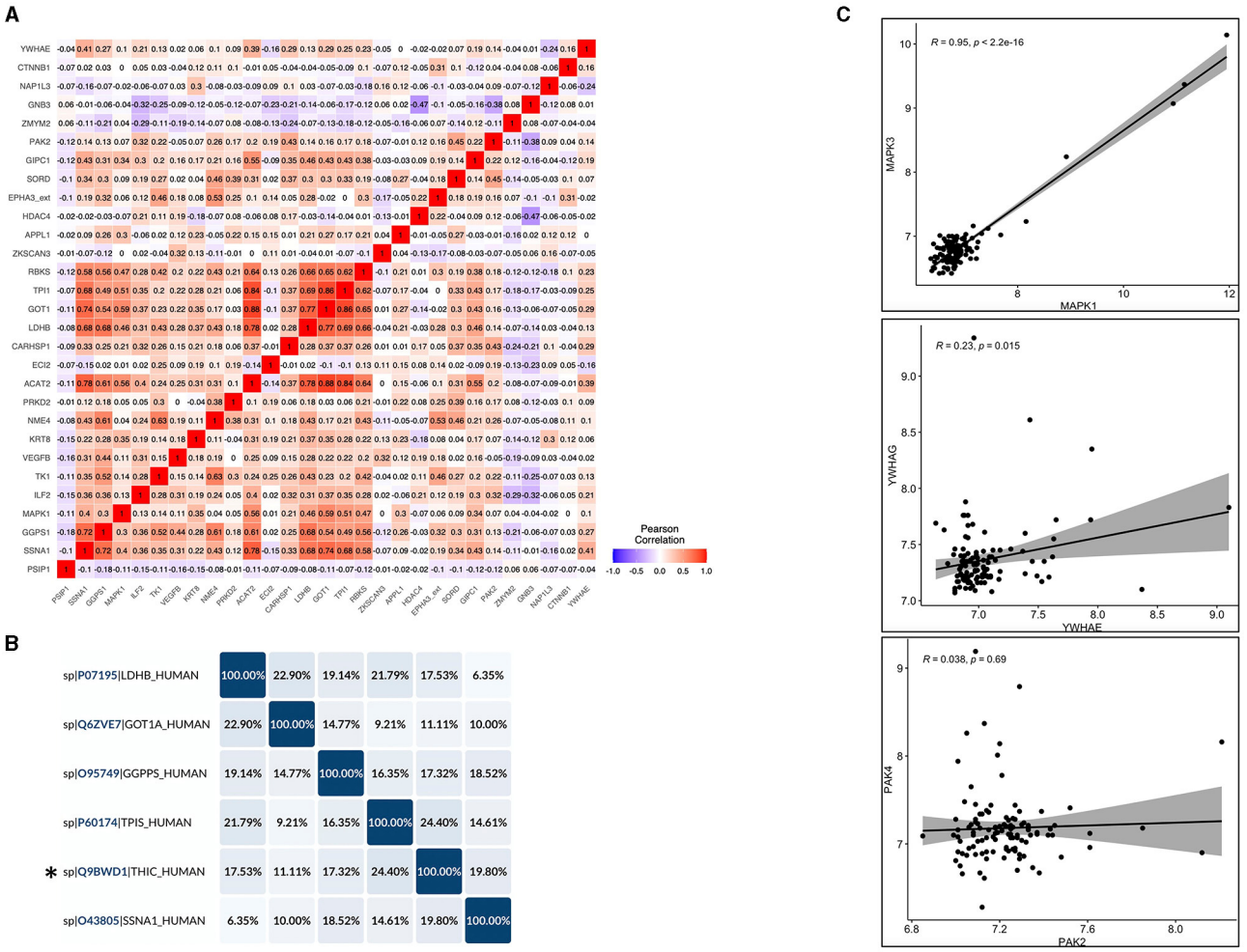

FIGURE 6
Cross-reactivity checks for the identified differential autoantibodies. **(A)** A correlation matrix of the differential autoantibodies using Pearson's correlation, red = high and blue = low. **(B)** Identity matrix, generated from aligning the corresponding protein sequences of the highly correlated autoantibodies ($R^2 \geq 0.7$) using Uniprot, *THIC corresponds to ACAT2. **(C)** Pearson correlation of the corresponding protein isoforms with >50% homology, correlation coefficients (R^2), and associated p-values are shown in each figure (top left).

statistically significant results, and SNCA did not pass the NCF threshold, leading to its exclusion from the statistical analysis. These previous studies predominantly employed Western blotting for autoantibody detection, and this methodological disparity could potentially explain the challenges in reproducing these findings within our cohort.

It is noteworthy that the majority of the identified autoantibodies in this study were overall downregulated in ASD compared to HCs. The cause of this downregulation and how it might be involved in ASD pathogenesis requires further investigation. However, the overall downregulation of autoantibodies in ASD does not indicate an underlying autoimmune pathology. The presence of higher concentrations of autoantibodies does not necessarily signify pathology; on the contrary, they might serve a protective role (Shoenfeld and Toubi, 2005). For instance, autoantibodies against dsDNA were negatively correlated with lupus nephritis in systemic lupus erythematosus patients; in other words, the higher the antibody titer, the lower the severity of the disease (Witte, 2008). Furthermore, anti-TCR antibodies that circulate in myasthenia gravis patients' peripheral blood are reactive against a specific T-cell population that expresses the Vβ5.1 TCR gene. This gene is largely responsible for the production of anti–acetylcholine receptor antibodies in patients with myasthenia gravis, thus inhibiting the proliferation and IFN-γ production of those cells and reducing the severity of the condition (Jambou et al., 2003). Another example of the protective role of autoantibodies against self-antigens was tested in the Alzheimer's disease mouse model, where administrating antibodies against β-amyloid, a protein responsible for plaque formation in Alzheimer's disease, resulted in reduced amyloid plaque formation in the brain and attenuated other pathological features of Alzheimer's disease (Schenk et al., 1999). This hypothesis was observed in humans as naturally occurring autoantibodies against β-amyloid were reduced in the cerebrospinal fluid of Alzheimer's disease patients compared to healthy controls (Du et al., 2001).

The majority of the identified differentially expressed autoantibodies correspond to cytosol and nuclear proteins; hence, they are expressed intracellularly. It is important to mention that autoantibodies production is not limited to extracellular and cell-surface proteins, but rather, there have been some instances where autoantibodies are generated against intracellular proteins. For example, autoantibodies against double-strand DNA are known to be present in systematic lupus erythematosus disorder (Rahman and Isenberg, 2008); autoantibodies against SSA and SSB are known to be present in Sjögren's syndrome (Routsias and Tzioufas, 2010); and autoantibodies against myeloperoxidase (P-ANCA) and proteinase 3 (p-ANCA) are present in vasculitides (Chen and Kallenberg, 2010). The mechanism by which the immune system is exposed to those antigens is thought to be through apoptosis, where the intracellular content of the cell is expressed on the surface of the apoptotic body (Casciola-Rosen et al., 1999). Another possible mechanism is antigen mimicry; for example, the Ro60 antigen, recognized by anti-Ro60 in systematic lupus erythematosus, shares similarities with a ribonucleoprotein found in *Mycobacterium smegmatis* as well as with a specific amino acid sequence (58–72) in the Epstein–Barr nuclear antigen-I (EBNA-I), a latent viral protein expressed by Epstein–Barr virus (McClain et al., 2005). However, the exact mechanism of how this takes place in the context of ASD is unknown.

Other examples of autoantibody targets that have been reported to have a protective role are autoantibodies against chemokines and cytokines. These autoantibodies protect against disease models such as multiple sclerosis and rheumatoid arthritis, thus confirming the importance of beneficial autoimmunity in controlling harmful self-directed immune responses (Wildbaum et al., 2003). In addition, the presence of natural autoantibodies that arise with no prior exposure to antigen plays a crucial role in clearing apoptotic cell bodies by marking them for macrophage-mediated phagocytosis (Elkon and Casali, 2008). These natural autoantibodies recognize intracellular antigens such as nucleosomes and phosphatidylserine in the apoptotic cell body.

To the best of our knowledge, our study is the first to perform autoantibody profiling using a large number of antigens for ASD individuals. However, it is important to acknowledge that our study faced limitations, primarily related to sample size, as the number of the HCs group was smaller than that of the cases. Subsequent studies are needed to validate our findings through larger sample sizes and to explore the role of these autoantibodies in the pathogenesis of ASD. Although we excluded sequence similarity among the candidate antigens, the potential for conformational molecular mimicry remains. Furthermore, our study uncovered a negative correlation between the majority of the identified autoantibodies and the age of ASD individuals. As a result, future longitudinal studies should include samples from ASD children to better elucidate this correlation and to validate our findings.

5. Conclusion

In conclusion, this study aimed to explore autoantibody reactivity against self-antigens in the serum of ASD individuals using a high-throughput assay. We identified 29 autoantibodies that were differentially expressed in ASD. These differential autoantibodies were reactive against proteins involved in axonal guidance, synaptic function, amino acid metabolism, fatty acid metabolism, and chromatin binding. In addition, we detected an overall decline in autoantibody concentration as ASD children's ages increased. This study was limited by the imbalanced number of participants and the significant difference, in terms of age and sex, between the studied groups. Therefore, validating our findings using a different cohort with a larger sample size is warranted. Furthermore, additional longitudinal investigations are necessary to accurately ascertain the sources and evolving patterns of these autoantibodies.

Data availability statement

The original contributions presented in the study are included in the article/Supplementary material, further inquiries can be directed to the corresponding author.

Ethics statement

The studies involving humans were approved by Qatar Biomedical Research Institute (QBRI). The studies were conducted in accordance with the local legislation and institutional requirements. Written informed consent for participation in this study was provided by the participants' legal guardians/next of kin.

Author contributions

AM: conceptualization, data curation, formal analysis, and writing—original draft. HE: data curation and formal analysis. KL: formal analysis. HA: project administration, resources, and writing—review and editing. FA-S: data curation (ADOS-2 scores) and writing—review and editing. JD, NA, ME, and OA: conceptualization and writing—review and editing. AA: conceptualization. LS: conceptualization, project coordination, and writing—review and editing. SA: project coordination. JB: writing—review and editing. OE-A: conceptualization, study design, supervision, and writing—review and editing. All authors have read and agreed to the published version of the manuscript.

Funding

This research was funded by Qatar Biomedical Research Institute (QBRI) under the Interdisciplinary Research Program, Grant Number: 2018 001. AM, a Ph.D. student funded by GSRA-QNRF (GSRA6-1-0616-19097). The funders had no role in the design and conduct of the study, in the collection, management, analysis, and interpretation of the data, in the preparation, review, or approval of the article or in the decision to submit the article for publication.

Acknowledgments

The authors thank all ASD and healthy subjects and their families for their valuable participation in this study. The authors would also like to extend their gratitude to QBRI and QNRF for funding this study.

Conflict of interest

KL and JB are employees of Sengenics, who commercialize the KREX arrays used in this study. JB is also a board member of Sengenics.

The remaining authors declare that the research was conducted in the absence of any commercial or financial relationships that could be construed as a potential conflict of interest.

Publisher's note

Supplementary material

The Supplementary Material for this article can be found online at: https://www.frontiersin.org/articles/10.3389/fnmol.2023.1222506/full#supplementary-material

References

Abou-Donia, M. B., Suliman, H. B., Siniscalco, D., Antonucci, N., and ElKafrawy, P. (2019). *De novo* blood biomarkers in autism: autoantibodies against neuronal and glial proteins. *Behav. Sci.* 9, 47. doi: 10.3390/bs9050047

Adeola, H. A., Smith, M., Kaestner, L., Blackburn, J. M., and Zerbini, L. F. (2016). Novel potential serological prostate cancer biomarkers using CT100+ cancer antigen microarray platform in a multi-cultural South African cohort. *Oncotarget* 7, 13945–13964. doi: 10.18632/oncotarget.7359

Adinolfi, M., Beck, S. E., Haddad, S. A., and Seller, M. J. (1976). Permeability of the blood-cerebrospinal fluid barrier to plasma proteins during foetal and perinatal life. *Nature* 259, 140–141. doi: 10.1038/259140a0

American Psychiatric Association (2013). *Diagnostic and Statistical Manual of Mental Disorders, 5th Edn.* Washington, DC: American Psychiatric Association.

Beeton-Kempen, N., Duarte, J., Shoko, A., Serufuri, J. M., John, T., Cebon, J., et al. (2014). Development of a novel, quantitative protein microarray platform for the multiplexed serological analysis of autoantibodies to cancer-testis antigens. *Int. J. Cancer.* 135, 1842–1851. doi: 10.1002/ijc.28832

Blackburn, J. M., Shoko, A., and Beeton-Kempen, N. (2012). Miniaturized, microarray-based assays for chemical proteomic studies of protein function. *Methods Mol. Biol.* 800, 133–162. doi: 10.1007/978-1-61779-349-3_10

Braunschweig, D., Ashwood, P., Krakowiak, P., Hertz-Picciotto, I., Hansen, R., Croen, L. A., et al. (2008). Autism: maternally derived antibodies specific for fetal brain proteins. *Neurotoxicology* 29, 226–231. doi: 10.1016/j.neuro.2007.10.010

Braunschweig, D., Krakowiak, P., Duncanson, P., Boyce, R., Hansen, R. L., Ashwood, P., et al. (2013). Autism-specific maternal autoantibodies recognize critical proteins in developing brain. *Transl. Psychiatry* 3, e277. doi: 10.1038/tp.2013.50

Brown, A., Yates, P. A., Burrola, P., Ortuño, D., Vaidya, A., Jessell, T. M., et al. (2000). Topographic mapping from the retina to the midbrain is controlled by relative but not absolute levels of EphA receptor signaling. *Cell* 102, 77–88. doi: 10.1016/S0092-8674(00)00012-X

Casciola-Rosen, L., Andrade, F., Ulanet, D., Wong, W. B., and Rosen, A. (1999). Cleavage by granzyme B is strongly predictive of autoantigen status: implications for initiation of autoimmunity. *J. Exp. Med.* 190, 815–826. doi: 10.1084/jem.190.6.815

Chen, M., and Kallenberg, C. G. (2010). ANCA-associated vasculitides–advances in pathogenesis and treatment. *Nat. Rev. Rheumatol.* 6, 653–664. doi: 10.1038/nrrheum.2010.158

Chylack, L. T. Jr., Fu, L., Mancini, R., Martin-Rehrmann, M. D., Saunders, A. J., Konopka, G., et al. (2004). Lens epithelium-derived growth factor (LEDGF/p75) expression in fetal and adult human brain. *Exp. Eye Res.* 79, 941–948. doi: 10.1016/j.exer.2004.08.022

Ding, Y., Li, Y., Lu, L., Zhang, R., Zeng, L., Wang, L., et al. (2015). Inhibition of nischarin expression promotes neurite outgrowth through regulation of PAK activity. *PLoS ONE* 10, e0144948. doi: 10.1371/journal.pone.0144948

Du, Y., Dodel, R., Hampel, H., Buerger, K., Lin, S., Eastwood, B., et al. (2001). Reduced levels of amyloid beta-peptide antibody in Alzheimer disease. *Neurology* 57, 801–805. doi: 10.1212/WNL.57.5.801

Edmiston, E., Ashwood, P., and Van de Water, J. (2017). Autoimmunity, autoantibodies, and autism spectrum disorder. *Biol. Psychiatry* 81, 383–390. doi: 10.1016/j.biopsych.2016.08.031

Elkon, K., and Casali, P. (2008). Nature and functions of autoantibodies. *Nat. Clin. Pract. Rheumatol.* 4, 491–498. doi: 10.1038/ncprheum0895

Frémin, C., Saba-El-Leil, M. K., Lévesque, K., Ang, S. L., and Meloche, S. (2015). Functional redundancy of ERK1 and ERK2 MAP kinases during development. *Cell Rep.* 12, 913–921. doi: 10.1016/j.celrep.2015.07.011

Hammarlund, M., Nix, P., Hauth, L., Jorgensen, E. M., and Bastiani, M. (2009). Axon regeneration requires a conserved MAP kinase pathway. *Science* 323, 802–806. doi: 10.1126/science.1165527

Heshmati, Y., Kharazi, S., Türköz, G., Chang, D., Kamali Dolatabadi, E., Boström, J., et al. (2018). The histone chaperone NAP1L3 is required for haematopoietic stem cell maintenance and differentiation. *Sci. Rep.* 8, 11202. doi: 10.1038/s41598-018-29518-z

Hewitson, L., Mathews, J. A., Devlin, M., Schutte, C., Lee, J., and German, D. C. (2021). Blood biomarker discovery for autism spectrum disorder: a proteomic analysis. *PLoS ONE* 16, e0246581. doi: 10.1371/journal.pone.0246581

Jambou, F., Zhang, W., Menestrier, M., Klingel-Schmitt, I., Michel, O., Caillat-Zucman, S., et al. (2003). Circulating regulatory anti-T cell receptor antibodies in patients with myasthenia gravis. *J. Clin. Invest.* 112, 265–274. doi: 10.1172/JCI200316039

Karsten, C. M., Pandey, M. K., Figge, J., Kilchenstein, R., Taylor, P. R., Rosas, M., et al. (2012). Anti-inflammatory activity of IgG1 mediated by Fc galactosylation and association of FcγRIIB and dectin-1. *Nat. Med.* 18, 1401–1406. doi: 10.1038/nm.2862

Lawrence, E. J., Arpag, G., Arnaiz, C., and Zanic, M. (2021). SSNA1 stabilizes dynamic microtubules and detects microtubule damage. *Elife* 10, 67282. doi: 10.7554/eLife.67282

Ludwig, R. J., Vanhoorelbeke, K., Leypoldt, F., Kaya, Z., Bieber, K., McLachlan, S. M., et al. (2017). Mechanisms of autoantibody-induced pathology. *Front. Immunol.* 8, 603. doi: 10.3389/fimmu.2017.00603

Maenner, M. J., Shaw, K. A., Bakian, A. V., Bilder, D. A., Durkin, M. S., Esler, A., et al. (2021). Prevalence and characteristics of autism spectrum disorder among children aged 8 years - autism and developmental disabilities monitoring network, 11 sites, United States 2018. *MMWR Surveill. Summ.* 70, 1–16. doi: 10.15585/mmwr.ss7011a1

Mannoor, K., Xu, Y., and Chen, C. (2013). Natural autoantibodies and associated B cells in immunity and autoimmunity. *Autoimmunity* 46, 138–147. doi: 10.3109/08916934.2012.748753

Mazón-Cabrera, R., Liesenborgs, J., Brône, B., Vandormael, P., and Somers, V. (2023). Novel maternal autoantibodies in autism spectrum disorder: implications for screening and diagnosis. *Front. Neurosci.* 17, 1067833. doi: 10.3389/fnins.2023.1067833

Mazón-Cabrera, R., Vandormael, P., and Somers, V. (2019). Antigenic targets of patient and maternal autoantibodies in autism spectrum disorder. *Front. Immunol.* 10, 1474. doi: 10.3389/fimmu.2019.01474

McClain, M. T., Heinlen, L. D., Dennis, G. J., Roebuck, J., Harley, J. B., and James, J. A. (2005). Early events in lupus humoral autoimmunity suggest initiation through molecular mimicry. *Nat. Med.* 11, 85–89. doi: 10.1038/nm1167

Mostafa, G. A., Bjørklund, G., Urbina, M. A., and Al-Ayadhi, L. Y. (2016). The positive association between elevated blood lead levels and brain-specific autoantibodies in autistic children from low lead-polluted areas. *Metab. Brain Dis.* 31, 1047–1054. doi: 10.1007/s11011-016-9836-8

Mostafa, G. A., El-Sherif, D. F., and Al-Ayadhi, L. Y. (2014). Systemic auto-antibodies in children with autism. *J. Neuroimmunol.* 272, 94–98. doi: 10.1016/j.jneuroim.2014.04.011

O'Roak, B. J., Vives, L., Girirajan, S., Karakoc, E., Krumm, N., Coe, B. P., et al. (2012). Sporadic autism exomes reveal a highly interconnected protein network of *de novo* mutations. *Nature* 485, 246–250. doi: 10.1038/nature10989

Park, J. S., Saeed, K., Jo, M. H., Kim, M. W., Lee, H. J., Park, C. B., et al. (2022). LDHB deficiency promotes mitochondrial dysfunction mediated oxidative stress and neurodegeneration in adult mouse brain. *Antioxidants* 11, 261. doi: 10.3390/antiox11020261

Piras, I. S., Haapanen, L., Napolioni, V., Sacco, R., Van de Water, J., and Persico, A. M. (2014). Anti-brain antibodies are associated with more severe cognitive and behavioral profiles in Italian children with Autism Spectrum Disorder. *Brain Behav. Immun.* 38, 91–99. doi: 10.1016/j.bbi.2013.12.020

Rahman, A., and Isenberg, D. A. (2008). Systemic lupus erythematosus. *N. Engl. J. Med.* 358, 929–939. doi: 10.1056/NEJMra071297

Ramirez-Celis, A., Becker, M., Nuño, M., Schauer, J., Aghaeepour, N., and Van de Water, J. (2021). Risk assessment analysis for maternal autoantibody-related autism (MAR-ASD): a subtype of autism. *Mol. Psychiatry* 26, 1551–1560. doi: 10.1038/s41380-020-00998-8

Routsias, J. G., and Tzioufas, A. G. (2010). B-cell epitopes of the intracellular autoantigens Ro/SSA and La/SSB: tools to study the regulation of the autoimmune response. *J. Autoimmun.* 35, 256–264. doi: 10.1016/j.jaut.2010.06.016

Saghazadeh, A., Ataeinia, B., Keynejad, K., Abdolalizadeh, A., Hirbod-Mobarakeh, A., and Rezaei, N. (2019). A meta-analysis of pro-inflammatory cytokines in autism spectrum disorders: effects of age, gender, and latitude. *J. Psychiatr. Res.* 115, 90–102. doi: 10.1016/j.jpsychires.2019.05.019

Schenk, D., Barbour, R., Dunn, W., Gordon, G., Grajeda, H., Guido, T., et al. (1999). Immunization with amyloid-beta attenuates Alzheimer-disease-like pathology in the PDAPP mouse. *Nature* 400, 173–177. doi: 10.1038/22124

Shoenfeld, Y., and Toubi, E. (2005). Protective autoantibodies: role in homeostasis, clinical importance, and therapeutic potential. *Arthritis Rheum.* 52, 2599–2606. doi: 10.1002/art.21252

Singh, V. K., Warren, R. P., Odell, J. D., Warren, W. L., and Cole, P. (1993). Antibodies to myelin basic protein in children with autistic behavior. *Brain Behav. Immun.* 7, 97–103. doi: 10.1006/brbi.1993.1010

Thomas, G. M., and Huganir, R. L. (2004). MAPK cascade signalling and synaptic plasticity. *Nat. Rev. Neurosci.* 5, 173–183. doi: 10.1038/nrn1346

Upadhya, D., Ogata, M., and Reneker, L. W. (2013). MAPK1 is required for establishing the pattern of cell proliferation and for cell survival during lens development. *Development* 140, 1573–1582. doi: 10.1242/dev.081042

Voineagu, I., Wang, X., Johnston, P., Lowe, J. K., Tian, Y., Horvath, S., et al. (2011). Transcriptomic analysis of autistic brain reveals convergent molecular pathology. *Nature* 474, 380–384. doi: 10.1038/nature10110

Wang, Z., Horowitz, H. W., Orlikowsky, T., Hahn, B. I., Trejo, V., Bapat, A. S., et al. (1999). Polyspecific self-reactive antibodies in individuals infected with human immunodeficiency virus facilitate T cell deletion and inhibit costimulatory accessory cell function. *J. Infect Dis.* 180, 1072–1079. doi: 10.1086/314974

Wang, Z., Qin, G., and Zhao, T. C. (2014). HDAC4: mechanism of regulation and biological functions. *Epigenomics* 6, 139–150. doi: 10.2217/epi.13.73

Wildbaum, G., Nahir, M. A., and Karin, N. (2003). Beneficial autoimmunity to proinflammatory mediators restrains the consequences of self-destructive immunity. *Immunity* 19, 679–688. doi: 10.1016/s1074-7613(03)00291-7

Williams, S. R., Aldred, M. A., Der Kaloustian, V. M., Halal, F., Gowans, G., McLeod, D. R., et al. (2010). Haploinsufficiency of HDAC4 causes brachydactyly mental retardation syndrome, with brachydactyly type E, developmental delays, and behavioral problems. *Am. J. Hum. Genet.* 87, 219–228. doi: 10.1016/j.ajhg.2010.07.011

Witte, T. (2008). IgM antibodies against dsDNA in SLE. *Clin. Rev. Allergy Immunol.* 34, 345–347. doi: 10.1007/s12016-007-8046-x

frontiers | Frontiers in Molecular Biosciences

TYPE Review
PUBLISHED 16 October 2023
DOI 10.3389/fmolb.2023.1216102

OPEN ACCESS

EDITED BY
Ashok Kumar,
All India Institute of Medical Sciences, Bhopal, India

REVIEWED BY
Renata Toscano Simões,
Faculdade Santa Casa BH, Brazil
Daria Chudakova,
Federal Biomedical Agency, Russia

*CORRESPONDENCE
Vadim Kumeiko,
vkumeiko@yandex.ru

RECEIVED 08 June 2023
ACCEPTED 04 September 2023
PUBLISHED 16 October 2023

CITATION
Penkova A, Kuziakova O, Gulaia V, Tiasto V, Goncharov NV, Lanskikh D, Zhmenia V, Baklanov I, Farniev V and Kumeiko V (2023), Comprehensive clinical assays for molecular diagnostics of gliomas: the current state and future prospects.
Front. Mol. Biosci. 10:1216102.
doi: 10.3389/fmolb.2023.1216102

Comprehensive clinical assays for molecular diagnostics of gliomas: the current state and future prospects

Alina Penkova[1], Olga Kuziakova[1], Valeriia Gulaia[1], Vladlena Tiasto[1], Nikolay V. Goncharov[1,2], Daria Lanskikh[1], Valeriia Zhmenia[1], Ivan Baklanov[1,2], Vladislav Farniev[1] and Vadim Kumeiko[1,2]*

[1]Institute of Life Sciences and Biomedicine, Far Eastern Federal University, Vladivostok, Russia, [2]A. V. Zhirmunsky National Scientific Center of Marine Biology, FEB RAS, Vladivostok, Russia

Glioma is one of the most intractable types of cancer, due to delayed diagnosis at advanced stages. The clinical symptoms of glioma are unclear and due to a variety of glioma subtypes, available low-invasive testing is not effective enough to be introduced into routine medical laboratory practice. Therefore, recent advances in the clinical diagnosis of glioma have focused on liquid biopsy approaches that utilize a wide range of techniques such as next-generation sequencing (NGS), droplet-digital polymerase chain reaction (ddPCR), and quantitative PCR (qPCR). Among all techniques, NGS is the most advantageous diagnostic method. Despite the rapid cheapening of NGS experiments, the cost of such diagnostics remains high. Moreover, high-throughput diagnostics are not appropriate for molecular profiling of gliomas since patients with gliomas exhibit only a few diagnostic markers. In this review, we highlighted all available assays for glioma diagnosing for main pathogenic glioma DNA sequence alterations. In the present study, we reviewed the possibility of integrating routine molecular methods into the diagnosis of gliomas. We state that the development of an affordable assay covering all glioma genetic aberrations could enable early detection and improve patient outcomes. Moreover, the development of such molecular diagnostic kits could potentially be a good alternative to expensive NGS-based approaches.

KEYWORDS

cancer molecular diagnostics, NGS panel, PCR, molecular markers of glioma, medical market

1 Introduction

Glioma is one of the most common forms of malignant tumors of the central nervous system that grow from glial cells in the brain and spinal cord. Glioma can diffusely infiltrate and affect surrounding brain tissue, which determines the many dramatic consequences for patients who have the disease. The manifestation of glioma is most characteristic for people aged over 50 years, is rare for those aged up to 30 years, and is distinctive for the male part of the population (Yang et al., 2022). The incidence of brain tumors per 100,000 people differs from region to region—the incidence is higher in Europe (5.5), North America (5.3), Australia/New Zealand (5.3), Western Asia (5.2), and Northern Africa (5.0). The lowest incidence is in South-Central Asia (1.8), sub-Saharan Africa (0.8), and Oceania excluding

Australia and New Zealand (0.5). However, these variations can be explained as true differences in the number of cases or an influence of the data collection method (Ostrom et al., 2015). Every year 80.000 primary cases of brain tumors are diagnosed in the United States with approximately 25% accounting for gliomas. The total number of glioblastoma cases annually is 12.000 (Mesfin and Al-Dhahir, 2022).

In 2016, the World Health Organization classified central nervous system tumors (CNS WHO 4) using molecular markers. Moreover, the updated WHO classification 2021 (WHO CNS 5) gives even higher priority to molecular diagnostics. As a result, new types of tumors were included in the classification. According to the latest WHO CNS5 2021, the prognosis and treatment of gliomas can vary significantly, depending on the glioma type (Louis et al., 2021). That is why it is necessary to develop universal diagnostic test systems to differentiate the diagnosis and select the appropriate treatment for gliomas. Nowadays, standard diagnostic methods that are based on histological examination remain not accurate due to the absence of a uniform evaluation method. Moreover, accurate histological classification can be hampered by insufficient or unrepresentative tissue samples (Coons et al., 1997; Nikiforova and Hamilton, 2011). To make a proper glioma molecular profiling, a modern laboratory infrastructure requires the establishment of several separated facilities, as its current classification requires fluorescence *in situ* hybridization (FISH) to detect large chromosomal aberrations, overexpression, loss-of-function analysis using immunohistochemistry (IHC), gene fusions examined by quantitative PCR (qPCR), single nucleotide substitutions/polymorphisms (SNPs) addressed by Sanger sequencing, and finally gene/promoter methylation studied by pyrosequencing. Only proper molecular characterization of glioma samples would result in better clinical management and realistic prognosis for the disease, as well as collecting representative data for researchers seeking the possible key to care.

Furthermore, one should not forget that there is a variety of glioma biomarkers that could be used for non-invasive diagnostics other than DNA sequence. The development of methods of diagnosis based on proteomics, lipidomics, and metabolomics was discussed recently (Gaca-Tabaszewska et al., 2022; Pienkowski et al., 2022). It was found that there is a metabolic difference in glioma with mutant or wild-type IDH1, with or without 1p/19q-codeletion (Goryńska et al., 2022). However, the use of such biomarkers has its limitations. They cannot be used to distinguish between the molecular subtypes of glioma or to monitor the genetic evolution of the tumor or its heterogeneity.

Since the clinical market still lacks a universal screening/diagnostic glioma assay based on one method and incorporating all molecular markers, we have reviewed all possible methods that could be applied to create such a diagnostic system. In this review, we list the commercially available NGS/PCR/FISH kits and describe their utility and suitability for glioma molecular profiling. Researchers can refer to this paper for developing screening or diagnostic glioma panels and clinicians can use it to choose a better available system.

In this study we are trying to summarize and review the existing methods for the diagnosis of glioma with the terms "*IDH1* molecular diagnostic," "glioma molecular diagnostic," "*1p/19q* molecular diagnostic," "(gene name)" PCR, "glioma NGS panel," and "(gene name)" NGS panel. Furthermore, we have highlighted new test systems that are used in clinical labs in different parts of the world and some promising methods. We analyzed the availability of next-generation sequencing (NGS) platforms globally by discovering national research centers in different countries.

In summary, despite NGS being the most sensitive and specific method to detect mutations in glioma and monitor its recurrence, there are many obstacles to making this technology universal in clinical diagnosis. Therefore, the requirement for a molecular diagnostic system could be solved by inventing one based on cost-effective widespread technology such as qPCR and ddPCR.

2 Gliomas molecular markers

Pathogenic DNA sequence alterations in glioma influence cell fate and the ability to evade standard treatment (Sharma, 2009). Adult-type diffuse gliomas are defined by the presence of pathogenic DNA sequence alterations in the isocytratedehidrogenese-1/2 gene (*IDH1/2*) (Sharma, 2009). They can be subclassified as either astrocytoma or oligodendroglioma by the presence of the tumor protein p53 (*TP53*) pathogenic alterations and alpha-thalassemia/intellectual disability X-linked syndrome (*ATRX*) loss in the first case, or by the revealing complete deletion of both of the short arm of chromosome 1 (*1p*) and the long arm of chromosome 19 (*19q*) (*1p/19q-co-deletion*) or telomerase reverse transcriptase (*TERT*) promoter (*p-TERT*) pathogenic DNA sequence alterations in the second (Figure 1). *p-TERT* pathogenic DNA sequence variants exclude the possibility of *ATRX* loss, as they both lead to the same consequence of telomerase activation within the tumor cell. Mutations in *IDH1/2* are associated with greater patient survival, however, *TP53* pathogenic variants occurring in *IDH*-mutant (*IDH1*-MT) tumors drop the survival rate significantly (Murnyak and Huang, 2021; Gulaia et al., 2022). The prognosis associated with *p-TERT* mutations is bivalent as patients carrying *IDH*-MT, *1p/19q*-codeletion, and promoter methylation of the O6-methylguanine-DNA methyltransferase (*p-MGMT*) favor in survival terms from the *p-TERT* co-occurrence (Arita et al., 2020; Vuong et al., 2020). Patients carrying wild-type (WT) *IDH* and mutant (MT) *p-TERT* have the poorest survival rate (Vuong et al., 2020).

Glioblastoma sequence alterations markers typically include *p-TERT* mutations, loss of cyclin-dependent kinase inhibitor 2A/B (*CDKN2A/B*) and phosphatase and tensin homolog (*PTEN*), amplification or truncation of epidermal growth factor receptor (*EGFR*), *TP53* pathogenic variants, as well as large chromosomal aberrations — 10 chromosome loss, 7 chromosome gain (*chr +7/-10*) (Figure 1).

According to the WHO 2021 classification, there is a wide range of molecular markers for the diagnosis of glioma that can be distinguished (Louis et al., 2021). Based on this classification we chose several DNA sequence alterations, such as *IDH1/2*, H3-3A, *ATRX*, *CDKN2A/B*, *1p/19q*-codeletion, *TERT*, MGMT, *EGFR*, that can be used as targets for diagnosis and evaluation of therapeutic response, as well as potential targets for successful treatment of glioma (Śledzińska et al., 2021; Miller, 2022; Yang et al., 2022).

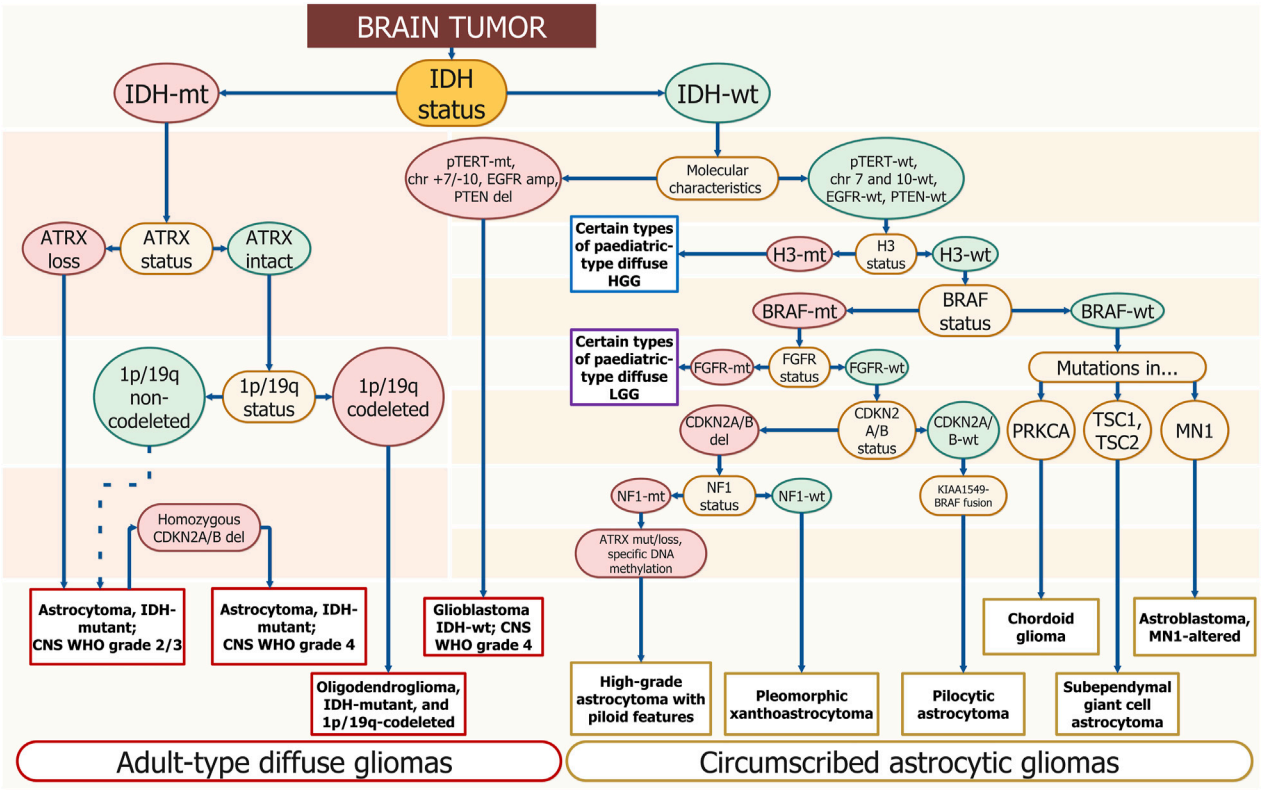

FIGURE 1
Schematic diagnostics path for diffuse glioma by gene/genomic alterations. The DNA sequence alterations are placed step by step for gradual diagnosis specification. The enquired DNA sequence alterations are annotated in yellow ellipses. Wild-type genotypes are placed in green ellipses and mutants are placed in red ones. The corresponding final diagnosis is placed in white rectangles; long ovals combine general diagnostic families — "Adult-type diffuse gliomas" and "Circumscribed astrocytic gliomas." Resembling algorithms were demonstrated in other studies but using different approaches and covering smaller amounts of diagnosis. The suggested scheme uses only molecular profiling to determine the type of tumor (Weller et al., 2021; Brat et al., 2022).

2.1 IDH

IDH catalyzes the oxidative decarboxylation of isocitrate to 2-oxoglutarate. *IDH1* is encoded by the *IDH1* gene and is a part of the isocitrate dehydrogenase isoenzymes, with the other two being *IDH2* and *IDH3*. *IDH1* protein is located in the cytoplasm, peroxisome, and endoplasmic reticulum, whereas *IDH2* is located in the mitochondrial matrix (Bleeker et al., 2010). The functions of *IDH1* and *IDH2* relate to cellular defense against oxidative stress, cellular metabolism in lipid synthesis, oxidative respiration, and oxygen-sensing signal transduction (Reitman and Yan, 2010).

IDH mutations represent an early event in gliomagenesis and may occur combined with TP53 pathogenic variants and *1p/19q* loss (Figure 1). Most *IDH1* DNA sequence alterations in gliomas occur as a single amino acid substitution with the hot spot at the arginine at codon 132 — *R132H* and cDNA coordinates—c.395G>A (Van Den Bent et al., 2016).

Low-grade gliomas (LGGs) with IDH-MT and *1p/19q*-codeletion have the most favorable clinical outcomes and are predictive of a positive response to alkylating chemotherapy (Weller et al., 2012). The combination of *IDH1* sequence variants and *p-MGMT* methylation status in malignant gliomas extends the survival rate more than either of the pathogenic variants (Śledzińska et al., 2021).

2.2 *1p/19q*-codeletion

1p/19q-codeletion is a chromosomal alteration that is described in oligodendrogliomas (Figure 1). It is a complete deletion of the short arm of chromosome 1 (*1p*) and the long arm of chromosome 19 (*19q*) (Brandner et al., 2022). Loss of *1p* and *19q* is an early event in oligodendroglioma tumorigenesis (Pinkham et al., 2015) and could be a result of an unbalanced whole-arm translocation between chromosomes 1 and 19 with the loss of the resulting hybrid chromosome (Griffin et al., 2006; Jenkins et al., 2006). Detection of *1p/19q* loss allows for identifying tumor type more accurately than routine histological evaluation (The Cancer Genome Atlas Research Network, 2015).

1p/19q-codeletion allows the prediction of the best treatment response within *IDH*-MT tumors to temozolomide (TMZ) (Kaloshi et al., 2007). *1p/19q*-codeletion is a predictor of prolonged survival in patients receiving PCV (combination of procarbazine, lomustine, and vincristine) chemotherapy followed by radiotherapy compared to radiotherapy alone (Weller et al., 2012).

2.3 H3-3A

H3.3 is a conserved histone protein, which is expressed outside the cell cycle and found at transcription start sites and in telomeric regions (Talbert and Henikoff, 2010; Armache et al., 2020). The *H3.3* histone is encoded by two different genes, *H3-3A* and *H3-3B*, which are located at *1q42.12* and *17q25.1,* respectively. Point mutations in *H3-3A* are associated with an epigenetic subgroup of high-grade gliomas (HGGs) and significantly worse outcomes (Khuong-Quang et al., 2012; Brat et al., 2018; Aldera and Govender, 2022).

The most common *H3-3A* pathogenic DNA sequence alteration is a single amino acid substitution at the positions *K27* or *G34* (Sturm et al., 2014; Lim et al., 2021). *H3 K27* alterations suppress the polycomb repressive complex 2 involved in epigenetic gene silencing; the tumorigenic mechanism of *H3.3 G34* has not yet been determined (Lim et al., 2021). Detection of an *H3 K27* or *H3 G34* mutation in a diffuse glioma, irrespective of histological grade, indicates high-grade biology (Korshunov et al., 2016; Brat et al., 2018).

Missense mutations in genes encoding histone *H3.3* isoforms occur in 50% of pediatric HGGs (Wang L. et al., 2022). A strong link was shown between *H3-3A* alterations and the age of HGG diagnosis. More often, the *H3-3A K27* mutation occurs in children and the *H3-3A* G34 mutation occurs in adolescents and young adults (Sturm et al., 2012; Wirsching and Weller, 2016). The WHO CNS5 classified tumors with alterations in *H3-3A* into a separate group, the pediatric type diffuse HGGs (Figure 1).

2.4 ATRX

ATRX is a gene located on the X-chromosome that encodes for an ATP-dependent helicase and provides nucleosome assembly, telomere maintenance, and histone *H3.3* deposition in transcriptionally silent genomic regions. There is a link between *ATRX* pathogenic DNA sequence alteration and a non-telomerase-dependent telomere lengthening mechanism called alternative lengthening of telomeres (ALT) promoting cellular immortality. Loss of *ATRX* results in genome instability, DNA damage, and global epigenetic dysregulation (Napier et al., 2015; Danussi et al., 2018). It is well known that loss of *ATRX* expression is significantly associated with *IDH*-MT (Ebrahimi et al., 2016; Chatterjee et al., 2018). However, the *ATRX* pathogenic variant is almost mutually exclusive with *1p/19q*-codeletion (Jiao et al., 2012) separating astrocytoma and oligodendroglioma (Figure 1).

It has been shown that *ATRX* pathogenic DNA sequence alteration correlates with glioma younger patient age, tumor histological features, and prognosis (Haase et al., 2018), as its mutations are frequently found in high-risk patients with a poor prognosis (van Gerven et al., 2022).

2.5 TERT

TERT is a rate-limiting enzyme for telomerase. DNA sequence alterations in *TERT* lead to the generation of two promoter-binding domains with the same structure, resulting in a multiplying of transcription activity. *TERT* reversely catalyzes telomerase production and maintains telomere ends by the addition of repeated sequences to the end of chromosomes (Huang et al., 2015).

The most common mutations are *C228T* (75%) and *C250T* (25%) (Mosrati et al., 2015). *TERT* promoter mutation generates identical 11 bp sequences that form a new binding site for the E26 transformation-specific transcription factor GA-binding protein, which selectively binds to the site and activates *TERT* (Chiba et al., 2017). Gliomas with the *p-TERT* mutation have shorter telomere lengths compared to gliomas without them, but at the same time expression of *TERT* is elevated (Arita et al., 2013; Heidenreich et al., 2015). *p-TERT* pathogenic variants are reported in 51% of all glioma types (Olympios et al., 2021) and together with *IDH*-WT constitute the most common genotype in glioblastoma (Figure 1) (Arita et al., 2016).

2.6 MGMT

MGMT is involved in cellular defense against mutagenesis and toxicity by cross-linking of double-stranded DNA by alkylating agents. The *MGMT* gene consists of five exons, and it is located on chromosome 10q26. The CpG-rich island covers a significant part of the *MGMT* promoter region including Exon 1. A minimal promoter and an enhancer region are located within the CpG island. In non-cancerous tissue, most CpG sites within the island are unmethylated. In tumors, the cytosines in CpG sites often carry a methyl group. These circumstances increase the affinity of proteins such as methyl-CpG-binding protein 2 and methyl-CpG-binding domain protein 2 to the DNA, which subsequently alters the chromatin structure and prevents binding of transcription factors leading to *MGMT* expression silencing (Nakagawachi et al., 2003).

Methylation of the gene promoter is associated with glioblastoma (Hosoya et al., 2022). Loss of chr 10q may also cause *MGMT* inactivation. Patients whose tumors show *p-MGMT* hypermethylation have longer overall survival (OS) from a combination of radiotherapy and TMZ (Stupp et al., 2005; Weller et al., 2012; Richard et al., 2020).

2.7 CDKN2A

The *CDKN2A* gene encodes multiple tumor suppressor 1 (*MTS1*) (Chen et al., 2021). The proteins that are encoded by *CDKN2A* (p16INK4A and p14ARF) and *CDKN2B* (p15INK4B) regulate the cell cycle and apoptosis and thus play the role of the tumor suppressor (Tesileanu et al., 2022). The homozygous *CDKN2A* deletion is a strongly unfavorable prognostic factor for survival outcomes of patients with *IDH*-MT or WT glioma (Lu et al., 2020; Varn et al., 2022). In diffuse *IDH*-MT astrocytoma, *CDKN2A* is a marker of the highest malignancy grade.

2.8 EGFR

EGFR (*HER1* or *ErbB1*) is a transmembrane tyrosine kinase located on chromosome band *7p12. EGFR* has a central role in cell division, migration, adhesion, differentiation, and apoptosis and is considered the most prominent oncogenes in *IDH*-WT

glioblastomas (Figure 1). There can be various types of genetic alterations of *EGFR* and include deletions, overexpression, and focal amplifications (Li et al., 2016).

The most common pathogenic DNA sequence alteration is amplification, when the *EGFR* gene locus is amplified to extremely high copy number levels (Turner et al., 2017; French et al., 2019), causing protein overexpression and subsequent secondary mutations, including intragenic deletions, point mutations, and gene fusions, which lead to intertumoral heterogeneity (Lee et al., 2006). One of the amplification mechanisms is the "double minute": extrachromosomal circular DNA fragments.

Another critical DNA sequence alteration is the deletion of 267 amino acids in the extracellular domain referred to as *EGFR*vIII (Gan et al., 2009) with subsequent loss of ability to bind canonical ligands. *EGFR*vIII is overexpressed in 50%–60% of *EGFR*-amplified glioblastomas (Heimberger et al., 2005) and constitutes a negative prognostic factor (Bonavia et al., 2012; Feng et al., 2014). *EGFR*vIII overexpression in the presence of *EGFR* amplification is the strongest indicator of a poor prognosis (Śledzińska et al., 2021).

2.9 PTEN

PTEN is a negative regulator of the phosphatidylinositol-3-kinase (*PI3K)/AKT* signaling pathway and is located on chromosome *10q23* (Chen et al., 2018). *PTEN* also promotes the stability and transcriptional activity of the *p53* in the nucleus and plays roles in chromosome stability, DNA repair, and cell cycle regulation. DNA sequence alterations in *PTEN* occur in dysplastic cerebellar gangliocytoma and glioblastoma (Benitez et al., 2017; Louis et al., 2021). *PTEN* loss is a marker of an unfavorable prognosis, induces macrophage M2 polarization, and promotes glioblastoma metastasis, growth, and angiogenesis (Ni et al., 2022).

2.10 Chromosome 7 gain and chromosome 10 Loss

chr +7/-10 are specific molecular alterations frequently observed in adult *IDH*-WT glioblastoma (Stichel et al., 2018; Vuong et al., 2019). This genetic aberration also leads to monoallelic loss of PTEN (*chr10*) or to EGFR amplification (*chr7*).

Thus, glioma markers vary from SNPs in metabolic enzymes to large chromosomal aberrations, with each marker determining the cancer cell fate decisions, as most mutually exclusive pathogenic variants determine histological glioma subtypes. Other molecular markers are also important for revealing tumor type. Following the WHO 2021 classification, a new diagnostic approach could be developed.

3 Existing methods for determining the glioma molecular profile

Molecular markers of gliomas include not only point mutations in genes *IDH1/2*, *TERT*, *BRAF* (B-Raf proto-oncogene, serine/threonine kinase), but also gene deletion (*CDKN2A/B*), fusion (*BRAF* with *KIAA1549*), amplification (*EGFR*), methylation (*MGMT*), and large chromosome deletion (*1p/19q* co-deletion) (Figure 2). There are "gold standard" methods for adult glioma molecular diagnostics, namely, immunohistochemistry (IHC), fluorescence *in situ* hybridization (FISH), and Sanger sequencing. In addition to these methods, there are alternative technologies that offer numerous potential benefits: microarray, variants of PCR, NGS, optical genome mapping, and MassArray.

3.1 Immunohistochemistry

Immunohistochemistry is an affordable and widely available technology that was first described by Coons et al., in 1941 (Jaiswal, 2016). This method provides diagnostic of the most significant molecular markers—*IDH1* R132H, *ATRX* loss, p53 aggregation in nuclei, *EGFR*vIII, *PARP1* expression, Ki-67, *EGFR* overexpression, *BRAF* V600E, *CDKN2A/B* loss, *CIC* and *FUBP1* loss (Figure 2), *MGMT* positive expression (not used in clinic because of difficult interpretation and variability (Sahara et al., 2021)), and *H3-3A* K27M (Tanboon et al., 2016). *1p/19q* co-deletion is not detectable by IHC but it is mutually exclusive to *ATRX* and *TP53* pathogenic DNA sequence alterations in *IDH1*-MT gliomas (The Cancer Genome Atlas Research Network, 2015). Furthermore, there are new perspective glioma markers found recently using IHC—*BCL7A* (Liu et al., 2021) and *SRSF1* (Broggi et al., 2021) correlate with favorable prognosis, whereas *TXNDC11* (Peng et al., 2021) predicts unfavorable prognosis.

According to different studies, the IHC sensitivity and specificity for detecting various markers are close to 80%–100% (Broggi et al., 2021). The utility of IHC in detecting *IDH* DNA sequence alterations was broadened with the new antibodies to find *IDH1* R132S (SMab-1), *IDH1* R132G (GMab-1), *IDH2* R172K, *IDH2* R172M, *IDH2* R172W (KMab-1, MMab-1, WMab-1), and multispecific *IDH1/2* monoclonal antibody—MsMab-1 detecting *IDH1* R132 H/S/G and *IDH2* R172M proteins (Babakoohi et al., 2017).

3.2 FISH

FISH is used for target hybridization of nuclear DNA to detect alterations and gene rearrangements in paraffin-embedded tissues. This technique allows pathologists to assess such significant biomarkers as *1p/19q*-codeletion, *EGFR* amplification, *PTEN* deletion, *CDKN2A/2B* deletion (Figure 2), *BRAF* V600E, and *NTRK* fusions (Horbinski et al., 2011). There is a new FISH application, G-FISH (graphene oxide quenching-based method), that is an original technique for the detection of various RNAs (lncRNAs, miRNAs, and mRNAs) in formalin-fixed paraffin-embedded (FFPE) tissue, frozen tissue, or living cells (Hwang et al., 2019). It is used for assessing miR-21 expression as a glioblastoma prognostic marker. FISH has become a routine procedure in testing *1p/19q* codeletion because it allows analysis of paraffin-embedded tissues, does not require references and controls, and is easy to interpret. The main disadvantages include the price of probes and the necessity to establish a special dark lab. The alternative method, namely, chromogenic *in situ* hybridization

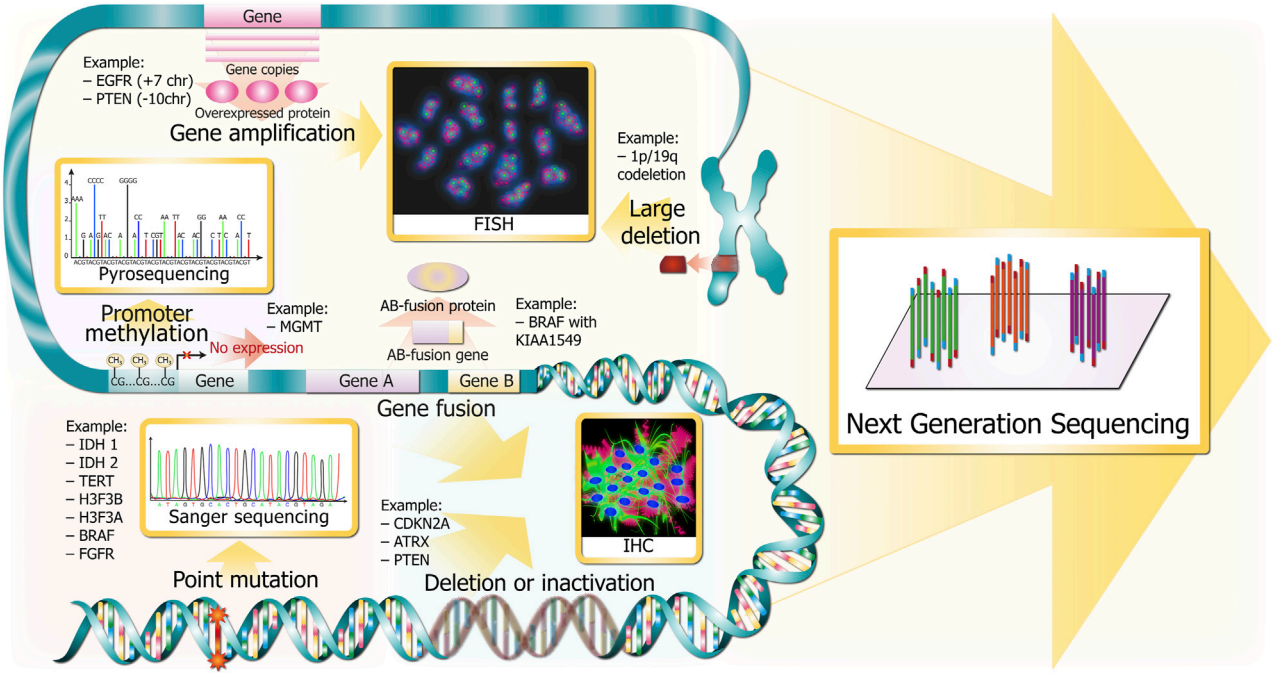

FIGURE 2
Glioma DNA sequence alterations and respective gold standards for clinical detection. Alterations are depicted in red and pink colors throughout the DNA molecule at several resolutions (from chromosomes in the upper part to single bases in the bottom). The methods for revealing the corresponding marker glioma DNA sequence alterations are depicted in golden squares and are linked with wide golden arrows.

(CISH), was proposed in 2013 (Lass et al., 2013) for the detection of *1p/19q* loss. According to the authors, CISH is a highly sensitive and low-cost method requiring merely a light microscope. However, data on the widespread usage of CISH in medical laboratories were not found. FISH could be used only for six markers and does not allow detection of the *IDH1* R132H pathogenic variant, which is essential in diagnostics. As a result, FISH must be used in common with IHC, NGS, or other methods.

There are cutting-edge imaging genomics methods referred to as OligoSTORM and OligoDNA-PAINT (Beliveau et al., 2017). Stochastic Optical Reconstruction Microscopy (STORM) and DNA-based Point Accumulation for Imaging in Nanoscale Topography (DNA-PAINT) enable various strategies of specific hybridization of fluorescent probes with oligos, which are used for switching individual fluorophores between dark and fluorescent states, or binding and unbinding individual labeled molecules to avoid overlapping images of single molecules. The usage of these technologies allows the resolution below 10 nm. This feature could be used in the diagnosis of glioma in creating an assay for *1p/19q*-codeletion, *chr +7/-10*, and *9p21* deletion in one reaction.

3.3 Sanger sequencing

Sanger sequencing was the first method to determine the DNA sequence. It has been the "gold standard" since 1977. Sanger sequencing could be used to spot various types of DNA sequence alterations, for example, SNPs and small indels. Despite the development of new sequencing technologies, such as next-generation sequencing (NGS), the Sanger method is still necessary as it produces DNA reads >500 bp with an accuracy of approximately 99.99% (Shendure and Ji, 2008). For gliomas, it is employed for the detection of important missense mutations such as *IDH1* R132, *IDH2* R172, *BRAF* V600, *TP53* R175/R248/R273, etc., (Figure 2).

3.4 Microarray

Microarray is a method that allows measuring gene expression from the complete genome in a single experiment. This technology is based on the specific hybridization of sample mRNA linked to fluorescent dyes with the spotted DNA sequences on the microarray. The intensity of fluorescence correlates with a gene expression and could be detected by a special laser (Tao et al., 2017). The variation of this technology is a comparative genomic hybridization (array-CGH), which enables the analysis of chromosomal copy-number variations (CNVs) (Ruano et al., 2010). Microarray could be used to predict the glioma's response to therapy, patient survival, and treatment outcomes according to the determination of upregulated and downregulated genes (Tao et al., 2017). There is a panel for glioma molecular diagnostics that detects DNA sequence alterations to find the cancer-associated copy-neutral loss of heterozygosity (Oncology Microarray - Targeted Gene and Region Panel, 2023). Chromosome microarray provides detection of 1p/19q-co-deletions, *chr +7/-10*, deletion of *CDKN2A/2B*, *PTEN*, and loss of heterozygosity (LOH) of *17q* (Buckner et al., 2017).

3.5 PCR or qPCR

3.5.1 High resolution melting

High resolution melting (HRM) is based on the melting temperature difference of small DNA fragments following PCR and is used to detect SNPs. There have been several applications for glioma molecular diagnosis, for instance, the ones based on the temperature difference between WT and MT fragments: IDH1/2 and *BRAF* diagnostics (Hatae et al., 2016), *TP53* assessment (Saito et al., 2021), *H3-3A*, and *H3-3B* (Yokogami et al., 2018). Other approaches increase the amount of MT allele and combine conventional PCR with COLD-PCR (co-amplification on low denaturation temperatures) for IDH1 R132H (Boisselier et al., 2010), as they are based on the statement that Tm of MT-WT heterodimers would be lower than Tm of MT-MT or WT-WT homodimers. There is a methylation-sensitive high resolution melting (MS-HRM) that is used for *p-MGMT* methylation analysis (Switzeny et al., 2016; Majchrzak-Celińska et al., 2020). However, this method has not been widely used both in clinical and scientific research since it does not allow determination of homo- or heterozygosity and is difficult to interpret.

3.5.2 Allele-specific qPCR

Allele-specific qPCR is actively used in clinical oncological diagnostics to assess common pathogenic variants, especially SNPs, in a variety of cancers. It is more sensitive and rather faster than Sanger sequencing. A wide range of allele-specific qPCR approaches are known, including probe-based chemistries (TaqMan, Scorpions, Molecular Beacons), modifications of primers and probes (locked nucleic acids (LNA), and minor groove binders (MGB). TaqMan is the most popular qPCR chemistry. This method uses specific hybridization of MT and WT probes with complementary sequences on target DNA. Each oligonucleotide probe has a fluorophore and a quencher on its ends and binds either to MT or WT DNA. During PCR, a polymerase destroys the probe and releases fluorophore and quencher, and since fluorophore is distanced from quencher, fluorescence can be detected. Allele-specific qPCR with fluorescent TaqMan probes was successfully established for mutations in *IDH1/2* (Catteau et al., 2014), *H3-3A* (Zhang et al., 2016), and other point mutations.

LNA base is a type of nucleic acid analog that contains a 2′-O, 4′-C methylene bridge. This modification restricts the flexibility of the ribofuranose ring, which significantly increases the primer specificity for the target mutation. Such primer modification is well-used in TERT promoter diagnostics (Diplas et al., 2019).

A comparative quantitative PCR (CQ-PCR) was developed based on quantitative analysis of gene copies from *1p* and *19q* relative to reference genes from unaltered chromosomes (Chaturbedi et al., 2012).

3.5.3 Peptide nucleic acid-mediated PCR technologies

Peptide nucleic acid-mediated PCR technologies (PNA) is an artificial DNA-oligonucleotide analog, where the phosphate-ribose backbone is replaced with a peptide-like amide backbone (N-(2-aminoethyl)glycine), which leads to increased stability of binding to DNA. Several variations of PNA application, e.g., PNAClamp, PANA RealTyper, PANA qPCR, and PANAMutyper, are united by a PNA probe hybridizing to complementary DNA sequence and precluding polymerase elongation. PNAClamp is used to specifically block the amplification of WT DNA and increase the synthesis of MT DNA. It provides accurate detection of 1% MT DNA in 50 ng of tissue and is applied to detect DNA sequence alterations in *BRAF*, *IDH1*, *IDH2*, *PIK3CA*, and *TERT* in tissue biopsy (Choi and PANAGENE, 2023). PANA RealTyper probe contains fluorophore and quencher, so the fluorescence signal is detected when the probe is annealed on target DNA, but if the PNA-DNA complex denatures the signal disappears. This PANA RealTyper is applied in the same manner as HRM analysis and is similar to PANA qPCR, whereas PANAMutyper combines both of the previously described techniques. PNA oligos are employed in diagnostic kits to assess glioma-associated pathogenic variants in liquid biopsy.

3.5.4 Droplet digital PCR

Droplet digital PCR (ddPCR) is now actively used to reveal pathogenic variants in samples with very low concentrations of tumor DNA, as it allows to determine as low as 2% of MT DNA. As profiling tumor tissues from the brain could be challenging because of tumor location and small sample size, currently, researchers are trying to adapt the use of cell-free tumor DNA (ctDNA) from cerebrospinal fluid (CSF) and plasma for revealing glioma molecular markers. Taking into account that the blood-brain barrier restricts the amount of ctDNA and generally brain tumors do not grow much in size because of space limits, the identification of glioma marker DNA sequence alterations in patient plasma is technically difficult (Mair and Mouliere, 2022). CSF is a more reliable ctDNA source for glioma patients, however, a lumbar puncture could be deleterious to patients and cannot be applied frequently. The sensitivity of ddPCR detection of *p-TERT* MT in patient plasma by ddPCR was 62.5% (Muralidharan et al., 2021). The technical ddPCR variation—BEAming comprises emulsion PCR and the flow cytometry to separate WT and MT DNA as different populations. However, the sensitivity of detecting ctDNA in glioma patients was less than 10% (Bettegowda et al., 2014).

3.6 NGS

NGS is a fast-growing cutting-edge methodology employing little amount of sample and is applicable to detect different types of DNA sequence alterations: SNPs, small indels, amplifications, big regions of LOH, and CNAs (Figure 2). NGS could be used for all essential pathogenic variants in glioma, and it is a more sensitive and specific method than IHC (Śledzińska et al., 2022). Plenty of NGS panels have been developed for glioma molecular diagnosis: glio-DNA panel (Tirrò et al., 2022) and GliomaSCAN (Shin et al., 2020). However, there is no CE-IVD or FDA-approved NGS panel, and not every hospital is able to establish NGS facilities due to its cost, unavailability of necessary specialists, and difficulties in providing consumables.

There are several types of NGS, specifically, pyrosequencing, sequencing by ligation, sequencing by synthesis, nanopore technology, and DNBseq.

3.6.1 Pyrosequencing

Pyrosequencing platform Roche 454 was the first NGS method. This platform uses emulsion PCR with the subsequent addition of a purified nucleotide, which incorporates into the DNA strand and results in the release of pyrophosphates. Then the series of enzyme reactions with pyrophosphate produces a flash of light (Jessri and Farah, 2014). The main advantages are long reads (approximately 700 bp), short run time, and high accuracy in homopolymer regions. This technology could be used to detect MGMT promoter methylation but is less effective than PCR-based alternatives due to its cost (Switzeny et al., 2016).

3.6.2 Sequencing by ligation (SBL)

SBL is based on the specific hybridization of known fluorescent oligonucleotides with target sequences. This method is good for detecting SNP and gross chromosome abnormalities (Slatko et al., 2018). Despite its high specificity and low rate of errors, it is very difficult to analyze the great amount of data (over 180 GB) and hence very rarely used for commercial platforms (Life TechnologiesTM SOLiD™ 5500XL) (Jessri and Farah, 2014).

3.6.3 Sequencing by synthesis

Sequencing by synthesis (SBS) is the most common NGS method for sequencing without using dideoxy terminators. Ion Torrent platforms use emulsion PCR and identification of nucleotide incorporated by the released H^+ ion by detecting the pH change. Illumina platforms utilize bridge PCR with fluorescent nucleotides incorporated in the growing DNA strand, and the optical detector catches fluorescent signals. After fluorophores are removed, the next nucleotides can be joined. However, it produces short reads with a high error rate (Jessri and Farah, 2014).

3.6.4 Nanopore

Nanopore technology is considered third-generation sequencing, as it enables real-time analysis of long strands. It measures differences between electronic changes in a special membrane, which depends on the nucleotide going through the nanopore. It does not require PCR amplification before and has a very high speed (400 bp per second) (How nanopore sequencing works, 2023). The downbreak is the comparatively low read accuracy as it produces ultra-long reads, of over 20kbp (Jain et al., 2018), and thus cannot be used for SNV detection (Kono and Arakawa, 2019).

3.6.5 DNBSeq

DNBSeq is a Chinese sequencing technology. The library preparation ligates nucleic acids to make a single-stranded DNA circle, which is replicated to produce DNA nanoball read by various sequencing platforms including BGISEQ-500 (Fehlmann et al., 2016), DNBSEQ-G400, and DNBSEQ-T7. This method is used for SNV and small indel detection. Although it produces short reads (around 50 bp), it shows high-quality results and deep coverage (Jeon et al., 2021).

3.6.6 CAPP-seq

Cancer Personalized Profiling by Deep Sequencing (CAPP-seq) is a personalized method for monitoring the tumor evolution in a patient without invasive procedures. In the first step, the molecular profile of the tumor is determined in tissue using NGS producing a unique specific library. The next step for monitoring disease relapse is to collect blood from the patient to search for circulating tumor DNA (ctDNA). CAPP-seq uses oligonucleotide probes with biotin specific to frequently mutated marker genes in a tumor. After hybridization with these probes, target DNA is cached by streptavidin sticking to biotin. However, CAPP-seq is unlikely to be applied for monitoring patients with glioma, as ctDNA is detected at extremely low concentrations in the blood due to the blood-CSF barrier (Newman et al., 2014; 2016).

3.7 Optical genome mapping

Optical genome mapping (OGM) is a new method for high-resolution detection of genomic structural variants, including loss, multiplication, rearrangement, and translocation of large genomic regions (Dremsek et al., 2021). DNA is labeled with the unique barcodes detected while DNA is moving through the nanochannel. Subsequently, the results are compared with the reference barcode pattern. OGM analyzes linearized DNA strands 200 kbp in length and is applicable to create maps covering the whole chromosome arm to detect indels larger than 500 bp, translocations larger than 50 kb, inversions larger than 30 kbp, duplications larger than 30 kb, and CNVs larger than 500 kb (Bionano, 2023). The limitations relate to the detection of aneuploidies, Robertsonian translocations, and other whole-arm translocations involving centromeres (Dremsek et al., 2021). OGM could become a prospective alternative to FISH.

3.8 Padlock probe-based amplification

A padlock probe is a linear oligonucleotide with two target complementary arms joined together by template-dependent ligation. After the ligation, there is a rolling circle amplification step leading to the formation of 1-μm-sized coiled structures. These structures could be visualized by FISH. This molecular analysis is performed directly in fixed cells or tissue (Nilsson et al., 1994; Larsson et al., 2004). There are several modifications of the padlock probe, for example, gap-fill ligation to assess SNPs *in situ* (Mignardi et al., 2015). In this method, target complementary arms form a 6-nucleotide gap. Then MT and WT probes are hybridized with the gap, but one of these two probes (e.g., WT) blocks rolling-circle amplification (RCA). As a result, only one variant (e.g., MT) is amplified. Padlock probes can be adapted for diagnostic fusion mutations (Chen et al., 2022). The base-specific *in situ* sequencing (BaSISS) method utilizes padlock probes with unique barcodes (Lomakin et al., 2022). The development of this methodology fosters multiplexing detection of SNP, CNA, and expression analysis, which can be employed in clinical diagnostics.

3.9 MassARRAY

MassARRAY genotyping is a simple, high-quality, cost-effective, and comparatively fast (~8.5 h) method providing simultaneous detection of SNPs, CNVs, indels, and methylation analysis. This technology is based on matrix-assisted laser desorption/ionization-

time of flight (MALDI-TOF) mass spectrometry. The procedure includes DNA extraction, PCR, and single base extension reaction with primer, which anneals directly before the hot spot polymorphic base and 'terminator' nucleotide (Ellis and Ong, 2017). After that, the mixture is transferred to the SpectroCHIP, which is placed in the MassARRAY mass spectrometer (The MassARRAY System from Agena Bioscience, 2023). The determination of the polymorphic base is carried out according to the difference in molecular weight of each nucleotide. This method allows accurate detection of up to 40 SNPs in one tube and could be performed in 24-, 96- or 384-well plates (The MassARRAY System from Agena Bioscience, 2023). The MassARRAY System is actively used both in clinical and scientific research because it does not require fluorescent detection or special rooms, can acquire many different analyses at one time, and the price of each sample is very low. There are developed panels for glioma diagnosis incorporating *1p/19q*-codeletion, *IDH1* R132, *IDH2* R172, *TERT* G228A, and G250A DNA sequence alterations (Pesenti et al., 2017). High accuracy, effectiveness, low cost, and speed make this method excellent for use in clinical laboratories. However, for now, the MassArray panel is not clinically approved.

All in all, there are a wide variety of methods for detecting glioma molecular markers because of the latter's high genetic heterogeneity and cellular plasticity. Currently, great expectations are invested in the NGS-based methods, which allow for all pathogenic variants to be covered by one technology and possess the ability to screen dozens to hundreds of patients simultaneously. Meanwhile, there are two techniques, namely, MassARRAY and ddPCR, that promise to revolutionize the glioma molecular profile. MassARRAY even exceeds the capacity of DNA sequence alteration detection by covering the possibility to enquire about the MGMT-promoter methylation along with SNPs and CNVs in a single experiment. On the other hand, ddPCR or qPCR could be used as a sensitive method to cover the genes related to therapeutic resistance/response in gliomas—*IDH1* R132H, *IDH2* R172K, *EGFR* and *MGMT* expression. Thus, we suggest these two alternatives to NGS-based techniques.

4 The market for glioma molecular profile

The biopharmaceutical companies provide their solutions with kits for researchers (research use only—RUO) and clinicians with CE-IVD certificate (European approval), FDA (United States), or National Medical Product Administration (NMPA, China) approval. Here, we summarize commercial offers of RUO and clinical kits available for glioma molecular profiling worldwide.

4.1 PCR kits

The easiest way to detect glioma marker DNA sequence alterations is to use a wide variety of PCR strategies discussed above. With PCR, we focused on the marker glioma SNP detection illustrated in Figure 1. We discovered that eight companies offer qPCR kits to identify DNA sequence alterations in *IDH1*, *IDH2*, *TERT*, *EGFR*, *BRAF*, *PIK3CA*, and methylation of *MGMT* promoter and *EGFR*vIII; two companies provide ddPCR kits for the determination of *IDH1* R132H and *IDH2* R172K mutations, *EGFR* amplification, *CDKN2A* loss of heterozygosity, and *TERT* CNV; one company promotes PNA PCR technology to detect DNA sequence alterations in *BRAF*, *IDH1*, *IDH2*, *PIK3CA*, and *TERT*.

The determination of *IDH1/2* mutations is offered by the majority of companies and most of their kits are clinically approved either by the FDA: Abbott (United States) (RealTime IDH1 | Abbott Molecular, 2023; RealTime IDH2 | Abbott Molecular, 2023) or CE-IVD: PANAGENE (South Korea) (Choi and PANAGENE, 2023), Genetron (China) (CANCER DIAGNOSTICS, 2023), EntroGen (United States) (IDH1/2 Mutation Detection Kit | EntroGen, Inc, 2023), Qiagen (Germany) (therascreen IDH1/2 RGQ PCR Kit CE, 2023). NeoGenomics (United States) promotes a kit for RUO (IDH1/IDH2 Mutation Analysis by PCR | NeoGenomics Laboratories, 2023). All companies except Abbott allow the use of their kits for glioma molecular diagnostics with DNA extracted from FEPE tissue. According to their guidelines, qPCR kits can catch as low as 1% mutant DNA in mixed samples.

Some companies, such as PANAGENE (South Korea) (Choi and PANAGENE, 2023), Genetron (China) (CANCER DIAGNOSTICS | GENETRON, 2023), JBS Science (United States) (TERT promoter −124 mutation Quantification kit – JBS Science, 2023), market kits to detect *hTERT* promoter DNA sequence alterations C228T and C250T. PANAGENE has a CE certificate and recommends its kit for CNS tumors diagnostics, Genetron allows the use of its kit for glioma profiling and has CE-IVD, and JBL Science offers a kit to identify C228T for RUO and it could be used only on Roche's LightCycler™.

Additionally, Genetron (China) provides an 8-gene kit comprising DNA sequence alterations in *EGFR*, *BRAF*, and *PIK3CA* (CANCER DIAGNOSTICS | GENETRON, 2023) approved for medical use by the National Medical Products Administration ("NMPA") in China. PANAGENE (South Korea) promotes a *PIK3CA* mutation detection kit that has CE-IVD. EntroGen (United States) offers a kit to detect *EGFR*vIII amplification (EGFRvIII Detection Kit, 2023).

The methylation of *MGMT* promoter analysis is designed by three companies only: EntroGen (United States) (MGMT Methylation Detection Kit | EntroGen, Inc, 2023), NeoGenomics (United States) (MGMT Promoter Methylation Analysis | NeoGenomics Laboratories, 2023), and Genmark Sağlık Ürünleri (Turkey) (geneMAP™ MGMT Methylation Analysis Kit MGM-RT50, 2023). EntroGen and Genmark kits are CE-approved and the NeoGenomics kit is New York-approved. EntroGen (United States) declared the ability of its kit to detect as low as 6.25% methylated DNA in mixed samples.

Despite neither of the ddPCR kits being clinically approved, Bio-Rad Laboratories (United States) and IdSolutions (France) offer very sensitive kits for revealing *IDH1* R132H, *IDH2* R172K, and *TERT*-promoter mutations. Bio-Rad also detects *EGFR* amplification and *CDKN2A* loss of heterozygosity. This technology is more sensitive than Sanger sequencing (Wolter et al., 2022) and could facilitate the development of liquid biopsy for glioma diagnostics. With their declared high sensitivity (<0.1%), these kits could be applied for DNA extracted from FFPE tissue and ctDNA extracted from plasma.

TABLE 1 FISH kits for the diagnosis of gliomas.

Regions important for the diagnosis of glioma	CytoCell	Abbott molecular	ZytoVision	Abnova
1p19q codeletion	1p36.32/1q25.2	1q25.2/1p36.3	1p36/1q25	1q43-q44/1q21.3 19q13.13/19q13.11
	19p13.2/19q13.33	19q13.3/19p13.2	19q13/19p13	
EGFR amplification	7p11.2	7p11.2	7p11.2	7p12
	7p11.1-q11.1	7p11.1-q11.1		
PTEN 10q	10q23.2-10q23.3	10p23	10p23.2-q23.31	10q23/10p11.22
CDKN2A/B deletion	CDKN2A deletion 9p21.3	CDK2A deletion 9p21	CDKN2A deletion 9p21.3	-
	9q12			
BRAF V600E	—	—	—	BRAF V600
BRAF fusion	KIAA1549/BRAF 7q35	—	—	KIAA1549/BRAF 7q34
TP53	—	17p13.1 CNV	17p13.1	17p13.1/9p21/18q21.2
Medical diagnostic license	CE-IVD, RUO	CE-IVD	CE-IVD	RUO

In summary, nowadays there is no PCR-based kit that would provide detection of enough pathological markers in glioma. However, there are CE-approved kits to assess mutations in *IDH1/2*, *p-TERT*, methylation of *p-MGMT*, and amplification of *EGFR*vIII. Although the most advantageous kits for glioma are based on ddPCR due to their high sensitivity, they are not clinically approved and are the most expensive as they require a special PCR cycler. Therefore, companies offer solutions utilizing conventional qPCR, which is cost-effective and could combine different essential diagnostic markers.

4.2 FISH

There are three main manufacturers in the FISH probe market, namely, Cytocell (United Kingdom), Abbot Molecular (United States), and ZytoVision (German), which provide clinically approved FISH kits for glioma profiling (Table 1). There is a Taiwan company, Abnowa, which produces FISH probes for RUO, however, it also uses mutation-specific FISH technology to detect DNA sequence alterations (mutaFISH™ (mutaFISH™ - Technologies - Support - Abnova, 2023)).

For glioma molecular profiling all these companies offer probes for detection of *1p/19q*-codeletion, *EGFR* amplification, and *PTEN*. Despite missing probes for the detection of *CDKN2A* deletion, Abnova developed *BRAF* V600E diagnostic probes. *BRAF* fusion is identified with probes from Cytocell and Abnova. The determination of *TP53* CNV is provided by Abbot Molecular, ZytoVision, and Abnova.

FISH is a gold standard for the diagnosis of chromosomal aberrations. Despite it being essential in the detection of *1p/19q*-codeletion and *chr +7/-10* in glioma, FISH is expensive, labor-consuming, and limited, making it difficult to create a cost-effective FISH kit for profiling different levels of DNA sequence alterations other than chromosomal rearrangements.

4.3 NGS panels

There are no targeted FDA or CE-IVD-certified NGS panels for patients with glioma. This could be due to the low incidence of glioma in the general population and the impossibility of non-invasive molecular diagnostics because of the difficulties in detecting ctDNA in patients with glioma unless it is at an advanced stage. However, the multi-cancer panels offered in the medical field could detect a part of the genes needed for diagnosing gliomas. Meanwhile, there are several RUO kits featured for the profiling of patients with glioma. An additional branch of the market for glioma molecular characterization is devoted to clinically certified diagnostic laboratories providing glioma DNA sequence alterations detection by NGS as a medical service. However, we were not able to comprehensively describe the latter, because the laboratories merely address the information related to patient sample handling and do not describe either the genes covered by the service or the platform used for NGS.

There are several FDA-approved pan-cancer NGS panels, namely, MSK-IMPACT (Memorial Sloan Kettering Cancer Center, New York, United States), FoundationOne Liquid CDx (Foundation Medicine, Cambridge, United States), and Guardant360 CDx (Guardant Health, Palo Alto, United States), with the two latter approved for liquid biopsy. The panels designed for ctDNA detection use barcode enrichment to identify rare DNA sequence alterations. Both panels can detect a rare pathogenic variant with the variant allele frequency (VAF) ranging from 0.40% to 0.82% and a probability of 95% (Vasseur et al., 2022). The panels have additional benefits by detecting CNVs important for the diagnosis of glioma (Jonsson et al., 2019; Sharaf et al., 2021) except for Guradant360 CDx. However, none of the multicancer panels incorporated *MGMT*-promoter methylation (Table 2). MSK-Impact can cover 468 genes, FoundationOne CDx assay can cover 324 genes, and Guardant360 CDx can cover 360 genes. The comparison of the panel performances revealed equal quality in

TABLE 2 Pan-cancer NGS panels that are available in the clinical and research markets with possible implementation for glioma molecular profiling.

Genes important for glioma molecular profiling	OncoDEEP from OncoDNA	Oncomine pan-cancer cell-free assay	Tempus xT	MSK-IMPACT	FoundationOne® liquid CDx	Guardant360 CDx	OncoScreen panel from burning Rock Dx	PGDx elio plasma complete
IDH1/2, BRAF, EGFR, KIT, TP53, CDKN2A, PTEN	+	+	+	+	+	+	+	+
p-TERT	-	-	+	+	+	+	-	+
H3-3A (H3F3A)	+	-	+	+	+	-	-	+
HIST1H3B	+	-	+	+	-	-	-	+
FUBP1	+	-	+	+	+	-	-	+
CIC, NOTCH1	+	-	+	+	+	-	+	+
CDKN2B, ATRX	+	+	-	+	+	-	+	+
1p/19q-codel	-	-	+	+	+	-	-	-
+7chr/-10chr	-	-	-	+	-	-	-	-
p-MGMT methylation	-	-	-	-	-	-	-	-
Platform	Illumina	Ion Torrent S5	Illumina HiSeq, NovaSeq 6000	Illumina HiSeq 2500	Illumina NovaSeq 6000	Illumina NextSeq 550	Illumina NextSeq 500	Illumina NextSeq
Biological material	FFPE tissue	ctDNA	FFPE tissue	FFPE tissue, ctDNA	FFPE tissue, ctDNA	ctDNA	FFPE tissue	ctDNA
Medical diagnostic license	CE-IVD	RUO	CE-IVD	FDA	FDA	FDA	CE-IVD	RUO

identifying mutational burden (Bevins et al., 2020), although the enrichment strategy is different. FoundationOne Liquid CDx and Guardant360 CDx use hybridization and capture-based enrichment utilizing oligonucleotides complementary to genes of interest, that serve as baits to capture hybridizing DNA fragments (Gaudin and Desnues, 2018). MSK-IMPACT exploits capturing beds with oligos hybridizing with target DNA fragments and amplified by ligation-mediated PCR.

Personal Genome Diagnostics (PGDx; Baltimore, United States) and NuProbe (Houston, United States) offer liquid biopsy pan-cancer panels for RUO. Both panels include important genes for glioma, however, PGDx elioTM plasma for solid tumors is intended for 500+ genes (Valkenburg et al., 2022) and can detect most of the glioma markers including *p-TERT* DNA sequence alterations (Alnajar et al., 2022) (Table 2). The NuProbe Pan-Cancer NGS panel covers 61 genes (NuProbe Launches Liquid Biopsy Pan-Cancer NGS Panel, 2023) and uses the special enrichment technique referred to as quantitative blocker displacement amplification (QBDA) for detecting rare genetic variants below 0.01% VAF (Dai et al., 2021). This feature could be potentially used for glioma ctDNA profiling. Due to the enrichment technique, the panel can be run with low-coverage sequencers, such as Illumina MiSeq and MiniSeq, which makes it cost-effective compared to other panels of the same size.

Tempus (Chicago, United States) offers a CE-certified NGS panel, Tempus xT, to search for DNA sequence alterations in 648 genes, including almost all important genes in glioma (Table 2), and could be used to detect *1p/19q*-codeletion (Beaubier et al., 2019) in patient tumor material (FFPE tissues). Another option is the clinical Tempus xF panel that is to be used for molecular profiling of ctDNA and covers 105 genes (Tempus xF - Clinical test - NIH Genetic Testing Registry GTR - NCBI, 2023) including glioma marker DNA sequence alterations except of ATRX, CIC, FUBP1, and TERT-promoter (Genomic Profiling - Tempus, 2023).

Illumina (San Diego, United States) sells TruSight Oncology 500/500 ctDNA RUO panel investigating 523 genes in tumor specimen or ctDNA (Wei et al., 2022) covering all glioma marker SNPs including p-TERT DNA sequence alterations (Kang et al., 2022). The possibility of identifying CNVs, such as *1p/19q* codeletion, for the diagnosis of glioma was proven only for the TruSight Tumor 170 panel (Na et al., 2019), which, however, lacks the important glioma diagnostic genes *ATRX*, *CIC*, *FUBP1*, and *CDKN2B*. EU market trades TruSight Oncology Comprehensive

examining 517 genes under CE-IVD certificate (TruSight Oncology Comprehensive EU, 2023). Myriad Genetics (Salt Lake City, United States) features the RUO NGS panel, Precise™ Tumor, for solid tumor characterization covering 523 genes by DNA sequencing and with most glioma-related SNPs, but missing *p-TERT* DNA sequence alterations (Precise™ Tumor | Molecular Profile Testing | Myriad Genetics, 2023).

Thermo Fisher Scientific (Waltham, United States) offers several NGS kits for cancer diagnostics—Oncomine Focus with 52 genes for solid tumors (Oncomine Focus Assay | Thermo Fisher Scientific, 2023), Oncomine Comprehensive Assay v3 with 161 genes, and Oncomine Comprehensive Assay Plus including 501 genes (Vestergaard et al., 2021), with the latter having the possibility to identify 1p/19q-codeletion (Ali et al., 2023). Additionally, the Oncomine Pan-Cancer Cell-Free Assay designed for ctDNA profiling detected 67% of DNA sequence alterations found in the corresponding primary tumor in CSF ctDNA from patients with CNS malignancies (Shah et al., 2021). Another option is the Ion AmpliSeq Cancer Hotspot panel, an assay covering 50 genes, that was investigated for the substitution of gold-standard techniques for tumor profiling (Lee et al., 2018). The panel has drawbacks for patients with glioma as it can be used only for the genomic DNA from tumor tissue and misses a lot of clinically important genes. All described Thermo Fisher NGS panels are RUO.

Mayo Clinic Laboratories (Rochester, United States) offers a MayoComplete Solid Tumor panel investigating SNVs and indels within 515 genes in the FFPE tissues (MCSTP - Overview: MayoComplete Solid Tumor Panel, Next-Generation Sequencing, Tumor, 2023). The panel can be used for profiling patients with glioma as it includes most of the essential glioma SNVs, missing only *p-TERT* DNA sequence alterations. There is a neuro-oncology panel (NONCP) covering 118 genes from tissue blocks. The panel could be used for profiling pediatric gliomas, but it misses the important diagnostic CNVs (NONCP - Overview: Neuro-Oncology Expanded Gene Panel with Rearrangement, Tumor, 2023). The Jackson Laboratory (Sacramento, United States) offers the JAX SOMASEQ NGS panel covering 517 genes for profiling patient DNA from FFPE tissues. It is compatible with Illumina Novaseq 6000 (JAX SOMASEQ - Clinical test - NIH Genetic Testing Registry GTR - NCBI, 2023) and could be used for the diagnosis of glioma, however, it misses *p-TERT* DNA sequence alterations, *p-MGMT* methylation, and important CNVs such as *1p/19q* codeletion. Paragon Genomics (Hayward, United States) offers the RUO CleanPlex OncoZoom Cancer Hotspot kit that examines 65 pro oncogenes and antioncogenes compatible with Illumina MiSeq and IonTorrent platforms (Zhu et al., 2021; CleanPlex OncoZoom Cancer Hotspot Kit for Cancer Profiling, 2023). CellMax Life (Sunnyvale, United States) developed CellMax-LBx to detect DNA sequence alterations in 73 genes in the ctDNA of various patients with cancer (Liu and Wang, 2022). So far, it lacks a medical certification but includes important glioma molecular markers, such as pathogenic DNA sequence alterations in *IDH1*, *IDH2*, *BRAF*, *CDKN2A*, *PTEN*, *NOTCH1*, and *TP53*.

Natera (Austin, United States) offers the Signatera NGS kit that is specially designed for ctDNA profiling and could be customized for a particular patient. Sequencing on corresponding tumor tissue and identification of the molecular markers might be used to search the patient's blood during relapse monitoring. Thus, there is a possibility to design a molecular residual disease monitoring system for each patient with glioma (Loupakis et al., 2021). Additionally, Altera is designed to profile 440 medically important genes by whole genome sequencing (WGS) including all glioma-relevant SNPs except for *p-TERT* DNA sequence alterations (Comprehensive Genomic Profiling, 2023). CD Genomics (New York, United States) features targeted NGS Glioma Gene Panel (Glioma Gene Panel Sequencing - CD Genomics, 2023) exploring 12 glioma-related genes in FFPE-tissues. The main disadvantages are the impossibility of *1p/19q*-codeletion detection, the large amount of DNA required (minimum 200 ng), and the compatibility only with the Illumina Hiseq platform. NeoGenomics Laboratories (Fort Myers, United States) provides an NGS service for detecting CNS tumor associated DNA sequence alterations in the FFPE tissue blocks, the NeoTYPE® Brain Tumor Profile (NeoTYPE® DNA & RNA - Brain | NeoGenomics Laboratories, 2023). It can be used for the detection of all essential glioma DNA sequence alterations plus *p-MGMT* methylation and *1p/19q*-codeletion. ArcherDx/Invitae (Boulder, United States) offers RUO LiquidPlex panel compatible with Illumina and detecting DNA sequence alterations in *IDH1*, *IDH2*, *BRAF*, *EGFR* and *TP53* (LiquidPlex ctDNA panel, 2023). The kit has the advantage of enrichment for rare ctDNA by amplifying highly fragmented DNA pieces typically sourced from tumors in contrast to long genomic DNA from white blood cells (Vendrell et al., 2020). A relatively low-cost solution could be the NGS Targeted Hotspot panel (CE-IVD certified) from EntroGen (Woodland Hills, United States), which covers 16 genes with several important genes for glioma (Śledzińska et al., 2022), allowing to profile up to 40 patient samples using Illumina MiniSeq or MiSeq (NGS Targeted Hotspot Panel 16 Kit | EntroGen, Inc, 2023). Personalis (Menlo Park, United States) offers a panel with 267 genes for solid tumor molecular profiling including most of the glioma-associated genes, but missing oligodendroglioma markers, namely, *FUBBP1*, *1p/19q*-codeletion, and *p-TERT* (Personalis | NeXT Dx, 2023).

Genes2Me Pvt. Ltd. (Gurgaon, India) introduced their own PanCan panel comprising oncological profiling of 524 genes (Next Generation Sequencing NGS Clinical Exome Sequencing Panels Assays | HLA Typing, 2023). However, we did not manage to find a comprehensive description of the genes used.

There are several NGS pan-cancer panels developed in China. Burning Rock Biotech produces CE-certificated panels, namely, OncoScreen spanning 295 genes including the one important for glioma profiling (Table 2) and OncoScreen Plus with 520 genes, both compatible with the Illumina platform (Tang et al., 2020). Onco PanScan (Genetron Health) is CE-approved and was designed to detect 309 microsatellite instability regions (Yang et al., 2023). RUO NGS kits are produced by Berry Genomics (BeiJianAn®) for whole-exome sequencing (WES), Novogene (NovoPM™ 2.0), AcornMed Biotechnology, AmoyDx (AmoyDx Comprehensive Panel; AmoyDx HANDLE Classic NGS Panel), GenePlus-Suzhou (Gene + OncoGlioma). Novogene Precision Medicine 2.0 (NovoPM™ 2.0) is a comprehensive test for all solid tumors profiling 484 genes (incorporating all glioma-related genes from Table 2) (NovoPM 2.0 - Novogene, 2023) intended for both tumor specimens and ctDNA. AmoyDx Comprehensive panel is intended for both tissue and liquid biopsy and is compatible with Illumina NextSeq 500 and NovaSeq 6000. AmoyDx HANDLE Classic NGS panel covers most

of the glioma-related genes (Comprehensive Panel_Amoydx, 2023; HANDLE Classic NGS Panel_Amoydx, 2023). Gene + OncoGlioma glioma gene test covers 1,021 genes and combines NGS with hybridization enrichment and pyrosequencing to analyze *MGMT* methylation status (Gene+|OncoGlioma, 2023).

ACT Genomics Co. Ltd. (Hong Kong) offers a RUO ACTOnco + kit that covers 440 genes with the glioma-related ones (*IDH1*, *IDH2*, *BRAF*, *CDKN2A*, *CDKN2B*, *CIC*, *FUBP1*, *NOTCH1*, etc.) for solid tumor molecular profiling compatible with the Ion Torrent platform (Jan et al., 2022). Geneseeq Technology Inc., the Chinese-Canadian company formerly known as Nanjing Geneseeq Technology Inc., developed GeneseeqPrime™ RUO for sequencing 425–437 solid tumor genes from biopsy or ctDNA (Geneseeq: Solid tumor genomic testing for precision oncology, 2023). The gene set includes *IDH1*, *IDH2*, *BRAF*, *CDKN2A/B*, *PTEN*, and *NOTCH1*, but misses *CIC*, *FUBP1*, *ATRX*, and *H3-3A* important for oligodendroglioma and astrocytoma diagnosis (Ye et al., 2022). Additionally, the Gliocan RUO kit is designed to sequence DNA sequence alterations in *IDH1*, *IDH2*, *ATRX*, *BRAF*, and *TP53*, along with detecting *1p/19q*-codeletion and *p-MGMT* methylation (Central Nervous System Tumors, 2023). However, it misses oligodendroglioma important pathogenic variants in *p-TERT*, *CIC*, *FUBP*, and *NOTCH1*.

Gendia (Antwerp, Belgium) offers the oncodiagnostics service for patient ctDNA screening over 50 genes, which includes several glioma-related genes, such as *IDH1*, *IDH2*, *NOTCH1*, *PTEN*, *BRAF*, *EGFR*, and *TP53* (Plessers, 2023), but there is no description of the NGS platform used for gene sequencing. Myriapod® NGS OncoDNA (Gosselies, Belgium) offers a CE-IVD kit - OncoDEEP for sequencing of 638 genes in FFPE tissues including all marker genes for glioma but missing important CNVs (*1p/19q*-codeletion and *chr +7/-10*) and p-MGMT methylation (OncoDEEP - Comprehensive biomarker test, 2023) (Table 2). Onco panel, offered by Diatech Pharmacogenetics (Jesi, Italy), has CE-IVD certification and covers 56 genes including usual glioma marker genes such as *BRAF, CDKN2A, EGFR, IDH1, IDH2, NOTCH,* and *TP53* (Marchetti et al., 2021; Eurofins Genomics, 2023). The panel includes several glioma-related genes and misses only the *p-TERT* mutation (Arildsen et al., 2019). CeGaT (CancerPrecision, 2023), missing only *p-TERT* and *H3-3A* for full glioma marker gene analysis; additionally, the possibility of 1p/19q-codeletion detection is not clear. NIMGenetics (Madrid, Spain) offers service for NGS cancer diagnostics, ONCONIM® Biomarker Broad Spectrum, for detecting SNPs, fusions, and SNVs in 52 genes from isolated patient sample DNA or FFPE tissues including *IDH1, IDH2, BRAF* and *EGFR* (Cáncer Somático, 2023). SOPHiA Solid Tumor Solution from SOPHiA GENETICS (Lausanne, Switzerland) has a CE certification and can detect glioma molecular markers such as *IDH1, IDH2, CDKN2A, BRAF, EGFR, TP53, p-TERT,* and *H3-3A* (SOPHiA Solid Tumor Solutions, 2023).

Glioma-specific NGS panels have been developed, however, we were not able to find some of them in the RUO or clinic markets. In this regard, we can merely summarize that there is ongoing research towards a panel specific for patients with glioma and that the market could be soon presented with a new targeted NGS kit. For instance, GlioSeq was distributed by the University of Pittsburgh Medical Center (Pittsburgh, United States) for sequencing 43 genes related to glioma (Nikiforova et al., 2016), and it can probably identify *1p/19q*-codeletion (Roy et al., 2019), although the methodology for identification was not described. CD Genomics (New York, United States) offers RUO Glioma Gene panel for sequencing of 12 glioma marker genes (Table 3) (Glioma Gene Panel Sequencing - CD Genomics, 2023); although it misses many important genes, it has the advantage of low-cost Illumina MiSeq utility. The Glio-DNA panel targets 65 genes including *p-MGMT* methylation, and *p-TERT* mutations, and can possibly identify the important CNVs (*1p/19q*-codeletion and *chr +7/-10*) (Tirrò et al., 2022). Italian researchers designed a glioma panel spanning 13 genes and a *p-TERT* region with the possibility of detecting *1p/19q*-codeletion (Guarnaccia et al., 2022). There is an Illumina MiniSeq compatible comprehensive glioma panel investigating 57 genes for SNPs and indels together with loss of heterozygosity in Chr1p, 6, 7, 9q, 10, 17, and 19q (Lorenz et al., 2020) (Table 3). A 20-gene NGS panel for gliomas compatible with the Ion Torrent platform was developed for molecular profiling of FFPE patient tissues (Zacher et al., 2017). GliomaSCAN is a big NGS panel comprising 232 genes for detecting most of the glioma markers, including SNPs, CNVs (*1p/19q*-codeletion and *chr +7/-10*), and amplifications (*EGFR, PDGFRA*) (Sa et al., 2019; Shin et al., 2020). CliomaSCAN is available on the Chinese market, but it is relatively big to be glioma-specific and ensure cost-effective screening or repeated monitoring and, probably, demands extensive sequencing power to override noise and artificial substitutions.

5 The ideal test system for the diagnosis of glioma

Preventive screening for glioma is not advisable due to the low incidence and low sensitivity of detecting ctDNA in low grades. However, the molecular phenotyping of gliomas can predict prognosis and temozolomide sensitivity and is also important for disease progression monitoring during relapses.

The ideal test system must 1) provide accurate diagnostics, 2) detect DNA sequence alterations in small amounts of different biological materials, 3) be cost-effective, 4) provide an opportunity to make a diagnosis with the available equipment, and 5) have high positive predictive value (PPV).

5.1 Provide accurate diagnosis

To provide accurate criteria for the diagnosis, the test system needs to incorporate all necessary markers that are sufficient for dividing glioma subtypes. The system should span all glioma marker mutations—DNA sequence alterations—*IDH1* R132, *IDH2* R172, *TP53* (W146, R175, R248, and R273), *p-TERT* (C250T and C228T), *BRAF* V600E, and *H3-3A* K27M; CNAs — *1p/19q*-codeletion and *chr +7/-10*; change in particular gene expression—gain of *EGFR*, *KIT*, and *PDGFRA*, loss of *ATRX*, *PTEN*, and *CDKN2A/B*; small indels—*EGFR*vIII; fusions—*BRAF-KIAA1549* (Figure 3) (Faulkner et al., 2015). However, in case of missing high throughput diagnostic methods, the preliminary assumption stems from the histological subtype and the glioma-specific genes could be enquired

TABLE 3 Glioma-specific NGS panels.

Genes important for glioma molecular profiling	GlioSeq	Glioma gene panel	Glio-DNA	13-Gene glioma panel	57-Gene comprehensive glioma panel	20-Gene glioma-tailored panel	GliomaSCAN
IDH1/2, BRAF, H3-3A (H3F3A), EGFR, TP53, CDKN2A, ATRX. PTEN	+	+	+	+	+	+	+
p-TERT	-	-	+	+	+	+	+
HIST1H3B	+	-	-	+	+	-	+
KIT	+	-	+	-	+	-	+
FUBP1, CDKN2B	+	-	+	-	+	+	+
CIC	+	+	+	-	+	+	+
NOTCH1	-	-	+	-	+	-	+
1p/19q-codel	+	-	+	+	+	-	+
+7chr/-10chr	-	-	+	-	+	-	+
p-MGMT methylation	-	-	+	-	-	-	-
Platform	Ion Torrent PGM	Illumina MiSeq	Ion Torrent PGM	Ion Torrent S5	Illumina MiniSeq	Ion Torrent PGM	Illumina HiSeq 2000
Biological material	brain biopsies, FFPE tissues	genomic DNA, FFPE tissues	FFPE tissues	FFPE tissues	FFPE tissues	frozen tissues, FFPE tissues	snap-frozen tissues
Availability on marker	+	+	-	-	-	-	+

sequentially. The strategy for the diagnosis of glioma is described in Supplementary Table S1.

Inherited DNA sequence alterations might predict glioma susceptibility, as a nearly 2-fold increase is seen in relatives of patients with glioma (Hemminki et al., 2009). Several inherited genetic alterations lead to a higher risk of glioma development, for instance, *TP53, TERT, CCDC26,* and *CDKN2B*.

Accurate diagnosis is also related to the specificity and sensitivity of the test system. Modern test systems pursue the highest possible sensitivity to diagnose as many people with the disease as feasible. However, high sensitivity should be balanced by high specificity in picking healthy people (Swift et al., 2020). Nowadays, there is a rising concern about false diagnosis/care/treatment referred to as overmedicalization, which can be avoided by focusing on the test system specificity and patient management in accordance with the real disease symptoms. When creating a test system, one needs to understand not only the purpose of use but also the possibility of misuse (inadvertently) of the diagnostic system, which may lead to unnecessary stress in false-positive patients. A good example is Prostate Specific Antigen, which has a sensitivity of 86% but a specificity of 33% (Swift et al., 2020). It is very good for revealing patients with prostate cancer but 67% of men receive false-positive results. With glioma one needs to be aware that patients diagnosed with glioblastoma tend to reject any treatment due to prominent adverse effects and fast ultimate mortality. Therefore, a diagnostics system should provide the same level of sensitivity and specificity.

5.2 Detect DNA sequence alterations in small amounts of different biological material

The gold standard of biological material for the detection of glioma DNA sequence alterations is a tumor piece or biopsy. However, the tumor biopsy in the case of patients with glioma is highly invasive and could cause the deterioration of the disease course. Typically, the glioma diagnosis is performed after the operation by histology and molecular testing, although prior knowledge could be obtained by the MRI visualization of tumor size and location. Nevertheless, the glioma molecular profile before the operation in cases of operation impossibility, or during multiple relapses, could provide additional information on patient prognosis and possible sensitivity to TMZ.

It is possible to use cerebrospinal fluid (CSF) for glioma genotyping as the content of ctDNA from dead glioma cells is sufficient and correlates with the source tumor profile (Miller et al., 2019). This allows for the monitoring of the glioma molecular progression with the relapses without obtaining biopsy samples (Martínez-Ricarte et al., 2018). Histone 3 DNA sequence alterations specific for pediatric gliomas can be identified in CSF using the ddPCR approach with a sensitivity of 87% (Panditharatna et al., 2018).

Another possibility is to use blood for detecting ctDNA, however, the sensitivity of using patient plasma is significantly lower than that of CSF (Juratli et al., 2018). The patients with glioma would have detectable plasma ctDNA only in 20%–50% of cases (Gao et al., 2022). Although, the study conducted in children has shown almost

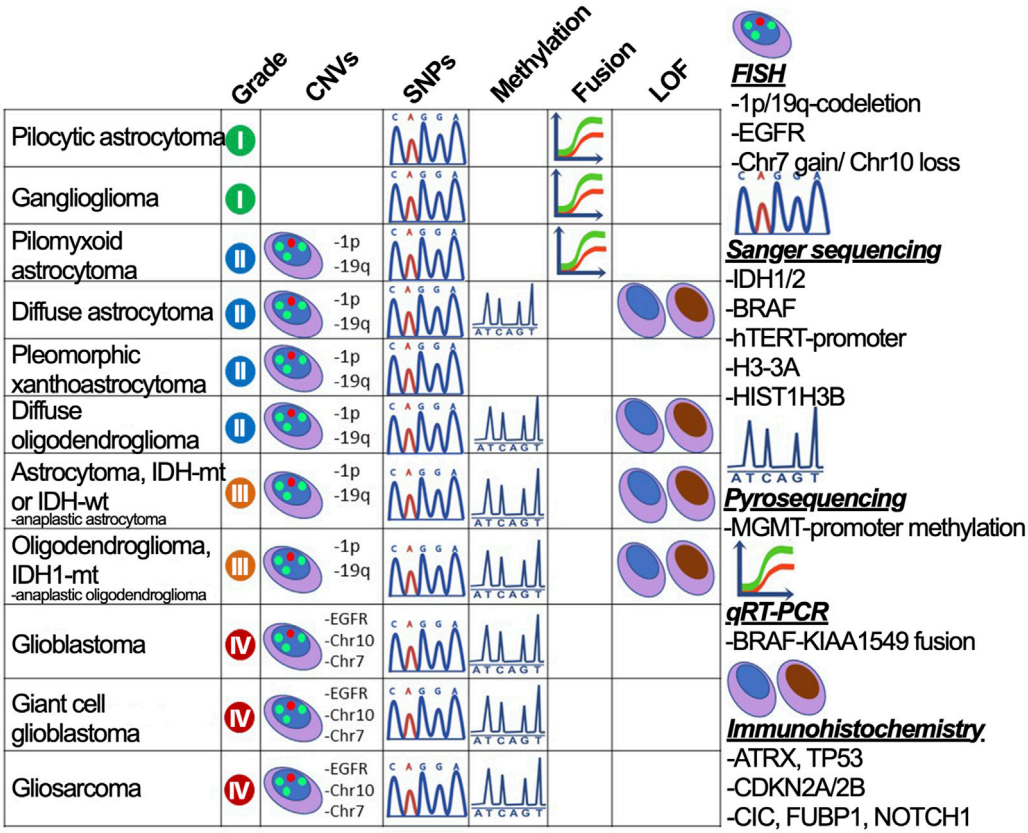

FIGURE 3
The strategy to divide gliomas into subtypes using gold standard diagnostic procedures. Glioma subdivisions are performed by searching for marker mutations (CNVs, SNPs, fusions, and protein loss-of-function) using methods graphically annotated and described on the right-hand side.

the same sensitivity in detecting H3 histone DNA sequence variants in plasma specimens (90%) compared to CSF (87%) (Panditharatna et al., 2018). Moreover, Guardant360 CDx markets the kit for the molecular characterization of any advanced solid tumor in the patient's blood plasma (GUARDANT368 cDX, 2023), but it misses the genes for oligodendroglioma diagnosis (Table 2).

Companies provide devices; for instance, chemagic™ instruments offered by PerkinElmer (cfDNA Isolation and Analysis Instruments|PerkinElmer, 2023), Roche sells hybridization-based enrichment kits, and QIAgen features a technique based on single primer extension (Lam et al., 2020).

There is an emerging technique called "sonobiopsy" to facilitate the ctDNA release in the blood with the means of sonication disruption of tumor cells and blood-CSF barrier, which was shown to increase the sensitivity of the glioma marker DNA sequence alteration detection for *EGFR*vIII and *p-TERT* SNVs (Pacia et al., 2022).

5.3 Be cost-effective (availability of a non-inexpensive test)

NGS technology is the most effective in terms of profiling patient materials and revealing SNVs as well as small indels. However, there is still no standard protocol to detect large chromosomal aberrations, such as *1p/19q*-codeletion and *chr +7/-10,* indispensable for glioma diagnosis. Despite a decreasing trend in NGS costs during the last few years, the costs of big pan-cancer panels are not affordable for routine patient surveillance, and big panel sizes could affect the sensitivity of marker identification and decrease the signal-to-noise ratio (Cohen et al., 2018). Thus, the usage of FDA-certified and CE-IVD-certified multicancer panels (Table 2) for glioma profiling/monitoring/prediction is questionable.

Additionally, there is no possibility to establish a sequencing unit and provide a linked technician and bioinformatician at every hospital. Nowadays, NGS can substitute all single-gene evaluation approaches. For instance, the diagnosis of glioma is based on inquiring about DNA sequence alterations in *IDH, TP53,* and *EGFR* and the presence of *1p/19q*-codeletion. For this purpose, we can use Sanger sequencing, qPCR, immunohistochemistry for SNPs and in FISH for chromosomal aberrations, however, NGS can replace all the mentioned techniques and reveal additional non-canonical polymorphisms.

5.4 Provide an opportunity to make a diagnosis with the available equipment

There is a possibility to use so-called targeted NGS focused on precise gene regions, for example, the cancer hot-spot panel traded by Ion Torrent covering 50 oncogenes with approximately

2,800 COSMIC mutations (Ion AmpliSeq™ Cancer Hotspot Panel v2, 2023), including glioma related DNA sequence alterations (Table 2). The targeted NGS technology allows for an increase in the number of sequenced patients and could lower the number of spent reagents per run (Plasmodium Diversity Network Africa et al., 2019).

NGS market in percentage of revenue for 2020 is separated as follows: North America — 40.5%, Europe — 28.3%, Asia-Pacific — 18.9%, South America — 7.8%, and Middle East and Africa — 4.5%. Some institutions in developing countries outsource the NGS to specialized laboratories in more developed countries (Ghilamicael et al., 2018; Tawfik et al., 2018; Mulenga et al., 2020). With this in mind, NGS technology is not available for patients in most regions partially due to difficulties with expensive equipment.

Nevertheless, the qPCR market is spread in major regions of the world, including North and Latin America, Europe, South and East Asia, Oceania, Middle and East, and Africa. The major advantage is that qPCR technology does not require high-quality instruments, special large rooms in labs, as FISH does, or a microscope with expensive antibodies, as IHC does.

5.5 Have a high positive predictive value (PPV)

CNS tumors are the most common cancer in the pediatric population (age range of 0–14 years) (Ostrom et al., 2019; Hauser, 2021). However, glioma is a rare type of cancer in the general adult population, and the probability of its occurrence peaks at the age of 36–59 years for different types (Molinaro et al., 2019). Hence, it is important that the healthcare system is prepared to screen only relevant subgroups of populations. These measures would prevent overdiagnosis and overtreatment.

6 Diagnostic strategy for the "ideal test system"

Molecular diagnostics requires a developed infrastructure. There is a need for stable electricity, low-temperature storage of mixes and samples, nuclease-free water, and trained personnel with relevant working time and wages. This is a problem that is still faced by developing countries and even developed countries in areas with low infrastructure (Abou Tayoun et al., 2014).

A survey conducted in 314 centers in 48 countries on the use of molecular diagnostics for gliomas has shown that molecular diagnostics is used in 235 centers (74.8%), and participants from all centers in 12 out of 48 countries (25%) stated that they do not have access to methods of molecular diagnosis of brain tumors. These 75% of centers that use molecular diagnostics in their clinical practice widely use such methods as FISH and/or CISH (216 centers, 69%), whereas 194 centers out of the 75% can perform other molecular diagnostics methods besides CISH/FISH aimed at analyzing the following: status *1p/19q* (72% of all centers), the methylation status of the *MGMT* promoter (53%), *BRAF* sequencing (50%), and *IDH1* mutation (47%) (Andreiuolo et al., 2016).

6.1 The pitfalls to performing high throughput diagnostics

The estimated cost of establishing an NGS facility ranges between $100K to $700K U.S. dollars (El-Metwally et al., 2014). On average, to cover the country's needs for sequencing there should be one sequencer per 2.4 million inhabitants. This is complicated to reach, especially for countries with large populations or countries with large skews in the distribution of the population over the territory.

The salary for NGS unit specialists in Italy is €61,670/year, €61,601/year, and €73,047/year for laboratory technicians, biologists, and pathologists, respectively (Pruneri et al., 2021). In Spain, a specialist technician is paid €33,155/year and a physician-oncologist receives €94,952/year (de Alava et al., 2022). The average salary of a molecular biologist in India is €3,748/year and for a bioinformatician, it is €7,369/year (Next-Generation Sequencing NGS Salary in India | PayScale, 2023). The gross salary in NGS facilities in lower and middle-income countries varies significantly, for instance, in South America, the average wage ranges from US$31,800 to US$45,500/year, while in China it ranges from US$39,000 to US$48,000/year, in Brazil it ranges from US$20,900 to US$37,000/year, in Russia it ranges from US$18,000 to US$31,800/year, and in India it ranges from US$11,700 to US$20,700/year. The information is provided by the website SalaryExpert (Institute, 2023).

Furthermore, establishing an NGS facility in a developing country could be far more expensive because of the added value of shipments, customs, and profit margin for local companies (Helmy et al., 2016). Typically, due to logistic issues, there are not many possibilities of delivering reagents that have to be transported in low-temperature conditions. Additional challenges include the lack of instrument maintenance personnel, the inability to quickly repair broken devices, the absence of qualified staff (especially for small towns), and limited access to up-to-date scientific literature (Helmy et al., 2016). The solution could be to establish/improve the research supply logistics, remove import duties on products for cutting-edge scientific research (NGS, mass spectrometry, and plasmids for gene editing), or elaborate diagnosis with other genotyping procedures, such as qPCR and allele-specific PCR).

6.2 The availability of NGS services throughout the world

In general, sequencing availability extremely varies throughout the world, with the highest concentration in the United States and Western Europe (Figure 4). Specifically, Illumina is the platform of choice for hospitals globally (Supplementary Figure S3) with the most frequent Illumina MiSeq accessibility due to relative low-cost of routine handling and high usage for clinical diagnostics. The second most popular platform is Oxford Nanopore Technologies with the device of choice, MinION, being utilized for long-read sequencing and usually employed by scientific institutions/universities for *de novo* genome assembly or low-cost WGS.

African countries face difficulties in providing patients with NGS services because of the pitfalls mentioned above. Nevertheless,

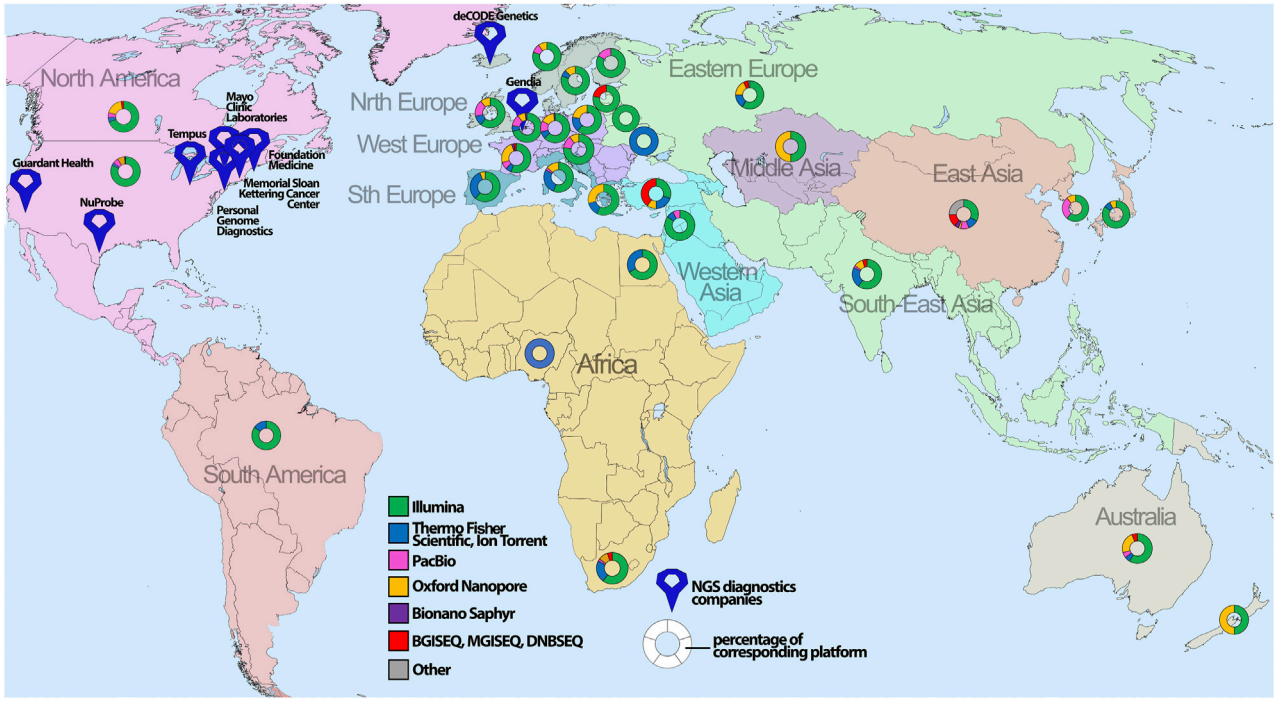

FIGURE 4
The global geographical distribution of sequencing platforms and technologies. The percentage of the corresponding sequencing platform analyzed for certain countries is depicted with map symbols of different colors and shapes showing the geographical location. The color annotates different NGS platforms, whereas size indicates the number of sequencers for the corresponding platform.

the sequencing of drug-resistant tuberculosis strains was performed utilizing Illumina iSeq 100 at Redeemer's University, in Ede, Nigeria. (Olawoye et al., 2021). The sequencing capacity of North Africa is concentrated in Egypt; for instance, Cairo University (Cairo, Egypt) possesses Illumina MiSeqDx and Ion Proton System, while Suez Canal University (Ismailia, Egypt) exploits Illumina MiSeq. Compared to the rest of Africa, South Africa has a much larger NGS capacity, and private companies utilize NGS for screening procedures and present a broad variety of NGS platforms from Chinese MGI-SEQ2000, all kinds of Illumina platforms to WGS sequencers such asPacBio Sequel II (Figure 4; Supplementary Figure S2).

Although India is considered a lower middle-income country, it possesses many NGS facilities (Supplementary Table S2). However, there is an issue with providing complete information about the advertised clinical services, thus some companies do not provide a description of the system they use for performing NGS analysis and do not mention whether they outsource this task to third parties (Salwan et al., 2020; Wen et al., 2020; Dash et al., 2021; Poonia et al., 2023). Indian Council of Medical Research claims that 84 institutes throughout the country possess an NGS facility (Next Generation Sequencing Capacity of India, 2023), however, it was difficult to confirm this as research institutions do not typically advertise the actual availability of their sequencing capacity. According to the available scientific research papers, several institutions were verified to have working NGS units (Supplementary Table S2). On the other hand, India has a wide variety of relatively small companies featuring NGS services. For instance, Genotypic Technology Pvt. Ltd. markets NGS employing the Nanopore platform (Next Generation Sequencing—Genotypic Technology Pvt. Ltd, 2023). Igenomix India offers whole genome sequencing technology for 24,000 genes but does not describe their platform. Eurofins Genomics India provides an opportunity to sequence a genome using Illumina NextSeq 500, Illumina HiSeq 2500 and Illumina NovaSeq. MedGenome Labs (Bengaluru, India) has a larger offer for various sequencing options, offering Illumina HiSeq X Ten, Illumina HiSeq 4000, Illumina NextSeq 500, Illumina MiSeq, Illumina HiSeq 2500, Illumina iScan, and Ion Proton System. Xcelris Labs (Ahmedabad, India) offers NGS sequencing on Illumina NextSeq500, Illumina MiSeq, GS FLX Titanium by Roche, Ion Proton System, and Roche 454 GSFLX + for pyrosequencing. Nucleome Informatics (Hyderabad, India) powers the genome sequencing on Bionano Saphyr, PacBio Sequel II, Illumina NovaSeq/HiSeq/iScan, as well as targeted gene sequencing with implication of Illumina MiSeq and Thermo Fisher GeneTitan. Biokart India provides transcriptome and genome sequencing, but does not describe properly the NGS platform used for these services. According to available publications, they have in use Illumina Miseq (Sajid et al., 2021) (Figure 4; Supplementary Table S2).

The Chinese NGS market is filled by big companies with targeted panels for prenatal diagnostics, cancer diagnostics, and diagnosis of rare hereditary diseases. For example, Berry Genomics markets an analog for Illumina NovaSeq500: NextSeq CN500, along with Illumina, PacBio, and Bionano devices (251). Similarly, Annoroad Gene Technology (Beijing) developed a sequencing machine analogous to Illumina NextSeq 500: NextSeq 550AR. CapitalBio Technology (Beijing) and Daan Gene (Guangzhou)

market analogous devices to Ion Torrent S5: BioelectronSeq 4000 Gene Sequencer and DA8600, respectively (Zeng et al., 2022). Genetron Health (Beijing) provides an option for the Ion Torrent platform featuring their sequencers GENETRON S5 and GENETRON S2000 along with Genetron Chef System. BGI Group offers MGI DNBseq™ technology along with BGISEQ-500 and more recent MGISEQ-2000 devices for transcriptome analysis, with the latter showing a comparable performance with the Illumina NextSeq 500 (Zeng et al., 2022), as well as DNBSEQ-T7 and DNBSEQ-G400 for WGS (Kanzi et al., 2020). GeneMind Biosciences (Shenzhen) developed sequencers: GenoLab M based on reversible termination of the fluorescent sequencing to identify optical signals from bases and Genocare 1600, which has the same optical signal technology but is implemented for single molecule sequencing. Shenzhen HYK Gene Technology features two sequencing devices: PSTAR-IIA and SeqExpert III-A without the description of the sequencing technology. Anxuyuan Biotechnology (Axbio Inc.) offers a fourth-generation sequencer AXP100 by combining Nanopore technology with single-molecule sequencing on the Biosensor-CMOS Platform implementing capacity sensor for proteins (Alhoshany et al., 2017). GenePlus-Suzhou (Suzhou) sells Gene + Seq-2000 and Gene + Seq-200 gene sequencers with the integrated DNBSEQ core technology (Wu et al., 2022). TIANGEN Biotech (Beijing) features transcriptome and genome sequencing using Illumina or BGI platforms. Biomarker Technology Corporation has a subdivision, BNKGene (Beijing), offering a wide variety of sequencing services, such as whole-transcriptome sequencing (WGS/WTS) on all kinds of platforms, e.g., PacBio Sequel, Nanopore PromethION, and GridION X5 MinION, Illumina NovaSeq, BGI DNBSEQ, and low-cost Bionano Irys. Guangzhou Huayin Health Medical Group (Guangzhou) has a subdivision, Huayin Biology, that trades sequencing services on Illumina HiSeq 3000, Illumina NextSeq 500, Illumina MiSeq, IonProton, and IonPGM. Novogene (Beijing) provides whole- and targeted genome sequencing on a variety of platforms, such as Illumina NovaSeq 6000, HiSeq X Ten and HiSeq 4000, PacBioSEQUEL II/IIE, and Nanopore PromethION. 3D Medicines (Shanghai) offers Illumina NovaSeq 6000 for sequencing services (Figure 4; Supplementary Table S2).

Similarly, the Russian NGS market is comprised of companies providing NGS devices or services and research institutions featuring services for exome/genome sequencing and data analysis. Russian companies do not provide the proprietary developed technology for sequencing but propose all kinds of platforms for WES/WGS such as Illumina, Ion Torrent, Nanopore, and DNBSEQ featured for research by R-pharm and Helicon, for clinical use by Genotek and Genoanalytica (Supplementary Table S2).

The global market for Europe and the United States is well characterized, thus we decided to point out the overall sequencing market research. Normanno et al. estimated the availability of oncological biomarker investigation in Europe. Multibiomarker test access through NGS services is high in Austria, Belgium, Cyprus, Denmark, Finland, France, Germany, Ireland, Portugal, Sweden, and the United Kingdom (100% of multi-biomarker access). Medium availability of NGS services was observed in Croatia, Czechia, Hungary, Netherlands, and Spain (75%–100% of multi-biomarker access), whereas there was low availability, accounting for less than 75% of multi-biomarker access, in Bulgaria, Estonia, Greece, Italy, Latvia, Lithuania, Luxembourg, Poland, Romania, Slovakia, and Slovenia (Normanno et al., 2022). In terms of support, governmental funding is received in a few European countries, namely, the United Kingdom, Belgium, Denmark, and the Netherlands (Phillips et al., 2021). Australia also possesses a governmental program for NGS development. Considering North America, WGS is not reimbursed while WES is funded in several provinces of Canada. However, the utility of WES is questionable as the time to receive results is delayed (2–6 months) and Canada outsources most of WES analysis abroad as the proper clinical NGS infrastructure is missing. The United States has private/public insurance coverage for clinical WGS and WES, which has been successfully used by more than half of insured individuals (Phillips et al., 2021).

Nevertheless, the largest NGS market is in the United States. Major companies such as Illumina, Thermo Fisher Scientific, Myriad Genetics, Roche, Bio-Rad Laboratories, and Perkin Elmer provide NGS services for both clinic and research. Alternative NGS operators are Oxford Nanopore Technologies in the United Kingdom, QiaGen from Germany, and Macrogen from South Korea. China's NGS market stands separately, with major companies such as MGI/BGI, Burning Rock, Novogene, and Berry Genomics, although Chinese offers of NGS services often provide an incomplete description of the sequencing technology or panels.

7 Discussion

In this review, it was observed that there is no comprehensive kit or test system to profile all the variety of glioma marker DNA sequence alterations, including SNVs, indels, amplifications, fusions, CNVs, and methylation status. First, there is no platform fully covering the complexity of glioma genetic variants because there is no methodology encompassing all the possible mutations in one single experiment. NGS panels are now highly invested in incorporating the most clinically relevant glioma mutations. However, so far, most of the targeted glioma panels reported in scientific papers remain inaccessible for even the RUO biomedical market, not to mention for *in vitro* clinical diagnosis.

Glioma molecular diagnostics provides an opportunity for precision oncology but remains an issue. To profile all subtyping DNA sequence alterations in a clinical lab there is a need to establish separate difficult procedures for SNPs (Sanger sequencing or qPCR), CNVs (FISH), amplification, or loss-of-function (IHC and *MGMT*-promoter methylation—pyrosequencing). This difficulty could be partially circumvented by building a clinical NGS testing facility and usage of pan-cancer panels certified for diagnosis. However, this approach is still expensive, because of the cost of building an appropriate unit and low demand for screening the general population due to low incidence in people under 60 years old (peaking incidence rate age is 70–79 years for glioblastoma and astrocytoma and 30–49 years for oligodendrogliomas) (Wang G.-M. et al., 2022). Additionally, there is no clinically approved glioma-specific NGS panel, and none of the developed panels could identify *MGMT*-promoter methylation relevant for predicting temozolomide responsiveness.

For prognostic and treatment response prediction, physicians could implement the shortened list of molecular markers, mainly DNA sequence alterations in *IDH1/2* affecting temozolomide response, *EGFR* amplification or truncation affecting the use of anti-*EGFR* therapy in glioma, and *p-TERT* mutations conferring a poor glioma prognosis (Killela et al., 2014). Both qPCR and ddPCR could be employed for SNP revealing, with the latter being more sensitive for determining mutations in blood and CSF ctDNA (Olympios et al., 2021). During the SARS-CoV-2 pandemic, the availability of ddPCR and qPCR has grown profoundly, spreading to small hospitals. The ddPCR segment is growing even faster, although ddPCR's high cost still precludes dissemination. However, there is no FDA-approved qPCR kit for detecting SNPs in patients with glioma, as the Abbott RealTime *IDH1/2* kits are approved for patients with acute myeloid leukemia. The European market has clinically certified qPCR kits for *IDH1/2* mutation detection from Qiagen and EntroGen, and *MGMT*-promoter methylation kits from EntroGen and Genmark Sağlık Ürünleri. Genetron Health provides qPCR kits for identifying DNA sequence alterations in *IDH1* and *p-TERT* approved by Chinese NMPA. Thus, glioma molecular profiling in clinics is either performed by diverse procedures (sending to clinically approved diagnostic labs providing services for mutation revealing) or represents an unmet need.

We suggest that the market should not consolidate hope only in the NGS segment but rather consider other perspectives for clinical development, such as qPCR, ddPCR, and MassArray, which could be developed for liquid biopsy and incorporate a wide spectrum of glioma-related mutations simultaneously.

Author contributions

Conceptualization, VG, VF, and VK; Investigation, VG, AP, OK, DL, and VZ; Writing—Original Draft, AP, OK, VG, VT, DL, and VZ; Writing—Review and Editing, NG, IB VG, VK, AP, OK, VT, and VF; Visualization, OK, VZ, and VG; Funding Acquisition, VK and NG. All authors contributed to the article and approved the submitted version.

Funding

AP, VG, VZ, DL, VF, and VK were funded by the Russian Science Foundation (RSF) Grant 20-15-00378; NG and IB were funded by the Russian Science Foundation (RSF) Grant 21-75-00100.

Conflict of interest

The authors declare that the research was conducted in the absence of any commercial or financial relationships that could be construed as a potential conflict of interest.

Publisher's note

All claims expressed in this article are solely those of the authors and do not necessarily represent those of their affiliated organizations, or those of the publisher, the editors and the reviewers. Any product that may be evaluated in this article, or claim that may be made by its manufacturer, is not guaranteed or endorsed by the publisher.

Supplementary material

The Supplementary Material for this article can be found online at: https://www.frontiersin.org/articles/10.3389/fmolb.2023.1216102/full#supplementary-material

References

Abou Tayoun, A. N., Burchard, P. R., Malik, I., Scherer, A., and Tsongalis, G. J. (2014). Democratizing molecular diagnostics for the developing world. *Am. J. Clin. Pathology* 141, 17–24. doi:10.1309/AJCPA1L4KPXBJNPG

Aldera, A. P., and Govender, D. (2022). Gene of the month: H3F3A and H3F3B. *J. Clin. Pathol.* 75, 1–4. doi:10.1136/jclinpath-2021-207751

Alhoshany, A., Sivashankar, S., Mashraei, Y., Omran, H., and Salama, K. N. (2017). A biosensor-CMOS platform and integrated readout circuit in 0.18-µm CMOS technology for cancer biomarker detection. *Sensors* 17, 1942. doi:10.3390/s17091942

Ali, R. H., Alateeqi, M., Jama, H., Alrumaidhi, N., Alqallaf, A., Mohammed, E. M., et al. (2023). Evaluation of the Oncomine Comprehensive Assay v3 panel for the detection of 1p/19q codeletion in oligodendroglial tumours. *J. Clin. Pathol.* 76, 103–110. doi:10.1136/jclinpath-2021-207876

Alnajar, H., Ravichandran, H., Figueiredo Rendeiro, A., Ohara, K., Al Zoughbi, W., Manohar, J., et al. (2022). Tumor-immune microenvironment revealed by Imaging Mass Cytometry in a metastatic sarcomatoid urothelial carcinoma with a prolonged response to pembrolizumab. *Cold Spring Harb. Mol. Case Stud.* 8, a006151. doi:10.1101/mcs.a006151

Andreiuolo, F., Mazeraud, A., Chrétien, F., and Pietsch, T. (2016). A global view on the availability of methods and information in the neuropathological diagnostics of CNS tumors: results of an international survey among neuropathological units. *Brain Pathol.* 26, 551–554. doi:10.1111/bpa.12383

Arildsen, N. S., Martin de la Fuente, L., Måsbäck, A., Malander, S., Forslund, O., Kannisto, P., et al. (2019). Detecting TP53 mutations in diagnostic and archival liquid-based Pap samples from ovarian cancer patients using an ultra-sensitive ddPCR method. *Sci. Rep.* 9, 15506. doi:10.1038/s41598-019-51697-6

Arita, H., Matsushita, Y., Machida, R., Yamasaki, K., Hata, N., Ohno, M., et al. (2020). TERT promoter mutation confers favorable prognosis regardless of 1p/19q status in adult diffuse gliomas with IDH1/2 mutations. *acta neuropathol. Commun.* 8, 201. doi:10.1186/s40478-020-01078-2

Arita, H., Narita, Y., Fukushima, S., Tateishi, K., Matsushita, Y., Yoshida, A., et al. (2013). Upregulating mutations in the TERT promoter commonly occur in adult malignant gliomas and are strongly associated with total 1p19q loss. *Acta Neuropathol.* 126, 267–276. doi:10.1007/s00401-013-1141-6

Arita, H., Yamasaki, K., Matsushita, Y., Nakamura, T., Shimokawa, A., Takami, H., et al. (2016). A combination of TERT promoter mutation and MGMT methylation status predicts clinically relevant subgroups of newly diagnosed glioblastomas. *acta neuropathol. Commun.* 4, 79. doi:10.1186/s40478-016-0351-2

Armache, A., Yang, S., Martínez de Paz, A., Robbins, L. E., Durmaz, C., Cheong, J. Q., et al. (2020). Histone H3.3 phosphorylation amplifies stimulation-induced transcription. *Nature* 583, 852–857. doi:10.1038/s41586-020-2533-0

Babakoohi, S., Lapidus, R. G., Faramand, R., Sausville, E. A., and Emadi, A. (2017). Comparative analysis of methods for detecting isocitrate dehydrogenase 1 and 2 mutations and their metabolic consequence, 2-hydroxyglutarate, in different neoplasms. *Appl. Immunohistochem. Mol. Morphol.* 25, 334–337. doi:10.1097/PAI.0000000000000342

Beaubier, N., Tell, R., Lau, D., Parsons, J. R., Bush, S., Perera, J., et al. (2019). Clinical validation of the tempus xT next-generation targeted oncology sequencing assay. *Oncotarget* 10, 2384–2396. doi:10.18632/oncotarget.26797

Beliveau, B. J., Boettiger, A. N., Nir, G., Bintu, B., Yin, P., Zhuang, X., et al. (2017). "Situ super-resolution imaging of genomic DNA with OligoSTORM and OligoDNA-PAINT," in Super-resolution microscopy *methods in molecular biology*. Editor H. Erfle (New York, NY: Springer New York), 231–252. doi:10.1007/978-1-4939-7265-4_19

Benitez, J. A., Ma, J., D'Antonio, M., Boyer, A., Camargo, M. F., Zanca, C., et al. (2017). PTEN regulates glioblastoma oncogenesis through chromatin-associated complexes of DAXX and histone H3.3. *Nat. Commun.* 8, 15223. doi:10.1038/ncomms15223

Bettegowda, C., Sausen, M., Leary, R. J., Kinde, I., Wang, Y., Agrawal, N., et al. (2014). Detection of circulating tumor DNA in early- and late-stage human malignancies. *Sci. Transl. Med.* 6, 224ra24. doi:10.1126/scitranslmed.3007094

Bevins, N., Sun, S., Gaieb, Z., Thorson, J. A., and Murray, S. S. (2020). Comparison of commonly used solid tumor targeted gene sequencing panels for estimating tumor mutation burden shows analytical and prognostic concordance within the cancer genome atlas cohort. *J. Immunother. Cancer* 8, e000613. doi:10.1136/jitc-2020-000613

Bionano (2023). Transforming the way the world sees the genome. *bionanogenomics*. Available at: https://bionano.com/(Accessed March 16, 2023).

Bleeker, F. E., Atai, N. A., Lamba, S., Jonker, A., Rijkeboer, D., Bosch, K. S., et al. (2010). The prognostic IDH1 R132 mutation is associated with reduced NADP+-dependent IDH activity in glioblastoma. *Acta Neuropathol.* 119, 487–494. doi:10.1007/s00401-010-0645-6

Boisselier, B., Marie, Y., Labussière, M., Ciccarino, P., Desestret, V., Wang, X., et al. (2010). Cold PCR HRM: a highly sensitive detection method for IDH1 mutations. *Hum. Mutat.* 31, 1360–1365. doi:10.1002/humu.21365

Bonavia, R., Inda, M. M., Vandenberg, S., Cheng, S.-Y., Nagane, M., Hadwiger, P., et al. (2012). EGFRvIII promotes glioma angiogenesis and growth through the NF-κB, interleukin-8 pathway. *Oncogene* 31, 4054–4066. doi:10.1038/onc.2011.563

Brandner, S., McAleenan, A., Jones, H. E., Kernohan, A., Robinson, T., Schmidt, L., et al. (2022). Diagnostic accuracy of 1p/19q codeletion tests in oligodendroglioma: a comprehensive meta-analysis based on a cochrane systematic review. *Neuropathol. Appl. Neurobio* 48, e12790. doi:10.1111/nan.12790

Brat, D. J., Aldape, K., Bridge, J. A., Canoll, P., Colman, H., Hameed, M. R., et al. (2022). Molecular biomarker testing for the diagnosis of diffuse gliomas. *Archives Pathology Laboratory Med.* 146, 547–574. doi:10.5858/arpa.2021-0295-CP

Brat, D. J., Aldape, K., Colman, H., Holland, E. C., Louis, D. N., Jenkins, R. B., et al. (2018). cIMPACT-NOW update 3: recommended diagnostic criteria for "Diffuse astrocytic glioma, IDH-wildtype, with molecular features of glioblastoma, WHO grade IV". *Acta Neuropathol.* 136, 805–810. doi:10.1007/s00401-018-1913-0

Broggi, G., Salvatorelli, L., Barbagallo, D., Certo, F., Altieri, R., Tirrò, E., et al. (2021). Diagnostic utility of the immunohistochemical expression of serine and arginine rich splicing factor 1 (SRSF1) in the differential diagnosis of adult gliomas. *Cancers* 13, 2086. doi:10.3390/cancers13092086

Buckner, J., Giannini, C., Eckel-Passow, J., Lachance, D., Parney, I., Laack, N., et al. (2017). Management of diffuse low-grade gliomas in adults — Use of molecular diagnostics. *Nat. Rev. Neurol.* 13, 340–351. doi:10.1038/nrneurol.2017.54

CANCER DIAGNOSTICS (2023). *Genetron*. Available at: https://en.genetronhealth.com/products-cancerOrMonitor.html (Accessed March 16, 2023).

Cáncer Somático (2023). OncoNIM, prosigna. *NIMGenetics*. Available at: https://www.nimgenetics.com/estudios-geneticos/mutaciones-somaticas/(Accessed March 18, 2023).

CancerPrecision (2023). *CeGaT GmbH*. Available at: https://www.cegat.com/diagnostics/tumor-diagnostics/cancerprecision/ (Accessed March 18, 2023).

Catteau, A., Girardi, H., Monville, F., Poggionovo, C., Carpentier, S., Frayssinet, V., et al. (2014). A new sensitive PCR assay for one-step detection of 12 IDH1/2 mutations in glioma. *acta neuropathol. Commun.* 2, 58. doi:10.1186/2051-5960-2-58

Central Nervous System Tumors (2023). *Geneseeq technology Inc. | A precision oncology company*. Available at: https://na.geneseeq.com/central-nervous-system-tumors/ (Accessed March 17, 2023).

cfDNA Isolation and Analysis Instruments (2023). *PerkinElmer*. Available at: https://www.perkinelmer.com/category/cfdna-isolation-and-analysis-instruments (Accessed March 19, 2023).

Chatterjee, D., Radotra, B., Kumar, N., Vasishta, R., and Gupta, S. (2018). IDH1, ATRX, and BRAFV600E mutation in astrocytic tumors and their significance in patient outcome in north Indian population. *Surg. Neurol. Int.* 9, 29. doi:10.4103/sni.sni_284_17

Chaturbedi, A., Yu, L., Linskey, M. E., and Zhou, Y. (2012). Detection of 1p19q deletion by real-time comparative quantitative PCR. *Biomark-Insights* 7, 9–17. doi:10.4137/BMI.S9003

Chen, C.-Y., Chen, J., He, L., and Stiles, B. L. (2018). Pten: tumor suppressor and metabolic regulator. *Front. Endocrinol.* 9, 338. doi:10.3389/fendo.2018.00338

Chen, Y., Su, F., Cheng, Y., He, X., and Li, Z. (2022). Sensitive detection of fusion transcripts with padlock probe-based continuous cascade amplification (P-CCA). *Analyst* 147, 2207–2214. doi:10.1039/D2AN00341D

Chen, Z., Guo, Y., Zhao, D., Zou, Q., Yu, F., Zhang, L., et al. (2021). Comprehensive analysis revealed that CDKN2A is a biomarker for immune infiltrates in multiple cancers. *Front. Cell. Dev. Biol.* 9, 808208. doi:10.3389/fcell.2021.808208

Chiba, K., Lorbeer, F. K., Shain, A. H., McSwiggen, D. T., Schruf, E., Oh, A., et al. (2017). Mutations in the promoter of the telomerase gene *TERT* contribute to tumorigenesis by a two-step mechanism. *Science* 357, 1416–1420. doi:10.1126/science.aao0535

Choi, W., and PANAGENE (2023). *Panagene*. Available at: http://panagene.com (Accessed March 16, 2023).

CleanPlex OncoZoom Cancer Hotspot Kit for Cancer Profiling (2023). *Paragon genomics*. Available at: https://www.paragongenomics.com/product/cleanplex-oncozoom-cancer-hotspot-panel/ (Accessed March 17, 2023).

Cohen, J. D., Li, L., Wang, Y., Thoburn, C., Afsari, B., Danilova, L., et al. (2018). Detection and localization of surgically resectable cancers with a multi-analyte blood test. *Science* 359, 926–930. doi:10.1126/science.aar3247

Comprehensive Genomic Profiling (2023). *Altera*. Available at: https://www.natera.com/oncology/signatera-advanced-cancer-detection/clinicians/altera/ (Accessed March 17, 2023).

Comprehensive Panel_Amoydx (2023). *Amoydx*. Available at: http://www.amoydiagnostics.com/productDetail_49.html (Accessed March 17, 2023).

Coons, S. W., Johnson, P. C., Scheithauer, B. W., Yates, A. J., and Pearl, D. K. (1997). Improving diagnostic accuracy and interobserver concordance in the classification and grading of primary gliomas. *Cancer* 79, 1381–1393. doi:10.1002/(SICI)1097-0142(19970401)79:7<1381::AID-CNCR16>3.0.CO;2-W

Dai, P., Wu, L. R., Chen, S. X., Wang, M. X., Cheng, L. Y., Zhang, J. X., et al. (2021). Calibration-free NGS quantitation of mutations below 0.01% VAF. *Nat. Commun.* 12, 6123. doi:10.1038/s41467-021-26308-6

Danussi, C., Bose, P., Parthasarathy, P. T., Silberman, P. C., Van Arnam, J. S., Vitucci, M., et al. (2018). Atrx inactivation drives disease-defining phenotypes in glioma cells of origin through global epigenomic remodeling. *Nat. Commun.* 9, 1057. doi:10.1038/s41467-018-03476-6

Dash, M., Somvanshi, V. S., Budhwar, R., Godwin, J., Shukla, R. N., and Rao, U. (2021). A rice root-knot nematode Meloidogyne graminicola-resistant mutant rice line shows early expression of plant-defence genes. *Planta* 253, 108. doi:10.1007/s00425-021-03625-0

de Alava, E., Pareja, M. J., Carcedo, D., Arrabal, N., García, J.-F., and Bernabé-Caro, R. (2022). Cost-effectiveness analysis of molecular diagnosis by next-generation sequencing versus sequential single testing in metastatic non-small cell lung cancer patients from a south Spanish hospital perspective. *Expert Rev. Pharmacoeconomics Outcomes Res.* 22, 1033–1042. doi:10.1080/14737167.2022.2078310

Diplas, B. H., Liu, H., Yang, R., Hansen, L. J., Zachem, A. L., Zhao, F., et al. (2019). Sensitive and rapid detection of *TERT* promoter and *IDH* mutations in diffuse gliomas. *Neuro-Oncology* 21, 440–450. doi:10.1093/neuonc/noy167

Dremsek, P., Schwarz, T., Weil, B., Malashka, A., Laccone, F., and Neesen, J. (2021). Optical genome mapping in routine human genetic diagnostics—its advantages and limitations. *Genes.* 12, 1958. doi:10.3390/genes12121958

Ebrahimi, A., Skardelly, M., Bonzheim, I., Ott, I., Mühleisen, H., Eckert, F., et al. (2016). ATRX immunostaining predicts IDH and H3F3A status in gliomas. *acta neuropathol. Commun.* 4, 60. doi:10.1186/s40478-016-0331-6

EGFRvIII Detection Kit (2023). *EntroGen, Inc*. Available at: http://entrogen.com/web3/egfrviii-detection-kit/ (Accessed March 16, 2023).

El-Metwally, S., Ouda, O. M., and Helmy, M. (2014). "Challenges in the next-generation sequencing field," in Next generation sequencing Technologies and Challenges in sequence assembly *SpringerBriefs in systems biology* (New York, NY: Springer New York), 45–49. doi:10.1007/978-1-4939-0715-1_5

Ellis, J. A., and Ong, B. (2017). "The MassARRAY® system for targeted SNP genotyping," in Genotyping *methods in molecular biology*. Editors S. J. White and S. Cantsilieris (New York, NY: Springer New York), 77–94. doi:10.1007/978-1-4939-6442-0_5

Eurofins Genomics (2023). *INVIEW liquid biopsy oncoprofiling (591 genes) (former GATCLiquid oncopanel all-in-one)*. Available at: https://eurofinsgenomics.eu/en/next-generation-sequencing/applications/oncology-solutions/inview-liquid-biopsy-oncoprofiling/ (Accessed March 17, 2023).

Faulkner, C., Ellis, H. P., Shaw, A., Penman, C., Palmer, A., Wragg, C., et al. (2015). BRAF fusion analysis in pilocytic astrocytomas: KIAA1549-BRAF 15-9 fusions are more frequent in the midline than within the cerebellum. *J. Neuropathol. Exp. Neurol.* 74, 867–872. doi:10.1097/NEN.0000000000000226

Fehlmann, T., Reinheimer, S., Geng, C., Su, X., Drmanac, S., Alexeev, A., et al. (2016). cPAS-based sequencing on the BGISEQ-500 to explore small non-coding RNAs. *Clin. Epigenet* 8, 123. doi:10.1186/s13148-016-0287-1

Feng, H., Hu, B., Vuori, K., Sarkaria, J. N., Furnari, F. B., Cavenee, W. K., et al. (2014). EGFRvIII stimulates glioma growth and invasion through PKA-dependent serine phosphorylation of Dock180. *Oncogene* 33, 2504–2512. doi:10.1038/onc.2013.198

French, P. J., Eoli, M., Sepulveda, J. M., de Heer, I., Kros, J. M., Walenkamp, A., et al. (2019). Defining EGFR amplification status for clinical trial inclusion. *Neuro-Oncology* 21, 1263–1272. doi:10.1093/neuonc/noz096

Gaca-Tabaszewska, M., Bogusiewicz, J., and Bojko, B. (2022). Metabolomic and lipidomic profiling of gliomas—a new direction in personalized therapies. *Cancers* 14, 5041. doi:10.3390/cancers14205041

Gan, H. K., Kaye, A. H., and Luwor, R. B. (2009). The EGFRvIII variant in glioblastoma multiforme. *J. Clin. Neurosci.* 16, 748–754. doi:10.1016/j.jocn.2008.12.005

Gao, Q., Zeng, Q., Wang, Z., Li, C., Xu, Y., Cui, P., et al. (2022). Circulating cell-free DNA for cancer early detection. *Innovation* 3, 100259. doi:10.1016/j.xinn.2022.100259

Gaudin, M., and Desnues, C. (2018). Hybrid capture-based next generation sequencing and its application to human infectious diseases. *Front. Microbiol.* 9, 2924. doi:10.3389/fmicb.2018.02924

Gene (2023). *OncoGlioma*. Available at: https://www.geneplus.cn/geneplus/trans/toCoreTechnology?page=clinical_OncoGlioma (Accessed March 17, 2023).

geneMAPTM MGMT Methylation Analysis Kit (MGM-RT50) (2023). *geneMAPTM*. Available at: https://www.genmark.com.tr/services/mgmt-methylation-analysis-kit/ (Accessed March 16, 2023).

Geneseeq: Solid tumour genomic testing for precision oncology (2023). *Geneseeq technology Inc. | A precision oncology company*. Available at: https://na.geneseeq.com/solid-tumors/ (Accessed March 17, 2023).

Genomic Profiling (2023). *Tempus*. Available at: https://www.tempus.com/oncology/genomic-profiling/ (Accessed March 16, 2023).

Ghilamicael, A. M., Boga, H. I., Anami, S. E., Mehari, T., and Budambula, N. L. M. (2018). Potential human pathogenic bacteria in five hot springs in Eritrea revealed by next generation sequencing. *PLoS ONE* 13, e0194554. doi:10.1371/journal.pone.0194554

Glioma Gene Panel Sequencing - *CD genomics* (2023). Available at: https://www.cd-genomics.com/diseasepanel/glioma-panel.html [Accessed March 17, 2023].

Goryńska, P. Z., Chmara, K., Kupcewicz, B., Goryński, K., Jaroch, K., Paczkowski, D., et al. (2022). Metabolomic phenotyping of gliomas: what can we get with simplified protocol for intact tissue analysis? *Cancers* 14, 312. doi:10.3390/cancers14020312

Griffin, C. A., Burger, P., Morsberger, L., Yonescu, R., Swierczynski, S., Weingart, J. D., et al. (2006). "Identification of der(1;19)(q10;p10)," in *Five oligodendrogliomas suggests mechanism of concurrent 1p and 19q loss: Journal of neuropathology and experimental neurology 65*, 988–994. doi:10.1097/01.jnen.0000235122.98052.8f

GUARDANT368 cDX (2023). *GUARDANT368 cDX*.

Guarnaccia, M., Guarnaccia, L., La Cognata, V., Navone, S. E., Campanella, R., Ampollini, A., et al. (2022). A targeted next-generation sequencing panel to genotype gliomas. *Life* 12, 956. doi:10.3390/life12070956

Gulaia, V., Shmelev, M., Romanishin, A., Shved, N., Farniev, V., Goncharov, N., et al. (2022). Single-nucleus transcriptomics of IDH1- and TP53-mutant glioma stem cells displays diversified commitment on invasive cancer progenitors. *Sci. Rep.* 12, 18975. doi:10.1038/s41598-022-23646-3

Haase, S., Garcia-Fabiani, M. B., Carney, S., Altshuler, D., Núñez, F. J., Méndez, F. M., et al. (2018). Mutant ATRX: uncovering a new therapeutic target for glioma. *Expert Opin. Ther. Targets* 22, 599–613. doi:10.1080/14728222.2018.1487953

HANDLE Classic NGS Panel_Amoydx (2023). *Amoydx*. Available at: http://www.amoydiagnostics.com/productDetail_38.html (Accessed March 17, 2023).

Hatae, R., Hata, N., Yoshimoto, K., Kuga, D., Akagi, Y., Murata, H., et al. (2016). Precise detection of IDH1/2 and BRAF hotspot mutations in clinical glioma tissues by a differential calculus analysis of high-resolution melting data. *PLoS ONE* 11, e0160489. doi:10.1371/journal.pone.0160489

Hauser, P. (2021). Classification and treatment of pediatric gliomas in the molecular era. *Children* 8, 739. doi:10.3390/children8090739

Heidenreich, B., Rachakonda, P. S., Hosen, I., Volz, F., Hemminki, K., Weyerbrock, A., et al. (2015). *TERT* promoter mutations and telomere length in adult malignant gliomas and recurrences. *Oncotarget* 6, 10617–10633. doi:10.18632/oncotarget.3329

Heimberger, A. B., Suki, D., Yang, D., Shi, W., and Aldape, K. (2005). The natural history of EGFR and EGFRvIII in glioblastoma patients. *J. Transl. Med.* 3, 38. doi:10.1186/1479-5876-3-38

Helmy, M., Awad, M., and Mosa, K. A. (2016). Limited resources of genome sequencing in developing countries: challenges and solutions. *Appl. Transl. Genomics* 9, 15–19. doi:10.1016/j.atg.2016.03.003

Hemminki, K., Tretli, S., Sundquist, J., Johannesen, T. B., and Granström, C. (2009). Familial risks in nervous-system tumours: a histology-specific analysis from Sweden and Norway. *Lancet Oncol.* 10, 481–488. doi:10.1016/S1470-2045(09)70076-2

Horbinski, C., Miller, C. R., and Perry, A. (2011). Gone FISHing: clinical lessons learned in brain tumor molecular diagnostics over the last decade. *Brain Pathol.* 21, 57–73. doi:10.1111/j.1750-3639.2010.00453.x

Hosoya, T., Takahashi, M., Honda-Kitahara, M., Miyakita, Y., Ohno, M., Yanagisawa, S., et al. (2022). MGMT gene promoter methylation by pyrosequencing method correlates volumetric response and neurological status in IDH wild-type glioblastomas. *J. Neurooncol* 157, 561–571. doi:10.1007/s11060-022-03999-5

How nanopore sequencing works (2023). *How nanopore sequencing works*. Available at: https://nanoporetech.com/support/how-it-works (Accessed March 16, 2023).

Huang, F. W., Bielski, C. M., Rinne, M. L., Hahn, W. C., Sellers, W. R., Stegmeier, F., et al. (2015). TERT promoter mutations and monoallelic activation of TERT in cancer. *Oncogenesis* 4, e176. doi:10.1038/oncsis.2015.39

Hwang, D. W., Choi, Y., Kim, D., Park, H. Y., Kim, K. W., Kim, M. Y., et al. (2019). Graphene oxide-quenching-based fluorescence *in situ* hybridization (G-FISH) to detect RNA in tissue: simple and fast tissue RNA diagnostics. *Nanomedicine Nanotechnol. Biol. Med.* 16, 162–172. doi:10.1016/j.nano.2018.12.004

IDH1/2 Mutation Detection Kit (2023). *EntroGen, Inc*. Available at: http://entrogen.com/web3/idh-12-mutation-detection-kit/ (Accessed March 16, 2023).

IDH1/IDH2 Mutation Analysis by PCR | *NeoGenomics laboratories* (2023). Available at: https://neogenomics.com/test-menu/idh1idh2-mutation-analysis-pcr [Accessed March 16, 2023].

Institute, E. E. R (2023). Global salary and cost of living data | compensation analysis tool - SalaryExpert. Available at: https://www.salaryexpert.com (Accessed March 19, 2023).

Ion AmpliSeqTM Cancer Hotspot Panel v2 (2023). *Ion AmpliSeqTM cancer Hotspot panel v2*. Available at: https://www.thermofisher.com/order/catalog/product/4475346?SID=srch-srp-4475346 (Accessed March 19, 2023).

Jain, M., Koren, S., Miga, K. H., Quick, J., Rand, A. C., Sasani, T. A., et al. (2018). Nanopore sequencing and assembly of a human genome with ultra-long reads. *Nat. Biotechnol.* 36, 338–345. doi:10.1038/nbt.4060

Jaiswal, S. (2016). Role of immunohistochemistry in the diagnosis of central nervous system tumors. *Neurol. India* 64, 502–512. doi:10.4103/0028-3886.181547

Jan, Y.-H., Tan, K. T., Chen, S.-J., Yip, T. T. C., Lu, C. tai, and Lam, A. K. (2022). Comprehensive assessment of actionable genomic alterations in primary colorectal carcinoma using targeted next-generation sequencing. *Br. J. Cancer* 127, 1304–1311. doi:10.1038/s41416-022-01913-4

JAX SOMASEQ (2023). *Clinical test - NIH genetic testing Registry (GTR) - NCBI*. Available at: https://www.ncbi.nlm.nih.gov/gtr/tests/596290/overview/ (Accessed March 17, 2023).

Jenkins, R. B., Blair, H., Ballman, K. V., Giannini, C., Arusell, R. M., Law, M., et al. (2006). A t(1;19)(q10;p10) mediates the combined deletions of 1p and 19q and predicts a better prognosis of patients with oligodendroglioma. *Cancer Res.* 66, 9852–9861. doi:10.1158/0008-5472.CAN-06-1796

Jeon, S. A., Park, J. L., Park, S.-J., Kim, J. H., Goh, S.-H., Han, J.-Y., et al. (2021). Comparison between MGI and Illumina sequencing platforms for whole genome sequencing. *Genes. Genom* 43, 713–724. doi:10.1007/s13258-021-01096-x

Jessri, M., and Farah, C. S. (2014). Next generation sequencing and its application in deciphering head and neck cancer. *Oral Oncol.* 50, 247–253. doi:10.1016/j.oraloncology.2013.12.017

Jiao, Y., Killela, P. J., Reitman, Z. J., Rasheed, B. A., Heaphy, C. M., de Wilde, R. F., et al. (2012). Frequent *ATRX*, *CIC*, *FUBP1* and *IDH1* mutations refine the classification of malignant gliomas. *Oncotarget* 3, 709–722. doi:10.18632/oncotarget.588

Jonsson, P., Lin, A. L., Young, R. J., DiStefano, N. M., Hyman, D. M., Li, B. T., et al. (2019). Genomic correlates of disease progression and treatment response in prospectively characterized gliomas. *Clin. Cancer Res.* 25, 5537–5547. doi:10.1158/1078-0432.CCR-19-0032

Juratli, T. A., Stasik, S., Zolal, A., Schuster, C., Richter, S., Daubner, D., et al. (2018). *TERT* promoter mutation detection in cell-free tumor-derived DNA in patients with *IDH* wild-type glioblastomas: a pilot prospective study. *Clin. Cancer Res.* 24, 5282–5291. doi:10.1158/1078-0432.CCR-17-3717

Kaloshi, G., Benouaich-Amiel, A., Diakite, F., Taillibert, S., Lejeune, J., Laigle-Donadey, F., et al. (2007). Temozolomide for low-grade gliomas: predictive impact of 1p/19q loss on response and outcome. *Neurology* 68, 1831–1836. doi:10.1212/01.wnl.0000262034.26310.a2

Kang, S. Y., Kim, D. G., Kim, H., Cho, Y. A., Ha, S. Y., Kwon, G. Y., et al. (2022). Direct comparison of the next-generation sequencing and iTERT PCR methods for the diagnosis of TERT hotspot mutations in advanced solid cancers. *BMC Med. Genomics* 15, 25. doi:10.1186/s12920-022-01175-2

Kanzi, A. M., San, J. E., Chimukangara, B., Wilkinson, E., Fish, M., Ramsuran, V., et al. (2020). Next generation sequencing and bioinformatics analysis of family genetic inheritance. *Front. Genet.* 11, 544162. doi:10.3389/fgene.2020.544162

Khuong-Quang, D.-A., Buczkowicz, P., Rakopoulos, P., Liu, X.-Y., Fontebasso, A. M., Bouffet, E., et al. (2012). K27M mutation in histone H3.3 defines clinically and biologically distinct subgroups of pediatric diffuse intrinsic pontine gliomas. *Acta Neuropathol.* 124, 439–447. doi:10.1007/s00401-012-0998-0

Killela, P. J., Pirozzi, C. J., Healy, P., Reitman, Z. J., Lipp, E., Rasheed, B. A., et al. (2014). Mutations in *IDH1*, *IDH2*, and in the *TERT* promoter define clinically distinct subgroups of adult malignant gliomas. *Oncotarget* 5, 1515–1525. doi:10.18632/oncotarget.1765

Kono, N., and Arakawa, K. (2019). Nanopore sequencing: review of potential applications in functional genomics. *Dev. Growth Differ.* 61, 316–326. doi:10.1111/dgd.12608

Korshunov, A., Capper, D., Reuss, D., Schrimpf, D., Ryzhova, M., Hovestadt, V., et al. (2016). Histologically distinct neuroepithelial tumors with histone 3 G34 mutation are molecularly similar and comprise a single nosologic entity. *Acta Neuropathol.* 131, 137–146. doi:10.1007/s00401-015-1493-1

Lam, S. N., Zhou, Y. C., Chan, Y. M., Foo, C. M., Lee, P. Y., Mok, W. Y., et al. (2020). Comparison of target enrichment platforms for circulating tumor DNA detection. *Sci. Rep.* 10, 4124. doi:10.1038/s41598-020-60375-x

Larsson, C., Koch, J., Nygren, A., Janssen, G., Raap, A. K., Landegren, U., et al. (2004). *In situ* genotyping individual DNA molecules by target-primed rolling-circle amplification of padlock probes. *Nat. Methods* 1, 227–232. doi:10.1038/nmeth723

Lass, U., Hartmann, C., Capper, D., Herold-Mende, C., von Deimling, A., Meiboom, M., et al. (2013). Chromogenic *in situ* hybridization is a reliable alternative to fluorescence *in situ* hybridization for diagnostic testing of 1p and 19q loss in paraffin-embedded gliomas: CISH vs. FISH in 1p/19q analysis in gliomas. *Brain Pathol.* 23, 311–318. doi:10.1111/bpa.12003

Lee, A., Lee, S.-H., Jung, C. K., Park, G., Lee, K. Y., Choi, H. J., et al. (2018). Use of the ion AmpliSeq cancer hotspot panel in clinical molecular pathology laboratories for analysis of solid tumours: with emphasis on validation with relevant single molecular pathology tests and the oncomine Focus assay. *Pathology - Res. Pract.* 214, 713–719. doi:10.1016/j.prp.2018.03.009

Lee, J. C., Vivanco, I., Beroukhim, R., Huang, J. H. Y., Feng, W. L., DeBiasi, R. M., et al. (2006). Epidermal growth factor receptor activation in glioblastoma through novel missense mutations in the extracellular domain. *PLoS Med.* 3, e485. doi:10.1371/journal.pmed.0030485

Li, X., Wu, C., Chen, N., Gu, H., Yen, A., Cao, L., et al. (2016). PI3K/Akt/mTOR signaling pathway and targeted therapy for glioblastoma. *Oncotarget* 7, 33440–33450. doi:10.18632/oncotarget.7961

Lim, K. Y., Won, J. K., Park, C.-K., Kim, S.-K., Choi, S. H., Kim, T., et al. (2021). H3 G34-mutant high-grade glioma. *Brain Tumor Pathol.* 38, 4–13. doi:10.1007/s10014-020-00378-8

LiquidPlex ctDNA panel (2023). *Archer*. Available at: https://archerdx.com/research-products/solid-tumor-research/liquidplex/ (Accessed March 17, 2023).

Liu, J., Gao, L., Ji, B., Geng, R., Chen, J., Tao, X., et al. (2021). BCL7A as a novel prognostic biomarker for glioma patients. *J. Transl. Med.* 19, 335. doi:10.1186/s12967-021-03003-0

Liu, S., and Wang, J. (2022). Current and future perspectives of cell-free DNA in liquid biopsy. *CIMB* 44, 2695–2709. doi:10.3390/cimb44060184

Lomakin, A., Svedlund, J., Strell, C., Gataric, M., Shmatko, A., Rukhovich, G., et al. (2022). Spatial genomics maps the structure, nature and evolution of cancer clones. *Nature* 611, 594–602. doi:10.1038/s41586-022-05425-2

Lorenz, J., Rothhammer-Hampl, T., Zoubaa, S., Bumes, E., Pukrop, T., Kölbl, O., et al. (2020). A comprehensive DNA panel next generation sequencing approach supporting diagnostics and therapy prediction in neurooncology. *acta neuropathol. Commun.* 8, 124. doi:10.1186/s40478-020-01000-w

Louis, D. N., Perry, A., Wesseling, P., Brat, D. J., Cree, I. A., Figarella-Branger, D., et al. (2021). The 2021 WHO classification of tumors of the central nervous system: a summary. *Neuro-Oncology* 23, 1231–1251. doi:10.1093/neuonc/noab106

Loupakis, F., Sharma, S., Derouazi, M., Murgioni, S., Biason, P., Rizzato, M. D., et al. (2021). Detection of molecular residual disease using personalized circulating tumor DNA assay in patients with colorectal cancer undergoing resection of metastases. *JCO Precis. Oncol.* 5, 1166–1177. doi:10.1200/PO.21.00101

Lu, V. M., O'Connor, K. P., Shah, A. H., Eichberg, D. G., Luther, E. M., Komotar, R. J., et al. (2020). The prognostic significance of CDKN2A homozygous deletion in IDH-mutant lower-grade glioma and glioblastoma: a systematic review of the contemporary literature. *J. Neurooncol* 148, 221–229. doi:10.1007/s11060-020-03528-2

Mair, R., and Mouliere, F. (2022). Cell-free DNA technologies for the analysis of brain cancer. *Br. J. Cancer* 126, 371–378. doi:10.1038/s41416-021-01594-5

Majchrzak-Celińska, A., Dybska, E., and Barciszewska, A. (2020). DNA methylation analysis with methylation-sensitive high-resolution melting (MS-HRM) reveals gene panel for glioma characteristics. *CNS Neurosci. Ther.* 26, 1303–1314. doi:10.1111/cns.13443

Marchetti, A., Barbareschi, M., Barberis, M., Buglioni, S., Buttitta, F., Fassan, M., et al. (2021). Real-world data on NGS diagnostics: a survey from the Italian society of pathology (SIAPeC) NGS Network. *Pathologica* 113, 262–271. doi:10.32074/1591-951X-324

Martínez-Ricarte, F., Mayor, R., Martínez-Sáez, E., Rubio-Pérez, C., Pineda, E., Cordero, E., et al. (2018). Molecular diagnosis of diffuse gliomas through sequencing of cell-free circulating tumor DNA from cerebrospinal fluid. *Clin. Cancer Res.* 24, 2812–2819. doi:10.1158/1078-0432.CCR-17-3800

MCSTP - Overview (2023). *MayoComplete solid tumor panel, next-generation sequencing, tumor*. Available at: https://www.mayocliniclabs.com/test-catalog/Overview/606162#Overview (Accessed March 17, 2023).

Mesfin, F. B., and Al-Dhahir, M. A. (2022). "Gliomas," in *StatPearls* (Treasure Island (FL): StatPearls). Available at: http://www.ncbi.nlm.nih.gov/books/NBK441874/ (Accessed March 12, 2023).

MGMT Methylation Detection Kit (2023). *EntroGen, Inc*. Available at: http://entrogen.com/web3/glioblastoma-panel/ (Accessed March 16, 2023).

MGMT Promoter Methylation Analysis (2023). *NeoGenomics laboratories*. Available at: https://neogenomics.com/test-menu/mgmt-promoter-methylation-analysis (Accessed March 16, 2023).

Mignardi, M., Mezger, A., Qian, X., La Fleur, L., Botling, J., Larsson, C., et al. (2015). Oligonucleotide gap-fill ligation for mutation detection and sequencing *in situ*. *Nucleic Acids Res.* 43, e151. doi:10.1093/nar/gkv772

Miller, A. M., Shah, R. H., Pentsova, E. I., Pourmaleki, M., Briggs, S., Distefano, N., et al. (2019). Tracking tumour evolution in glioma through liquid biopsies of cerebrospinal fluid. *Nature* 565, 654–658. doi:10.1038/s41586-019-0882-3

Miller, J. J. (2022). Targeting IDH-mutant glioma. *Neurotherapeutics* 19, 1724–1732. doi:10.1007/s13311-022-01238-3

Molinaro, A. M., Taylor, J. W., Wiencke, J. K., and Wrensch, M. R. (2019). Genetic and molecular epidemiology of adult diffuse glioma. *Nat. Rev. Neurol.* 15, 405–417. doi:10.1038/s41582-019-0220-2

Mosrati, M. A., Malmström, A., Lysiak, M., Krysztofiak, A., Hallbeck, M., Milos, P., et al. (2015). *TERT* promoter mutations and polymorphisms as prognostic factors in primary glioblastoma. *Oncotarget* 6, 16663–16673. doi:10.18632/oncotarget.4389

Mulenga, R. M., Miano, D. W., Kaimoyo, E., Akello, J., Nzuve, F. M., Al Rwahnih, M., et al. (2020). First report of southern bean mosaic virus infecting common bean in Zambia. *Plant Dis.* 104, 1880. doi:10.1094/PDIS-11-19-2390-PDN

Muralidharan, K., Yekula, A., Small, J. L., Rosh, Z. S., Kang, K. M., Wang, L., et al. (2021). *TERT* promoter mutation analysis for blood-based diagnosis and monitoring of gliomas. *Clin. Cancer Res.* 27, 169–178. doi:10.1158/1078-0432.CCR-20-3083

Murnyak, B., and Huang, L. E. (2021). Association of TP53 alteration with tissue specificity and patient outcome of IDH1-mutant glioma. *Cells* 10, 2116. doi:10.3390/cells10082116

mutaFISHTM (2023). *Technologies - support - Abnova*. Available at: http://www.abnova.com/support/technologies.asp?switchfunctionid=%7B0EB5007F-F70F-4D70-BF2A-C5739393C48E%7D (Accessed March 16, 2023).

Na, K., Kim, H.-S., Shim, H. S., Chang, J. H., Kang, S.-G., and Kim, S. H. (2019). Targeted next-generation sequencing panel (TruSight tumor 170) in diffuse glioma: a single institutional experience of 135 cases. *J. Neurooncol* 142, 445–454. doi:10.1007/s11060-019-03114-1

Nakagawachi, T., Soejima, H., Urano, T., Zhao, W., Higashimoto, K., Satoh, Y., et al. (2003). Silencing effect of CpG island hypermethylation and histone modifications on O6-methylguanine-DNA methyltransferase (MGMT) gene expression in human cancer. *Oncogene* 22, 8835–8844. doi:10.1038/sj.onc.1207183

Napier, C. E., Huschtscha, L. I., Harvey, A., Bower, K., Noble, J. R., Hendrickson, E. A., et al. (2015). ATRX represses alternative lengthening of telomeres. *Oncotarget* 6, 16543–16558. doi:10.18632/oncotarget.3846

NeoTYPE DNA and RNA - Brain (2023). *NeoGenomics laboratories*. Available at: https://neogenomics.com/test-menu/neotyper-dna-rna-brain (Accessed March 17, 2023).

Newman, A. M., Bratman, S. V., To, J., Wynne, J. F., Eclov, N. C. W., Modlin, L. A., et al. (2014). An ultrasensitive method for quantitating circulating tumor DNA with broad patient coverage. *Nat. Med.* 20, 548–554. doi:10.1038/nm.3519

Newman, A. M., Lovejoy, A. F., Klass, D. M., Kurtz, D. M., Chabon, J. J., Scherer, F., et al. (2016). Integrated digital error suppression for improved detection of circulating tumor DNA. *Nat. Biotechnol.* 34, 547–555. doi:10.1038/nbt.3520

Next Generation Sequencing Capacity of India (2023). *Next generation sequencing capacity of India*. Available at: https://www.icmr.gov.in/cnextgenseq.html (Accessed March 19, 2023).

Next Generation Sequencing (2023). *Genotypic technology Pvt. Ltd*. Available at: https://www.genotypic.co.in/next-generation-sequencing/ (Accessed March 19, 2023).

Next Generation Sequencing (NGS) Clinical Exome Sequencing Panels Assays (2023). *HLA typing*. Available at: https://www.genes2me.com/next-generation-sequencing-clinical-panels (Accessed March 17, 2023).

Next-Generation Sequencing (NGS) Salary in India (2023). *PayScale*. Available at: https://www.payscale.com/research/IN/Skill=Next-Generation_Sequencing_(NGS)/Salary (Accessed March 19, 2023).

Ngs Targeted Hotspot Panel 16 Kit, (2023). *EntroGen, Inc*. Available at: http://entrogen.com/web3/ngs-targeted-hotspot-panel-16-kit/ (Accessed March 17, 2023).

Ni, X., Wu, W., Sun, X., Ma, J., Yu, Z., He, X., et al. (2022). Interrogating glioma-M2 macrophage interactions identifies Gal-9/Tim-3 as a viable target against *PTEN* -null glioblastoma. *Sci. Adv.* 8, eabl5165. doi:10.1126/sciadv.abl5165

Nikiforova, M. N., and Hamilton, R. L. (2011). Molecular diagnostics of gliomas. *Archives Pathology Laboratory Med.* 135, 558–568. doi:10.1043/2010-0649-RAIR.1

Nikiforova, M. N., Wald, A. I., Melan, M. A., Roy, S., Zhong, S., Hamilton, R. L., et al. (2016). Targeted next-generation sequencing panel (GlioSeq) provides comprehensive genetic profiling of central nervous system tumors. *Neuro Oncol.* 18, 379–387. doi:10.1093/neuonc/nov289

Nilsson, M., Malmgren, H., Samiotaki, M., Kwiatkowski, M., Chowdhary, B. P., and Landegren, U. (1994). Padlock probes: circularizing oligonucleotides for localized DNA detection. *Science* 265, 2085–2088. doi:10.1126/science.7522346

NONCP - Overview (2023). *Neuro-oncology expanded gene panel with rearrangement, tumor*. Available at: https://www.mayocliniclabs.com/test-catalog/overview/603047#Overview (Accessed March 17, 2023).

Normanno, N., Apostolidis, K., Wolf, A., Al Dieri, R., Deans, Z., Fairley, J., et al. (2022). Access and quality of biomarker testing for precision oncology in Europe. *Eur. J. Cancer* 176, 70–77. doi:10.1016/j.ejca.2022.09.005

NovoPM 2.0 (2023). *Novogene*. Available at: https://www.novogene.com/eu-en/services/clinical-diagnostics/clinical-panels/oncology/novopm-2-0/# (Accessed March 17, 2023).

NuProbe Launches Liquid Biopsy Pan-Cancer NGS Panel (2023). *Prnewswire*. Available at: https://www.prnewswire.com/news-releases/nuprobe-launches-liquid-biopsy-pan-cancer-ngs-panel-301231271.html (Accessed March 16, 2023).

Olawoye, I. B., Uwanibe, J. N., Kunle-Ope, C. N., Davies-Bolorunduro, O. F., Abiodun, T. A., Audu, R. A., et al. (2021). Whole genome sequencing of clinical samples reveals extensively drug resistant tuberculosis (XDR TB) strains from the Beijing lineage in Nigeria, West Africa. *Sci. Rep.* 11, 17387. doi:10.1038/s41598-021-96956-7

Olympios, N., Gilard, V., Marguet, F., Clatot, F., Di Fiore, F., and Fontanilles, M. (2021). TERT promoter alterations in glioblastoma: a systematic review. *Cancers* 13, 1147. doi:10.3390/cancers13051147

OncoDEEP (2023). *Comprehensive biomarker test*. Available at: https://www.oncodna.com/en/healthcare-providers/our-diagnostic-solutions/oncodeep/ (Accessed March 17, 2023).

Oncology Microarray (2023). *Targeted gene and region panel*. Available at: https://knightdxlabs.ohsu.edu/home/test-details?id=Oncology+Microarray+-+Targeted+Gene+and+Region+Panel (Accessed March 16, 2023).

Oncomine Focus Assay (2023). *Thermo Fisher scientific*. Available at: https://www.thermofisher.com/ru/ru/home/clinical/preclinical-companion-diagnostic-development/oncomine-oncology/oncomine-focus-assay.html (Accessed March 17, 2023).

Ostrom, Q. T., Cioffi, G., Gittleman, H., Patil, N., Waite, K., Kruchko, C., et al. (2019). CBTRUS statistical report: primary brain and other central nervous system tumors diagnosed in the United States in 2012–2016. *Neuro-Oncology* 21, v1–v100. doi:10.1093/neuonc/noz150

Ostrom, Q. T., Gittleman, H., Stetson, L., Virk, S. M., and Barnholtz-Sloan, J. S. (2015). "Epidemiology of gliomas," in *Current understanding and treatment of gliomas cancer treatment and research*. Editors J. Raizer and A. Parsa (Cham: Springer International Publishing), 1–14. doi:10.1007/978-3-319-12048-5_1

Pacia, C. P., Yuan, J., Yue, Y., Xu, L., Nazeri, A., Desai, R., et al. (2022). Sonobiopsy for minimally invasive, spatiotemporally-controlled, and sensitive detection of glioblastoma-derived circulating tumor DNA. *Theranostics* 12, 362–378. doi:10.7150/thno.65597

Panditharatna, E., Kilburn, L. B., Aboian, M. S., Kambhampati, M., Gordish-Dressman, H., Magge, S. N., et al. (2018). Clinically relevant and minimally invasive tumor surveillance of pediatric diffuse midline gliomas using patient-derived liquid biopsy. *Clin. Cancer Res.* 24, 5850–5859. doi:10.1158/1078-0432.CCR-18-1345

Peng, P., Cheng, F., Dong, Y., Chen, Z., Zhang, X., Guo, D., et al. (2021). High expression of TXNDC11 indicated unfavorable prognosis of glioma. *Transl. Cancer Res. TCR* 10, 5040–5051. doi:10.21037/tcr-21-1326

Personalis (2023). *NeXT Dx*. Personalis. Available at: https://www.personalis.com/products/next-dx/ (Accessed April 11, 2023).

Pesenti, C., Paganini, L., Fontana, L., Veniani, E., Runza, L., Ferrero, S., et al. (2017). Mass spectrometry-based assay for the molecular diagnosis of glioma: concomitant detection of chromosome 1p/19q codeletion, and *IDH1*, *IDH2*, and *TERT* mutation status. *Oncotarget* 8, 57134–57148. doi:10.18632/oncotarget.19103

Phillips, K. A., Douglas, M. P., Wordsworth, S., Buchanan, J., and Marshall, D. A. (2021). Availability and funding of clinical genomic sequencing globally. *BMJ Glob. Health* 6, e004415. doi:10.1136/bmjgh-2020-004415

Pienkowski, T., Kowalczyk, T., Garcia-Romero, N., Ayuso-Sacido, A., and Ciborowski, M. (2022). Proteomics and metabolomics approach in adult and pediatric glioma diagnostics. *Biochimica Biophysica Acta (BBA) - Rev. Cancer* 1877, 188721. doi:10.1016/j.bbcan.2022.188721

Pinkham, M. B., Telford, N., Whitfield, G. A., Colaco, R. J., O'Neill, F., and McBain, C. A. (2015). FISHing tips: what every clinician should know about 1p19q analysis in gliomas using fluorescence *in situ* hybridisation. *Clin. Oncol.* 27, 445–453. doi:10.1016/j.clon.2015.04.008

Plasmodium Diversity Network Africa, Ghansah, A., Kamau, E., Amambua-Ngwa, A., Ishengoma, D. S., Maiga-Ascofare, O., et al. (2019). Targeted next generation sequencing for malaria research in Africa: current status and outlook. *Malar. J.* 18, 324. doi:10.1186/s12936-019-2944-2

Plessers, S. (2023). *Cancer screening | CT-DNA. Kankerscreening - cancer screening (TURI - BOC - CTDNA)*. Available at: https://www.kankerscreening.net/ct-dna/?lang=en (Accessed March 17, 2023).

Poonia, A., Mishra, S., Sirohi, P., Chaudhary, R., Germain, H., and Chauhan, H. (2023). *Improved thermotolerance in transgenic barley by overexpressing a heat shock factor gene (TaHsfA6b) from wheat*. doi:10.22541/au.158057216.61888397

PreciseTM Tumor (2023). *Molecular profile testing | Myriad genetics*. Available at: https://myriad.com/genetic-tests/precise-tumor/ (Accessed March 16, 2023).

Pruneri, G., De Braud, F., Sapino, A., Aglietta, M., Vecchione, A., Giusti, R., et al. (2021). Next-generation sequencing in clinical practice: is it a cost-saving alternative to a single-gene testing approach? *PharmacoEconomics Open* 5, 285–298. doi:10.1007/s41669-020-00249-0

RealTime IDH1 (2023). *Abbott molecular*. Available at: https://www.molecular.abbott/us/en/products/oncology/realtime-idh1 (Accessed March 16, 2023).

RealTime IDH2 (2023). *Abbott molecular*. Available at: https://www.molecular.abbott/us/en/products/oncology/realtime-idh2 (Accessed March 16, 2023).

Reitman, Z. J., and Yan, H. (2010). Isocitrate dehydrogenase 1 and 2 mutations in cancer: alterations at a crossroads of cellular metabolism. *JNCI J. Natl. Cancer Inst.* 102, 932–941. doi:10.1093/jnci/djq187

Richard, S., Tachon, G., Milin, S., Wager, M., and Karayan-Tapon, L. (2020). Dual *MGMT* inactivation by promoter hypermethylation and loss of the long arm of chromosome 10 in glioblastoma. *Cancer Med.* 9, 6344–6353. doi:10.1002/cam4.3217

Roy, S., Agnihotri, S., El Hallani, S., Ernst, W. L., Wald, A. I., Santana dos Santos, L., et al. (2019). Clinical utility of GlioSeq next-generation sequencing test in pediatric and young adult patients with brain tumors. *J. Neuropathology Exp. Neurology* 78, 694–702. doi:10.1093/jnen/nlz055

Ruano, Y., Mollejo, M., de Lope, A. R., Hernández-Moneo, J. L., Martínez, P., and Meléndez, B. (2010). "Microarray-based comparative genomic hybridization (Array-CGH) as a useful tool for identifying genes involved in glioblastoma (GB)," in *Cancer susceptibility methods in molecular biology*. Editor M. Webb (Totowa, NJ: Humana Press), 35–45. doi:10.1007/978-1-60761-759-4_3

Sa, J. K., Kim, S. H., Lee, J.-K., Cho, H. J., Shin, Y. J., Shin, H., et al. (2019). Identification of genomic and molecular traits that present therapeutic vulnerability to HGF-targeted therapy in glioblastoma. *Neuro-Oncology* 21, 222–233. doi:10.1093/neuonc/noy105

Sahara, N., Hartanto, R., Yoshuantari, N., Dananjoyo, K., Widodo, I., Malueka, R., et al. (2021). Diagnostic accuracy of immunohistochemistry in detecting MGMT methylation status in patients with glioma. *Asian Pac J. Cancer Prev.* 22, 3803–3808. doi:10.31557/APJCP.2021.22.12.3803

Saito, K., Yokogami, K., Maekawa, K., Sato, Y., Yamashita, S., Matsumoto, F., et al. (2021). High-resolution melting effectively pre-screens for TP53 mutations before direct sequencing in patients with diffuse glioma. *Hum. Cell.* 34, 644–653. doi:10.1007/s13577-020-00471-2

Sajid, M., Srivastava, S., Kumar, A., Kumar, A., Singh, H., and Bharadwaj, M. (2021). Bacteriome of moist smokeless tobacco products consumed in India with emphasis on the predictive functional potential. *Front. Microbiol.* 12, 784841. doi:10.3389/fmicb.2021.784841

Salwan, R., Sharma, V., Sharma, A., and Singh, A. (2020). Molecular imprints of plant beneficial Streptomyces sp. AC30 and AC40 reveal differential capabilities and strategies to counter environmental stresses. *Microbiol. Res.* 235, 126449. doi:10.1016/j.micres.2020.126449

Shah, M., Takayasu, T., Zorofchian Moghadamtousi, S., Arevalo, O., Chen, M., Lan, C., et al. (2021). Evaluation of the oncomine pan-cancer cell-free assay for analyzing circulating tumor DNA in the cerebrospinal fluid in patients with central nervous system malignancies. *J. Mol. Diagnostics* 23, 171–180. doi:10.1016/j.jmoldx.2020.10.013

Sharaf, R., Pavlick, D. C., Frampton, G. M., Cooper, M., Jenkins, J., Danziger, N., et al. (2021). FoundationOne CDx testing accurately determines whole arm 1p19q codeletion status in gliomas. *Neuro-Oncology Adv.* 3, vdab017. doi:10.1093/noajnl/vdab017

Sharma, H. S. (2009). "Preface: new concepts of psychostimulants induced neurotoxicity," in *International review of neurobiology* (Elsevier), xv–xvi. doi:10.1016/S0074-7742(09)88019-7

Shendure, J., and Ji, H. (2008). Next-generation DNA sequencing. *Nat. Biotechnol.* 26, 1135–1145. doi:10.1038/nbt1486

Shin, H., Sa, J. K., Bae, J. S., Koo, H., Jin, S., Cho, H. J., et al. (2020). Clinical targeted next-generation sequencing panels for detection of somatic variants in gliomas. *Cancer Res. Treat.* 52, 41–50. doi:10.4143/crt.2019.036

Slatko, B. E., Gardner, A. F., and Ausubel, F. M. (2018). Overview of next-generation sequencing technologies. *Curr. Protoc. Mol. Biol.* 122, e59. doi:10.1002/cpmb.59

Śledzińska, P., Bebyn, M. G., Furtak, J., Kowalewski, J., and Lewandowska, M. A. (2021). Prognostic and predictive biomarkers in gliomas. *IJMS* 22, 10373. doi:10.3390/ijms221910373

Śledzińska, P., Bebyn, M., Szczerba, E., Furtak, J., Harat, M., Olszewska, N., et al. (2022). Glioma 2021 WHO classification: the superiority of NGS over IHC in routine diagnostics. *Mol. Diagn Ther.* 26, 699–713. doi:10.1007/s40291-022-00612-3

SOPHiA Solid Tumor Solutions (2023). *SOPHiA GENETICS*. Available at: https://www.sophiagenetics.com/clinical/oncology/solid-tumors/sophia-solid-tumor-solutions/ (Accessed March 18, 2023).

Stichel, D., Ebrahimi, A., Reuss, D., Schrimpf, D., Ono, T., Shirahata, M., et al. (2018). Distribution of EGFR amplification, combined chromosome 7 gain and chromosome 10 loss, and TERT promoter mutation in brain tumors and their potential for the reclassification of IDHwt astrocytoma to glioblastoma. *Acta Neuropathol.* 136, 793–803. doi:10.1007/s00401-018-1905-0

Stupp, R., Mason, W. P., van den Bent, M. J., Weller, M., Fisher, B., Taphoorn, M. J. B., et al. (2005). Radiotherapy plus concomitant and adjuvant temozolomide for glioblastoma. *N. Engl. J. Med.* 352, 987–996. doi:10.1056/NEJMoa043330

Sturm, D., Bender, S., Jones, D. T. W., Lichter, P., Grill, J., Becher, O., et al. (2014). Paediatric and adult glioblastoma: multiform (epi)genomic culprits emerge. *Nat. Rev. Cancer* 14, 92–107. doi:10.1038/nrc3655

Sturm, D., Witt, H., Hovestadt, V., Khuong-Quang, D.-A., Jones, D. T. W., Konermann, C., et al. (2012). Hotspot mutations in H3F3A and IDH1 define distinct epigenetic and biological subgroups of glioblastoma. *Cancer Cell.* 22, 425–437. doi:10.1016/j.ccr.2012.08.024

Swift, A., Heale, R., and Twycross, A. (2020). What are sensitivity and specificity? *Evid. Based Nurs.* 23, 2–4. doi:10.1136/ebnurs-2019-103225

Switzeny, O. J., Christmann, M., Renovanz, M., Giese, A., Sommer, C., and Kaina, B. (2016). MGMT promoter methylation determined by HRM in comparison to MSP and pyrosequencing for predicting high-grade glioma response. *Clin. Epigenet* 8, 49. doi:10.1186/s13148-016-0204-7

Talbert, P. B., and Henikoff, S. (2010). Histone variants — Ancient wrap artists of the epigenome. *Nat. Rev. Mol. Cell. Biol.* 11, 264–275. doi:10.1038/nrm2861

Tanboon, J., Williams, E. A., and Louis, D. N. (2016). The diagnostic use of immunohistochemical surrogates for signature molecular genetic alterations in gliomas. *J. Neuropathol. Exp. Neurol.* 75, 4–18. doi:10.1093/jnen/nlv009

Tang, Y., Li, Y., Wang, W., Lizaso, A., Hou, T., Jiang, L., et al. (2020). Tumor mutation burden derived from small next generation sequencing targeted gene panel as an initial screening method. *Transl. Lung Cancer Res.* 9, 71–81. doi:10.21037/tlcr.2019.12.27

Tao, Z., Shi, A., Li, R., Wang, Y., Wang, X., and Zhao, J. (2017). Microarray bioinformatics in cancer-a review. *J. BUON* 22, 838–843.

Tawfik, S. A., Azab, M. M., Ahmed, A. A. A., and Fayyad, D. M. (2018). Illumina MiSeq sequencing for preliminary analysis of microbiome causing primary endodontic infections in Egypt. *Int. J. Microbiol.* 2018, 2837328–2837415. doi:10.1155/2018/2837328

Tempus xF (2023). *Clinical test - NIH genetic testing Registry (GTR) - NCBI*. Available at: https://www.ncbi.nlm.nih.gov/gtr/tests/569040/ (Accessed March 16, 2023).

TERT promoter -124 mutation Quantification kit (2023). *JBS science*. Available at: https://jbs-science.com/pcr-quantification-kits/3-tert-promoter-124-mutation-quantification-kit/ (Accessed March 16, 2023).

Tesileanu, C. M. S., Vallentgoed, W. R., French, P. J., and van den Bent, M. J. (2022). Molecular markers related to patient outcome in patients with IDH-mutant astrocytomas grade 2 to 4: a systematic review. *Eur. J. Cancer* 175, 214–223. doi:10.1016/j.ejca.2022.08.016

The Cancer Genome Atlas Research Network, Brat, D. J., Verhaak, R. G., Aldape, K. D., Yung, W. K, Salama, S. R., Cooper, L. A., et al. (2015). Comprehensive, integrative genomic analysis of diffuse lower-grade gliomas. *N. Engl. J. Med.* 372, 2481–2498. doi:10.1056/NEJMoa1402121

The MassARRAY System from Agena Bioscience (2023). *The MassARRAY system from Agena bioscience*. Available at: https://www.agenabio.com/products/massarray-system/ (Accessed March 16, 2023).

therascreen IDH1/2 RGQ PCR Kit CE (2023). *Therascreen IDH1/2 RGQ PCR Kit CE*. Available at: https://www.qiagen.com/de/products/diagnostics-and-clinical-research/oncology/therascreen-solid-tumor/therascreen-idh1-2-rgq-pcr-kit-ce (Accessed March 16, 2023).

Tirrò, E., Massimino, M., Broggi, G., Romano, C., Minasi, S., Gianno, F., et al. (2022). A custom DNA-based NGS panel for the molecular characterization of patients with diffuse gliomas: diagnostic and therapeutic applications. *Front. Oncol.* 12, 861078. doi:10.3389/fonc.2022.861078

TruSight Oncology Comprehensive (EU) (2023). *TruSight oncology comprehensive*. Available at: https://emea.illumina.com/products/by-type/ivd-products/trusight-oncology-comprehensive.html (Accessed March 16, 2023).

Turner, K. M., Deshpande, V., Beyter, D., Koga, T., Rusert, J., Lee, C., et al. (2017). Extrachromosomal oncogene amplification drives tumour evolution and genetic heterogeneity. *Nature* 543, 122–125. doi:10.1038/nature21356

Valkenburg, K. C., Caropreso, V., Fox, J., Gault, C., Georgiadis, A., Gerding, K. M., et al. (2022). Abstract 72: comprehensive liquid biopsy profiling enabled by PGDx elio plasmacomplete to facilitate precision oncology through decentralized access to testing. *Cancer Res.* 82, 72. doi:10.1158/1538-7445.AM2022-72

Van Den Bent, M. J., Bromberg, J. E. C., and Buckner, J. (2016). "Low-grade and anaplastic oligodendroglioma," in *Handbook of clinical neurology* (Elsevier), 361–380. doi:10.1016/B978-0-12-802997-8.00022-0

van Gerven, M. R., Bozsaky, E., Matser, Y. A. H., Vosseberg, J., Taschner-Mandl, S., Koster, J., et al. (2022). Mutational spectrum of *ATRX* aberrations in neuroblastoma and associated patient and tumor characteristics. *Cancer Sci.* 113, 2167–2178. doi:10.1111/cas.15363

Varn, F. S., Johnson, K. C., Martinek, J., Huse, J. T., Nasrallah, M. P., Wesseling, P., et al. (2022). Glioma progression is shaped by genetic evolution and microenvironment interactions. *Cell.* 185, 2184–2199.e16. doi:10.1016/j.cell.2022.04.038

Vasseur, D., Sassi, H., Bayle, A., Tagliamento, M., Besse, B., Marzac, C., et al. (2022). Next-generation sequencing on circulating tumor DNA in advanced solid cancer: swiss army knife for the molecular tumor board? A review of the literature focused on FDA approved test. *Cells* 11, 1901. doi:10.3390/cells11121901

Vendrell, J. A., Quantin, X., Serre, I., and Solassol, J. (2020). Combination of tissue and liquid biopsy molecular profiling to detect transformation to small cell lung carcinoma during osimertinib treatment. *Ther. Adv. Med. Oncol.* 12, 1758835920974192. doi:10.1177/1758835920974192

Vestergaard, L. K., Oliveira, D. N. P., Poulsen, T. S., Høgdall, C. K., and Høgdall, E. V. (2021). Oncomine™ comprehensive assay v3 vs. Oncomine™ comprehensive assay plus. *Cancers* 13, 5230. doi:10.3390/cancers13205230

Vuong, H. G., Nguyen, T. Q., Ngo, T. N. M., Nguyen, H. C., Fung, K.-M., and Dunn, I. F. (2020). The interaction between TERT promoter mutation and MGMT promoter methylation on overall survival of glioma patients: a meta-analysis. *BMC Cancer* 20, 897. doi:10.1186/s12885-020-07364-5

Vuong, H. G., Tran, T. T. K., Ngo, H. T. T., Pham, T. Q., Nakazawa, T., Fung, K. -M., et al. (2019). Prognostic significance of genetic biomarkers in isocitrate dehydrogenase-wild-type lower-grade glioma: the need to further stratify this tumor entity – a meta-analysis. *Eur. J. Neurol.* 26, 379–387. doi:10.1111/ene.13826

Wang, G.-M., Cioffi, G., Patil, N., Waite, K. A., Lanese, R., Ostrom, Q. T., et al. (2022a). Importance of the intersection of age and sex to understand variation in incidence and survival for primary malignant gliomas. *Neuro-Oncology* 24, 302–310. doi:10.1093/neuonc/noab199

Wang, L., Shao, L., Li, H., Yao, K., Duan, Z., Zhi, C., et al. (2022b). Histone H3.3 G34-mutant diffuse gliomas in adults. *Am. J. Surg. Pathology* 46, 249–257. doi:10.1097/PAS.0000000000001781

Wei, B., Kang, J., Kibukawa, M., Arreaza, G., Maguire, M., Chen, L., et al. (2022). Evaluation of the TruSight oncology 500 assay for routine clinical testing of tumor mutational burden and clinical utility for predicting response to pembrolizumab. *J. Mol. Diagnostics* 24, 600–608. doi:10.1016/j.jmoldx.2022.01.008

Weller, M., Stupp, R., Hegi, M. E., van den Bent, M., Tonn, J. C., Sanson, M., et al. (2012). Personalized care in neuro-oncology coming of age: why we need MGMT and 1p/19q testing for malignant glioma patients in clinical practice. *Neuro-Oncology* 14, iv100–iv108. doi:10.1093/neuonc/nos206

Weller, M., van den Bent, M., Preusser, M., Le Rhun, E., Tonn, J. C., Minniti, G., et al. (2021). EANO guidelines on the diagnosis and treatment of diffuse gliomas of adulthood. *Nat. Rev. Clin. Oncol.* 18, 170–186. doi:10.1038/s41571-020-00447-z

Wen, S., Wang, G., Yang, Z., Wang, Y., Rao, M., Lu, Q., et al. (2020). Next-generation sequencing combined with conventional sanger sequencing reveals high molecular diversity in actinidia virus 1 populations from kiwifruit grown in China. *Front. Microbiol.* 11, 602039. doi:10.3389/fmicb.2020.602039

Wirsching, H.-G., and Weller, M. (2016). The role of molecular diagnostics in the management of patients with gliomas. *Curr. Treat. Options Oncol.* 17, 51. doi:10.1007/s11864-016-0430-4

Wolter, M., Felsberg, J., Malzkorn, B., Kaulich, K., and Reifenberger, G. (2022). Droplet digital PCR-based analyses for robust, rapid, and sensitive molecular diagnostics of gliomas. *acta neuropathol. Commun.* 10, 42. doi:10.1186/s40478-022-01335-6

Wu, X., Zhao, J., Yang, L., Nie, X., Wang, Z., Zhang, P., et al. (2022). Next-generation sequencing reveals age-dependent genetic underpinnings in lung adenocarcinoma. *J. Cancer* 13, 1565–1572. doi:10.7150/jca.65370

Yang, K., Wu, Z., Zhang, H., Zhang, N., Wu, W., Wang, Z., et al. (2022). Glioma targeted therapy: insight into future of molecular approaches. *Mol. Cancer* 21, 39. doi:10.1186/s12943-022-01513-z

Yang, Y., Zhang, Y., Zhao, D., Li, X., and Ma, T. (2023). A novel PRKAR1A::MET fusion dramatic response to crizotinib in a patient with unresectable lung cancer. *Clin. Lung Cancer* 24, e50–e54. doi:10.1016/j.cllc.2022.10.001

Ye, J., Ma, Y., Ou, Q., Yan, J., Ye, B., and Li, Y. (2022). Long-term clinical benefit in EGFR-mutant lung adenocarcinoma with local squamous cell carcinoma transformation after EGFR TKI resistance: a case report. *Front. Oncol.* 12, 883367. doi:10.3389/fonc.2022.883367

Yokogami, K., Yamasaki, K., Matsumoto, F., Yamashita, S., Saito, K., Tacheva, A., et al. (2018). Impact of PCR-based molecular analysis in daily diagnosis for the patient with gliomas. *Brain Tumor Pathol.* 35, 141–147. doi:10.1007/s10014-018-0322-3

Zacher, A., Kaulich, K., Stepanow, S., Wolter, M., Köhrer, K., Felsberg, J., et al. (2017). Molecular diagnostics of gliomas using next generation sequencing of a glioma-tailored gene panel: next generation molecular diagnostics of gliomas. *Brain Pathol.* 27, 146–159. doi:10.1111/bpa.12367

Zeng, H.-H., Yang, Z., Qiu, Y.-B., Bashir, S., Li, Y., and Xu, M. (2022). Detection of a novel panel of 24 genes with high frequencies of mutation in gastric cancer based on next-generation sequencing. *WJCC* 10, 4761–4775. doi:10.12998/wjcc.v10.i15.4761

Zhang, R., Han, J., Daniels, D., Huang, H., and Zhang, Z. (2016). Detecting the H3F3A mutant allele found in high-grade pediatric glioma by real-time PCR. *J. Neurooncol* 126, 27–36. doi:10.1007/s11060-015-1936-5

Zhu, Y., Allard, G. M., Ericson, N. G., George, T. C., Kunder, C. A., and Lowe, A. C. (2021). Identification and characterization of effusion tumor cells (ETCs) from remnant pleural effusion specimens. *Cancer Cytopathol.* 129, 893–906. doi:10.1002/cncy.22483

frontiers | Frontiers in Molecular Neuroscience

TYPE Original Research
PUBLISHED 27 October 2023
DOI 10.3389/fnmol.2023.1276726

OPEN ACCESS

EDITED BY
Gal Bitan,
University of California, Los Angeles, United States

REVIEWED BY
Jennifer McGuire,
University of Cincinnati, United States
Michelle Theus,
Virginia Tech, United States

*CORRESPONDENCE
Feng Zheng
✉ dr.feng.zheng@gmail.com
Hefan He
✉ 15860905262@163.com;
✉ 15860905262@fjmu.edu.cn

RECEIVED 12 August 2023
ACCEPTED 11 October 2023
PUBLISHED 27 October 2023

CITATION
Chen X, Wang X, Liu Y, Guo X, Wu F, Yang Y, Hu W, Zheng F and He H (2023) Plasma D-dimer levels are a biomarker for in-hospital complications and long-term mortality in patients with traumatic brain injury. *Front. Mol. Neurosci.* 16:1276726. doi: 10.3389/fnmol.2023.1276726

Plasma D-dimer levels are a biomarker for in-hospital complications and long-term mortality in patients with traumatic brain injury

Xinli Chen[1], Xiaohua Wang[1], Yingchao Liu[1], Xiumei Guo[2], Fan Wu[1], Yushen Yang[1], Weipeng Hu[2], Feng Zheng[2]* and Hefan He[1]*

[1]Department of Anesthesiology, The Second Affiliated Hospital of Fujian Medical University, Quanzhou, China, [2]Department of Neurosurgery, The Second Affiliated Hospital of Fujian Medical University, Quanzhou, China

Introduction: Traumatic brain injury (TBI) is a major health concern worldwide. D-dimer levels, commonly used in the diagnosis and treatment of neurological diseases, may be associated with adverse events in patients with TBI. However, the relationship between D-dimer levels, TBI-related in-hospital complications, and long-term mortality in patients with TBI has not been investigated. Here, examined whether elevated D-dimer levels facilitate the prediction of in-hospital complications and mortality in patients with TBI.

Methods: Overall, 1,338 patients with TBI admitted to our institute between January 2016 and June 2022 were retrospectively examined. D-dimer levels were assessed within 24 h of admission, and propensity score matching was used to adjust for baseline characteristics.

Results: Among the in-hospital complications, high D-dimer levels were associated with electrolyte metabolism disorders, pulmonary infections, and intensive care unit admission ($p < 0.05$). Compared with patients with low (0.00–1.54 mg/L) D-dimer levels, the odds of long-term mortality were significantly higher in all other patients, including those with D-dimer levels between 1.55 mg/L and 6.35 mg/L (adjusted hazard ratio [aHR] 1.655, 95% CI 0.9632.843), 6.36 mg/L and 19.99 mg/L (aHR 2.38, 95% CI 1.416–4.000), and >20 mg/L (aHR 3.635, 95% CI 2.195–6.018; $p < 0.001$). D-dimer levels were positively correlated with the risk of death when the D-dimer level reached 6.82 mg/L.

Conclusion: Overall, elevated D-dimer levels at admission were associated with adverse outcomes and may predict poor prognosis in patients with TBI. Our findings will aid in the acute diagnosis, classification, and management of TBI.

KEYWORDS

traumatic brain injury, D-dimer, biomarker, in-hospital complications, long-term mortality, prognosis prediction

1. Introduction

Traumatic brain injury (TBI) is a major health concern worldwide, affecting an estimated 54–60 million people annually. Moreover, according to the European Union, TBI contributes to 37% of all injury-related deaths worldwide (Vos et al., 2016; Maas et al., 2022). TBI is a systemic disease that can lead to organ dysfunction, including infections, respiratory and renal failure, myocardial injury, and multiple organ dysfunction in the acute phase, thereby increasing the length of hospital stays and costs (Stocchetti and Zanier, 2016). After discharge, many patients with TBI require long-term rehabilitation to address physical disability, cognitive impairment, and psychological disorders, which impose considerable economic burdens on families and society (Wiles et al., 2023). In addition, the poor prognosis of TBI substantially impacts patients, families, and healthcare providers. Therefore, early assessment of TBI is crucial for identifying critically ill patients, guiding treatment decisions, and establishing realistic expectations.

In clinical management, repeated computed tomography (CT) and the Glasgow Coma Scale (GCS) score aid in the evaluation of TBI. However, CT scans expose patients to ionizing radiation, and the potential long-term effects on children and pregnant women remain unclear. Furthermore, patients with severe TBI face risks during transportation and CT examinations (Kamiya et al., 2015; Riemann et al., 2023). The GCS score, determined based on the patient's symptoms and the evaluator's judgment, does not provide an accurate reflection of the extent of brain injury (Maas et al., 2017). Thus, at present, the commonly used diagnostic and classification methods are insufficient for all TBI groups. A convenient and sensitive objective index that reflects injury severity is required to supplement the diagnosis and prognosis of TBI (Maas et al., 2022; Nelson et al., 2023; Riemann et al., 2023).

Nearly two-thirds of patients with severe TBI have abnormalities on coagulation tests at admission (Maegele et al., 2017). Prior studies have shown that coagulation disorders strongly predict TBI prognosis, and coagulation disorders increase mortality risk and adverse outcomes by nine and 30 times, respectively, in patients with TBI (Greuters et al., 2011; Maegele et al., 2017). Coagulation dysfunction after TBI may be secondary to tissue damage, hypotension, and upregulation of inflammation, leading to an imbalance of coagulation and fibrinolysis pathways (Anderson et al., 2021). The coagulation system, which forms a thrombus to stop bleeding, and the fibrinolytic system, which dissolves a thrombus following tissue repair, work in harmony to establish hemostasis mechanisms. However, because of the exhaustion of coagulation factors and amplification of the fibrinolytic system in cases of severe trauma, the fibrinolytic system tends to become relatively overactive. This could lead to catastrophic and progressing coagulopathy (Maegele et al., 2017). After TBI, coagulation and fibrinolysis imbalances lead to a bleeding tendency, which increases the risk of progressive bleeding injury and intracranial hemorrhage and worsens the prognosis (Folkerson et al., 2015).

Cross-linked fibrin produces D-dimers. In a study of TBI-induced coagulation process changes, D-dimer levels reacted rapidly and increased within a few minutes of TBI (Zhang et al., 2018). Studies have found that brain-derived cellular microvesicles, a type of microvesicle that is rich in tissue factors and phosphatidylserine, are rapidly released into the circulation through the damaged blood–brain barrier after TBI, inducing systemic hypercoagulability and rapidly developing into consumptive coagulation dysfunction (Tian et al., 2015). This change is consistent with the time shift in which D-dimer peaks rapidly after TBI, while prolonged prothrombin time and partial prothrombin kinase peak later (Zhang et al., 2018). According to previous studies, patients with brain parenchymal damage show a significant correlation between serum D-dimer levels and tissue factor levels (Suehiro et al., 2019). Compared to other tissues, the brain parenchyma has a higher tissue factor per unit weight. This increased tissue factor per unit weight makes the brain parenchyma more susceptible to conspicuous coagulation and the related hyperfibrinolysis, especially in cases of severe head trauma (Echigo et al., 2017). We speculate that the brain-derived cellular microvesicles and tissue factor may be the reason for the early increase in D-dimer in TBI.

D-dimer is commonly used to diagnose and treat neurological diseases because it is inexpensive and convenient. Elevated levels of D-dimer have been observed in the peripheral blood of patients with central nervous system diseases such as aneurysmal subarachnoid hemorrhage (Fang et al., 2022) and stroke (Qiu et al., 2023), indicating activation of systemic coagulation. Furthermore, D-dimer assessment is also useful for evaluating venous thrombosis, pulmonary embolism, and early diffuse intravascular coagulation following TBI (Wada et al., 2017; Chen et al., 2023). Therefore, it is worth investigating whether D-dimer levels are associated with adverse events during hospitalization and long-term prognosis after discharge in patients with TBI.

Recent studies have linked hyperfibrinolysis to tissue damage and trauma severity in patients with and without TBI (Hayakawa et al., 2017). Among patients with TBI, those with elevated peripheral blood D-dimer levels were found to be at risk of progressive hemorrhagic injury (Xu et al., 2020). Furthermore, D-dimer levels were found to predict a poor neurological prognosis 6 months after discharge in patients with isolated TBI (Fujiwara et al., 2022). Additionally, measurement of the D-dimer level can reduce unnecessary CT scans for head trauma assessment in children with TBI (Berger et al., 2015; Langness et al., 2018). Understanding the prognostic factors aids in TBI severity assessment and treatment planning. However, the relationship between D-dimer levels, TBI in-hospital complications, and long-term mortality in patients with TBI have not yet been investigated. These relationships should be studied to improve the diagnosis and treatment of brain trauma. Here, we hypothesized that D-dimer levels are associated with in-hospital complication rates and long-term mortality in patients. This large single-center cohort study examined the relationship between D-dimer levels, TBI complications, and mortality rates. This is the first study to explore this association.

2. Materials and methods

2.1. Study design

In this retrospective, single-center cohort study, patient data were obtained from the electronic medical records of patients admitted to the Second Affiliated Hospital of Fujian Medical University between January 2016 and June 2022. Clinical features and results were obtained from the electronic medical records and reviewed by a trained team of physicians. The data collected included details on sex, age, pre-existing medical conditions, clinical test results, clinical diagnosis and treatment, complications, and long-term follow-up.

This study adhered to the tenets of the Declaration of Helsinki and was approved by the Ethics Committee of the Second Affiliated Hospital of Fujian Medical University (2022, No. 523). Each patient or their authorized representative was verbally informed about the purpose of the study and the potential risks of participating at the time of admission and agreed to an anonymous analysis of personal data for scientific purposes. Referring to other retrospective study designs, the requirement for informed consent can be waived for anonymous data (Filion et al., 2016). As a supplement to the informed consent procedure, the patients or their authorized signed the informed consent form at the last follow-up of each patient.

2.2. Patient selection

The inclusion criteria for this study were as follows: (1) patients diagnosed with TBI by neurosurgeons based on neuroimaging and managed in accordance with the "Guidelines for the Management of Severe Traumatic Brain Injury" and (2) patients without severe trauma to other organs.

The exclusion criteria were as follows: (1) patients with a history of coagulation disorders; (2) patients who received anticoagulant therapy or blood replacement therapy that may lead to coagulopathy before admission; (3) patients with diseases that affect D-dimer levels, such as malignant tumors, uremia, cirrhosis, and immune system diseases; (4) lack of D-dimer test results within 24 h of admission; (5) incomplete medical records; and (6) loss to follow-up.

2.3. D-dimer measurement

For this study, the exposure variable was the concentration of D-dimer in the blood. Blood samples were collected from patients with TBI within 24 h of admission. The patients were divided into four groups according to their D-dimer levels. As the upper limit of the detection machine was 20 mg/L, the highest D-dimer level group had D-dimer levels higher than 20 mg/L; patients with D-dimer levels below 20 mg/L were divided into three groups according to the percentile method. Finally, the baseline cut points of the four groups were 0.00–1.54 (n = 326), 1.55–6.35 (n = 325), 6.36–19.99 (n = 324), and ≥ 20.00 mg/L (n = 363).

2.4. Outcome measures

The primary outcome was long-term mortality (defined as mortality at the longest follow-up). Secondary outcomes were 1-year mortality (defined as mortality at the 1-year follow-up), 1-month mortality (defined as mortality at the 1-month follow-up), and in-hospital complications. In-hospital complications included serum electrolyte disorder, hypoproteinemia, cardiac complications (including cardiac insufficiency, arrhythmia, myocardial damage), urinary complications (renal insufficiency, urinary tract infection, diabetes insipidus), traumatic coagulopathy, pulmonary infection, admission to the intensive care unit (ICU), gastrointestinal complications (gastrointestinal dysfunction, gastrointestinal infection, gastrointestinal ulcer, gastrointestinal perforation, gastrointestinal bleeding), hypohepatia, stress hyperglycemia, deep vein thrombosis, seizures, and intracranial infection.

2.5. Follow-up

Patients were discharged between January 1, 2016, and May 31, 2022, and the follow-up ended on December 31, 2022. The average follow-up time was 2.8 years, ranging from 0.5 to 6.9 years. According to the follow-up guidelines for discharged patients in our research center, each patient was followed up by a doctor at 1 month, 3 months, 6 months, and 1 year after discharge, and their health status was recorded; the surviving patients who had been discharged for more than 1 year were followed up at least once a year. If the patient died, the follow-up was stopped and the date of death was recorded.

2.6. Data collection and clinical assessment

Medical records of patients with TBI were retrospectively analyzed. We extracted the following information: demographic data (age and sex), medical history (hypertension and diabetes), Glasgow Coma Scale (GCS) score at admission, and whether surgery was performed in this hospital. Laboratory test data were also collected within 24 h of admission, including the D-dimer concentration, hemoglobin (HB) concentration, platelet (Plt) count, fibrinogen (Fib) concentration, activated partial thromboplastin time (APTT), thrombin time (TT), and prothrombin time (PT). We also recorded the occurrence of complications at the hospital.

2.7. Statistical analysis

R version 4.0.3 (R Core Team, 2020) and IBM SPSS 26 (IBM Corporation, 2019) were used for all statistical analyses. Continuous baseline data are presented as mean with the standard deviation and were compared using analysis of variance. Chi-square tests were used to compare the counts (frequencies) of categorical variables. $p < 0.05$ was considered to indicate statistical significance in all two-sided significance tests. For categorical variables, all missing values were encoded as other variables, and multiple inferences were used for continuous variables.

Propensity score matching (PSM) reduced the bias of confounding variables (age, GCS score, and surgical treatment) and other important biomarkers (HB concentration, Plt count, fibrinogen concentration, APTT, TT, and PT). The similar groups were matched 1:1, and the matching tolerance was 0.20 SD. D-dimer levels and patient factors determined that a logistic regression score > 0.1 was significant. The PSM-adjusted dataset was subsequently analyzed.

The median method was used to divide D-dimer levels into high- and low-level groups to assess their relationship with in-hospital complications. A binary logistic regression model was used to identify the predictive outcome indicators. The multivariate logistic regression model included all univariate variables with bilateral p values <0.05 to determine the outcome variables associated with D-dimer levels.

Kaplan–Meier analysis was used to examine the unadjusted overall survival rate, while the log-rank test was used to determine significant differences between groups. Multivariate Cox regression

analysis was used to examine D-dimer levels and mortality rates. Hazard ratios and 95% confidence intervals (CIs) are presented. The multivariate analysis incorporated significant ($p < 0.05$) univariate variables.

To investigate the dose–response relationship between death and D-dimer levels, we constructed a restricted cubic spline (RCS) curve. The cubic spline was adjusted for confounding factors to detect a possible nonlinear relationship between the D-dimer level as a continuous variable and long-term mortality.

D-dimer levels were assessed using receiver operating characteristic (ROC) curves to predict death at different times. The area under the ROC curve (AUC) estimates the discrimination ability.

3. Results

3.1. Patient characteristics

This cohort study included 1,338 patients with TBI (Figure 1). The baseline characteristics of the patients, stratified by D-dimer levels, are presented in Table 1. The D-dimer levels of the four groups were as follows: G1 (0.00–1.54, $n = 326$), G2 (1.55–6.35, $n = 325$), G3 (6.36–19.99, $n = 324$), and G4 (≥20, $n = 363$). The mean age, GCS, surgical treatment, and laboratory index test results (HB concentration, Plt count, Fib concentration, APTT, TT, and PT) differed between the four groups ($p < 0.05$). In contrast, there were no significant differences in sex and previous medical history (hypertension or diabetes) ($p > 0.05$).

3.2. Association between D-dimer levels and in-hospital complications

The hospitalization complications are presented in Table 2. We divided the patients into two groups according to a median D-dimer cut-off value of 6.85 mg/L. After a preliminary comparison, we found that high D-dimer levels were associated with serum electrolyte disorders, hypoproteinemia, cardiac complications, urinary system complications, coagulation disorders, pulmonary infection, ICU admission, gastrointestinal complications, liver dysfunction, stress hyperglycemia, deep vein thrombosis, seizures, and intracranial infection during hospitalization ($p < 0.05$). After adjustment by multivariate logistic regression analysis, compared with low D-dimer levels, high D-dimer levels had significant value in predicting serum electrolyte disorders, hypoproteinemia, cardiac complications, urinary complications, coagulation disorders, pulmonary infection, and ICU admission ($p < 0.05$). Correlation analysis after PSM adjustment showed significant differences between high D-dimer levels and

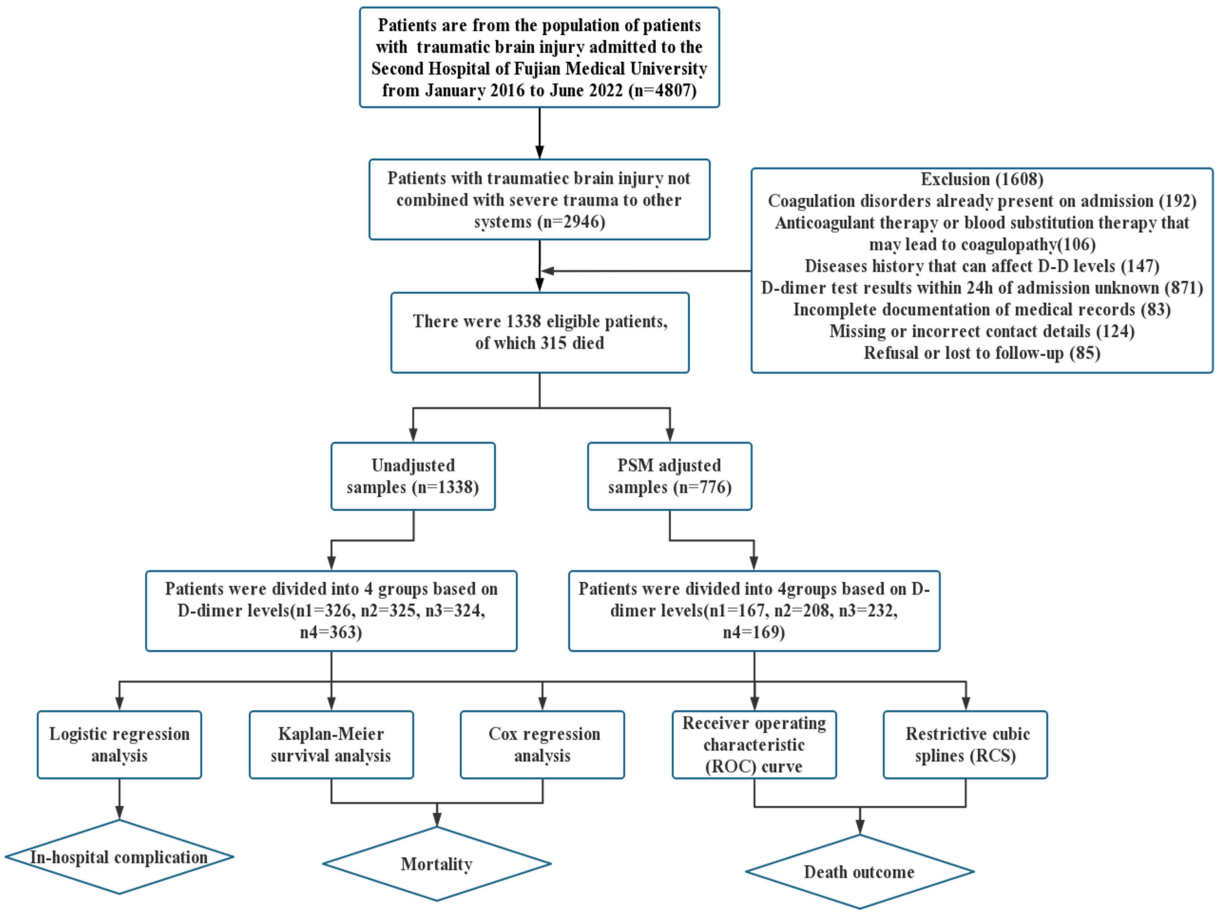

FIGURE 1
Flow chart of the patient selection process and statistical analysis method.

TABLE 1 Baseline patient characteristics stratified by baseline D-dimer levels.

Patient Characteristics	D-Dimer Groups (mg/L)				
	G1[a]	G2[b]	G3[c]	G4[d]	*p*-value for trend
Mean age, years (SD)	45.7 (22.6)	45.5 (22.9)	47.0 (22.0)	52.7 (20.6)	<0.001
Sex					
Male	222 (68.1)	229 (70.5)	207 (63.9)	243 (66.9)	0.347
Female	104 (31.9)	96 (29.5)	117 (36.1)	120 (32.7)	0.347
Medical history					
Hypertension	78 (23.9)	84 (25.8)	66 (20.4)	81 (22.3)	0.393
Diabetes	31 (9.5)	28 (8.6)	29 (9.0)	44 (12.1)	0.392
Glasgow Coma Scale score					
13–15	291 (89.3)	224 (68.9)	183 (56.5)	125 (34.4)	<0.001
9–12	18 (5.5)	47 (14.5)	60 (18.5)	42 (11.6)	
3–8	17 (5.2)	54 (16.6)	81 (25.0)	196 (54.0)	
Surgical treatment					
Yes	83 (25.5)	71 (21.8)	74 (22.8)	178 (49.0)	<0.001
No	243 (74.5)	254 (78.2)	250 (77.2)	185 (51.0)	
Mean baseline biomarker concentrations (SD)					
Hemoglobin, g/L	132.2 (17.3)	128.2 (20.8)	128.1 (22.9)	124.7 (22.6)	<0.001
Platelet, 10^9/L	257.5 (84.2)	243.1 (83.8)	232.1 (82.5)	217.1 (73.3)	<0.001
Fibrinogen, g/L	3.0 (1.2)	2.9 (1.8)	2.6 (1.2)	2.1 (1.1)	<0.001
Activated partial thromboplastin time, s	28.2 (5.4)	27.4 (5.1)	27.4 (6.3)	31.4 (16.9)	<0.001
Thrombin time, s	17.1 (2.8)	16.9 (3.0)	17.2 (2.2)	18.9 (6.2)	<0.001
Prothrombin time, s	13.0 (8.3)	12.5 (1.8)	12.8 (2.4)	13.6 (3.4)	0.017

[a]G1, Group 1: D-dimer level of 10.00–1.54 ($n_1 = 326$); [b]G2, Group 2: D-dimer level of 1.55–6.35 ($n_2 = 325$); [c]G3, Group 3: D-dimer level of 6.36–19.99 ($n_3 = 324$); [d]G4, Group 4: D-dimer level ≥ 20 ($n_4 = 363$).

serum electrolyte disorder, pulmonary infection, and ICU admission ($p < 0.05$).

3.3. Association between D-dimer levels and mortality

The Kaplan–Meier analysis showed that death events during follow-up were more common in patients with higher D-dimer levels ($p < 0.001$) (Figure 2). The 1-month, 1-year, and long-term survival rates of patients in G4 were significantly lower than those of patients in G1, G2, and G3, and the trend in the survival curve among the four groups was significantly different ($p < 0.001$). A similar trend was observed in the 1-month, 1-year, and long-term survival curves.

Cox regression models were used to further analyze mortality in patients with different D-dimer levels. In univariate analysis, higher D-dimer levels were independently associated with the risk of death, with significantly higher long-term mortality in groups G2, G3, and G4 than in G1 ($p < 0.001$, Table 3). In addition, age, sex, GCS, surgical treatment, HB concentration, Plt count, Fib concentration, APTT, TT, and PT were independent predictors of long-term mortality, and were, therefore, included in the multivariate Cox regression analysis model (Table 4). The results showed that compared to patients in G1 and G2 (aHR 1.655, 95% CI 0.963–2.843), patients in G3 (aHR 2.38, 95% CI 1.416–4.000) and G4 (aHR 3.635, 95% CI 2.195–6.018) had higher long-term mortality ($p < 0.001$; Table 3). After PSM-adjusted analysis, the trend remained significant ($p < 0.001$; Table 3). We found a similar trend in the 1-month and 1-year mortality rates (Tables 3–6).

Subgroup analyses were performed to explore whether the interaction of other variables would affect the value of D-dimer levels in predicting mortality outcomes (Figure 3). After setting age, surgical treatment, GCS score, HB concentration, Plt count, fibrinogen concentration, PT, APTT, and TT as separate subgroups, the correlation between D-dimer levels and long-term mortality remained of high predictive value ($p < 0.001$).

3.4. Predictive value of D-dimer levels for death outcomes

Time-related ROC curves were used to further explore the predictive value of D-dimer levels for the occurrence of death (Figure 4). The results showed that D-dimer levels had different predictive abilities for mortality outcomes at different times. The AUC for long-term mortality was 0.759 (95%CI: 0.720–0.799), while the AUC of 1-year mortality and 1-month mortality was 0.790 (95%CI: 0.761–0.819) and 0.787 (95%CI: 0.755–0.812), respectively. Among them, D-dimer was a long-term prognostic predictor of TBI; the cut-off values were 15.6,

TABLE 2 In-hospital complications stratified by low and high D-dimer levels.

Outcomes	Unadjusted		Multivariable Regression Adjustment		Propensity Score Adjustment	
	OR (95% CI)	*p*-value	OR (95% CI)	*p*-value	OR (95% CI)	*p*-value
Serum electrolyte disorder	2.059 (1.603–2.644)	<0.001	1.57 (1.19–2.071)	0.001	1.562 (1.129–2.162)	0.007
Hypoproteinemia	2.162 (1.559–2.998)	<0.001	1.455 (1.005–2.106)	0.047	1.269 (0.826–1.95)	0.276
Cardiac complication	4.44 (1.936–10.181)	<0.001	3.12 (1.307–7.46)	0.01	2.037 (0.813–5.105)	0.129
Urinary complication	3.551 (2.255–5.591)	<0.001	1.743 (1.057–2.874)	0.029	1.569 (0.864–2.848)	0.139
Traumatic coagulopathy	5.007 (2.065–12.141)	<0.001	2.85 (1.098–7.399)	0.031	0.831 (0.252–2.746)	0.14
Pulmonary infection	3.109 (2.477–3.902)	<0.001	1.888 (1.402–2.543)	<0.001	1.362 (1.017–1.824)	0.038
Admission to intensive care unit	6.18 (4.027–9.482)	<0.001	2.495 (1.488–4.185)	0.001	1.926 (1.081–3.43)	0.026
Gastrointestinal complications	2.113 (1.379–3.237)	0.001	1.123 (0.69–1.828)	0.641	0.848 (0.482–1.491)	0.566
Hypohepatia	2.206 (1.591–3.057)	<0.001	1.255 (0.871–1.809)	0.223	1.138 (0.728–1.779)	0.57
Stress hyperglycemia	6.609 (1.486–29.401)	0.013	2.308 (0.487–10.948)	0.292	2.52 (0.486–13.066)	0.271
Deep venous thrombosis	3.711 (1.031–13.363)	0.045	2.485 (0.639–9.667)	0.189	2.01 (0.366–11.041)	0.422
Seizures	1.559 (1.003–2.423)	0.049	1.021 (0.623–1.672)	0.934	1.542 (0.86–2.765)	0.146
Intracranial infection	2.678 (1.178–6.089)	0.019	2.409 (0.882–6.579)	0.086	3.395 (0.927–12.432)	0.065

OR, odds ratio; CI, confidence interval.

12.53, and 15.95 mg/L for long-term death events, 1-year death events, and 1-month death events, respectively. The best predictive value for the ROC curve was achieved at these cut-off concentrations. After PSM adjustment, the AUC of the ROC curve at different time points was >0.6, indicating predictive significance.

In addition, RCS models were used to flexibly and visually predict the relationship between D-dimer levels and long-term mortality in patients with TBI (Figure 5). As shown in Figure 5, the risk of long-term death was relatively low at D-dimer levels <6.820 mg/L. The predicted D-dimer concentration was 6.820 mg/L (6.860 mg/L after PSM adjustment). The risk of death began to increase rapidly, and the HR increased with an increase in D-dimer levels, showing a positive correlation ($p < 0.001$).

4. Discussion

TBI is a global health concern due to its association with high mortality rates, disability, and poor prognosis (Wiles et al., 2023). Therefore, early and accurate assessment of injuries is crucial to promptly identify critically ill patients, guide treatment decisions, and establish realistic expectations for the disease. However, the current diagnostic and grading criteria for TBI that are used in clinical practice fail to accurately evaluate all patients (Maas et al., 2022). Therefore, an objective index that can reflect the severity of trauma is urgently required to supplement existing schemes (Maas et al., 2022). The role of D-dimers in the evaluation of TBI has been a topic of interest. It reflects the high fibrinolytic state of the coagulation system and is often used to evaluate venous thrombosis and pulmonary embolism after TBI (Chen et al., 2023). For changes in coagulation function in patients with TBI, D-dimer can respond quickly in the early stages, and changes can be detected in the blood within minutes after TBI (Zhang et al., 2018). Prior studies have shown that D-dimer concentrations in the peripheral blood positively correlate with the risk of progressive hemorrhagic injury in patients with TBI and that D-dimer levels in patients with isolated TBI are associated with poor neurological prognosis 6 months after discharge (Xu et al., 2020; Fujiwara et al., 2022). However, there are no existing studies on the correlation between D-dimer levels and the incidence of complications or long-term mortality during hospitalization in patients with TBI.

Studies have revealed that TBI can have widespread pathophysiological effects on peripheral organs, such as the heart, lungs, gastrointestinal tract, liver, and kidneys, due to autonomic nervous system disorders and systemic inflammatory response (McDonald et al., 2020). By preventing or improving non-neurological complications, such as pneumonia, heart failure, and renal failure, the prognosis of a considerable number of patients can be significantly improved (Robba et al., 2020). In this large single-center cohort study, we found that the D-dimer level at admission was an independent predictor of complications during hospitalization after TBI. High D-dimer levels are associated with serum electrolyte disorders, hypoproteinemia, cardiac complications, urinary complications, coagulation disorders, pulmonary infections, ICU admission, gastrointestinal complications, liver dysfunction, stress hyperglycemia, deep vein thrombosis, epilepsy, and intracranial infections during hospitalization. In the present study, serum electrolyte disorder, pulmonary infection, and admission to the ICU remained significant after multivariate adjustment and PSM adjustment of the sample data and have been reported to be significantly associated with high mortality in patients with TBI (Longhi et al., 2017; Sundman et al., 2017; Sharma et al., 2019; Tsai et al., 2020).

In our study, the D-dimer level was identified as an independent predictor of short- and long-term mortality after TBI. Several small studies have assessed the short-term mortality and poor prognosis in patients with TBI. For example, studies have found that higher levels of D-dimer are associated with higher in-hospital, 28-day (Allard et al., 2009; Lee et al., 2018), and 30-day mortality (Yuan et al., 2012). Fujiwara et al. analyzed a multicenter TBI database and found that

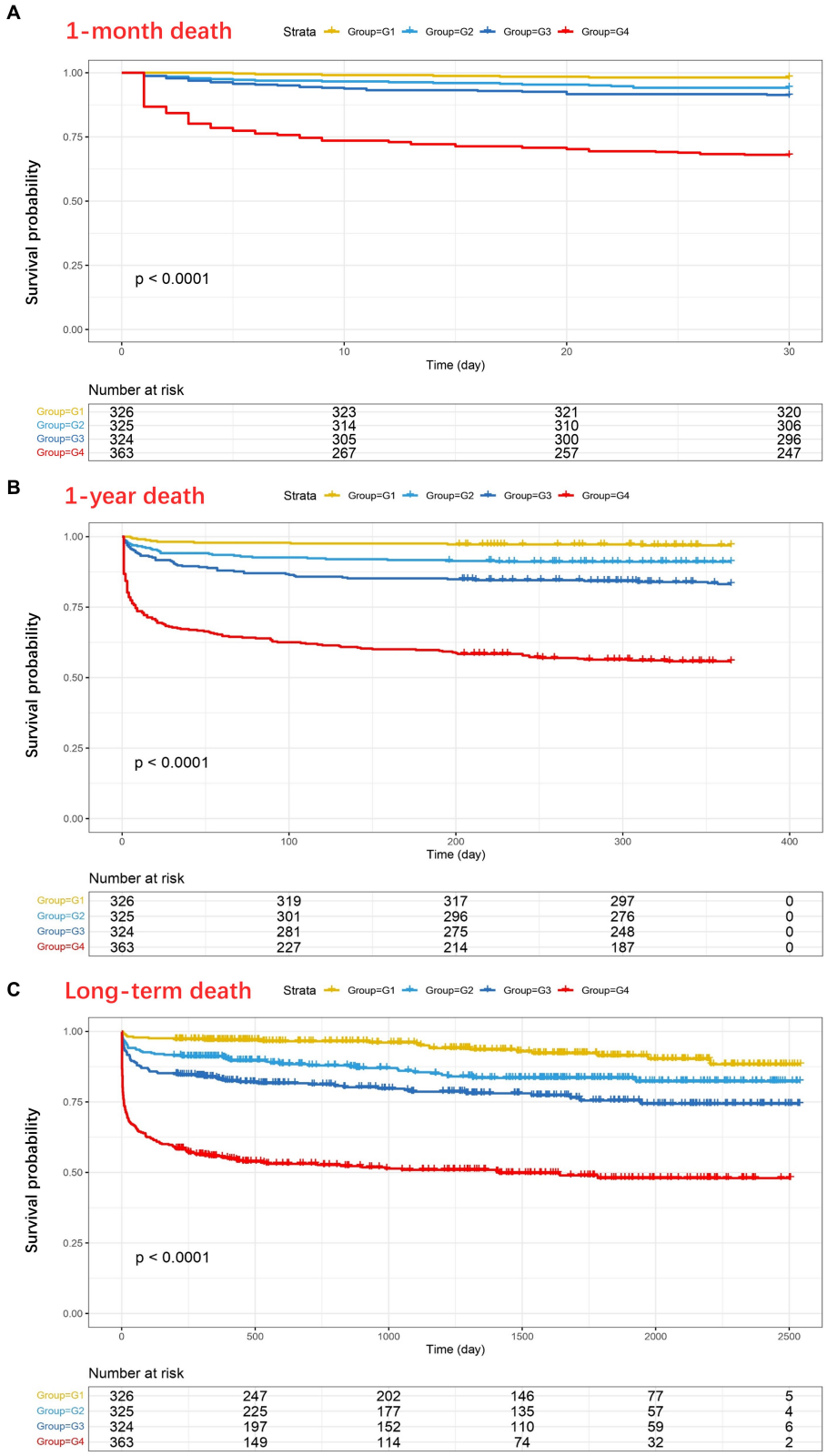

FIGURE 2
Kaplan–Meier analysis showing the four groups of D-dimer levels in relation to 1-month mortality **(A)**, 1-year mortality **(B)**, and long-term mortality **(C)** after traumatic brain injury (TBI) ($P_a < 0.0001$, $P_b < 0.0001$, $P_c < 0.0001$). As shown in **(C)**, at 2500 days, 5, 4, 6, and 2 patients in the four groups (G1–G4, respectively) did not experience any outcome events and were still being followed up with.

TABLE 3 Unadjusted and adjusted associations between quartiles of D-dimer levels and mortality.

Outcome	D-Dimer level (mg/L)	No. of deaths (%)	Unadjusted HR (95% CI)	*p*-value	Multivariable regression adjusted HR (95% CI)	*p*-value	PSM-adjusted HR (95% CI)	*p*-value
1-month mortality	0.00–1.54	6 (0.8)	Ref	<0.001	Ref	<0.001	Ref	<0.001
	1.55–6.35	19 (5.8)	3.232 (1.291–8.093)		2.314 (0.822–6.512)		3.302 (1.104–9.878)	
	6.36–19.99	29 (9.0)	5.014 (2.082–12.077)		2.531 (0.926–6.916)		1.629 (0.502–5.288)	
	≥20	117 (32.2)	20.852 (9.178–47.376)		5.413 (2.037–14.386)		7.882 (2.771–22.424)	
1-year mortality	0.00–1.54	10 (3.1)	Ref	<0.001	Ref	<0.001	Ref	<0.001
	1.55–6.35	29 (8.9)	2.998 (1.461–6.152)		2.227 (0.984–5.042)		2.384 (1.008–5.639)	
	6.36–19.99	54 (16.7)	5.788 (2.948–11.366)		3.482 (1.6–7.576)		2.516 (1.084–5.839)	
	≥20	160 (44.1)	18.79 (9.916–35.608)		5.9 (2.747–12.675)		6.413 (2.873–14.317)	
Long-term mortality	0.00–1.54	22 (6.7)	Ref	<0.001	Ref	<0.001	Ref	<0.001
	1.55–6.35	47 (14.5)	2.254 (1.358–3.739)		1.655 (0.963–2.843)		2.34 (1.14–4.803)	
	6.36–19.99	69 (22.3)	3.511 (2.173–5.674)		2.38 (1.416–4)		2.316 (1.14–4.7)	
	≥20	177 (48.8)	10.284 (6.598–16.03)		3.635 (2.195–6.018)		5.023 (2.534–9.955)	

HR, hazard ratio; CI, confidence interval; PSM, propensity score matching.

TABLE 4 Multivariate analysis for long-term mortality.

Characteristics	Unadjusted		Multivariable regression adjustment	
	HR (95% CI)	*p*-value	aHR (95% CI)	*p*-value
Age, year, mean	1.034 (1.027–1.04)	<0.001	1.039 (1.031–1.048)	<0.001
Sex				
Female	1 [Reference]		1 [Reference]	
Male	1.297 (1.013–1.663)	0.039	1.352 (1.036–1.765)	0.027
Medical history				
Hypertension	1.738 (1.375–2.197)	<0.001	1.053 (0.796–1.392)	0.718
Diabetes	1.861 (1.371–2.524)	<0.001	1.108 (0.779–1.578)	0.567
Glasgow Coma Scale score				
13–15	1 [Reference]	<0.001	1 [Reference]	<0.001
9–12	3.802 (2.608–5.544)	<0.001	2.700 (1.817–4.012)	<0.001
3–8	10.991 (8.333–14.496)	<0.001	6.835 (4.886–9.562)	<0.001
Surgical treatment	2.923 (2.342–3.648)	<0.001	1.040 (0.803–1.348)	0.766
Baseline biomarker concentrations				
Hemoglobin, g/L	0.988 (0.983–0.993)	<0.001	0.997 (0.991–1.002)	0.22
Platelet, 10^9/L	0.996 (0.994–0.997)	<0.001	1.001 (1.000–1.003)	0.067
Fibrinogen, g/L	0.866 (0.781–0.96)	0.006	0.990 (0.907–1.080)	0.814
Activated partial thromboplastin time, s	1.025 (1.021–1.03)	<0.001	1.010 (1.003–1.017)	0.004
Thrombin time, s	1.056 (1.041–1.071)	<0.001	1.027(1.005–1.049)	0.014
Prothrombin time, s	1.025 (1.015–1.034)	<0.001	1.021 (1.004–1.039)	0.015
D-Dimer, mg/L				
G1	1 [Reference]	<0.001	1 [Reference]	<0.001
G2	2.254 (1.358–3.739)	0.002	1.655 (0.963–2.843)	0.068
G3	3.511 (2.173–5.674)	<0.001	2.380 (1.416–4.000)	0.001
G4	10.284 (6.598–16.03)	<0.001	3.635 (2.195–6.018)	<0.001

CI, confidence interval; G1, Group 1: D-dimer level of 10.00–1.54 ($n_1 = 326$); G2, Group 2: D-dimer level of 1.55–6.35 ($n_2 = 325$); G3, Group 3: D-dimer level of 6.36–19.99 ($n_3 = 324$); G4, Group 4: D-dimer level ≥ 20 ($n_4 = 363$).

TABLE 5 Multivariate analysis for 1-month mortality.

Characteristics	Unadjusted		Multivariable regression adjustment	
	HR (95% CI)	*p*-value	aHR (95% CI)	*p*-value
Age, year, mean	1.02 (1.013–1.028)	<0.001	1.021 (1.011–1.031)	<0.001
Sex				
Female	1 [Reference]		1 [Reference]	
Male	1.216 (0.873–1.694)	0.247	–	–
Medical history				
Hypertension	1.146 (0.814–1.615)	0.435	–	–
Diabetes	1.761 (1.167–2.656)	0.007	1.083 (0.676–1.736)	0.74
GCS score				
13–15	1 [Reference]	<0.001	1 [Reference]	<0.001
9–12	7.964 (4.252–14.916)	<0.001	6.28 (3.313–11.902)	<0.001
3–8	23.83 (14.17–40.077)	<0.001	14.619 (8.226–25.982)	<0.001
Surgical treatment	2.76 (2.044–3.727)	<0.001	0.714 (0.509–1.001)	0.051
Baseline biomarker concentrations				
Hemoglobin, g/L	0.989 (0.983–0.996)	0.001	1.001 (0.995–1.008)	0.663
Platelet, 10^9/L	0.995 (0.993–0.997)	<0.001	1 (0.998–1.002)	0.969
Fibrinogen, g/L	0.668 (0.569–0.784)	<0.001	0.94 (0.83–1.064)	0.328
Activated partial thromboplastin time, s	1.025 (1.02–1.03)	<0.001	1.006 (0.999–1.013)	0.1
Thrombin time, s	1.064 (1.05–1.079)	<0.001	1.027 (1.005–1.051)	0.018
Prothrombin time, s	1.03 (1.02–1.039)	<0.001	1.03 (1.012–1.049)	0.001
D-Dimer, mg/L				
G1	1 [Reference]	<0.001	1 [Reference]	<0.001
G2	3.232 (1.291–8.093)	0.012	2.314 (0.822–6.512)	0.112
G3	5.014 (2.082–12.077)	<0.001	2.531 (0.926–6.916)	0.07
G4	20.852 (9.178–47.376)	<0.001	5.413 (2.037–14.386)	0.001

CI, confidence interval; HR, hazard ratio; G1, Group 1: D-dimer level of 10.00–1.54 ($n_1 = 326$); G2, Group 2: D-dimer level of 1.55–6.35 ($n_2 = 325$); G3, Group 3: D-dimer level of 6.36–19.99 ($n_3 = 324$); G4, Group 4: D-dimer level ≥ 20 ($n_4 = 363$).

D-dimer levels at admission were associated with poor GOS scores and mortality at 6 months (Fujiwara et al., 2022). Our 1-month and 1-year mortality results are similar to these findings, indicating that D-dimer levels are associated with short-term mortality in patients with TBI, which further supports the credibility of our study. However, to the best of our knowledge, previous studies have not discussed the relationship between long-term mortality and poor prognosis with D-dimer levels in patients with TBI. In the present study, through long-term follow-up observations, a large sample of prognostic data was collected over a long duration. The average follow-up time was 2.8 years, and the longest follow-up time was 6.9 years. Relatively complete prognostic data were available, which could be used to determine the correlation between D-dimer levels and long-term mortality of patients with TBI and provide further evidence supporting the role of D-dimer levels in the prediction of poor prognosis. We found a possible dose–response relationship between elevated D-dimer levels and patient mortality. The odds of mortality were significantly higher in patients with higher D-dimer levels than in patients with lower D-dimer levels.

In addition, in most previous studies, the methods used to determine the correlation between D-dimer levels and TBI were relatively simple. For example, Simone et al. found that the D-dimer level can be used as an evaluation method to reduce the use of unnecessary CT examinations in children with TBI through ROC model analysis (Langness et al., 2018), and Xu et al. (2020) found that the ratio of D-dimer/Fib can predict the incidence of progressive hemorrhagic injury after TBI through logistic regression and the ROC model. In this study, various statistical methods and models were used to determine the relationship between D-dimer levels and patient mortality at different time points. These methods included Kaplan–Meier survival analysis, Cox multivariate regression, an ROC model, RCS model, and subgroup analysis. The use of these statistical approaches and models enhanced the rigor of the study's statistical methods and design. Furthermore, previous studies failed to account for confounding bias. In our study, we addressed the issue by excluding confounding factors such as age, GCS score, surgery, and other blood test indicators. This allowed us to determine whether the D-dimer level was an independent predictor of death in patients with TBI. The dataset was adjusted using PSM to verify the reliability of the results. After adjusting for confounding factors and performing subgroup analysis, our findings remained significant, which is one of the advantages of our study.

TABLE 6 Multivariate analysis for 1-year mortality.

Patient characteristics	Unadjusted		Multivariable regression adjustment	
	HR (95% CI)	*p*-value	aHR (95% CI)	*p*-value
Age, year, mean	1.027 (1.02–1.033)	<0.001	1.028 (1.02–1.036)	<0.001
Sex				
Female	1 [Reference]		1 [Reference]	
Male	1.315 (0.997–1.734)	0.052	–	–
Medical history				
Hypertension	1.312 (0.997–1.726)	0.052	–	–
Diabetes	1.645 (1.161–2.332)	0.005	1 (0.672–1.488)	>0.999
GCS score				
13–15	1 [Reference]	<0.001	1 [Reference]	<0.001
9–12	5.852 (3.649–9.386)	<0.001	4.256 (2.61–6.941)	<0.001
3–8	18.419 (12.704–26.704)	<0.001	10.811 (7.056–16.566)	<0.001
Surgical treatment	2.919 (2.28–3.737)	<0.001	0.885 (0.666–1.174)	0.396
Baseline biomarker concentrations				
Hemoglobin, g/L	0.988 (0.983–0.993)	<0.001	1 (0.995–1.006)	0.982
Platelet, 10^9/L	0.995 (0.994–0.997)	<0.001	1 (0.999–1.002)	0.85
Fibrinogen, g/L	0.811 (0.721–0.913)	0.001	1.007 (0.917–1.106)	0.883
Activated partial thromboplastin time, s	1.026 (1.021–1.03)	<0.001	1.009 (1.002–1.016)	0.011
Thrombin time, s	1.06 (1.046–1.075)	<0.001	1.027 (1.005–1.05)	0.016
Prothrombin time, s	1.028 (1.019–1.037)	<0.001	1.028 (1.011–1.045)	0.001
D-Dimer, mg / L				
G1	1 [Reference]	<0.001	1 [Reference]	<0.001
G2	2.998 (1.461–6.152)	0.003	2.227 (0.984–5.042)	0.055
G3	5.788 (2.948–11.366)	<0.001	3.482 (1.6–7.576)	0.002
G4	18.79 (9.916–35.608)	<0.001	5.9 (2.747–12.675)	<0.001

CI, confidence interval; G1, Group 1: D-dimer level of 10.00–1.54 ($n_1 = 326$); G2: Group 2: D-dimer level of 1.55–6.35 ($n_2 = 325$); G3, Group 3: D-dimer level of 6.36–19.99 ($n_3 = 324$); G4, Group 4: D-dimer level ≥ 20 ($n_4 = 363$); HR, hazard ratio.

There is no direct pathological evidence indicating the association between D-dimer levels and death in patients with TBI. Based on a literature review, we speculate that the following mechanisms may be involved. First, the D-dimer levels may indicate the severity of tissue damage. In mild TBI, elevated D-dimer levels on admission are independently associated with intracranial structural disorders (Sugimoto et al., 2017); in severe TBI, acute D-dimer levels predict hematoma expansion (Suehiro et al., 2014), and hyperfibrinolysis is more damaging than low fibrinolysis (Hayakawa et al., 2017). D-dimer levels also predict the occurrence of progressive hemorrhagic brain injury after TBI (Xu et al., 2020). In addition, D-dimer regulates the local immune response, stimulates the synthesis of monocytes, and releases pro-inflammatory cytokines, such as interleukin-6, which may contribute to diseased tissue edema and hematoma formation in various diseases (Welch et al., 2016). Elevated D-dimer levels are also associated with intracranial lesions and poor prognosis in patients with cerebral infarction and subarachnoid hemorrhage (Fang et al., 2022; Qiu et al., 2023). Thus, D-dimer levels may indicate brain tissue damage and prognosis. Second, local brain lesions after TBI can alter body coagulation, thereby increasing D-dimer levels. In the acute phase of TBI, tissue factors are released from the damaged blood–brain barrier into the entire body, rapidly increasing plasma D-dimer levels (Kwaan, 2020). Tissue factors promoting fibrinolysis and prothrombin conversion (Suehiro et al., 2019). Thrombin degrades fibrin into the D-dimer and fibrin degradation products. Thrombin-related proteins cause post-traumatic immunosuppression, inflammation, and breakdown of the blood–brain barrier. Low tissue blood perfusion after TBI worsens the imbalance of these coagulation and fibrinolysis systems, causing brain tissue damage and post-traumatic changes in other organs (Kwaan, 2020; Medcalf et al., 2020), resulting in poor prognosis.

This study has several limitations that should be taken into consideration when interpreting our results. First, the retrospective study design limited our ability to establish causality and was susceptible to bias from unmeasured factors. Second, we only assessed one biomarker; however, additional markers may be helpful for risk classification (Böhm et al., 2022). Third, our investigation solely focused on all-cause mortality and did not explore the association between D-dimer levels and cause-specific mortality. According to a previous study, D-dimer levels can influence cardiovascular, cancerous, and non-cardiovascular non-cancerous mortality. Therefore, the association between

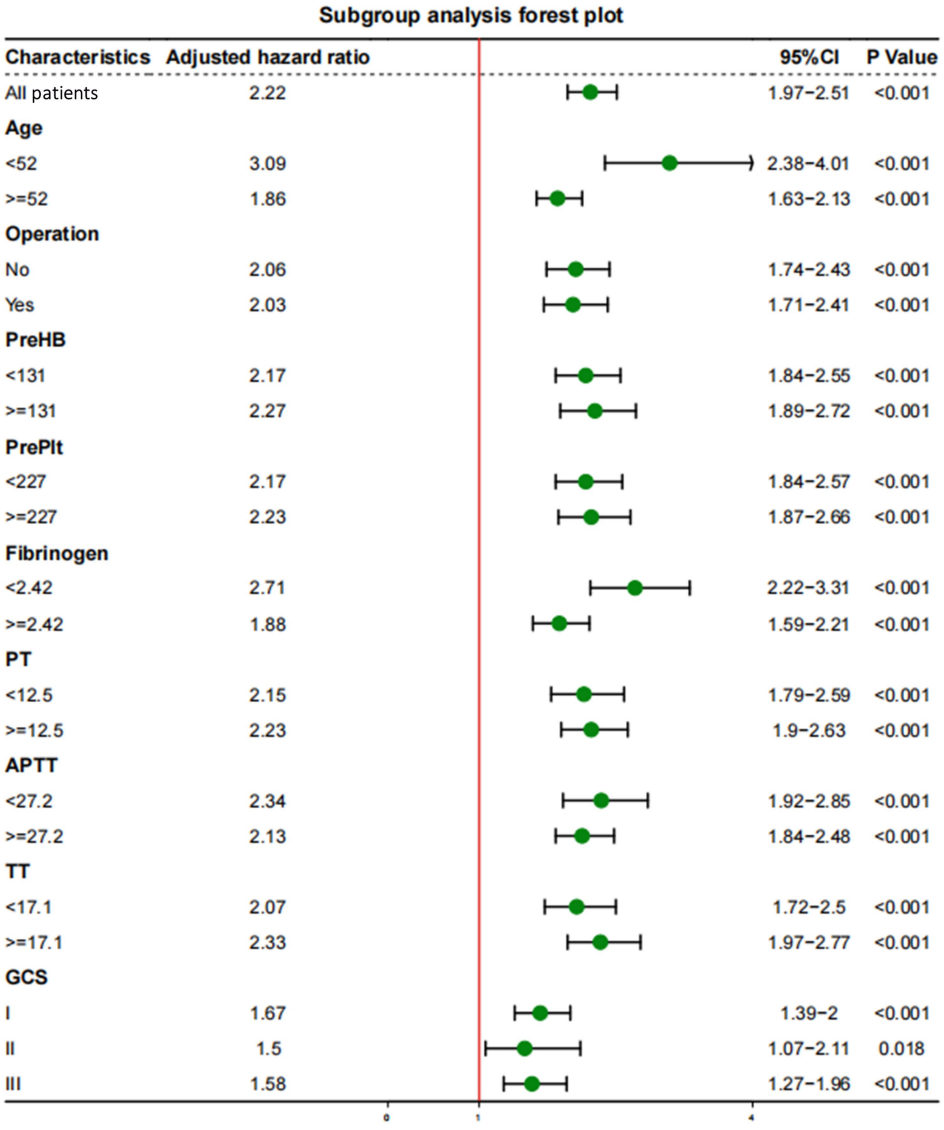

FIGURE 3
Subgroup analyses of the association between D-dimer levels and long-term mortality with a multivariate model adjusted for age, operation treatment, Glasgow Coma Scale (GCS) score, and concentrations of hemoglobin (HB), platelets (Plt), fibrinogen, prothrombin time (PT), activated partial thromboplastin time (APTT), and thrombin time (TT).

D-dimer levels and cause-specific mortality should be investigated in future studies(Simes et al., 2018). Fourth, for the long-term prognosis of patients with TBI, we only evaluated adverse outcomes such as death, and there was a lack of recording and analysis of other adverse prognostic states such as paralysis, loss of motor and sensory function, and cognitive dysfunction, and the Glasgow Outcome Scale (Asami et al., 2022) scores were not recorded. Fifth, differences in the time of blood collection and facilities may have resulted in variations in D-dimer levels, which may affect the accuracy of our findings (Asami et al., 2022). In the future, we hope to obtain more accurate and comprehensive follow-up data by implementing a prospective, multicenter, and large-sample design to optimize our research.

In summary, based on the predictive value of D-dimer levels for complications and short- and long-term mortality in patients with TBI during hospitalization, we believe that D-dimer detection is a promising approach for the early assessment of all patients with TBI. As a blood test index, D-dimer can be measured in the acute phase of TBI rapidly and at a low cost. It not only facilitates the prompt identification and diagnosis of patients with different severities of injury but also potentially guides early clinical treatment and long-term rehabilitation measures for patients with TBI (Maegele et al., 2017). The D-dimer test can reduce the need for sophisticated testing tools such as CT and MRI in patients with mild TBI, which will lower treatment costs and radiation exposure. Furthermore, it enables early intervention and the use of targeted measures to improve outcomes in patients with moderate to severe TBI (Foaud et al., 2014). This development is expected to substantially impact how patients with TBI are assessed and treated.

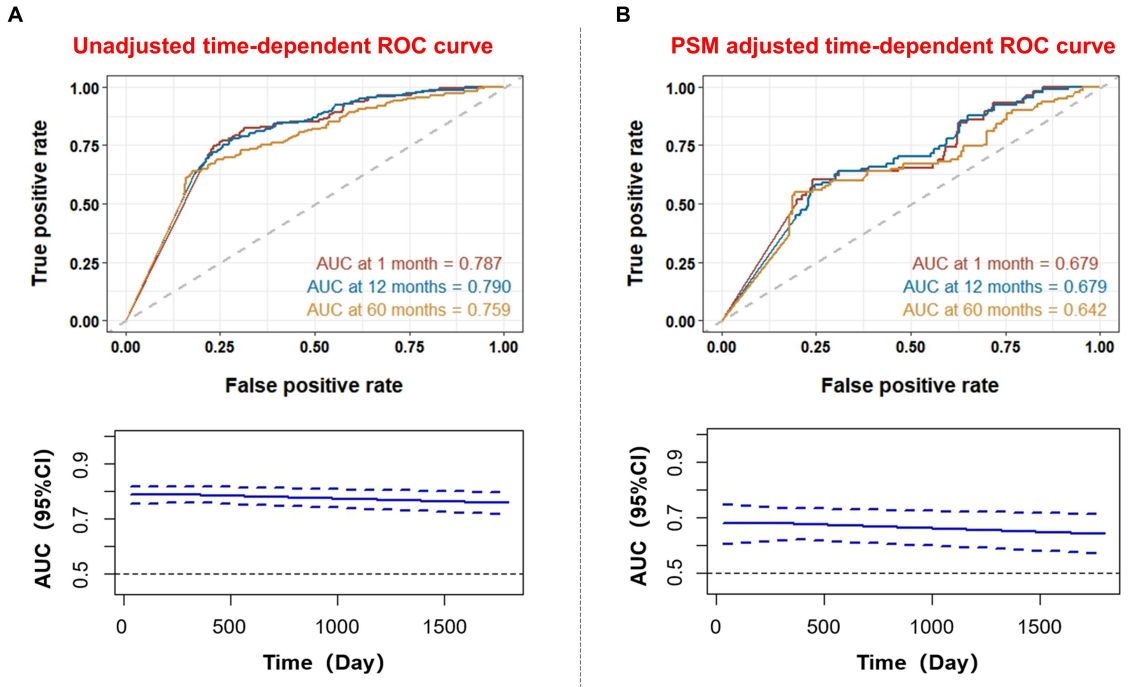

FIGURE 4
Time-dependent receiver operating characteristic curve for prediction of D-dimer levels in patients with traumatic brain injury. **(A)** Unadjusted time-dependent ROC curve; **(B)** PSM adjusted time-dependent ROC curve. AUC, area under the curve; ROC, receiver operating characteristic; PSM, propensity score matching.

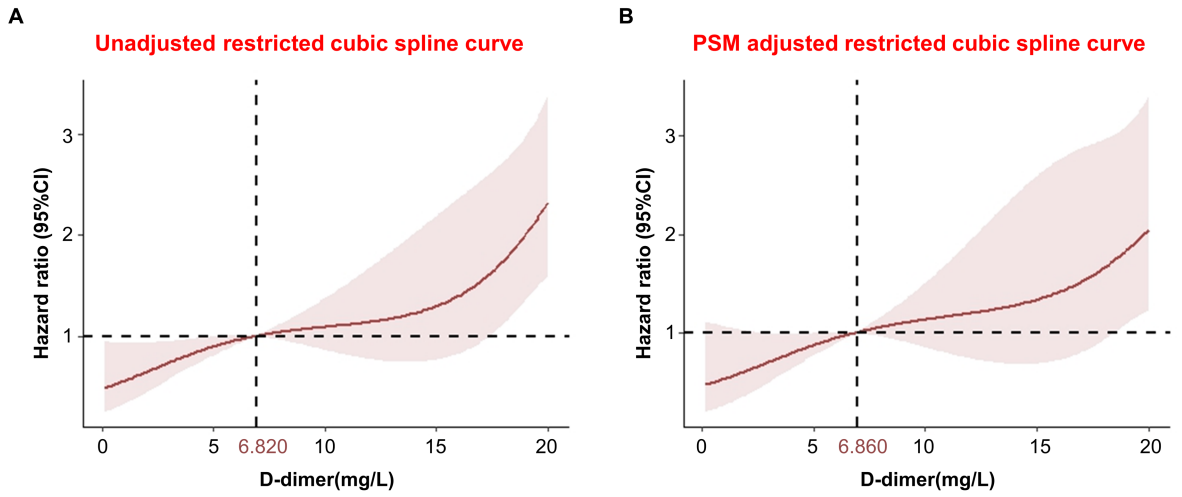

FIGURE 5
Restricted cubic spline showing the association between D-dimer levels and long-term mortality. **(A)** Unadjusted restricted cubic spline curve; **(B)** PSM adjusted restricted cubic spline curve. CI, confidence interval; PSM, propensity score matching.

5. Conclusion

In conclusion, our results revealed that in patients with TBI, high D-dimer levels within 24 h of admission were associated with complications such as electrolyte metabolism disorders, pulmonary infections, and ICU admission during hospitalization ($p < 0.05$) (Figure 6). Additionally, we observed a dose–response relationship between elevated D-dimer levels and patient mortality. The odds of mortality were significantly higher in patients with higher D-dimer levels than in those with lower D-dimer levels ($p < 0.001$) (Figure 6).

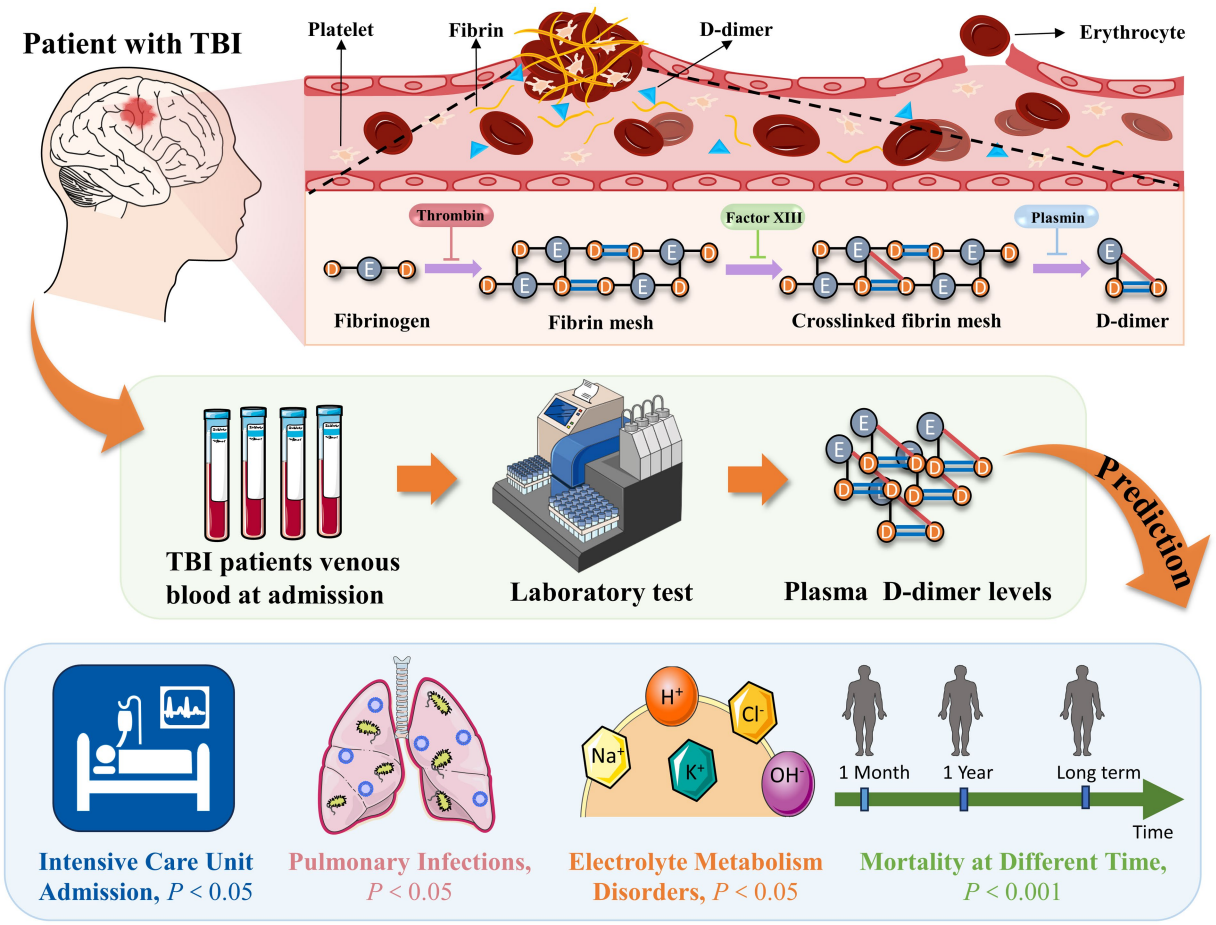

FIGURE 6
High D-dimer levels within 24 h of admission were associated with complications and mortality in TBI patients. TBI, traumatic brain injury.

In the future, this blood marker may help to timely identify patients at risk of poor prognosis and tailor treatment plans for these patients, thereby reducing mortality and improving prognosis. Furthermore, our findings may also facilitate the exploration of new therapeutic targets in the future. However, further studies are required to validate our results and elucidate the underlying mechanisms between the correlation of D-dimer levels and clinical outcomes.

Data availability statement

The datasets presented in this article are not readily available due to privacy or ethical restrictions. Requests to access the datasets should be directed to the corresponding author.

Ethics statement

The studies involving humans were approved by the Ethics Committee of the Second Affiliated Hospital of Fujian Medical University. The studies were conducted in accordance with the local legislation and institutional requirements. Written informed consent for participation in this study was provided by the participants' legal guardians/next of kin.

Author contributions

XC: Conceptualization, Formal analysis, Validation, Writing – original draft, Methodology. XW: Data curation, Investigation, Writing – original draft. YL: Data curation, Investigation, Writing – original draft. XG: Data curation, Investigation, Writing – original draft. FW: Project administration, Writing – original draft. YY: Project administration, Writing – original draft. WH: Supervision, Writing – review & editing. FZ: Supervision, Writing – review & editing. HH: Conceptualization, Funding acquisition, Writing – original draft, Supervision, Writing – review & editing.

Funding

The author(s) declare financial support was received for the research, authorship, and/or publication of this article. This research was supported by the Natural Science Foundation of

Fujian Province (2020 J01227), the Medical Innovation Science and Technology Project of Fujian Province (2020CXA047), the Science and Technology Bureau Project of Quanzhou (2021C054R), and the Science and Technology Bureau Project of Quanzhou (2022C036R).

Acknowledgments

We would like to thank the Department of Medical Record, the Second Affiliated Hospital of Fujian Medical University, which helped us with data selection in the initial stages. We would also like to thank Editage (www.editage.cn) for English language editing.

Conflict of interest

The authors declare that the research was conducted in the absence of any commercial or financial relationships that could be construed as a potential conflict of interest.

Publisher's note

References

Allard, C. B., Scarpelini, S., Rhind, S. G., Baker, A. J., Shek, P. N., Tien, H., et al. (2009). Abnormal coagulation tests are associated with progression of traumatic intracranial hemorrhage. *J. Trauma* 67, 959–967. doi: 10.1097/TA.0b013e3181ad5d37

Anderson, T. N., Farrell, D. H., and Rowell, S. E. (2021). Fibrinolysis in traumatic brain injury: diagnosis, management, and clinical considerations. *Semin. Thromb. Hemost.* 47, 527–537. doi: 10.1055/s-0041-1722970

Asami, M., Nakahara, S., Miyake, Y., Kanda, J., Onuki, T., Matsuno, A., et al. (2022). Serum D-dimer level as a predictor of neurological functional prognosis in cases of head injuries caused by road traffic accidents. *BMC Emerg. Med.* 22:51. doi: 10.1186/s12873-022-00613-9

Berger, R. P., Fromkin, J., Rubin, P., Snyder, J., Richichi, R., and Kochanek, P. (2015). Serum D-dimer concentrations are increased after pediatric traumatic brain injury. *J. Pediatr.* 166, 383–388. doi: 10.1016/j.jpeds.2014.10.036

Böhm, J. K., Schaeben, V., Schäfer, N., Güting, H., Lefering, R., Thorn, S., et al. (2022). Extended coagulation profiling in isolated traumatic brain injury: a CENTER-TBI analysis. *Neurocrit. Care.* 36, 927–941. doi: 10.1007/s12028-021-01400-3

Chen, D., Luo, J., Zhang, C., Tang, L., Deng, H., Chang, T., et al. (2023). Venous thrombus embolism in polytrauma: special attention to patients with traumatic brain injury. *J. Clin. Med.* 12:1716. doi: 10.3390/jcm12051716

Echigo, T., Shiomi, N., Nozawa, M., Okada, M., Kato, F., and Hiraizumi, S. (2017). An evaluation and treatment strategy according to the age group and focal brain vs diffuse brain injury type for coagulation-fibrinolysis abnormalities of severe head trauma. *Neurotraumatology* 40, 38–42. doi: 10.32187/neurotraumatology.40.1_38

Fang, F., Wang, P., Yao, W., Wang, X., Zhang, Y., Chong, W., et al. (2022). Association between D-dimer levels and long-term mortality in patients with aneurysmal subarachnoid hemorrhage. *Neurosurg. Focus.* 52:E8. doi: 10.3171/2021.12.FOCUS21512

Filion, K. B., Azoulay, L., Platt, R. W., Dahl, M., Dormuth, C. R., Clemens, K. K., et al. (2016). A multicenter observational study of incretin-based drugs and heart failure. *N. Engl. J. Med.* 374, 1145–1154. doi: 10.1056/NEJMoa1506115

Foaud, H. M., Labib, J. R., Metwally, H. G., and El-Twab, K. M. (2014). Plasma D-dimer as a prognostic marker in ICU admitted Egyptian children with traumatic brain injury. *J. Clin. Diagn. Res.* 8, PC01–PC06. doi: 10.7860/JCDR/2014/9489.4784

Folkerson, L. E., Sloan, D., Cotton, B. A., Holcomb, J. B., Tomasek, J. S., and Wade, C. E. (2015). Predicting progressive hemorrhagic injury from isolated traumatic brain injury and coagulation. *Surgery* 158, 655–661. doi: 10.1016/j.surg.2015.02.029

Fujiwara, G., Okada, Y., Sakakibara, T., Yamaki, T., and Hashimoto, N. (2022). The association between D-dimer levels and long-term neurological outcomes of patients with traumatic brain injury: an analysis of a nationwide observational neurotrauma database in Japan. *Neurocrit. Care.* 36, 483–491. doi: 10.1007/s12028-021-01329-7

Greuters, S., van den Berg, A., Franschman, G., Viersen, V. A., Beishuizen, A., Peerdeman, S. M., et al. (2011). Acute and delayed mild coagulopathy are related to outcome in patients with isolated traumatic brain injury. *Crit. Care* 15:R2. doi: 10.1186/cc9399

Hayakawa, M., Maekawa, K., Kushimoto, S., Kato, H., Sasaki, J., Ogura, H., et al. (2017). Hyperfibrinolysis in severe isolated traumatic brain injury may occur without tissue hypoperfusion: a retrospective observational multicentre study. *Crit. Care* 21:222. doi: 10.1186/s13054-017-1811-1

Kamiya, K., Ozasa, K., Akiba, S., Niwa, O., Kodama, K., Takamura, N., et al. (2015). Long-term effects of radiation exposure on health. *Lancet* 386, 469–478. doi: 10.1016/S0140-6736(15)61167-9

Kwaan, H. C. (2020). The central role of fibrinolytic response in trauma-induced coagulopathy: a hematologist's perspective. *Semin. Thromb. Hemost.* 46, 116–124. doi: 10.1055/s-0039-3402428

Langness, S., Ward, E., Halbach, J., Lizardo, R., Davenport, K., Bickler, S., et al. (2018). Plasma D-dimer safely reduces unnecessary CT scans obtained in the evaluation of pediatric head trauma. *J. Pediatr. Surg.* 53, 752–757. doi: 10.1016/j.jpedsurg.2017.08.017

Lee, D. H., Lee, B. K., Noh, S. M., and Cho, Y. S. (2018). High fibrin/fibrinogen degradation product to fibrinogen ratio is associated with 28-day mortality and massive transfusion in severe trauma. *Eur. J. Trauma Emerg. Surg.* 44, 291–298. doi: 10.1007/s00068-017-0844-0

Longhi, L., Ferri, F., Cavalleri, G., and Lorini, L. (2017). Cardiac function following traumatic brain injury. *Crit. Care Med.* 45, e1193–e1194. doi: 10.1097/CCM.0000000000002616

Maas, A. I. R., Menon, D. K., Adelson, P. D., Andelic, N., Bell, M. J., Belli, A., et al. (2017). Traumatic brain injury: integrated approaches to improve prevention, clinical care, and research. *Lancet Neurol.* 16, 987–1048. doi: 10.1016/S1474-4422(17)30371-X

Maas, A. I. R., Menon, D. K., Manley, G. T., Abrams, M., Åkerlund, C., Andelic, N., et al. (2022). Traumatic brain injury: progress and challenges in prevention, clinical care, and research. *Lancet Neurol.* 21, 1004–1060. doi: 10.1016/S1474-4422(22)00309-X

Maegele, M., Schöchl, H., Menovsky, T., Maréchal, H., Marklund, N., Buki, A., et al. (2017). Coagulopathy and haemorrhagic progression in traumatic brain injury: advances in mechanisms, diagnosis, and management. *Lancet Neurol.* 16, 630–647. doi: 10.1016/S1474-4422(17)30197-7

McDonald, S. J., Sharkey, J. M., Sun, M., Kaukas, L. M., Shultz, S. R., Turner, R. J., et al. (2020). Beyond the brain: peripheral interactions after traumatic brain injury. *J. Neurotrauma* 37, 770–781. doi: 10.1089/neu.2019.6885

Medcalf, R. L., Keragala, C. B., and Draxler, D. F. (2020). Fibrinolysis and the immune response in trauma. *Semin. Thromb. Hemost.* 46, 176–182. doi: 10.1055/s-0040-1702170

Nelson, L. D., Temkin, N. R., Barber, J., Brett, B. L., Okonkwo, D. O., McCrea, M. A., et al. (2023). Functional recovery, symptoms, and quality of life 1 to 5 years after traumatic brain injury. *JAMA Netw. Open* 6:e233660. doi: 10.1001/jamanetworkopen.2023.3660

Qiu, K., Jia, Z. Y., Cao, Y., Zhao, L. B., Zu, Q., Shi, H. B., et al. (2023). Emergency admission plasma D-dimer: a novel predictor for symptomatic intracranial hemorrhage after thrombectomy in acute ischemic stroke. *J. NeuroInterv. Surg.*:jnis-2022-019719. doi: 10.1136/jnis-2022-019719

Riemann, L., Mikolic, A., Maas, A., Unterberg, A., and Younsi, A.Collaborative European NeuroTrauma Effectiveness Research in Traumatic Brain Injury (CENTER-TBI) Investigators and Participants (2023). Computed tomography lesions and their association with global outcome in young people with mild traumatic brain injury. *J. Neurotrauma* 40, 1243–1254. doi: 10.1089/neu.2022.0055

Robba, C., Bonatti, G., Pelosi, P., and Citerio, G. (2020). Extracranial complications after traumatic brain injury: targeting the brain and the body. *Curr. Opin. Crit. Care* 26, 137–146. doi: 10.1097/MCC.0000000000000707

Sharma, R., Shultz, S. R., Robinson, M. J., Belli, A., Hibbs, M. L., O'Brien, T. J., et al. (2019). Infections after a traumatic brain injury: the complex interplay between the immune and neurological systems. *Brain Behav. Immun.* 79, 63–74. doi: 10.1016/j.bbi.2019.04.034

Simes, J., Robledo, K. P., White, H. D., Espinoza, D., Stewart, R. A., Sullivan, D. R., et al. (2018). D-dimer predicts long-term cause-specific mortality, cardiovascular events, and cancer in patients with stable coronary heart disease: LIPID study. *Circulation* 138, 712–723. doi: 10.1161/CIRCULATIONAHA.117.029901

Stocchetti, N., and Zanier, E. R. (2016). Chronic impact of traumatic brain injury on outcome and quality of life: a narrative review. *Crit. Care* 20:148. doi: 10.1186/s13054-016-1318-1

Suehiro, E., Fujiyama, Y., Kiyohira, M., Motoki, Y., Nojima, J., and Suzuki, M. (2019). Probability of soluble tissue factor release lead to the elevation of D-dimer as a biomarker

for traumatic brain injury. *Neurol. Med. Chir. (Tokyo)* 59, 63–67. doi: 10.2176/nmc.oa.2018-0254

Suehiro, E., Koizumi, H., Fujiyama, Y., Yoneda, H., and Suzuki, M. (2014). Predictors of deterioration indicating a requirement for surgery in mild to moderate traumatic brain injury. *Clin. Neurol. Neurosurg.* 127, 97–100. doi: 10.1016/j.clineuro.2014.10.007

Sugimoto, K., Suehiro, E., Shinoyama, M., Sadahiro, H., Haji, K., Fujiyama, Y., et al. (2017). D-dimer elevation as a blood biomarker for detection of structural disorder in mild traumatic brain injury. *J. Neurotrauma* 34, 3245–3248. doi: 10.1089/neu.2017.5240

Sundman, M. H., Chen, N. K., Subbian, V., and Chou, Y. H. (2017). The bidirectional gut-brain-microbiota axis as a potential nexus between traumatic brain injury, inflammation, and disease. *Brain Behav. Immun.* 66, 31–44. doi: 10.1016/j.bbi.2017.05.009

Tian, Y., Salsbery, B., Wang, M., Yuan, H., Yang, J., Zhao, Z., et al. (2015). Brain-derived microparticles induce systemic coagulation in a murine model of traumatic brain injury. *Blood* 125, 2151–2159. doi: 10.1182/blood-2014-09-598805

Tsai, Y. C., Wu, S. C., Hsieh, T. M., Liu, H. T., Huang, C. Y., Chou, S. E., et al. (2020). Association of stress-induced hyperglycemia and diabetic hyperglycemia with mortality in patients with traumatic brain injury: analysis of a propensity score-matched population. *Int. J. Environ. Res. Public Health* 17:4266. doi: 10.3390/ijerph17124266

Vos, T., Allen, C., Arora, M., Barber, R. M., Bhutta, Z. A., Brown, A., et al. (2016). Global, regional, and national incidence, prevalence, and years lived with disability for 310 diseases and injuries, 1990–2015: a systematic analysis for the global burden of disease study 2015. *Lancet* 388, 1545–1602. doi: 10.1016/S0140-6736(16)31678-6

Wada, T., Gando, S., Maekaw, K., Katabami, K., Sageshima, H., Hayakawa, M., et al. (2017). Disseminated intravascular coagulation with increased fibrinolysis during the early phase of isolated traumatic brain injury. *Crit. Care* 21:219. doi: 10.1186/s13054-017-1808-9

Welch, R. D., Ayaz, S. I., Lewis, L. M., Unden, J., Chen, J. Y., Mika, V. H., et al. (2016). Ability of serum glial fibrillary acidic protein, ubiquitin C-terminal hydrolase-L1, and S100B to differentiate normal and abnormal head computed tomography findings in patients with suspected mild or moderate traumatic brain injury. *J. Neurotrauma* 33, 203–214. doi: 10.1089/neu.2015.4149

Wiles, M. D., Braganza, M., Edwards, H., Krause, E., Jackson, J., and Tait, F. (2023). Management of traumatic brain injury in the non-neurosurgical intensive care unit: a narrative review of current evidence. *Anaesthesia* 78, 510–520. doi: 10.1111/anae.15898

Xu, D. X., Du, W. T., Li, X., Wu, Z. X., and Yu, G. F. (2020). D-dimer/fibrinogen ratio for the prediction of progressive hemorrhagic injury after traumatic brain injury. *Clin. Chim. Acta* 507, 143–148. doi: 10.1016/j.cca.2020.04.022

Yuan, F., Ding, J., Chen, H., Guo, Y., Wang, G., Gao, W. W., et al. (2012). Predicting outcomes after traumatic brain injury: the development and validation of prognostic models based on admission characteristics. *J. Trauma Acute Care Surg.* 73, 137–145. doi: 10.1097/TA.0b013e31824b00ac

Zhang, J., Zhang, F., and Dong, J. F. (2018). Coagulopathy induced by traumatic brain injury: systemic manifestation of a localized injury. *Blood* 131, 2001–2006. doi: 10.1182/blood-2017-11-784108

frontiers | Frontiers in Neuroscience

TYPE Original Research
PUBLISHED 23 November 2023
DOI 10.3389/fnins.2023.1222345

OPEN ACCESS

EDITED BY
Ana Semeano,
Northeastern University, United States

REVIEWED BY
Naushad Khan,
Hamad Medical Corporation, Qatar
Andrew P. Lavender,
Federation University Australia, Australia
Huaqiu Zhang,
Huazhong University of Science and Technology, China

*CORRESPONDENCE
Yan Zhao
✉ doctoryanzhao@whu.edu.cn
Haoli Ma
✉ mahaoli@whu.edu.cn

RECEIVED 14 May 2023
ACCEPTED 30 October 2023
PUBLISHED 23 November 2023

CITATION
Zeng R, Li S, Yu J, Ma H and Zhao Y (2023) Performance of plasma von Willebrand factor in acute traumatic brain injury: relations to severity, CT findings, and outcomes. *Front. Neurosci.* 17:1222345. doi: 10.3389/fnins.2023.1222345

Performance of plasma von Willebrand factor in acute traumatic brain injury: relations to severity, CT findings, and outcomes

Rong Zeng[1], Shaoping Li[1], Jiangtao Yu[1], Haoli Ma[2]* and Yan Zhao[1]*

[1]Emergency Center, Zhongnan Hospital of Wuhan University, Wuhan, Hubei, China, [2]Department of Biological Repositories, Zhongnan Hospital of Wuhan University, Wuhan, China

Background: von Willebrand factor (VWF) has been widely recognized as a biomarker for endothelial cell activation in trauma and inflammation. Traumatic brain injury (TBI) is characterized by cerebral vascular injury and subsequent inflammation. The objective of this study was to investigate the correlation between VWF levels and clinical severity, as well as imaging abnormalities, in TBI patients. Additionally, the predictive value of VWF for patient outcomes was assessed.

Methods: We conducted a prospective study to recruit acute TBI patients who were admitted to the emergency department within 24 h. Healthy individuals from the medical examination center were recruited as the control group. This study aimed to compare the accuracy of VWF in discriminating TBI severity and imaging abnormalities with the Glasgow Coma Scale (GCS) and Rotterdam computed tomography (CT) scores. We also analyzed the predictive value of these outcomes using the Glasgow Outcome Scale (GOS) and 6-month mortality.

Results: The plasma concentration of VWF in TBI patients (84.7 ± 29.7 ng/ml) was significantly higher than in healthy individuals (40 ± 8.8 ng/ml). There was a negative correlation between VWF levels and GCS scores, as well as a positive correlation between VWF levels and Rotterdam CT scores. The area under the curve (AUC) for VWF in discriminating mild TBI was 0.76 (95% CI: 0.64, 0.88), and for predicting negative CT findings, it was 0.82 (95% CI: 0.72, 0.92). Meanwhile, the AUC of VWF in predicting mortality within 6 months was 0.70 (95% CI: 0.56, 0.84), and for a GOS score lower 4, it was 0.78 (95% CI: 0.67, 0.88). Combining VWF with either the GCS or Rotterdam CT score improved the prediction ability compared to using VWF alone.

Conclusion: VWF levels were significantly elevated in patients with TBI compared with healthy individuals. Furthermore, VWF levels demonstrated a negative correlation with GCS scores and a positive correlation with Rotterdam CT scores. In terms of predicting mortality, VWF alone was not sufficient, but its predictive power was enhanced when combined with either the Rotterdam CT score or GCS. These findings suggest that VWF may serve as a potential biomarker for assessing the severity and prognosis of TBI patients.

KEYWORDS

traumatic brain injury, VWF, GCS, GOS, Rotterdam CT score, 6-month mortality

Introduction

Traumatic brain injury (TBI) is one of the most common diseases in the emergency department and a leading cause of death and disability, imposing a significant economic burden on individuals and society (Hyder et al., 2007). Globally, over 50 million people experience TBI annually, with a high likelihood of TBI incidents occurring throughout their lifetimes (Tang et al., 2020).

TBI progresses rapidly, presents numerous complications, and has a high mortality rate. Therefore, timely and accurate evaluation of TBI patients is very important for distinguishing between those who need emergency surgery and those who need conservative observation (Hon et al., 2019; Vavilala et al., 2019; Al-Hajj et al., 2021; Miller et al., 2021). Accurate diagnosis, triage, and treatment are essential for TBI patients, who are typically stratified based on the Glasgow Coma Scale (GCS), which assesses neurological dysfunction by evaluating eye, verbal, and motor responses. The GCS categorizes TBI severity as severe (GCS 3–8), moderate (GCS 9–12), and mild (GCS 13–15) TBI. However, the GCS has several limitations, often resulting in an inaccurate classification of TBI severity (Stocchetti et al., 2004). Cranial computer tomography (CT) scans are commonly used in the early stages to determine the severity of brain injuries. Although repeated CT scans improve diagnostic accuracy, they also increase the risk of radiation exposure (Brenner and Hall, 2007). Moreover, CT examination may not detect relatively minor lesions (Papa et al., 2012). Although magnetic resonance imaging (MRI) offers higher sensitivity and specificity, it is not suitable for patients with severe conditions requiring continuous mechanical ventilation (Tokshilykova et al., 2020). Its high cost and limited accessibility restrict its use for repeated monitoring of TBI progression. The Glasgow Outcome Scale (GOS) is often used to evaluate clinical outcome variables, including survival and neurological assessment, in TBI patients, but it also has some limitations (Corral et al., 2007; Lu et al., 2012). Therefore, there is a need to explore new methods for detecting changes in the brain structure or function that may have important implications for prognosis (Kurca et al., 2006).

In recent years, there has been an increasing focus on experimental and clinical studies aimed at identifying blood-based biomarkers for the diagnosis and prognostic evaluation of TBI (Anada et al., 2018). Inflammation is one of the main pathophysiological mechanisms of TBI (Abdul-Muneer et al., 2015). The impact or shear force experienced by cerebral blood vessels during TBI can lead to compression, damage, or a cascade of reactions due to brain tissue contusion and edema (Nawashiro et al., 1995; DeWitt and Prough, 2003). These injuries may result in cerebral vessel rupture, hemorrhage, and thrombosis, which can subsequently cause severe consequences such as stroke. Therefore, when addressing TBI, it is crucial to not only focus on the damage to brain tissue itself but also closely monitor cerebrovascular injuries. von Willebrand factor (VWF) serves as a critical factor in promoting platelet recruitment to the site of vascular injury and regulating hemostasis during vascular injury (Xu et al., 2019). Furthermore, VWF has recently been demonstrated to play a role in promoting inflammatory processes and blood–brain barrier (BBB) damage in mice with cerebral hemorrhage (Zhu et al., 2016).

Therefore, our study aims to determine whether there is any difference in plasma VWF levels between TBI patients and healthy individuals. At the same time, the relationship between VWF expression and the severity, imaging abnormalities, and prognosis of acute TBI was studied.

Abbreviations: TBI, traumatic brain injury; ELISA, enzyme-linked immunosorbent assay; GCS, Glasgow Coma Scale; CT, computer tomography; GO, Gene Oncology; GOS, Glasgow Outcome Scale; MRI, magnetic resonance imaging; VWF, von Willebrand factor; ROC, receiver operating characteristic; AUC, area under the curve; CI, confidence interval; ICU, intensive care unit.

Methods

Study design

We prospectively recruited TBI patients who visited emergency department of Zhongnan Hospital of Wuhan University between August 2020 and December 2020. Additionally, healthy individuals from the medical examination center during the same period were recruited as control participants. The primary focus of this study was to explore the effectiveness of VWF in identifying the severity and prognosis of TBI.

Ethic information

This study was approved by Medical Ethical Committee of Zhongnan Hospital of Wuhan University (approval number 2020121). All procedures were carried out in accordance with the principles outlined in the Code of Ethics of The World Medical Association for experiments involving humans (Declaration of Helsinki) as well as the guidelines for research on health databases (Declaration of Taipei). All data were acquired after informed consent were obtained from the patients.

Patient inclusion

Consecutive TBI patients who were admitted to the emergency department were recruited for this study. The inclusion criteria were patients aged over 18 years old with acute TBI and no obvious injuries at other sites. However, patients who were pregnant or had a history of hematologic disorders, malignant tumors, uremia, heart failure, severe systemic diseases, chronic TBI, epilepsy, neurological diseases, psychiatric diseases, or intracranial hemorrhage were excluded. Patients who did not undergo brain CT scanning within 24 h after injury were also excluded. Additionally, healthy individuals aged over 18 years old from the medical examination center were recruited as control participants.

Definition of TBI and severity

Clinical TBI diagnostic criteria included a history of traumatic injury, consciousness alterations, and neurological injury based on CT scanning. The severity assessment of TBI was based solely on the lowest GCS score obtained either at the scene of the accident or in the emergency department. A GCS value of 3–8 was considered severe, 9–12 as moderate, and 13–15 as mild TBI.

Rotterdam CT score

The Rotterdam CT score is a widely used radiological scoring system for assessing the severity of TBI on CT scans (Huang et al., 2012). In this study, we employed the Rotterdam CT score to evaluate the extent of TBI in our patient cohort. The status of the basal cisterns was assessed and classified into three categories: normal (score 0), compressed (score 1), or absent (score 2). Midline shift was evaluated and categorized as either 0–5 millimeters (score 0) or above 5 millimeters (score 1). The presence or absence of an epidural hematoma was documented as a score of 0 or 1, respectively. Additionally, the presence of traumatic subarachnoid hemorrhage or intraventricular hemorrhage was recorded as a score of 1 accordingly. Finally, one point was added to the total score. Two independent radiologists, who were blinded to the patient's clinical information, reviewed the CT scans and assigned scores based on predefined criteria. To ensure inter-rater reliability, a subset of CT scans was randomly selected and independently assessed by both radiologists. Inter-rater agreement was determined using the intraclass correlation coefficient (ICC). All CT scans were performed using standardized acquisition protocols and interpreted by experienced radiologists. Any discrepancies in the scoring were resolved through discussion and consensus.

Data collection outcomes

After obtaining informed consent from patients, we collected information on participants and their blood samples. Relevant data, such as age, sex, GCS score, Rotterdam CT score, and GOS score, were extracted from the medical database. The blood samples of the participants were obtained within 1 h of admission. Samples were centrifuged and stored at −80°C for further detection.

VWF measurements

The plasma concentration of VWF was analyzed by a commercial ELISA kit (CEA833Hu, Cloud-Clone Corp., China) in accordance with the manufacturer's instructions.

Statistical analysis

Continuous data were presented as mean ± standard error (SD), and categorical data were presented as numbers (percentage). All data were analyzed using GraphPad Prism (Version 8.0.1; GraphPad Software Inc.). Statistical methods, including *t*-tests and Wilcoxon rank-sum tests, were selected based on the characteristics of the data. Pearson's rank correlation was used for correlation analysis. The discriminatory ability of the parameters was assessed by comparing the area under the receiver operating characteristic curve (AUROC). Statistical significance was defined as a two-tailed $P < 0.05$.

Results

Characteristics of patients and healthy individuals

A total of 110 participants, consisting of 69 TBI patients and 41 healthy individuals, were included in our study. The flowchart in Figure 1 provides an overview of the patient inclusion process. There was no significant difference in age between the two groups. However, the TBI group had a significantly higher proportion of male patients compared to the control group. The main causes of TBI were vehicle accidents, falls, and assaults. Based on the GCS score, approximately 70%, 6%, and 25% of the patients were categorized as having mild, moderate, and severe TBI, respectively. Furthermore, 37.7% of the patients had a normal CT report (Figure 2A), while the majority (62.3%) exhibited positive CT findings, including contusion (Figure 2B), extradural hematoma (Figure 2C), subdural hematoma (Figure 2D), subarachnoid hemorrhage (Figure 2E), and hemorrhage with midline shift (Figure 2F). In terms of outcomes, 15.9% of the patients had a GOS score of 1–2, indicating a poor outcome, while 84.1% had a GOS score of 3–5, indicating a moderate-to-good outcome. Additionally, the 6-month all-cause mortality rate was 13% (Table 1). In our study, individuals aged 60 and above were classified as elderly. Within the healthy control group and TBI group, the elderly represent 22% and 43.5% of the total population, respectively.

Correlation between plasma VWF level and clinical parameters

The TBI group ($n = 69$) had a significantly higher plasma concentration of VWF (84.68 ± 29.72 ng/ml) compared with the healthy individuals ($n = 41$) (39.97 ± 8.79 ng/ml, $p < 0.0001$, Figure 3A). The *post-hoc* power after data collection was 1. Furthermore, the level of VWF in patients with mild TBI (76.8 ± 29.0 ng/ml) or negative CT findings (63.9 ± 27.3 ng/ml) was significantly lower than that in non-mild TBI (102.8 ± 23.0 ng/ml) or positive CT findings (97.2 ± 223.6 ng/ml, all $p < 0.001$, Figures 3B, C). Among TBI patients, a VWF level of 78.26 ng/mL had the highest discriminatory power to differentiate TBI patients from healthy individuals (AUC, 0.89, sensitivity, 67%, specificity, 98%, Figure 3D). Moreover, VWF had an AUC of 0.76 (95% CI: 0.64, 0.88, Figure 3E) for discriminating mild TBI and 0.82 (95% CI: 0.72, 0.92, Figure 3F) for predicting negative CT findings. Furthermore, we analyzed the correlation between VWF, GCS, and CT scores in TBI patients. We found a negative correlation between

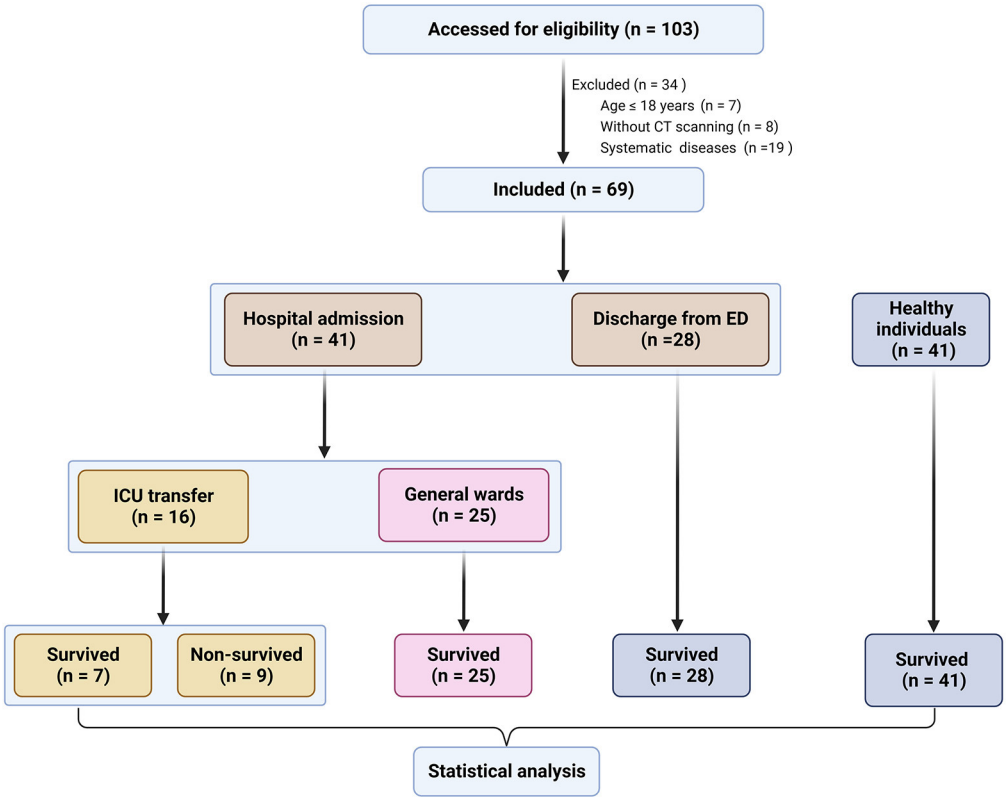

FIGURE 1
Flowchart of the selection of patients with traumatic brain injury (TBI) and healthy individuals. ED, emergency department; ICU, intensive care unit; CT, computed tomography.

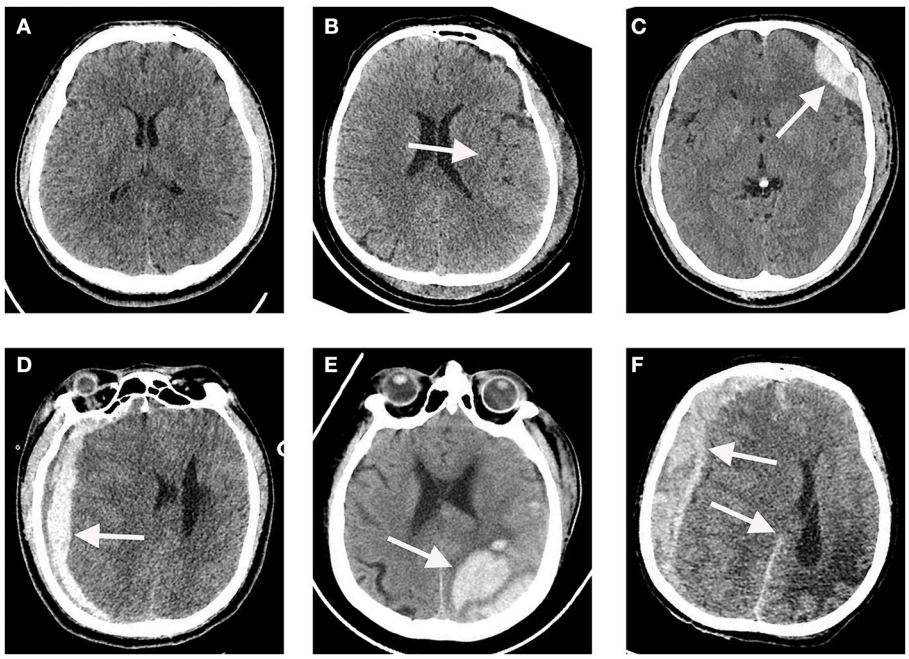

FIGURE 2
Representative CT images of a traumatic brain injury (TBI) and a normal CT scan. **(A)** Normal CT scan. **(B)** Cerebral contusion. **(C)** Extradural hematoma. **(D)** Subdural hematoma. **(E)** Subarachnoid hemorrhage. **(F)** Hemorrhage with midline shift. The white arrows indicate lesion regions.

TABLE 1 Demographic and clinical characteristics of the participants.

	TBI ($n = 69$)	Con ($n = 41$)	*P*-value
Age, (IQR)	53.0 (37.5–73.5)	50.0 (43–58.5)	0.253
Sex, *n* (%)			
Men	53 (76.8%)	23 (56.1%)	0.023
Women	16 (23.2%)	18 (43.9%)	
Non-elderly (<60 years)	39 (56.5%)	32 (78%)	
Elderly (≥60 years)	30 (43.5%)	9 (22%)	
Mechanisms, *n* (%)			
Fall	26 (37.7%)		
Assault	11 (15.9%)		
Vehicle accident	32 (46.4%)		
GCS, (%)			
Mild 13–15	48 (69.6%)		
Moderate 9–12	4 (5.8%)		
Severe 3–8	17 (24.6%)		
CT findings, *n* (%)			
CT positive scans	43 (62.3%)		
CT negative scans	26 (37.7%)		
GOS, (%)			
GOS 1–2	11 (15.9%)		
GOS 3–5	58 (84.1%)		
6-month mortality, *n* (%)	3/23 (13%)		

TBI, traumatic brain injury; GCS, Glasgow Coma Scale; CT, computed tomography; GOS, Glasgow Outcome Scal; VWF, von Willebrand factor.

GCS and CT score ($r = -0.642$, $p < 0.0001$, Figure 3G), indicating that patients with lower GCS scores were more likely to have severe brain structural damage detected by CT scanning. Additionally, VWF was negatively correlated with the GCS score ($r = -0.447$, $p < 0.0001$, Figure 3H) and significantly positively correlated with the CT score ($r = 0.464$, $p < 0.0001$, Figure 3I). Additionally, within the TBI group and the healthy control group, we separately examined the potential impact of age and gender on VWF levels. Our results showed that neither age nor gender had any significant influence on VWF levels (Supplementary Figure 1).

VWF improves prediction of clinical recovery

There were eight patients who died in the hospital and one patient who died within 6 months of discharge. The predictive ability of VWF for 6-month mortality was evaluated, and it was found to have an area under the curve (AUC) of 0.70. However, this did not reach the threshold for statistical significance (Table 2, $p = 0.06$). When combined with either CT score or GCS, VWF showed improved predictive ability ($p < 0.0001$). Given that a GOS score of ≤ 4 is closely associated with morbidity, the discriminatory power of VWF in predicting patients with a GOS of ≤ 4 was also analyzed. VWF demonstrated an AUC of 0.77 ($p < 0.0001$) for GOS ≤ 4. Similarly, the combined use of VWF with either a GCS or CT score showed improved predictive ability. These findings indicate that VWF alone is not sufficient for predicting 6-month mortality, but it can effectively identify patients at high risk of morbidity following TBI. Therefore, combining VWF with either the CT score or the GCS significantly enhances the predictive ability.

Discussion

A blood-based biomarker associated with pathophysiological mechanisms can aid in the identification of TBI, prediction and monitoring of recovery post-injury, and guidance for clinical treatment (Lippa et al., 2020). TBI inevitably results in vascular injury or blood flow disorders; hence, it is essential to explore biomarkers associated with TBI-related vascular injury. Previous clinical studies have shown that VWF, released from injured endothelial cells and activated platelets during acute injury, significantly elevates plasma VWF levels (Yokota et al., 2002; Tang et al., 2013). However, there is a paucity of studies investigating whether VWF can differentiate between TBI patients and healthy individuals or serve as a biomarker for evaluating TBI severity.

In this study, plasma levels of VWF were measured in patients with acute TBI and healthy individuals. The study aimed to analyze the relationship between VWF and the GCS, Rotterdam CT score, and GOS. The findings revealed that patients with acute TBI had higher plasma VWF levels compared to healthy individuals. Additionally, VWF levels were negatively correlated with GCS scores and significantly positively correlated with Rotterdam CT scores. While VWF alone was not sufficient to predict mortality, its predictive power improved when combined with either the Rotterdam CT score or GCS. Furthermore, our study demonstrates that VWF levels have the capability to differentiate between patients with unfavorable outcomes (GOS 1–4) and those with favorable outcomes (GOS 5) subsequent to TBI. Previous research has demonstrated that VWF serves as a sensitive indicator of endothelial cell activation (Ward et al., 2020). In the context of traumatic injury, an appropriate concentration of VWF can effectively control bleeding and reduce hemorrhage (Holcomb et al., 2015; Ng et al., 2015). Additionally, a high concentration of VWF independently increases the risk of deep vein thrombosis formation (Setiawan et al., 2020). The excessive release of VWF can lead to the formation of emboli within blood vessels, resulting in compromised blood flow and exacerbated ischemic injury (Nguyen et al., 2008). VWF is promising as a monitoring marker of systemic injury in brain trauma or critical diseases (Plautz et al., 2020). Our findings provide evidence of a significant correlation between the concentration of VWF and both the severity and prognosis of acute TBI. These findings are consistent with the results reported in previous clinical studies (De Oliveira et al., 2007; Sandsmark et al., 2019). In TBI, rupture of blood vessels and impaired endothelial cells can lead to increased release of VWF, contributing to platelet aggregation and thrombus formation. This can result in microcirculatory disturbances and local ischemia,

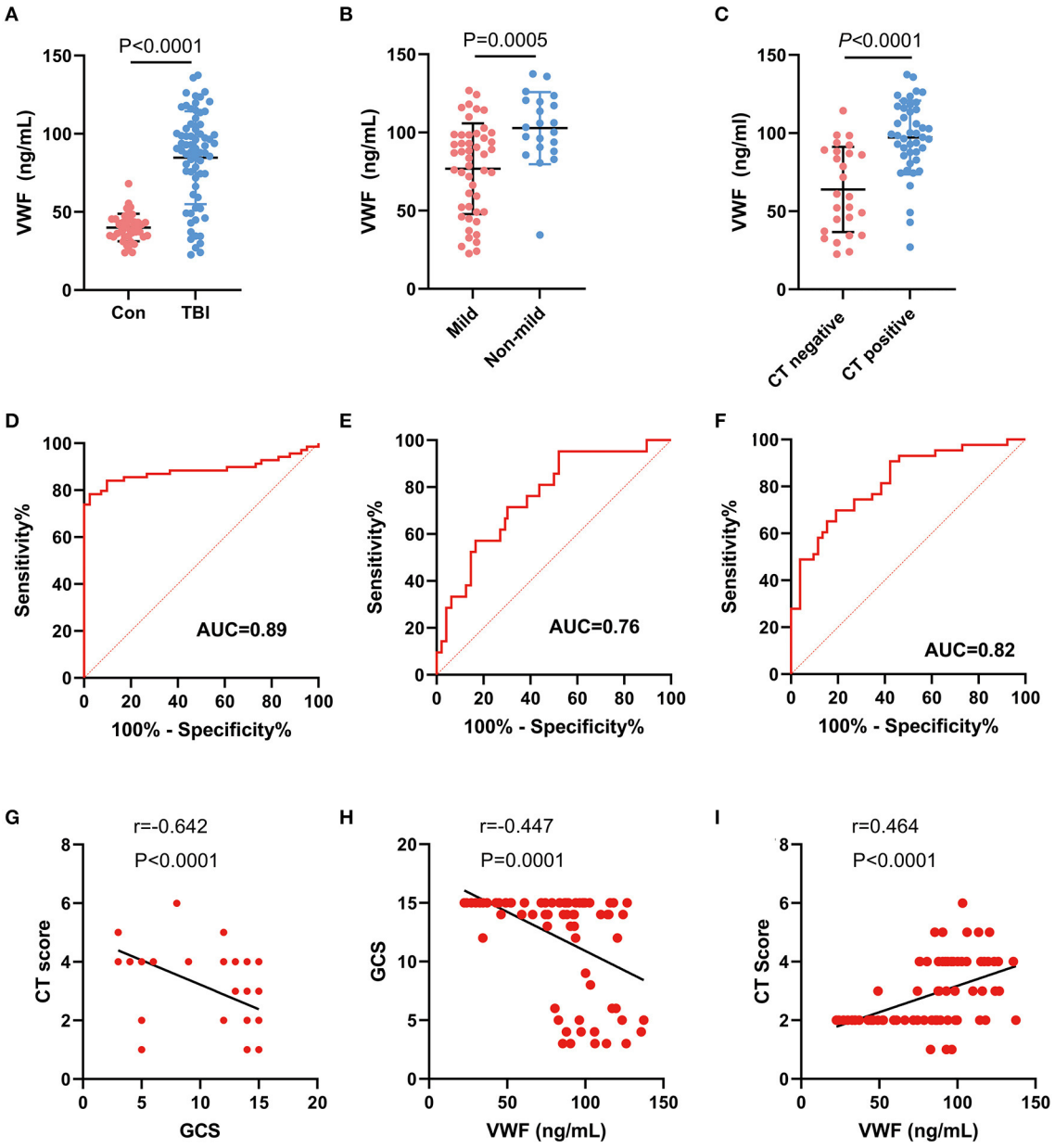

FIGURE 3
Correlation between plasma VWF level and clinical parameters. **(A)** Difference in plasma VWF concentrations between the control group and TBI patients ($p < 0.001$). **(B)** The level of VWF in patients with mild TBI (76.8 ± 29.0 ng/ml) was significantly lower than that in non-mild TBI (102.8 ± 23.0 ng/ml, $p < 0.001$). **(C)** The level of VWF in patients with negative CT findings (63.9 ± 27.3 ng/ml) was significantly lower than that in patients with positive CT findings (97.2 ± 223.6 ng/ml, $p < 0.001$). **(D)** ROC curve of plasma VWF levels for discriminating TBI patients from healthy individuals. **(E)** ROC curve of plasma VWF levels for discriminating mild TBI from non-mild TBI. **(F)** ROC curve of plasma VWF levels for discriminating negative CT findings from positive CT findings. **(G)** A negative correlation between GCS and CT score ($r = -0.642$, $p < 0.0001$). **(H)** A negative correlation between GCS score and VWF concentration ($r = -0.45$, $p < 0.0001$). **(I)** A positive correlation between VWF and CT score ($r = 0.46$, $p < 0.0001$).

further exacerbating brain injury (Lu et al., 2004; Wu et al., 2018). Moreover, TBI-induced endothelial injury and an inflammatory response can increase vascular permeability. VWF, through its binding to receptors on the endothelial cell surface, facilitates vascular leakage in TBI (Zhu et al., 2016; Aymé et al., 2017; Wu et al., 2018). Excessive VWF may promote the extravasation of blood components into brain tissue, leading to edema and an inflammatory response. In addition to its roles in coagulation and vascular biology, VWF is also involved in modulating the inflammatory process (Chauhan et al., 2008). It can interact with inflammatory mediators, influencing the activation and migration of inflammatory cells. In TBI, VWF may impact the development and recovery of injury by modulating the inflammatory response. However, further investigation is necessary to establish VWF as a reliable biomarker for the diagnosis and prognosis of acute TBI.

This study has several limitations. First, due to the location of our department in the emergency department, our study focused primarily on assessing outcomes during the ED visit or

TABLE 2 Discrimination power of the VWF, CT score, and GCS for mortality and GOS≤4 in TBI patients.

	Mortality			GOS ≤ 4	
	AUC	*P*-value		AUC	*P*-value
GCS	0.13	$P < 0.0001$	GCS	0.14	$P < 0.0001$
CT Score	0.86	$P < 0.0001$	CT Score	0.83	$P < 0.0001$
VWF	0.70	$P = 0.06$	VWF	0.77	$P < 0.0001$
GCS + VWF	0.87	$P < 0.0001$	GCS + VWF	0.90	$P < 0.0001$
CT + VWF	0.88	$P < 0.0001$	CT + VWF	0.87	$P < 0.0001$
CT + GCS	0.91	$P < 0.0001$	CT + GCS	0.90	$P < 0.0001$
VWF + CT + GCS	0.90	$P < 0.0001$	VWF + CT + GCS	0.91	$P < 0.0001$

VWF, von Willebrand factor; CT, computed tomography; GCS, Glasgow Coma Scale; GOS, Glasgow Outcome Scale; TBI, traumatic brain injury; AUC, area under the receiver operating characteristic curve.

initial presentation. Long-term follow-up and evaluation of VWF levels, GCS scores, and detailed prognosis were not conducted. Second, the diagnostic and predictive value of VWF in diseases other than TBI or in combination with other injuries remains unknown. Third, the findings of this study are limited to a single location and a relatively small sample size, which may restrict the generalizability of the results. Finally, further research is necessary to identify additional blood biomarkers and enhance the accuracy and reliability of TBI diagnosis and prognosis.

Conclusion

Plasma VWF concentrations were found to be significantly higher in patients with acute TBI compared to healthy individuals. In patients with acute TBI, VWF levels showed a negative correlation with GCS scores and a positive correlation with CT scores and TBI severity. However, the ability of VWF alone to predict mortality in acute TBI patients was limited, and its predictive value was enhanced when combined with Rotterdam CT scores or GCS scores. Therefore, VWF may serve as a potential biomarker for the diagnosis of acute TBI.

Data availability statement

The datasets presented in this study can be found in online repositories. The names of the repository/repositories and accession number(s) can be found in the article/Supplementary material.

Ethics statement

The studies involving humans were approved by Medical Ethics Committee of Zhongnan Hospital of Wuhan University. The studies were conducted in accordance with the local legislation and institutional requirements. The participants provided their written informed consent to participate in this study. Written informed consent was obtained from the individual(s) for the publication of any potentially identifiable images or data included in this article.

Author contributions

RZ, YZ, and HM conceived and designed the experiments. SL performed the data analysis. RZ and SL wrote the manuscript. All authors reviewed and approved the manuscript.

Acknowledgments

The authors thank the Emergency Diagnostic and Therapeutic Center of Central China in the Zhongnan Hospital of Wuhan University.

Conflict of interest

The authors declare that the research was conducted in the absence of any commercial or financial relationships that could be construed as a potential conflict of interest.

Publisher's note

Supplementary material

The Supplementary Material for this article can be found online at: https://www.frontiersin.org/articles/10.3389/fnins.2023.1222345/full#supplementary-material

References

Abdul-Muneer, P. M., Chandra, N., and Haorah, J. (2015). Interactions of oxidative stress and neurovascular inflammation in the pathogenesis of traumatic brain injury. *Mol. Neurobiol.* 51, 966–979. doi: 10.1007/s12035-014-8752-3

Al-Hajj, S., Hammoud, Z., Colnaric, J., Ataya, M., Macaron, M. M., Kadi, K., et al. (2021). Characterization of traumatic brain injury research in the middle east and north africa region: a systematic review. *Neuroepidemiology.* 10, 1–12. doi: 10.1159/000511554

Anada, R. P., Wong, K. T., Jayapalan, J. J., Hashim, O. H., and Ganesan, D. (2018). Panel of serum protein biomarkers to grade the severity of traumatic brain injury. *Electrophoresis* 39, 2308–2315. doi: 10.1002/elps.201700407

Aymé, G., Adam, F., Legendre, P., Bazaa, A., Proulle, V., Denis, C. V., et al. (2017). A novel single-domain antibody against von willebrand factor A1 domain resolves leukocyte recruitment and vascular leakage during inflammation-brief report. *Arterioscler. Thromb Vasc. Biol.* 37, 1736–1740. doi: 10.1161/ATVBAHA.117.309319

Brenner, D. J., and Hall, E. J. (2007). Computed tomography–an increasing source of radiation exposure. *N. Engl. J. Med.* 357, 2277–2284. doi: 10.1056/NEJMra072149

Chauhan, A. K., Kisucka, J., Brill, A., Walsh, M. T., Scheiflinger, F., and Wagner, D. D. (2008). ADAMTS13: a new link between thrombosis and inflammation. *J. Exp. Med.* 205, 2065–2074. doi: 10.1084/jem.20080130

Corral, L., Ventura, J. L., Herrero, J. I., Monfort, J. L., Juncadella, M., Gabarrós, A., et al. (2007). Improvement in GOS and GOSE scores 6 and 12 months after severe traumatic brain injury. *Brain Inj.* 21, 1225–1231. doi: 10.1080/02699050701727460

De Oliveira, C. O., Reimer, A. G., Da Rocha, A. B., Grivicich, I., Schneider, R. F., Roisenberg, I., et al. (2007). Plasma von Willebrand factor levels correlate with clinical outcome of severe traumatic brain injury. *J. Neurotrauma* 24, 1331–1338. doi: 10.1089/neu.2006.0159

DeWitt, D. S., and Prough, D. S. (2003). Traumatic cerebral vascular injury: the effects of concussive brain injury on the cerebral vasculature. *J. Neurotrauma* 20, 795–825. doi: 10.1089/089771503322385755

Holcomb, J. B., Tilley, B. C., Baraniuk, S., Fox, E. E., Wade, C. E., Podbielski, J. M., et al. (2015). Transfusion of plasma, platelets, and red blood cells in a 1:1:1 vs a 1:1:2 ratio and mortality in patients with severe trauma: the PROPPR randomized clinical trial. *JAMA* 313, 471–482. doi: 10.1001/jama.2015.12

Hon, K. L., Leung, A. K. C., and Torres, A. R. (2019). Concussion: a global perspective. *Semin Pediatr. Neurol.* 30, 117–127. doi: 10.1016/j.spen.2019.03.017

Huang, Y. H., Deng, Y. H., Lee, T. C., and Chen, W. F. (2012). Rotterdam computed tomography score as a prognosticator in head-injured patients undergoing decompressive craniectomy. *Neurosurgery* 71, 80–85. doi: 10.1227/NEU.0b013e3182517aa1

Hyder, A. A., Wunderlich, C. A., Puvanachandra, P., Gururaj, G., and Kobusingye, O. C. (2007). The impact of traumatic brain injuries: a global perspective. *NeuroRehabilitation* 22, 341–353. doi: 10.3233/NRE-2007-22502

Kurca, E., Sivák, S., and Kucera, P. (2006). Impaired cognitive functions in mild traumatic brain injury patients with normal and pathologic magnetic resonance imaging. *Neuroradiology* 48, 661–669. doi: 10.1007/s00234-006-0109-9

Lippa, S. M., Werner, J. K., Miller, M. C., Gill, J. M., Diaz-Arrastia, R., and Kenney, K. (2020). Recent advances in blood-based biomarkers of remote combat-related traumatic brain injury. *Curr. Neurol. Neurosci. Rep.* 20, 54. doi: 10.1007/s11910-020-01076-w

Lu, D., Mahmood, A., Goussev, A., Qu, C., Zhang, Z. G., and Chopp, M. (2004). Delayed thrombosis after traumatic brain injury in rats. *J. Neurotrauma* 21, 1756–1766. doi: 10.1089/neu.2004.21.1756

Lu, J., Marmarou, A., and Lapane, K. L. (2012). Impact of GOS misclassification on ordinal outcome analysis of traumatic brain injury clinical trials. *J. Neurotrauma* 29, 719–726. doi: 10.1089/neu.2010.1746

Miller, G. F., Daugherty, J., Waltzman, D., and Sarmiento, K. (2021). Predictors of traumatic brain injury morbidity and mortality: examination of data from the national trauma data bank: predictors of TBI morbidity and mortality. *Injury* 52, 1138–1144. doi: 10.1016/j.injury.2021.01.042

Nawashiro, H., Shima, K., and Chigasaki, H. (1995). Immediate cerebrovascular responses to closed head injury in the rat. *J. Neurotrauma* 12, 189–197. doi: 10.1089/neu.1995.12.189

Ng, C., Motto, D. G., and Di Paola, J. (2015). Diagnostic approach to von Willebrand disease. *Blood* 125, 2029–2037. doi: 10.1182/blood-2014-08-528398

Nguyen, T. C., Han, Y. Y., Kiss, J. E., Hall, M. W., Hassett, A. C., Jaffe, R., et al. (2008). Intensive plasma exchange increases a disintegrin and metalloprotease with thrombospondin motifs-13 activity and reverses organ dysfunction in children with thrombocytopenia-associated multiple organ failure. *Crit. Care Med.* 36, 2878–2887. doi: 10.1097/CCM.0b013e318186aa49

Papa, L., Lewis, L. M., Falk, J. L., Zhang, Z., Silvestri, S., Giordano, P., et al. (2012). Elevated levels of serum glial fibrillary acidic protein breakdown products in mild and moderate traumatic brain injury are associated with intracranial lesions and neurosurgical intervention. *Ann. Emerg. Med.* 59, 471–483. doi: 10.1016/j.annemergmed.2011.08.021

Plautz, W. E., Matthay, Z. A., Rollins-Raval, M. A., Raval, J. S., Kornblith, L. Z., Neal, M. D. (2020). Von Willebrand factor as a thrombotic and inflammatory mediator in critical illness. *Transfusion.* 60, S158–S166. doi: 10.1111/trf.15667

Sandsmark, D. K., Bogoslovsky, T., Qu, B. X., Haber, M., Cota, M. R., Davis, C., et al. (2019). Changes in plasma von willebrand factor and cellular fibronectin in MRI-defined traumatic microvascular injury. *Front. Neurol.* 10, 246. doi: 10.3389/fneur.2019.00246

Setiawan, B., Permatadewi, C. O., de Samakto, B., Bugis, A., Naibaho, R. M., Pangarsa, E. A., et al. (2020). Von Willebrand factor:antigen and ADAMTS-13 level, but not soluble P-selectin, are risk factors for the first asymptomatic deep vein thrombosis in cancer patients undergoing chemotherapy. *Thromb J.* 18, 33. doi: 10.1186/s12959-020-00247-6

Stocchetti, N., Pagan, F., Calappi, E., Canavesi, K., Beretta, L., Citerio, G., et al. (2004). Inaccurate early assessment of neurological severity in head injury. *J. Neurotrauma* 21, 1131–1140. doi: 10.1089/neu.2004.21.1131

Tang, N., Yin, S., Sun, Z., and Pan, Y. (2013). Time course of soluble P-selectin and von Willebrand factor levels in trauma patients: a prospective observational study. *Scand. J. Trauma Resusc. Emerg. Med.* 21, 70. doi: 10.1186/1757-7241-21-70

Tang, Y. L., Fang, L. J., Zhong, L. Y., Jiang, J., Dong, X. Y., and Feng, Z. (2020). Hub genes and key pathways of traumatic brain injury: bioinformatics analysis and in vivo validation. *Neural Regen. Res.* 15, 2262–2269. doi: 10.4103/1673-5374.284996

Tokshilykova, A. B., Sarkulova, Z. N., Kabdrakhmanova, G. B., Utepkaliyeva, A. P., Tleuova, A. S., and Satenov, Z. K. (2020). Neuron-specific markers and their correlation with neurological scales in patients with acute neuropathologies. *J. Mol. Neurosci.* 70, 1267–1273. doi: 10.1007/s12031-020-01536-5

Vavilala, M., King, M., and Yang, J. (2019). The Pediatric Guideline Adherence and Outcomes (PEGASUS) programme in severe traumatic brain injury: a single-centre hybrid implementation and effectiveness study. *Lancet Child Adolesc. Health* 3, 23–34. doi: 10.1016/S2352-4642(18)30341-9

Ward, S. E., Curley, G. F., Lavin, M., Fogarty, H., Karampini, E., McEvoy, N. L., et al. (2020). Von Willebrand factor propeptide in severe coronavirus disease 2019 (COVID-19): evidence of acute and sustained endothelial cell activation. *Br. J. Haematol.* 192, 714–719. doi: 10.1111/bjh.17273

Wu, Y., Liu, W., Zhou, Y., Hilton, T., Zhao, Z., Liu, W., et al. (2018). von Willebrand factor enhances microvesicle-induced vascular leakage and coagulopathy in mice with traumatic brain injury. *Blood* 132, 1075–1084. doi: 10.1182/blood-2018-03-841932

Xu, E. R., von Bülow, S., Chen, P. C., Lenting, P. J., Kolšek, K., Aponte-Santamaría, C., et al. (2019). Structure and dynamics of the platelet integrin-binding C4 domain of von Willebrand factor. *Blood* 133, 366–376. doi: 10.1182/blood-2018-04-843615

Yokota, H., Naoe, Y., Nakabayashi, M., Unemoto, K., Kushimoto, S., Kurokawa, A., et al. (2002). Cerebral endothelial injury in severe head injury: the significance of measurements of serum thrombomodulin and the von Willebrand factor. *J. Neurotrauma* 19, 1007–1015. doi: 10.1089/089771502760341929

Zhu, X., Cao, Y., Wei, L., Cai, P., Xu, H., Luo, H., et al. (2016). von Willebrand factor contributes to poor outcome in a mouse model of intracerebral haemorrhage. *Sci. Rep.* 6, 35901. doi: 10.1038/srep35901

frontiers | Frontiers in Molecular Neuroscience

TYPE Original Research
PUBLISHED 05 December 2023
DOI 10.3389/fnmol.2023.1298560

OPEN ACCESS

EDITED BY
Hai Sun,
The State University of New Jersey, United States

REVIEWED BY
Sung Ung Kang,
Johns Hopkins University, United States
Sangjune Kim,
Chungbuk National University, Republic of Korea

*CORRESPONDENCE
José M. Salas-Pacheco
✉ jsalas_pacheco@hotmail.com
Ada A. Sandoval-Carrillo
✉ adda-sandoval@hotmail.com

RECEIVED 21 September 2023
ACCEPTED 13 November 2023
PUBLISHED 05 December 2023

CITATION
Salas-Leal AC, Salas-Pacheco SM, Hernández-Cosaín EI, Vélez-Vélez LM, Antuna-Salcido EI, Castellanos-Juárez FX, Méndez-Hernández EM, La Llave-León O, Quiñones-Canales G, Arias-Carrión O, Sandoval-Carrillo AA and Salas-Pacheco JM (2023) Differential expression of *PSMC4*, *SKP1*, and *HSPA8* in Parkinson's disease: insights from a Mexican mestizo population. *Front. Mol. Neurosci.* 16:1298560. doi: 10.3389/fnmol.2023.1298560

Differential expression of *PSMC4*, *SKP1*, and *HSPA8* in Parkinson's disease: insights from a Mexican mestizo population

Alma C. Salas-Leal[1], Sergio M. Salas-Pacheco[1], Erik I. Hernández-Cosaín[1], Lilia M. Vélez-Vélez[1], Elizabeth I. Antuna-Salcido[1], Francisco X. Castellanos-Juárez[1], Edna M. Méndez-Hernández[1], Osmel La Llave-León[1], Gerardo Quiñones-Canales[2], Oscar Arias-Carrión[3], Ada A. Sandoval-Carrillo[1]* and José M. Salas-Pacheco[1]*

[1]Instituto de Investigación Científica, Universidad Juárez del Estado de Durango, Durango, México, [2]Hospital General Santiago Ramón y Cajal-ISSSTE, Durango, México, [3]Unidad de Trastornos del Movimiento y Sueño, Hospital General Dr. Manuel Gea González, Ciudad de México, México

Parkinson's disease (PD) is a complex neurodegenerative condition characterized by alpha-synuclein aggregation and dysfunctional protein degradation pathways. This study investigates the differential gene expression of pivotal components (*UBE2K*, *PSMC4*, *SKP1*, and *HSPA8*) within these pathways in a Mexican-Mestizo PD population compared to healthy controls. We enrolled 87 PD patients and 87 controls, assessing their gene expression levels via RT-qPCR. Our results reveal a significant downregulation of *PSMC4*, *SKP1*, and *HSPA8* in the PD group (p = 0.033, p = 0.003, and p = 0.002, respectively). Logistic regression analyses establish a strong association between PD and reduced expression of *PSMC4*, *SKP1*, and *HSPA8* (OR = 0.640, 95% CI = 0.415–0.987; OR = 0.000, 95% CI = 0.000–0.075; OR = 0.550, 95% CI = 0.368–0.823, respectively). Conversely, *UBE2K* exhibited no significant association or expression difference between the groups. Furthermore, we develop a gene expression model based on *HSPA8*, *PSMC4*, and *SKP1*, demonstrating robust discrimination between healthy controls and PD patients. Notably, the model's diagnostic efficacy is particularly pronounced in early-stage PD. In conclusion, our study provides compelling evidence linking decreased gene expression of *PSMC4*, *SKP1*, and *HSPA8* to PD in the Mexican-Mestizo population. Additionally, our gene expression model exhibits promise as a diagnostic tool, particularly for early-stage PD diagnosis.

KEYWORDS

Parkinson's disease, *UBE2K*, *PSMC4*, *SKP1*, *HSPA8*, protein degradation systems

1 Introduction

Parkinson's disease (PD) stands as a multifaceted neurodegenerative disorder characterized by the progressive degeneration of dopaminergic neurons. Nevertheless, the intricate mechanisms underlying this condition remain shrouded in uncertainty. Emerging evidence has spotlighted dysregulation in the clearance and degradation of alpha-synuclein

as a pivotal player in the pathogenesis of neuronal demise in PD (Mehra et al., 2019; Jankovic and Tan, 2020). At the crux of this degradation nexus lies the concerted interplay among chaperones, the ubiquitin-proteasome system (UPS), and autophagy-lysosomal pathways.

The UPS pathway orchestrates the disposal of damaged proteins through a meticulous tagging process involving three key enzymes: activating enzyme E1, conjugating enzyme E2, and ligase enzyme E3 (Chen and Dou, 2010). Subsequent to this tagging, the protein-ubiquitin conjugates are recognized and degraded by the 26S proteasome, a large proteolytic assembly resident within the cytosol and nucleus of eukaryotic cells. This proteasome is composed of a 20S core particle and a 19S regulatory particle (Jarome and Devulapalli, 2018).

Intriguingly, prior inquiries into the expression of genes associated with these degradation machineries in blood and brain tissues of individuals afflicted by PD, including *PSMC4* (an integral component of the 19S proteasomal particle), *SKP1* (an essential constituent of the SCF complex endowed with E3 ubiquitin ligase activity), *UBE2K* (an ubiquitin-conjugating enzyme E2K), and *HSPA8* (a 70kDa heat shock protein exerting chaperone functions), have yielded divergent results (Grunblatt et al., 2004; Mandel et al., 2005, 2012b; Molochnikov et al., 2012; Su et al., 2018). This divergence may stem from genetic disparities among diverse populations, imparting an element of complexity to our understanding of PD etiology.

Thus, the principal objective of our study is to scrutinize the expression profiles of these genes in peripheral blood samples sourced from the Mexican-mestizo population. By doing so, we aim to ascertain whether these gene expression patterns possess the potential to serve as a risk profile for PD.

2 Materials and methods

2.1 Study participants and ethical criteria

We collected samples from a cohort of 87 PD patients and 87 healthy, age-matched controls devoid of familial or personal histories of neurodegenerative diseases. PD diagnoses were confirmed by neurologists employing the United Kingdom Parkinson's disease Society Brain Bank (UKPDSBB) diagnostic criteria. Participants were recruited from three prominent public hospitals located in central and northwest Mexico: Hospital General Dr. Manuel Gea Gonzalez in Mexico City, Hospital General 450, and Hospital General Santiago Ramón y Cajal in Durango City. This study secured the ethical approval of each participating hospital's ethics committee.

All procedures adhered strictly to the ethical principles outlined in the 1964 Helsinki Declaration and its subsequent amendments. Informed written consent was obtained from all participants, with the additional requirement of a family member's consent for each participant. Pertinent patient data, encompassing age, gender, presence of depression, cognitive status, age of disease onset, and Unified Parkinson's disease Rating Scale (UPDRS) scores, were meticulously documented.

2.2 Blood collection, RNA extraction, cDNA synthesis, and RT-qPCR

Venous whole blood was collected from the subjects in Tempus Blood RNA tubes and reserved at −80 C until RNA extraction. We processed samples according to the manufacturer protocol to extract total RNA using MagMAX for Stabilized Blood Tubes RNA Isolation kit (Life Technologies, Norway). We then synthesized cDNA using a High-Capacity cDNA Reverse Transcription kit (Applied Biosystems, Carlsbad, CA, USA) according to the manufacturer's instructions. Concentration and purity of RNA and cDNA were determined using NanoDrop 2000 spectrophotometer (Thermo Fisher Scientific Inc., Germering, Germany) and cDNA was stored at −20 C until further evaluation. Gene expression levels of *UBE2K, HSPA8, SKP1*, and *PSMC4* were measured through relative quantification (RQ) of 125 ng/mL of cDNA by Real-time quantitative PCR (RT-qPCR) using a QuantStudio 3 System (Applied Biosystems, Carlsbad, CA, USA) with TaqMan assays (*UBE2K* assay ID Hs00193507_m1, *HSPA8* assay ID Hs03044880_gH, *SKP1* assay ID Hs00429069_m1 and *PSMC4* assay ID Hs00197826_m1, Applied Biosystems). The expression was normalized to the *RPLP0* gene (*RPLP0* assay ID Hs00420895_gH, Applied Biosystems). The reaction conditions were: initial hold of 10 min at 95 C; 40 cycles of denaturation for 15 s at 95 C and annealing for 1 min at 60 C.

2.3 Statistical methods

Statistical analyses were executed using SPSS Statistics 20.0 software. Quantitative data are presented as mean ± standard deviation (SD). For normally distributed parameters, differences were assessed using a two-tailed t-test, while non-parametric tests were applied to analyze mRNA and protein levels. Logistic regression was employed to investigate the association between mRNA expression and PD, with significant P-values retaining relevance in constructing predictive classifier models. Receiver operating characteristic curve (ROC) data were derived from predictive probabilities generated via multivariate logistic regression, encompassing all PD patients and a subset of early-stage PD patients (those with less than 5 and 3 years of disease evolution). Correlations were evaluated via Spearman correlation with the two-tailed test of significance. P-value < 0.05 was considered statistically significant.

3 Results

3.1 Demographic and clinical characteristics

Table 1 presents a comprehensive overview of the demographic and clinical attributes of both the PD cases and control subjects. Comparative analysis of these variables between the two groups unveiled significant differences on the presence of depression ($p = 0.040$).

10.3389/fnmol.2023.1298560

TABLE 1 Demographic and clinical characteristics of study participants.

	PD $n = 87$	Control $n = 87$	p
Age ± SD	70.4 ± 9.27	70.03 ± 9.19	0.793[+]
Gender			
Female	42 (48.3%)	42 (48.3%)	1[++]
Male	45 (51.7%)	45 (51.7%)	
Minimum Age	53	53	
Maximum Age	94	92	
Depression (HAM-D)	67 (77.2%)	53 (61.3%)	0.040[++]
Cognitive impairment (MMSE)	44 (51.2%)	45 (52.3%)	0.890[++]
Age of onset ± SD	64.9 ± 9.6		
PD Early stage (smaller or equal to 5 years of diagnosis)	52 (59.8%)		
PD Early stage (smaller or equal to 3 years of diagnosis)	31 (17.8%)		
UPDRS total score ± SD	68.6 ± 31.3		
UPDRS PART I ± SD	10.5 ± 6.9		
UPDRS PART II ± SD	14.9 ± 9.4		
UPDRS PART III ± SD	39.9 ± 19.7		
UPDRS PART IV ± SD	2.3 ± 4.8		

[+]Student t-test, [++]chi-square test.

3.2 Gene expression profiles

Figure 1 provides a graphical representation of the observed gene expression levels in both the PD and control groups. Utilizing Relative Quantification (RQ) analysis, we identified a significant reduction in the expression levels of *HSPA8*, *SKP1*, and *PSMC4* among PD cases ($p = 0.002$, $p = 0.003$, and $p = 0.033$, respectively). To further elucidate their relevance to PD, logistic regression analysis was conducted, adjusting for sex and age (Table 2). The results unequivocally substantiated the associations of *HSPA8*, *SKP1*, and *PSMC4* with PD. However, *UBE2K* exhibited no statistically significant association with the disease.

3.3 Influence of depression on gene expression

We observed a notable disparity in the frequency of depression between the PD and control groups (Table 1), consequently, we conducted a gene expression association analysis considering while adjusting for sex, age, and depression. The findings revealed that, even after factoring in depression, the previously established associations for *HSPA8* and *SKP1* remained statistically significant (Table 3).

3.4 Correlation analysis of gene expression

An exploratory analysis of gene expression within the control group unveiled intriguing interrelationships among the four genes under scrutiny. Specifically, we observed a positive correlation between the expression levels of *HSPA8*, *UBE2K*, and *PSMC4*. Conversely, *SKP1* exhibited a negative correlation with these three genes (Figure 2A). Similar results were observed when testing the PD group, except for the correlation between *SKP1* and *PSMC4*, which was not statistically significant ($p = 0.165$, Figure 2B). Furthermore, a correlation analysis within the PD group revealed no significant correlation between PD severity (measured with UPDRS) and the expression levels of *SKP1A* ($p = 0.455$), *PSMC4* ($p = 0.655$), *UBE2K* ($p = 0.305$) and *HSPA8* ($p = 0.786$).

3.5 Predictive utility of gene expression

To assess the potential utility of gene expression as a prognostic biomarker for PD, we constructed Receiver Operating

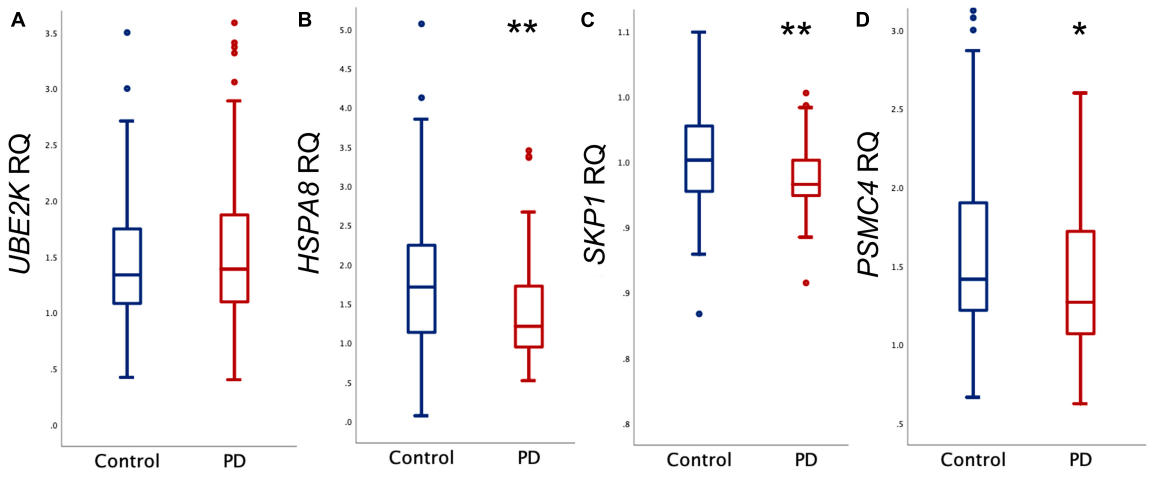

FIGURE 1
Relative quantification (RQ) of mRNA. Comparison between control and PD groups of mRNA levels of **(A)** *UBE2K*, **(B)** *HSPA8*, **(C)** *SKP1*, and **(D)** *PSMC4*. Outliers are denoted by dots. $^{**}p < 0.005$, $^{*}p < 0.05$.

TABLE 2 Association of gene expression levels with PD adjusted by sex and age.

	OR*	95% CI	*p*
UBE2K	0.943	0.711–1.250	0.681
HSPA8	0.550	0.368–0.823	0.004
SKP1	0.000	0.000–0.075	0.012
PSMC4	0.640	0.415–0.987	0.044

OR, Odds Ratio; CI, confidence interval. *Adjusted by sex and age.

TABLE 3 Association of gene expression levels with PD adjusted by sex, age and depression.

	OR*	95% CI	*p*
UBE2K	1.041	0.758–1.430	0.803
HSPA8	0.461	0.278–0.764	0.003
SKP1	0.000	0.000–0.000	0.001
PSMC4	0.798	0.499–1.278	0.348

OR, Odds Ratio; CI, confidence interval. *Adjusted by sex, age and depression.

Characteristic (ROC) curves based on predictive values derived from logistic regression. We formulated three distinct models, each contingent on the duration of PD evolution (**Figure 3**). Evaluation of these curves unveiled increasing values for the Area under the Curve (AUC), signifying that a shorter duration of PD evolution positively impacts the predictive value of the model. At a cut-off point of 0.25 it was possible to distinguish between PD individuals and healthy controls with sensitivity and specificity values of 77% and 72.3%, respectively (**Figure 3C**).

4 Discussion

In this study, we delved into the gene expression profiles of *UBE2K*, *HSPA8*, *SKP1*, and *PSMC4* within both control and PD cohorts to evaluate their potential implications in the pathogenesis of PD. Our findings unveiled marked reductions in the gene expression levels of *HSPA8*, *SKP1*, and *PSMC4* in the PD group in comparison to the control group.

The *PSMC4* gene encodes the proteasomal protein S6 ATPase, a constituent of the 19S regulatory subunit essential for the assembly of the 26S proteasome (Dahlmann, 2016). Previous investigations have identified the presence of the *PSMC4* protein in Lewy bodies, demarcating their periphery within dopaminergic neurons of the substantia nigra (Grünblatt et al., 2018). Notably, our observations concerning *PSMC4* gene expression in blood align with prior reports (Molochnikov et al., 2012). Similar reductions in mRNA levels of *PSMC4* within the substantia nigra pars compacta (SNpc) of the brain have been documented in PD patients when compared to controls (Grunblatt et al., 2004; Grünblatt, 2012). The correlation between gene expression levels, protein presence in the SNpc, and localization within Lewy bodies in post-mortem SN samples from PD patients suggests the potential biological relevance of our findings derived from blood samples (Marx et al., 2007; Grünblatt et al., 2018). Recent research indicated a decreased expression of *PSMC4* mRNA, particularly evident after 3 years of disease progression, and established a correlation with disease severity. Nevertheless, this correlation, while noteworthy, did not achieve the requisite strength to be incorporated into a predictive PD classifier model (Rabey et al., 2020).

The *SKP1* gene encodes the SKP1 protein, involved in the formation of the SCF complex, endowed with E3 ubiquitin ligase activity. This intricate assembly plays a pivotal role in identifying target proteins for degradation via the ubiquitin-proteasome system, primarily through interactions with F-box proteins (Zheng et al., 2002). SKP1 exhibits the ability to directly interact with FBXO7, an F-box protein implicated in the regulation of alpha-synuclein (Zhao et al., 2013; Conedera et al., 2016). Perturbations in SKP1 function could potentially contribute to PD development by disrupting the proper degradation of proteins, leading to an accrual of misfolded proteins (Mandel et al., 2012a). Consistent with our findings, reduced expression levels of *SKP1* in both the SNpc and blood have been documented in PD (Grunblatt et al., 2004; Mandel et al., 2009; Molochnikov et al., 2012). It is important to underscore that silencing of *SKP1* has been experimentally demonstrated to promote the accumulation of cytoplasmic inclusions reminiscent of Lewy bodies while concurrently exerting a negative regulatory effect on *HSPA8* gene expression (Fishman-Jacob et al., 2009; Mandel et al., 2012a). *In vitro* studies have further validated that SKP1 deficiency exacerbates PD pathology, culminating in the formation of Lewy body-like inclusions and ensuing neuronal demise (Mandel et al., 2012b). Notably, our identification of a negative correlation between *SKP1* expression and all three genes within our control group implies that SKP1 may potentially exert its effects only in the presence of cellular damage. Consequently, normal *SKP1* expression might not suffice to deter PD progression in the absence of underlying cellular damage.

HSC70 protein, encoded by the *HSPA8* gene, stands as an integral component of Lewy bodies in PD (Grünblatt et al., 2018). This chaperone protein, orchestrates the selective degradation of proteins, maintaining cellular proteostasis through chaperone-mediated autophagy, a process contingent on lysosomes (Nie et al., 2021). Our findings regarding *HSPA8* expression harmonize with prior assessments encompassing transcript and protein levels in both peripheral blood and brain tissues (Grunblatt et al., 2004; Tanaka, 2009; Alvarez-Erviti et al., 2010; Papagiannakis et al., 2015). Nonetheless, it is worth noting that Molochnikov et al. (2012) reported an elevation in *HSPA8* expression levels in PD patients, although the biological significance of this elevation was not explained.

The differential expression profiles observed in our study suggest potential perturbations in protein degradation pathways within our study population, which could underlie the abnormal aggregation of proteins integral to Lewy bodies and consequently impact dopaminergic neuron function.

Our comprehensive ROC curve analysis illuminates the potential utility of *HSPA8*, *PSMC4*, and *SKP1* gene expression levels as effective discriminators between healthy controls and individuals with PD. Similar results in a multi- center study in the German, Italian and Israeli population suggest the ability of a five-gene panel, including *HSPA8*, *PSMC4*, *SKP1* and *UBE2K*, to diagnose early/mild PD in Italy, Germany, and Israel populations (Molochnikov et al., 2012).

As depicted in **Figure 3**, this discriminatory capacity is further augmented when PD has a shorter duration. These observations collectively indicate that the expression levels of these genes

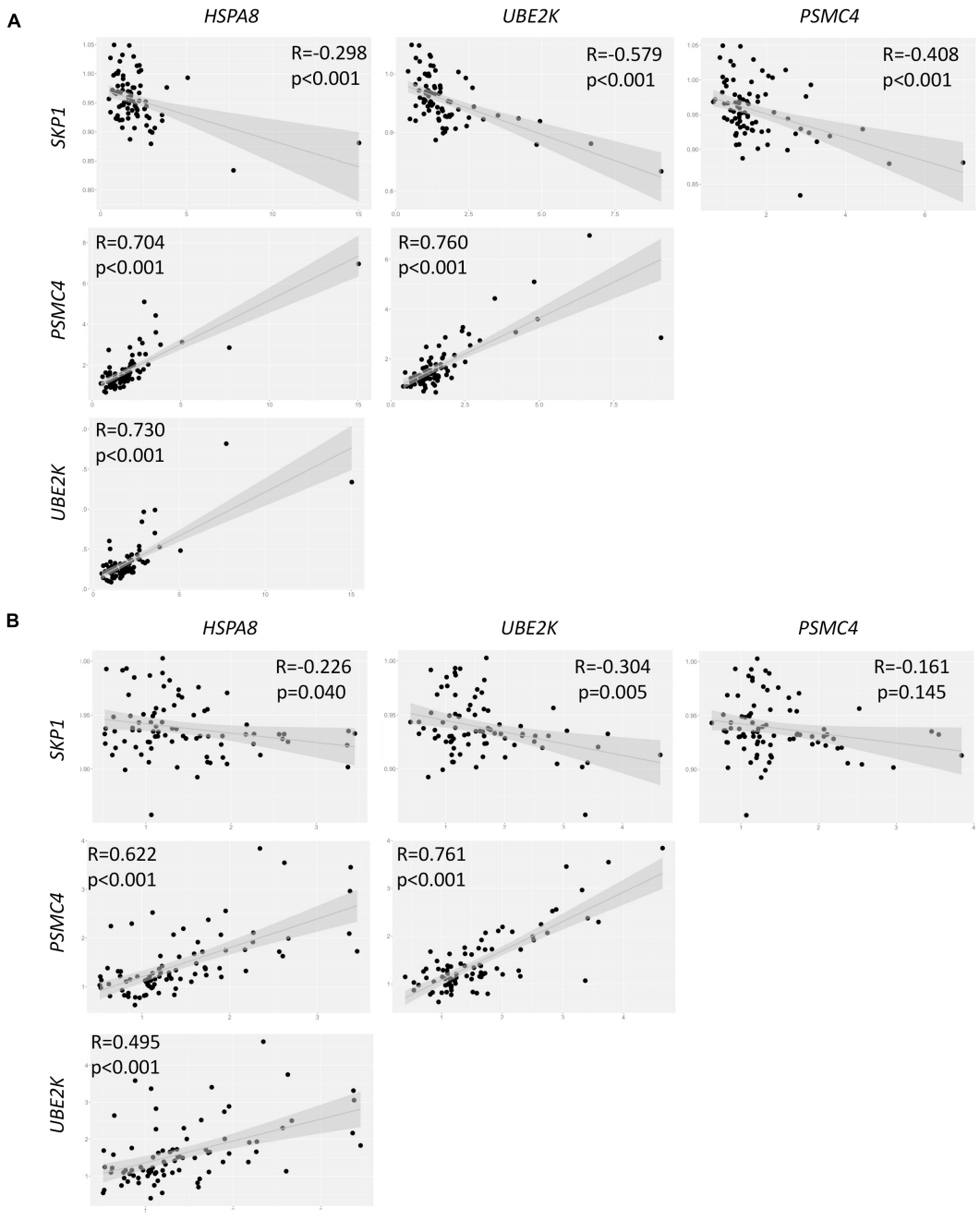

FIGURE 2
Correlation analysis of gene expression in both control **(A)** and PD **(B)** groups. R = Spearman correlations coefficient.

experience significant reductions during the early stages of PD. Importantly, these reductions may be partially ameliorated through medication-induced epigenetic modifications.

Previously, it has been shown that the accuracy of clinical diagnosis for PD could range from 53–74% (Tolosa et al., 2006). More recently, accuracies ranging from 69% to over 90% have been reported in some populations with advanced symptoms (Rizzo et al., 2016). However, a recent study describes an accuracy of 26% in clinical diagnoses for PD in patients with recent symptom onset (Prajjwal et al., 2023). Our model suggests an accuracy of 79.1% for predicting PD in the early stage, as indicated by the AUC values obtained, suggesting it as a promising tool for PD prediction.

One noteworthy limitation of our study resides in the fact that all PD patients were undergoing L-dopa treatment, a factor that has been previously suggested to potentially influence gene expression patterns (Taravini et al., 2016). Reports indicated that L-dopa influenced DNA methylation, resulting in reduced expression of the *SNCA* gene. Nevertheless, it was suggested that its epigenetic influence on other genes could have been possible (Schmitt et al., 2015; Guhathakurta et al., 2017; Song et al., 2017).

The variances in our findings when compared to other populations underscore the necessity of exploring associations between single nucleotide polymorphisms (SNPs) and gene expression to elucidate these disparities (Soldner et al., 2016;

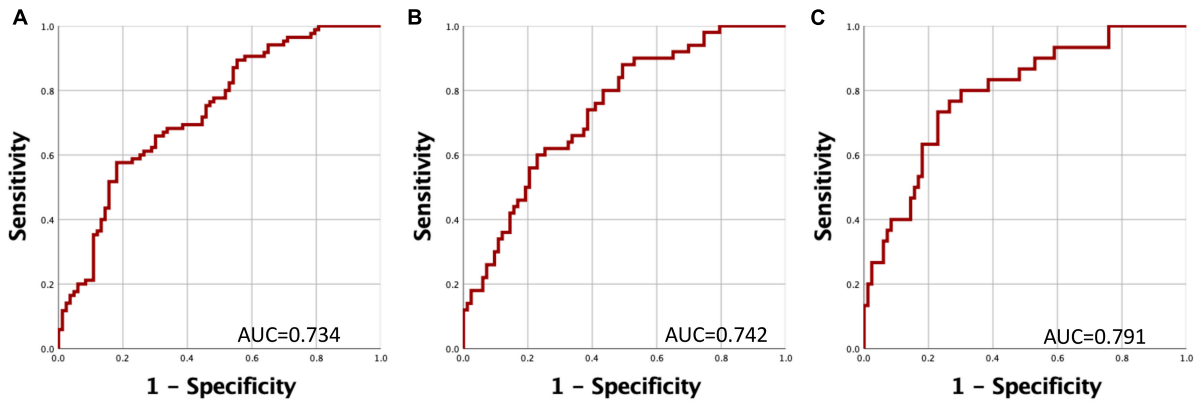

FIGURE 3
Receiver Operating Characteristic (ROC) Curves for Discriminating Between PD Patients and Controls. The curve represents the relationship between specificity and sensitivity based on the predictive probability derived from gene expression levels of *HSPA8*, *SKP1*, and *PSMC4*. **(A)** Comparison of PD patients versus healthy controls. **(B)** Comparison of PD patients with a disease duration of less than 5 years versus healthy controls. **(C)** Comparison of PD patients with a disease duration of less than 3 years versus healthy controls.

Salas-Leal et al., 2021). Consequently, future endeavors should encompass genotyping to modulate transcript variants, shedding light on these discrepancies. Additionally, the execution of cohort studies will be indispensable in delineating the potential utility of our model as a predictive tool for PD.

Data availability statement

The raw data supporting the conclusions of this article will be made available by the authors, without undue reservation.

Ethics statement

The studies involving humans were approved by the Comité de ética del Hospital General Dr. Manuel Gea González, Comité de ética del Hospital General 450 and Comité de ética del Hospital General Santiago Ramón y Cajal. The studies were conducted in accordance with the local legislation and institutional requirements. Written informed consent for participation in this study was provided by the participants' legal guardians/next of kin.

Author contributions

AS-L: Conceptualization, Methodology, Writing—original draft. SS-P: Data curation, Formal analysis, Methodology, Writing—review and editing. EH-C: Data curation, Formal analysis, Writing—review and editing. LV-V: Investigation, Methodology, Writing—review and editing. EA-S: Investigation, Methodology, Writing—review and editing. FC-J: Investigation, Methodology, Writing—review and editing. EM-H: Data curation, Methodology, Writing—review and editing. OL-L: Data curation, Formal analysis, Writing—review and editing. GQ-C: Data curation, Investigation, Writing—review and editing. OA-C: Data curation, Formal analysis, Writing—review and editing. AS-C: Conceptualization, Formal analysis, Funding acquisition, Supervision, Writing—review and editing. JS-P: Conceptualization, Methodology, Supervision, Visualization, Writing—review and editing.

Funding

The author(s) declare financial support was received for the research, authorship, and/or publication of the article. This study was supported by the grants from CONACyT (FOSISS 2014:233092 and CB 2015:253857 giving to AS-C).

Acknowledgments

We would like to thank all the participants in the project and their families for their willingness and cooperation throughout the development of this study.

Conflict of interest

The authors declare that the research was conducted in the absence of any commercial or financial relationships that could be construed as a potential conflict of interest.

Publisher's note

References

Alvarez-Erviti, L., Rodriguez-Oroz, M., Cooper, J., Caballero, C., Ferrer, I., Obeso, J., et al. (2010). Chaperone-mediated autophagy markers in Parkinson disease brains. *Arch. Neurol.* 67, 1464–1472. doi: 10.1001/archneurol.2010.198

Chen, D., and Dou, Q. (2010). The ubiquitin-proteasome system as a prospective molecular target for cancer treatment and prevention. *Curr. Protein Pept. Sci.* 11, 459–470. doi: 10.2174/138920310791824057

Conedera, S., Apaydin, H., Li, Y., Yoshino, H., Ikeda, A., Matsushima, T., et al. (2016). FBXO7 mutations in Parkinson's disease and multiple system atrophy. *Neurobiol. Aging* 40:192.e1–192.e5. doi: 10.1016/j.neurobiolaging.2016.01.003

Dahlmann, B. (2016). Mammalian proteasome subtypes: Their diversity in structure and function. *Arch. Biochem. Biophys.* 591, 132–140. doi: 10.1016/j.abb.2015.12.012

Fishman-Jacob, T., Reznichenko, L., Youdim, M., and Mandel, S. A. (2009). A sporadic Parkinson disease model via silencing of the ubiquitin-proteasome/E3 ligase component SKP1A. *J. Biol. Chem.* 284, 32835–32845. doi: 10.1074/jbc.M109.034223

Grünblatt, E. (2012). Parkinson's disease: Molecular risk factors. *Parkinsonism Relat. Disord.* 18, S45–S48. doi: 10.1016/S1353-8020(11)70016-5

Grunblatt, E., Mandel, S., Jacob-Hirsch, J., Zeligson, S., Amariglio, N., Rechavi, G., et al. (2004). Gene expression profiling of parkinsonian substantia nigra pars compacta; alterations in ubiquitin-proteasome, heat shock protein, iron and oxidative stress regulated proteins, cell adhesion/cellular matrix and vesicle trafficking genes. *J. Neural Transm.* 111, 1543–1573. doi: 10.1007/s00702-004-0212-1

Grünblatt, E., Ruder, J., Monoranu, C., Riederer, P., Youdim, M., and Mandel, S. (2018). Differential alterations in metabolism and proteolysis-related proteins in human Parkinson's Disease substantia nigra. *Neurotox Res.* 33, 560–568. doi: 10.1007/s12640-017-9843-5

Guhathakurta, S., Bok, E., Evangelista, B., and Kim, Y. (2017). Deregulation of α-synuclein in Parkinson's disease: Insight from epigenetic structure and transcriptional regulation of SNCA. *Prog. Neurobiol.* 154, 21–36. doi: 10.1016/j.pneurobio.2017.04.004

Jankovic, J., and Tan, E. (2020). Parkinson's disease: Etiopathogenesis and treatment. *J. Neurol. Neurosurg. Psychiatry* 91, 795–808. doi: 10.1136/jnnp-2019-322338

Jarome, T., and Devulapalli, R. (2018). The ubiquitin-proteasome system and memory: Moving beyond protein degradation. *Neurosci* 24, 639–651. doi: 10.1177/1073858418762317

Mandel, S., Fishman-Jacob, T., and Youdim, M. (2009). Modeling sporadic Parkinson's disease by silencing the ubiquitin E3 ligase component, SKP1A. *Parkinsonism Relat. Disord.* 15(Suppl. 3), S148–S151. doi: 10.1016/S1353-8020(09)70803-X

Mandel, S., Fishman-Jacob, T., and Youdim, M. (2012b). Targeting Skp1, an ubiquitin E3 ligase component found decreased in sporadic Parkinsons Disease. *Neurodegener. Dis.* 10, 220–223. doi: 10.1159/000333223

Mandel, S., Fishman-Jacob, T., and Youdim, M. (2012a). Genetic reduction of the E3 ubiquitin ligase element, SKP1A and environmental manipulation to emulate cardinal features of Parkinson's disease. *Parkinsonism Relat. Disord.* 18(Suppl. 1), S177–S179. doi: 10.1016/S1353-8020(11)70055-4

Mandel, S., Grunblatt, E., Riederer, P., Amariglio, N., Jacob-Hirsch, J., Rechavi, G., et al. (2005). Gene expression profiling of sporadic Parkinson's disease substantia nigra pars compacta reveals impairment of ubiquitin-proteasome subunits. SKP1A, aldehyde dehydrogenase, and chaperone HSC-70. *Ann. N. Y. Acad. Sci.* 1053, 356–375. doi: 10.1196/annals.1344.031

Marx, F., Soehn, A., Berg, D., Melle, C., Schiesling, C., Lang, M., et al. (2007). The proteasomal subunit S6 ATPase is a novel synphilin-1 interacting protein–implications for Parkinson's disease. *FASEB J. Off. Publ. Fed. Am. Soc. Exp. Biol.* 21, 1759–1767. doi: 10.1096/fj.06-6734com

Mehra, S., Sahay, S., and Maji, S. (2019). α-Synuclein misfolding and aggregation: Implications in Parkinson's disease pathogenesis. *Biochim. Biophys. Acta Proteins Proteomics* 1867, 890–908. doi: 10.1016/j.bbapap.2019.03.001

Molochnikov, L., Rabey, J., Dobronevsky, E., Bonuccelli, U., Ceravolo, R., Frosini, D., et al. (2012). A molecular signature in blood identifies early Parkinson's disease. *Mol. Neurodegener.* 7:26. doi: 10.1186/1750-1326-7-26

Nie, T., Tao, K., Zhu, L., Huang, L., Hu, S., Yang, R., et al. (2021). Chaperone-mediated autophagy controls the turnover of E3 ubiquitin ligase MARCHF5 and regulates mitochondrial dynamics. *Autophagy* 17, 2923–2938. doi: 10.1080/15548627.2020.1848128

Papagiannakis, N., Xilouri, M., Koros, C., Stamelou, M., Antonelou, R., Maniati, M., et al. (2015). Lysosomal alterations in peripheral blood mononuclear cells of Parkinson's disease patients. *Mov. Disord.* 30, 1830–1834. doi: 10.1002/mds.26433

Prajjwal, P., Flores Sanga, H., Acharya, K., Tango, T., John, J., and Rodriguez, R. (2023). Parkinson's disease updates: Addressing the pathophysiology, risk factors, genetics, diagnosis, along with the medical and surgical treatment. *Ann. Med. Surg.* 85, 4887–4902. doi: 10.1097/MS9.0000000000001142

Rabey, J., Yarden, J., Dotan, N., Mechlovich, D., Riederer, P., and Youdim, M. (2020). Creation of a gene expression classifier for predicting Parkinson's disease rate of progression. *J. Neural. Transm.* 127, 755–762. doi: 10.1007/s00702-020-02194-y

Rizzo, G., Copetti, M., Arcuti, S., Martino, D., Fontana, A., and Logroscino, G. (2016). Accuracy of clinical diagnosis of Parkinson disease: A systematic review and meta-analysis. *Neurology* 86, 566–576. doi: 10.1212/WNL.0000000000002350

Salas-Leal, A., Salas-Pacheco, S., Gavilán-Ceniceros, J., Castellanos-Juárez, F., Méndez-Hernández, E., and La Llave-León, O. (2021). α-syn and SNP rs356219 as a potential biomarker in blood for Parkinson's disease in Mexican Mestizos. *Neurosci. Lett.* 754:135901. doi: 10.1016/j.neulet.2021.135901

Schmitt, I., Kaut, O., Khazneh, H., deBoni, L., Ahmad, A., Berg, D., et al. (2015). L-dopa increases α-synuclein DNA methylation in Parkinson's disease patients in vivo and in vitro. *Mov. Disord.* 30, 1794–1801. doi: 10.1002/mds.26319

Soldner, F., Stelzer, Y., Shivalila, C., Abraham, B., Latourelle, J., Barrasa, M., et al. (2016). Parkinson-associated risk variant in distal enhancer of α-synuclein modulates target gene expression. *Nature* 533, 95–99. doi: 10.1038/nature17939

Song, J., Kim, B., Nguyen, D., Samidurai, M., and Choi, S. (2017). Levodopa (L-DOPA) attenuates endoplasmic reticulum stress response and cell death signaling through DRD2 in SH-SY5Y neuronal cells under α-synuclein-induced toxicity. *Neuroscience* 358, 336–348. doi: 10.1016/j.neuroscience.2017.06.060

Su, J., Huang, P., Qin, M., Lu, Q., Sang, X., Cai, Y., et al. (2018). Reduction of HIP2 expression causes motor function impairment and increased vulnerability to dopaminergic degeneration in Parkinson's disease models. *Cell Death Dis.* 9:1020. doi: 10.1038/s41419-018-1066-z

Tanaka, K. (2009). The proteasome: Overview of structure and functions. *Proc. Jpn. Acad. Ser. B Phys. Biol. Sci.* 85, 12–36. doi: 10.2183/pjab.85.12

Taravini, I., Larramendy, C., Gomez, G., Saborido, M., Spaans, F., Fresno, C., et al. (2016). Contrasting gene expression patterns induced by levodopa and pramipexole treatments in the rat model of Parkinson's disease. *Neuropharmacology* 101, 576–589. doi: 10.1016/j.neuropharm.2015.04.018

Tolosa, E., Wenning, G., and Poewe, W. (2006). The diagnosis of Parkinson's disease. *Lancet Neurol.* 5, 75–86. doi: 10.1016/S1474-4422(05)70285-4

Zhao, T., Severijnen, L., van der Weiden, M., Zheng, P., Oostra, B., Hukema, R., et al. (2013). FBXO7 immunoreactivity in α-synuclein-containing inclusions in Parkinson disease and multiple system atrophy. *J. Neuropathol. Exp. Neurol.* 72, 482–488. doi: 10.1097/NEN.0b013e318293c586

Zheng, N., Schulman, B., Song, L., Miller, J., Jeffrey, P., Wang, P., et al. (2002). Structure of the Cul1-Rbx1-Skp1-F boxSkp2 SCF ubiquitin ligase complex. *Nature* 416, 703–709. doi: 10.1038/416703a

frontiers | Frontiers in Molecular Neuroscience

TYPE Original Research
PUBLISHED 08 January 2024
DOI 10.3389/fnmol.2023.1288930

OPEN ACCESS

EDITED BY
Gal Bitan,
University of California, Los Angeles, United States

REVIEWED BY
Nicolas Sergeant,
Institut National de la Santé et de la Recherche Médicale (INSERM), France
Lenka Hromadkova,
Case Western Reserve University, United States

*CORRESPONDENCE
Bin Xu
✉ bxu@nccu.edu
Andy J. Liu
✉ andy.liu@duke.edu

RECEIVED 11 September 2023
ACCEPTED 29 November 2023
PUBLISHED 08 January 2024

CITATION
Wu L, Arvai S, Wang S-HJ, Liu AJ and Xu B (2024) Differential diagnosis of mild cognitive impairment of Alzheimer's disease by Simoa p-tau181 measurements with matching plasma and CSF.
Front. Mol. Neurosci. 16:1288930.
doi: 10.3389/fnmol.2023.1288930

Differential diagnosis of mild cognitive impairment of Alzheimer's disease by Simoa p-tau181 measurements with matching plasma and CSF

Ling Wu[1,2], Stephanie Arvai[3], Shih-Hsiu J. Wang[2,3,4], Andy J. Liu[2,3,4]* and Bin Xu[1,2,5]*

[1]Biomanufacturing Research Institute and Technology Enterprise (BRITE), North Carolina Central University, Durham, NC, United States, [2]Duke-UNC Alzheimer's Disease Research Center, Durham, NC, United States, [3]Department of Neurology, Duke University Medical Center, Durham, NC, United States, [4]Department of Pathology, Duke University Medical Center, Durham, NC, United States, [5]Department of Pharmaceutical Sciences, North Carolina Central University, Durham, NC, United States

Alzheimer's disease (AD) is characterized by a long preclinical phase. Although late-stage AD/dementia may be robustly differentiated from cognitively normal individuals by means of a clinical evaluation, PET imaging, and established biofluid biomarkers, disease differentiation between cognitively normal and various subtypes of mild cognitive impairment (MCI) remains a challenging task. Differential biomarkers for early-stage AD diagnosis with accessible biofluid samples are urgently needed. Misfolded phosphorylated tau aggregates (p-tau) are present in multiple neurodegenerative diseases known as "tauopathies", with the most common being AD. P-tau181 is a well-established p-tau biomarker to differentiate AD dementia from non-AD pathology. However, it is unclear if p-tau181 is capable of diagnosing MCI, an early AD stage, from cognitively normal subjects, or if it can discriminate MCI subtypes amnestic MCI (aMCI) from non-amnestic MCI (naMCI). Here we evaluated the capability of p-tau181 in diagnosing MCI from cognitively normal subjects and discriminating aMCI from naMCI subtypes. We collected matching plasma and CSF samples of a clinically diagnosed cohort of 35 cognitively normal, 34 aMCI, 17 naMCI, and 31 AD dementia cases (total 117 participants) with supplemental CSF Aβ42 and total tau AD biomarker levels and performed Simoa p-tau181 assays. The diagnostic capabilities of Simoa p-tau181 assays to differentiate these cohorts were evaluated. We found (i) p-tau181 can robustly differentiate MCI or aMCI from cognitively normal cohorts with matching plasma and CSF samples, but such differentiation is weaker in diagnosing naMCI from cognitively normal groups, (ii) p-tau181 is not capable of differentiating aMCI from naMCI cohorts, and (iii) either factor of Aβ or total tau burden markedly improved differentiation power to diagnose aMCI from cognitively normal group. Plasma and CSF p-tau181 levels may serve as a promising biomarker for diagnosing aMCI from normal controls in the preclinical phase. But more robust new biomarkers are needed to differentiate naMCI from cognitively normal cases or to discriminate between MCI subtypes, aMCI from naMCI.

KEYWORDS

Alzheimer's disease, mild cognitive impairment, p-tau181 biomarker, early diagnosis, matching plasma and CSF pre-mortem samples

Introduction

Accumulation of tau neurofibrillary tangles (NFTs) and Aβ amyloid plaques are two neuropathological features of Alzheimer's disease (AD) (Braak and Braak, 1991; Lee et al., 2001; Selkoe, 2001). NFTs are made from hyperphosphorylated tau, a neuron-enriched, microtubule (MT) associated protein. Under non-pathological conditions, tau is minimally phosphorylated, highly soluble and shows little tendency to form aggregates. After phosphorylation and other post-translational modifications (Wesseling et al., 2020), however, tau aggregates into insoluble, paired helical and straight filaments, tightly packed bundles of which constitute the NFTs thought to be neurotoxic and important in the pathogenesis of AD and related tauopathies. AD is a slowly progressing disease. It can take 15–20 years to develop noticeable neuropathological changes that lead to cognitive impairment and behavioral abnormalities (Vermunt et al., 2019). Therefore, early detection of AD is critical for devising novel treatment strategies that may prevent or slow down progression to severe dementia, which significantly impacts the quality of life and cost of care.

Mild cognitive impairment (MCI) is considered an early disease stage of AD where subtle cognitive changes can be detected by neurocognitive tests but the ability to perform daily activities independently is preserved. MCI is classified as amnestic MCI (aMCI) and non-amnestic MCI (naMCI), with the former primarily affecting memory and the latter affecting cognitive functions other than memory. Individuals with aMCI have a higher rate of conversion to AD dementia (Grundman, 2004), and thus aMCI may represent preclinical stages of AD (Petersen et al., 2006). In contrast, individuals with naMCI have a higher rate of progression to other types of dementia, such as dementia with Lewy bodies (Ferman et al., 2013). Diagnostic assays to detect AD-related changes at MCI stage and differentiate aMCI from naMCI are therefore critical to identify patients at pre-clinical stage of AD for targeted early intervention. Significant progress has been made in the last few years in the clinical diagnosis of AD, such as the development of sensitive Single Molecular Array (Simoa) assays for site-specific phospho-tau epitope detection (such as p-tau181, p-tau217, and p-tau231) to differentiate AD from non-AD with brain tissues, CSF and blood samples (Rissin et al., 2010; Blennow et al., 2015; Janelidze et al., 2020; Ashton et al., 2021, 2022; Thijssen et al., 2021). However, MCI diagnosis and MCI subgroups discrimination remain a significant challenge.

In this study, we sought to evaluate the capabilities of Simoa p-tau181 test as a molecular biomarker for differential diagnosis of mild cognitive impairment of Alzheimer's disease with matching plasma and CSF samples. Simoa p-tau181 test is a FDA-approved digitizing biomarker developed for low-abundance detection in plasma or CSF and translated for clinical diagnostic evaluation of Alzheimer's disease (Mielke et al., 2018; Karikari et al., 2020). Current study focuses on p-tau181 utility for MCI diagnosis from cognitively normal cohorts and for MCI subgroups (aMCI and naMCI) discrimination, in part because p-tau181 is one of the best characterized molecular biomarker for AD diagnosis. Using a clinically diagnosed set of cognitively normal, aMCI, naMCI, and AD dementia cohorts (total 117 participants), we first demonstrated that p-tau181 is capable of differentiating MCI subjects from cognitively normal cohorts with high confidence in matching plasma and CSF samples (p = 0.0009 in plasma and $p < 0.0001$ in CSF). While our data showed that p-tau181 is able to diagnose aMCI, it is less capable to differentiate naMCI from cognitively normal individuals. Furthermore, our data demonstrated p-tau181 is not capable of differentiating aMCI from naMCI cohorts. Thirdly, either factor of being Aβ-positive or total tau-positive markedly improved differentiation performance to diagnose aMCI with p-tau181 from cognitively normal group.

Abbreviations: AD, Alzheimer's disease; aMCI, amnestic MCI; AUC, area under the curve; CN, cognitively normal; CSF, cerebrospinal fluid; MCI, mild cognitive impairment; MMSE, mini-Mental State Examination; MoCA, Montreal Cognitive Assessment; naMCI, non-amnestic MCI; NFT, neurofibrillary tangle; PET, positron emission tomography; PMCA, protein misfolding cyclic amplification; PTM, post-translational modification; ROC, receiver operating characteristics; RT-QuIC, real-time quaking-induced conversion; Simoa, Single molecular array.

Materials and methods

Study participants

Clinical diagnosis of dementia, MCI, and cognitively normal was based on a clinical evaluation at the Duke Memory Disorder clinic. Cognitively normal participants were recruited separately and their cognitive status was determined by the patients' functional status. Cognitive status of MCI and AD patients was determined by a combination of patients' (or their family members') stated symptoms, their functional status (activities of daily living, ADLs, and instrumental activities of daily living, iADLs), and the Montreal Cognitive Assessment (MoCA) neuropsychological evaluation. Demographic information, clinical diagnosis, CSF Aβ and total tau biomarker data of total 117 participants included in this study are summarized in **Table 1** and obtained from the Duke University Department of Neurology's BioBank.

Plasma and CSF sample collection and handling

Blood samples were collected and handled as described elsewhere (Palmqvist et al., 2019; Janelidze et al., 2020). Briefly, blood samples were collected at the same time as CSF samples, and the collection was performed during a clinically indicated lumbar puncture visit with participants not fasting. Blood samples were collected and analyzed according to a standardized protocol. For each study participant, blood was collected in EDTA-plasma tubes and centrifuged (2000 g, 4°C) for 10 min. After centrifugation, plasma from all tubes were combined, mixed, and 1 mL was aliquoted into polypropylene tubes and stored at −80°C within 30 to 60 min of collection. Lumbar CSF samples were collected through a standard spinal tap procedure performed at the Duke Memory Disorders clinic. The laboratory technicians performing the biochemical analyses of plasma and CSF biospecimens were blinded to the clinical data.

TABLE 1 Demographic and characteristics of study participants (N = 117).

	CN (35)	aMCI (34)	naMCI (17)	AD (31)	P-value
Age (mean ± SD), years	67.4 ± 16.8	72.1 ± 8.5	70.6 ± 9.7	72.7 ± 9.2	0.12 (CN vs. AD) 0.16 (CN vs. aMCI) 0.43 (CN vs. naMCI)
Sex, Female (%)	24 (68.6)	20 (58.8)	6 (35.3)	18 (58.1)	
MoCA score (mean ± SD)	NA	22.8 ± 2.3	22.2 ± 3.9	16.9 ± 5.1	9.7×10^{-7} (aMCI vs. AD) 3.1×10^{-4} (naMCI vs. AD)
Aβ (mean ± SD), pg/ml	NA	1040.8 ± 420.1	1119.2 ± 495.6	815.9 ± 309.8	0.017 (aMCI vs. AD) 0.032 (naMCI vs. AD)
Total tau (mean ± SD), pg/ml	NA	282.9 ± 133.1	266.8 ± 175.2	309.8 ± 185.6	0.51 (aMCI vs. AD) 0.43 (naMCI vs. AD)

Abbreviations: CN, cognitively normal; aMCI, amnestic MCI; naMCI, non-amnestic MCI; AD, Alzheimer's disease; MoCA, Montreal cognitive assessment test; NA, not available.

Measurement of CSF Aβ and total tau levels

For the entire cohort, Aβ and total tau concentrations were measured using β-amyloid (1–42) and hTau Ag ELISA tests. Aβ42 and total tau levels were measured on the Roche Elecsys system. These measurements were performed by Clinical Laboratory Improvement Amendments (CLIA)-certified Mayo Clinic Laboratories following manufacturers' instructions. CSF Aβ42 and total tau cut-offs follow Mayo Clinic reference values: Aβ42 at 1026 pg/ml and total tau cut-off at 238 pg/ml (Hansson et al., 2018).

Matching plasma and CSF p-tau181 Simoa measurements

P-tau181 Simoa measurements were performed in a Quanterix HD-X instrumentation platform in the Molecular Genomics Core of the Duke Molecular Physiology Institute. Matching plasma and CSF p-tau181 measurements used high precision Quanterix Simoa p-tau181 Advantage V2 kit (cat #103714; Quanterix Corp., Billerica, MA, USA): 7.7% for coefficient of variation (CV) between runs, 6.5% for CV within runs, and 3.7% of CV between instruments. Calibrators were run in triplicates, internal low and high controls were measured in duplicates, and matching plasma and CSF p-tau181 Simoa were measured in singlicates. CSF samples were diluted 1:10 on bench manually using vendor's diluent and all plasma samples used 1:4 dilution onboard. The coefficient of variation for an average number of enzyme per bead (AEB CV) for each calibrator was controlled within 20% per vendor's instruction. R^2 values for triplicated calibrator curve fitting were controlled with 0.95 or above.

MoCA evaluation

The MoCA test is a brief cognitive screening tool with high sensitivity and specificity for detecting MCI as currently conceptualized in patients performing in the normal range on the mini-Mental State Examination (MMSE) (Nasreddine et al., 2005). It is a 10-min cognitive screening tool to assist first-line physicians in detection of MCI, a clinical state that often progresses to dementia.

Statistical analysis

Plasma or CSF p-tau181 levels, or plasma/CSF p-tau181 ratios in cognitively normal, MCI, AD dementia or MCI subgroups with varying Aβ42 or total tau burden were plotted in box-whisker format in GraphPad Prism software (version 9.0). Each box-whisker plot shows levels for minimum (Q0), 25th percentile (Q1), 50th percentile (Q2 or median), 75th percentile (Q3) and maximum (Q4). The differences between various comparing groups were analyzed with non-parametric Mann-Whitney test as implemented within GraphPad Prism software. Detailed statistical analysis results are listed in **Supplementary Tables 1, 2**. P-values < 0.05 were considered significant. The specificity and sensitivity of plasma or CSF p-tau181 with the specific comparing groups were determined based on the area under the curve (AUC) of receiver operating characteristics (ROC) analysis. The 95% confidence interval ($CI_{95\%}$) of AUC was calculated with Wilson/Brown method. Demographic factor of sex in relation to p-tau181 Simoa measurement levels in plasma or CSF was analyzed by non-parametric Mann-Whitney test in GraphPad Prism 9.3.1. P-values < 0.05 were considered significant.

Correlation analysis

The non-parametric Spearman's correlation coefficients between p-tau181 levels versus age, p-tau181 levels in plasma versus CSF in cognitively normal (CN), MCI, or AD dementia groups, or CSF p-tau181 versus CSF Aβ or total tau level were calculated using GraphPad Prism 9.3.1. R-values > 0.60 are considered strong correlation, r values between 0.40–0.59 as moderate correlation, and $r < 0.39$ as weak or no correlation.

Results

Demographic and clinical characteristics

The basic demographic and clinical characteristics of the participants are shown in **Table 1**. The AD dementia group did not differ significantly in age from those for aMCI or naMCI groups. These groups were on average 3–5 years older than the cognitively normal group but these differences were not statistically significant

(p = 0.12 for AD vs. CN, p = 0.16 for aMCI vs. CN, and p = 0.43 for naMCI vs. CN, respectively). The percentage of females in AD group (58.1%) is similar to that of aMCI group (58.8%). Cognitively normal group had higher female percentage (68.6%) and naMCI group had a lower percentage of females (35.3%). As expected, MoCA scores for the AD group were significantly lower than the aMCI or naMCI groups ($p = 9.7 \times 10^{-7}$ and $p = 3.1 \times 10^{-4}$, respectively); CSF Aβ42 levels were decreased in the AD group versus those in aMCI or naMCI groups (p = 0.017 or p = 0.032, respectively); and total tau levels were elevated but not statistically different in AD cohorts versus those in aMCI or naMCI groups (p = 0.51 and p = 0.43, respectively).

P-tau181 is capable to diagnose both AD and MCI from cognitively normal subjects

Significantly higher concentrations of both plasma and CSF p-tau181 were found in AD group (n = 31; $p < 0.0001$ for both plasma and CSF) and MCI cohort (n = 51; p = 0.0009 for plasma samples and $p < 0.0001$ for CSF samples) compared with cognitively normal group (n = 12 for plasma samples and n = 39 for CSF samples) (Figures 1A, C; Supplementary Table 1). Receiving operating characteristic (ROC) analyses for the classification of AD vs. CN or MCI vs. CN showed similarly significant differential power for plasma (AUC = 0.89 for AD vs. CN; AUC = 0.80 for MCI vs. CN), and CSF (AUC = 0.87 for AD vs. CN; AUC = 0.85 for MCI vs. CN) (Figures 1B, D).

P-tau181 can robustly diagnose aMCI, but not naMCI, from cognitively normal subjects

If MCI cohorts were broken down into aMCI and naMCI subgroups, differentiation between these two MCI subgroups are somewhat different from cognitively normal subjects. P-tau181 can robustly diagnose aMCI: its levels in aMCI were significantly higher than those in CN cohorts (p = 0.0003 for plasma samples and $p < 0.0001$ for CSF samples; Figures 2A, C; Supplementary Table 1) and ROC analyses for the classification of aMCI vs. CN showed high sensitivity and specificity (AUC = 0.84 for plasma samples and AUC = 0.90 for CSF samples; Figures 2B, D). However, differentiation of naMCI from CN cohorts was not as robust: even though p-tau181 levels were still significantly higher statistically (p = 0.0391 in plasma and p = 0.0067 in CSF; Figures 2A, C; Supplementary Table 1), separation in ROC analyses was only moderate (AUC = 0.72 in plasma and AUC = 0.75 in CSF; Figures 2B, D).

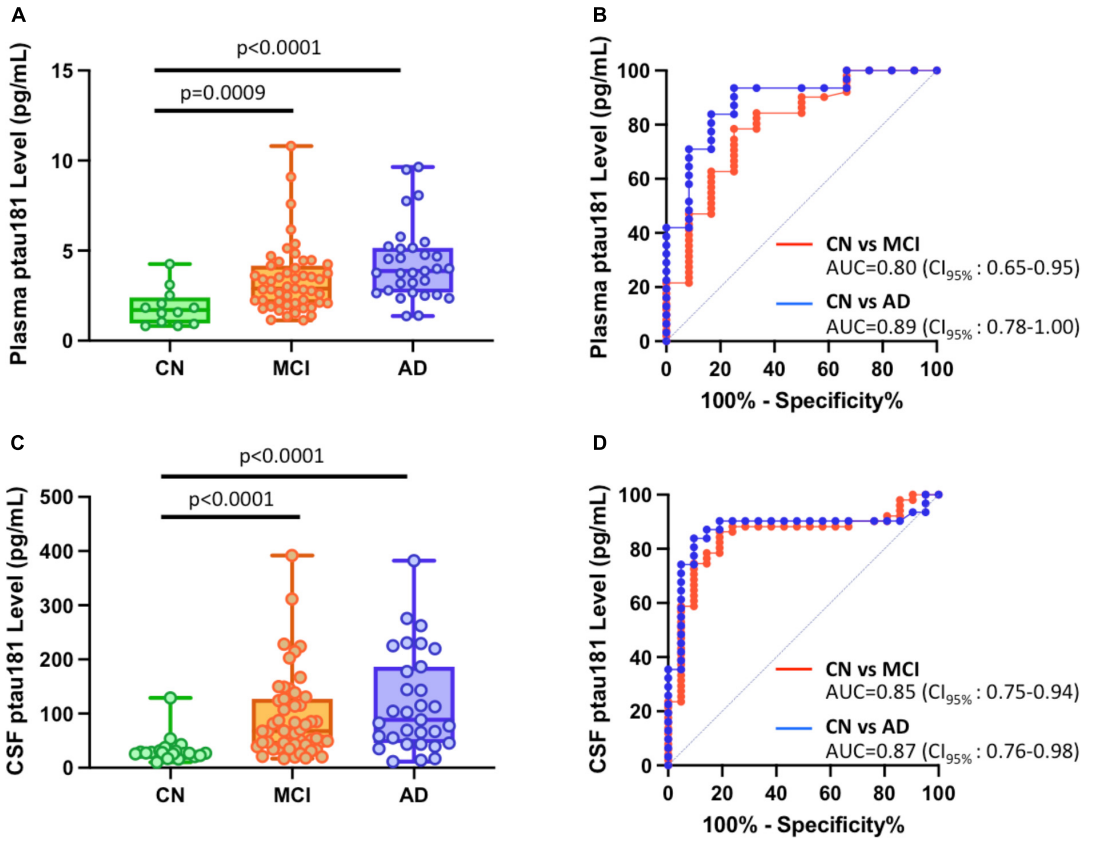

FIGURE 1
Differential capabilities of Simoa plasma and CSF p-tau181 measurements in cognitively normal (CN), MCI, and Alzheimer's disease (AD) dementia cohorts. **(A,C)** Box and whisker plot of p-tau181 in plasma panel **(A)**, and CSF panel **(C)** for CN, MCI and AD subjects. **(B,D)** ROC curves discriminating among controls, MCI and AD dementia for the p-tau181 levels in plasma panel **(B)** and CSF panel **(D)**.

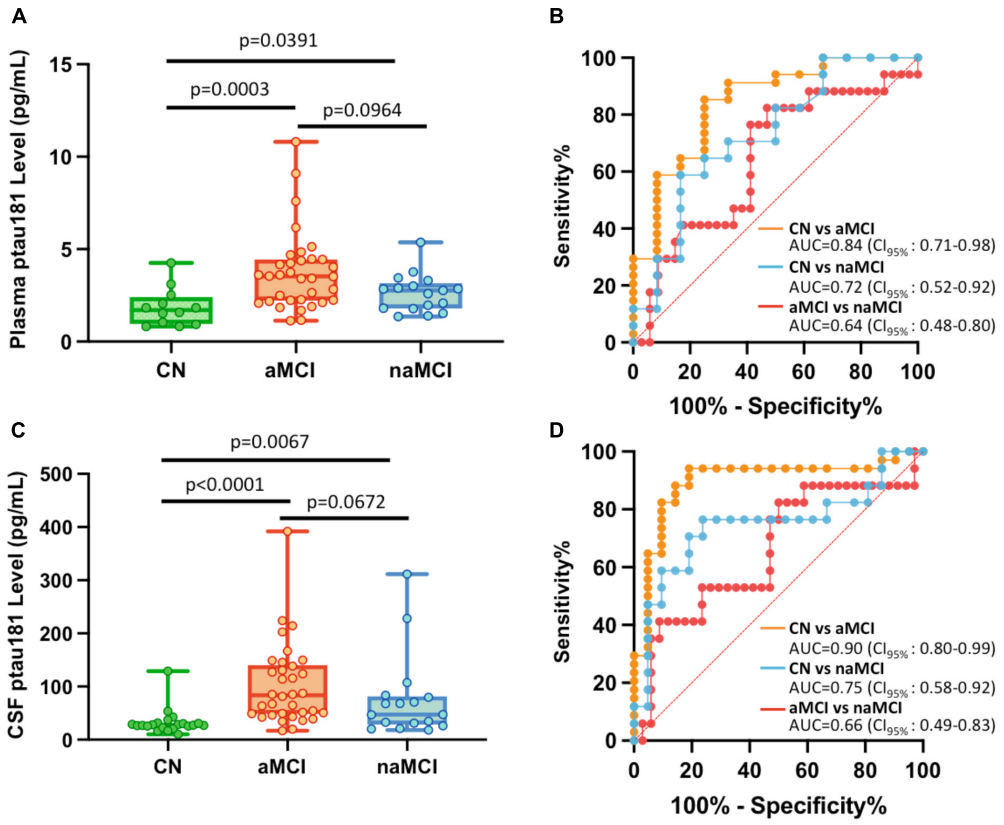

FIGURE 2
Differential capabilities of Simoa plasma and CSF p-tau181 measurements in cognitively normal (CN), amnestic MCI (aMCI), and non-amnestic MCI (naMCI) cohorts. **(A,C)** Box and whisker plot of p-tau181 in plasma panel **(A)**, and CSF panel **(C)** for CN, aMCI and naMCI subjects. **(B,D)** ROC curves discriminating among controls, aMCI and naMCI for the p-tau181 levels in plasma panel **(B)** and CSF panel **(D)**.

P-tau181 is not capable to differentiate aMCI from naMCI cohorts

To determine if plasma or CSF p-tau181 levels can differentiate aMCI cohorts from naMCI subjects, p-tau181 levels of these two MCI subgroups were compared. We found that p-tau181 is not capable of differentiating aMCI from naMCI cohorts: p-tau181 levels were not statistically different between aMCI samples from naMCI samples (p = 0.0964 in plasma and p = 0.0672 in CSF; Figures 2A, C; Supplementary Table 1). Furthermore, ROC analyses demonstrated that p-tau181 levels, with its low discriminatory power in both plasma (AUC = 0.64; Figure 2B) and CSF samples (AUC = 0.66; Figure 2D), would not be clinically useful (AUC $\leq$ 0.75) to differentiate aMCI from naMCI cohorts.

P-tau181 has high probability to diagnose Aβ-positive or total tau-positive aMCI subjects from cognitively normal subjects

We first investigated how Aβ or total tau burden each affects the differentiation of aMCI groups from cognitively normal cohort. While patients with Aβ-positive (aMCI A+) or Aβ-negative (aMCI A−), and total tau positive (aMCI N+) or negative (aMCI N−) groups all showed statistically higher plasma or CSF p-tau181 levels (Figures 3A–D, left panels; Supplementary Table 1), the differentiation capabilities of Aβ-negative or total tau negative groups vs. cognitively normal group remain relatively low (AUCs range from 0.73 to 0.83) compared with corresponding Aβ-positive and total tau positive groups (AUCs range from 0.88 to 0.96; Figures 3A–D, right panels). P-tau181 showed high probability to diagnose both Aβ-positive or total tau-positive aMCI groups from cognitively normal subjects (AUC $\geq$ 0.88).

We further classified aMCI subgroups into two total tau-positive groups (aMCI A+N+ and aMCI A−N+) and two total tau-negative groups (aMCI A−N− and aMCI A+N−). We used "N+" or "N-" for total tau-positive or total tau-negative based on the ATN classification system (amyloid, tau, neurodegeneration) (Jack et al., 2018), where each individual is rated for the presence of β-amyloid (CSF Aβ or amyloid PET: "A"), hyperphosphorylated tau (CSF p-tau or tau PET: "T"), and neurodegeneration (CSF total tau or atrophy on structural MRI, fluorodeoxyglucose (FDG)-PET: "N") (Ebenau et al., 2020). In this study, A, N status was determined based on CSF biomarker Aβ and total tau levels (see Materials and methods section). Our results showed that tau-positive aMCI subgroups have significantly higher p-tau181 concentrations in both plasma (p = 0.0004 for aMCI A+N+ vs. CN and p = 0.0068 for aMCI A−N+ vs. CN; Figure 4A; Supplementary Table 1) and CSF samples (p < 0.0001 for both aMCI A+N+ vs. CN and aMCI A−N+ vs. CN; Figure 4C; Supplementary Table 1).

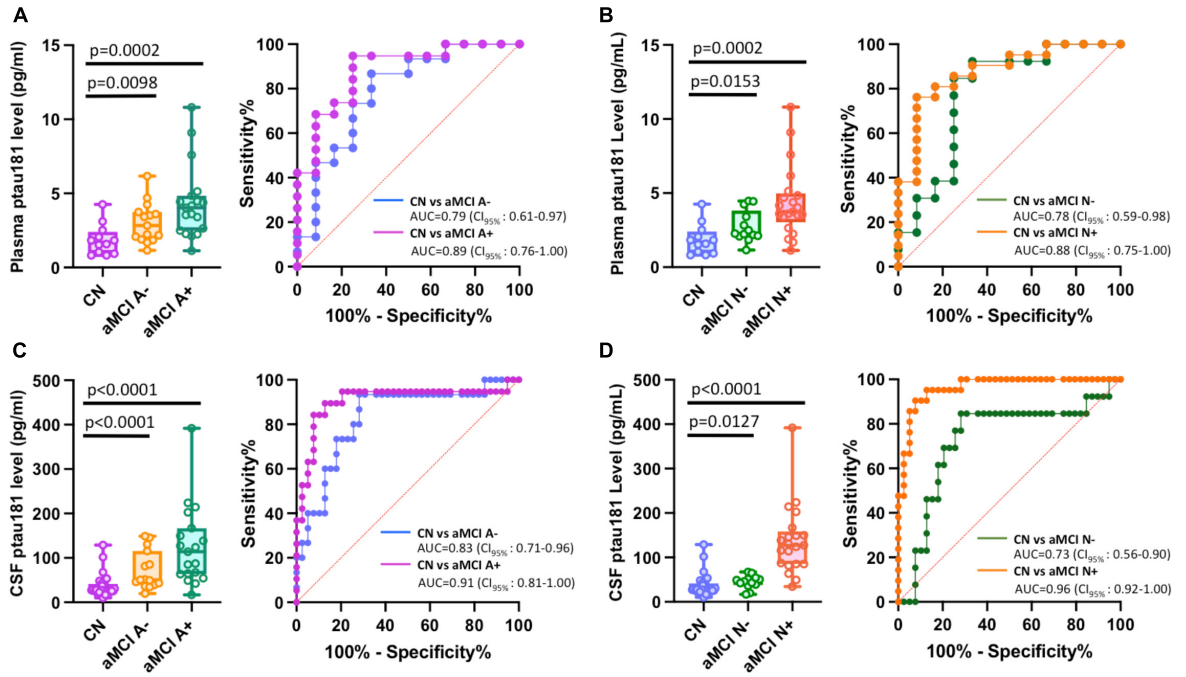

FIGURE 3
Impact of Aβ or total tau burden in differentiating among amnestic MCI (aMCI) subgroups using Simoa plasma or CSF p-tau181 measurements. **(A–D)** Left panels are box and whisker plots of p-tau181 in plasma panel **(A,B)**, and CSF panel **(C,D)** for cognitively normal groups versus aMCI subjects with positive or negative Aβ burdens (aMCI A+ or aMCI A−) or total tau burdens (aMCI N+ or aMCI N−). Right panels show ROC curves discriminating corresponding two aMCI subgroups for the p-tau181 levels in plasma or CSF.

Corresponding ROC analyses also showed excellent discriminatory power for p-tau181: AUC = 0.89 for aMCI A+N+ vs. CN and AUC = 0.85 for aMCI A−N+ vs. CN in plasma measurements (Figure 4B); AUC = 0.98 for aMCI A+N+ vs. CN and AUC = 0.95 for aMCI A−N+ vs. CN in CSF measurements (Figure 4D). In contrast, tau-negative aMCI subgroups had less degree of significant elevation or did not show statistically significant elevation in p-tau181 concentrations in plasma (p = 0.0125 for aMCI A+N− vs. CN and p = 0.1364 for aMCI A−N− vs. CN; Figure 4A; Supplementary Table 1) and CSF samples (p = 0.0525 for aMCI A+N− vs. CN and p = 0.0748 for aMCI A−N− vs. CN; Figure 4C; Supplementary Table 1). Corresponding ROC analyses also showed less prominent discriminatory power for p-tau181: AUC = 0.86 for aMCI A+N− vs. CN and AUC = 0.71 for aMCI A−N− vs. CN in plasma measurements (Figure 4B); AUC = 0.79 for aMCI A+N− vs. CN and AUC = 0.78 for aMCI A−N− vs. CN in CSF measurements (Figure 4D). Due to relatively small number of total naMCI cohort (n = 17), subgroup classifications of naMCI group into Aβ and total tau biomarker positive or negative was not performed.

Plasma/CSF p-tau181 ratio as a potential biomarker for differentiation

We further evaluated the ratio of plasma/CSF of p-tau181 for matching biofluid samples to test if such ratio could be a useful biomarker for MCI differentiation. We found while the aMCI cohort shows a trend of reduced plasma/CSF ratio compared to those of cognitively normal cohort or naMCI cohort, such reduction was not enough to be statistically significant (p = 0.069 for CN vs. aMCI; p = 0.215 for aMCI vs. naMCI; Supplementary Figure 1A; Supplementary Table 2). In separate comparisons of aMCI vs. CN (p = 0.106), aMCI A+ vs. CN (p = 0.0268), and aMCI N+ vs. CN (p = 0.0035), we found Aβ and total tau positivity improve the differentiation power of p-tau181 to separate aMCI from cognitively normal cohort (Supplementary Figure 1B; Supplementary Table 2). This data further supports our existing conclusion above that p-tau181 has high probability to diagnose Aβ-positive or total tau-positive aMCI subjects from cognitively normal subjects (Figure 3).

CSF p-tau181 has strong, positive correlation with total tau burden in both aMCI and naMCI cohorts but weak and negative correlation with Aβ burden in both MCI subgroups

We investigated if CSF p-tau181 level in aMCI or naMCI cohorts correlated with CSF total tau or Aβ burden, or other demographic factors such as sex and age. Not surprisingly, our data showed CSF p-tau181 levels have strong and positive correlation with CSF total tau burden in both aMCI (r = 0.74; Figure 5A) and naMCI cohort (r = 0.83; Figure 5B). Interestingly, CSF p-tau181 levels were negatively correlated with CSF Aβ burden in aMCI cohort (r = −0.32; Figure 5C) or in naMCI cohort (r = −0.69; Figure 5D). Plasma and CSF p-tau181 levels have

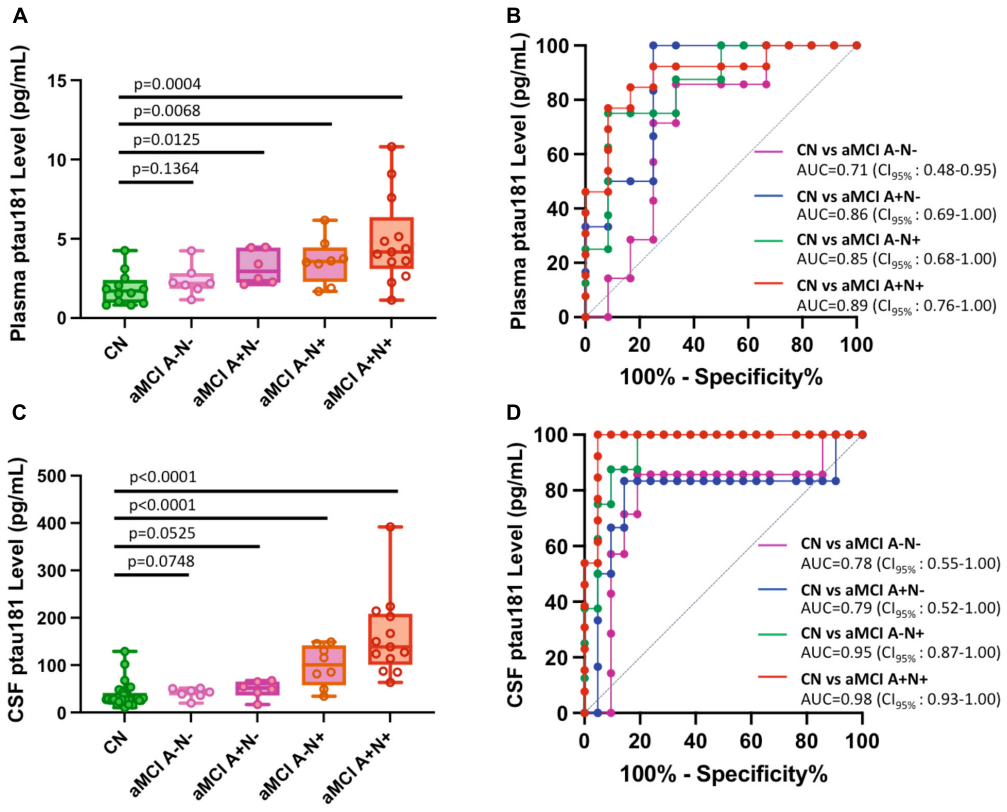

FIGURE 4
Differential capabilities of Simoa plasma or CSF p-tau181 levels in separating various amnestic MCI (aMCI) cohorts from cognitively normal (CN) subjects: Impact of Aβ and total tau burden. **(A,C)** Box and whisker plot of p-tau181 in plasma panel **(A)**, and CSF panel **(C)** for CN and aMCI subjects with positive or negative Aβ or total tau burdens. Panel **(B,D)** ROC curves discriminating among controls and various subclassified aMCI for the p-tau181 levels in plasma panel **(B)** and CSF panel **(D)**.

no significant differences between male versus female in both aMCI and naMCI cohorts (*P*-values range from 0.29 to 0.77; Supplementary Figure 2). In terms of demographic factor of age, plasma and CSF p-tau181 levels have no correlations with age in aMCI cohort ($r = 0.21$ or $r = 0.20$; Supplementary Figures 3A, C). Plasma and CSF p-tau181 levels have moderate correlation with naMCI group ($r = 0.55$ or $r = 0.48$; Supplementary Figures 3B, D). Due to limited data of MoCA scores (not every patient completed the MoCA test or was available to review), correlation between p-tau181 with MoCA score was not evaluated.

Plasma and CSF p-tau181 levels have significant correlation with each other

We further investigated if CSF p-tau181 levels correlated with plasma p-tau181 concentrations in various subgroups or combined groups. Our data suggested CSF p-tau181 concentration has significant, positive correlation with corresponding cohort's plasma p-tau181 levels: $r = 0.76$ for CN group (Supplementary Figure 4A); $r = 0.56$ for MCI group and $r = 0.55$ for aMCI group (Supplementary Figures 4B, D); $r = 0.49$ for AD dementia group (Supplementary Figure 4C); and $r = 0.63$ for combined CN, MCI, and AD groups (Supplementary Figure 4E).

Discussion

Recently, there is a growing research interest in early diagnosis and intervention for individuals with mild cognitive impairment (MCI). Diagnostic assays to detect AD-related changes at MCI stage are critical to identify patients at preclinical stage of AD for targeted early intervention. Furthermore, new biomarkers to differentiate subclasses of MCI (aMCI and naMCI), which will likely develop into different types of dementias, are of high translational utilities for targeted therapy in clinical healthcare. While much remains to be investigated, several recent p-tau biomarker studies began to test their potential for MCI diagnosis and progression from MCI to AD dementia. Plasma p-tau181 levels were found to be elevated in Aβ+ cognitively unimpaired, Aβ+ MCI, and Aβ+ AD dementia compared to those in Aβ− cognitively unimpaired and non-AD disease groups (Janelidze et al., 2020). In a separate study, plasma p-tau181 and PET centiloid scale alone or in combination with other biomarkers were found to produce high predictive value in predicting future cognitive stage transition (Kwon et al., 2023). CSF p-tau235 levels were elevated in amyloid-positive MCI cases compared to amyloid-negative cognitively unimpaired cohorts (Lantero-Rodriguez et al., 2021). A recent study of p-tau217 study comparing 10 plasma p-tau assays in prodromal AD cohorts suggested that mass-spectrometry-based measures of p-tau217 was able to identify MCI patients who will subsequently progress to AD

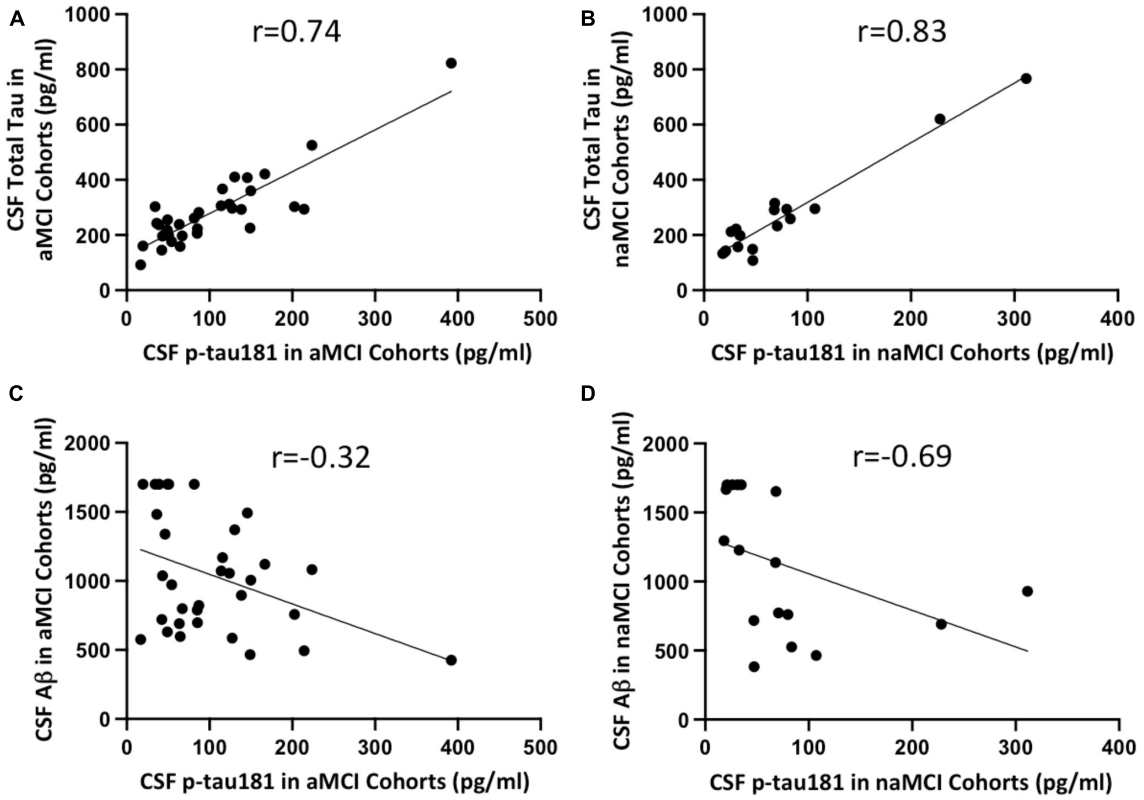

FIGURE 5
Correlation between CSF Simoa p-tau181 and CSF total tau in aMCI **(A)** and naMCI **(B)** cohorts, and between CSF Simoa p-tau181 and CSF Aβ in aMCI **(C)** and naMCI **(D)** cohorts. Correlation coefficient *r* values were calculated using non-parametric Spearman's correlation tests.

dementia with high probability (AUC = 0.932) whereas other non-mass spectrometry-based Simoa, Lumipulse immunoassay, Meso Scale Discovery immunoassay, and Splex immunoassay yielded wide AUC range from 0.688–0.889 in predicting future progression to AD dementia (Janelidze et al., 2023). A recent study suggested plasma p-tau217 predicted cognitive decline in patients with pre-clinical AD (Mattsson-Carlgren et al., 2023). To our knowledge, no p-tau biomarker studies have been reported on diagnosing MCI subclasses aMCI and naMCI from cognitively normal subjects, and on discriminating aMCI from naMCI cohorts.

Our data suggest that p-tau181 is not sensitive enough to differentiate naMCI from cognitively normal cohort and to discriminate aMCI from naMCI as in both cases the discriminating power scores were well below 0.80 (AUC = 0.72 in plasma samples and AUC = 0.75 in CSF samples for naMCI vs. cognitive normal group; AUC = 0.68 in plasma samples and AUC = 0.66 in CSF samples for aMCI vs. naMCI). It is unclear if the relatively small case number of naMCI (n = 17) affected the discriminating power. Therefore, future studies with larger cohort number of naMCI should be evaluated to further clarify this question. More importantly, other p-tau biomarkers should be evaluated or new p-tau biomarkers should be developed for these differential translational applications. Several p-tau biomarkers (p-tau217, p-tau231, and p-tau235) are well-established markers to diagnose AD dementia from non-AD controls. A recent meta-analysis suggested that p-tau217 had better discriminative accuracy for MCI than p-tau181 and p-tau231 (Chen et al., 2022). We recently showed that a new neuropathological biomarker p-tau198 had capability to diagnose MCI cohorts from cognitively normal subjects in brain tissues (Wu et al., 2022a). Therefore, it will be interesting in the future to evaluate these promising p-tau biomarkers or to develop novel p-tau biomarkers for plasma and CSF tests.

Our analysis demonstrated that aMCI diagnosis with p-tau181 biomarker noticeably improves in the Aβ-positive (aMCI A+ and aMCI N+ in **Figure 3**), total tau-positive MCI cohorts (aMCI A−N+ and aMCI A+N+ in **Figure 4**), or using plasma/CSF p-tau181 ratio as a biomarker (**Supplementary Figure 1B**). This is consistent with common clinical practice of using a combination of biomarkers (site-specific p-tau, Aβ, total tau, ApoE ε4 etc.) for more accurate diagnosis. Multi-factorial nature of AD disease etiology has been well recognized with respect to AD biomarker and therapeutic development (Gustaw-Rothenberg et al., 2010; DeTure and Dickson, 2019). It is intriguing that Aβ-positive and total tau-negative aMCI group has nearly the same differentiation power as Aβ-negative and total tau-negative aMCI from cognitively normal group (AUC = 0.79 for the former and 0.78 for the latter, **Figure 4D**) whereas Aβ-positive aMCI group has noticeably higher differentiation power than Aβ-negative aMCI group from cognitively normal group (AUC = 0.91 for the former and 0.83 for the latter, right panel of **Figure 3C**). We speculate the cause for this difference is that our Aβ-positive aMCI group (aMCI A+ in **Figure 3**) contains both total tau negative or total tau

positive cohorts, and highly significant elevation in p-tau181 levels in Aβ− and total tau-double positive aMCI cases vs. cognitively normal group compensated for the very little elevation in p-tau181 levels in Aβ-positive and total tau-negative aMCI cohorts vs. CN cohort (**Figures 4C, D**).

Over fifty post-translational modification (PTM) sites in tau protein have been identified, which include dozens of phosphorylation sites, and multiple sites with other modifications such as acetylation and ubiquitination (Wesseling et al., 2020). PTMs of tau proteins lead to structural and molecular diversity that may be linked to disease staging and contribute to AD clinical heterogeneity and disease progression (Arakhamia et al., 2020; Dujardin et al., 2020; Xia et al., 2021). Different tau PTMs may occur at different AD stages in a sequential fashion, and specific combinations of PTMs were proposed to reflect progressive steps in the process of tau fibril formation and AD disease progression (Wesseling et al., 2020; Wu et al., 2022a). Therefore, more sensitive and specific p-tau or other tau PTM-based biomarkers may remain to be discovered. Alternatively, other sensitive detection methods applicable to amplify misfolded protein seeds, such as real-time quaking-induced conversion (RT-QuIC) and protein misfolding cyclic amplification (PMCA) may be developed and applied to the challenging MCI diagnosis with accessible plasma and CSF biospecimens (Salvadores et al., 2014; Wang et al., 2019, 2023; Wu et al., 2022b).

Conclusion

We showed that plasma and CSF p-tau181 levels can robustly differentiate MCI or aMCI from cognitively normal cohorts, but such differentiation is weaker in diagnosing naMCI from cognitively normal groups. Furthermore, p-tau181 biomarker is not capable of differentiating aMCI from naMCI cohorts. Thirdly, incorporation of either factor of Aβ or total tau burden markedly improved differentiation power to diagnose aMCI from cognitively normal group. Therefore, we conclude that plasma and CSF p-tau181 levels are a promising biomarker for diagnosing aMCI from normal controls in the preclinical phase. But more robust new biomarkers are needed to differentiate naMCI from cognitively normal cases or to discriminate between MCI subtypes, aMCI from naMCI.

Data availability statement

The original contributions presented in the study are included in the article/**Supplementary material**, further inquiries can be directed to the corresponding authors.

Ethics statement

The studies involving humans were approved by the Duke University IRB; North Carolina Central University IRB. The studies were conducted in accordance with the local legislation and institutional requirements. All participants of the Duke Department of Neurology Biospecimen Bank provided written informed consent. All human samples obtained from the Biospecimen Bank were de-identified and without any protected health information.

Author contributions

LW: Data curation, Formal analysis, Funding acquisition, Investigation, Methodology, Validation, Visualization, Writing—original draft, Writing—review and editing. SA: Data curation, Investigation, Methodology, Validation, Writing—review and editing. S-HJW: Data curation, Formal analysis, Funding acquisition, Investigation, Methodology, Validation, Writing—review and editing. AL: Data curation, Formal analysis, Investigation, Methodology, Project administration, Resources, Supervision, Validation, Writing—review and editing. BX: Conceptualization, Data curation, Formal analysis, Funding acquisition, Investigation, Methodology, Project administration, Resources, Supervision, Validation, Visualization, Writing—original draft, Writing—review and editing.

Funding

The author(s) declare financial support was received for the research, authorship, and/or publication of the article. This study was supported in part by the Duke Clinical and Translational Science Institute Collaborative Research Award (BX and S-HJW), Biomarkers Across Neurodegenerative Diseases (BAND) Program of Alzheimer's Association (Grant #19-614848) (BX), North Carolina Biotech Center Translational Grant Award #2023-TRG-0015 (BX, S-HJW, and AL), National Institute of Health grants R01 AG067607 (BX), P30 AG072958 to S-HJW and Duke-UNC Alzheimer's Disease Research Center (ADRC) and for Duke-UNC ADRC REC Scholar Award (LW).

Acknowledgments

We would like to thank the Department of Neurology of Duke University's School of Medicine BioBank for CN, MCI, and AD dementia plasma and CSF access and Duke Molecular Physiology Institute Molecular Genomics Core for Quanterix Simoa HD-X Automated Immunoassay Analyzer access. We thank reviewer for insightful comment on the potential of using plasma/CSF p-tau181 ratio as a differentiation biomarker.

Conflict of interest

The authors declare that the research was conducted in the absence of any commercial or financial relationships that could be construed as a potential conflict of interest.

The authors declared that they were an editorial board member of Frontiers, at the time of submission. This had no impact on the peer review process and the final decision.

Publisher's note

Supplementary material

The Supplementary Material for this article can be found online at: https://www.frontiersin.org/articles/10.3389/fnmol.2023.1288930/full#supplementary-material

SUPPLEMENTARY FIGURE 1
Differential capabilities based on plasma/CSF p-tau181 ratio. **(A)** Box and whisker plot of percent ratio of plasma/CSF p-tau181 in cognitively normal, aMCI, and naMCI cohorts. **(B)** Box and whisker plot of percent ratio of plasma/CSF p-tau181 in cognitively normal, aMCI, aMCI A+ and aMCI N+ cohorts. Statistical *P*-values in both panels were calculated using non-parametric Mann-Whitney test.

SUPPLEMENTARY FIGURE 2
Scatter plots of the p-tau181 levels in aMCI or naMCI cohorts in relation with demographic factor sex. Upper panels **(A,B)** show Simoa p-tau181 measurements in plasma and lower panels **(C,D)** show corresponding p-tau181 levels in CSF. Statistical *P*-values were calculated using non-parametric Mann-Whitney test.

SUPPLEMENTARY FIGURE 3
Scatter plots of the p-tau181 levels in aMCI or naMCI cohorts in relation with demographic factor age. Upper panels **(A,B)** show Simoa p-tau181 measurements in plasma and lower panels **(C,D)** show corresponding p-tau181 levels in CSF. Correlation coefficient *R* values were calculated using non-parametric Spearman's correlation tests.

SUPPLEMENTARY FIGURE 4
Correlation between plasma and CSF Simoa p-tau181 measurements in the individual cohort of **(A)** cognitively normal (CN), **(B)** MCI, **(C)** AD dementia, **(D)** amnestic MCI (aMCI), and **(E)** combined cohorts of CN, MCI, AD subjects. Correlation coefficient *r* values were calculated using non-parametric Spearman's correlation tests.

References

Arakhamia, T., Lee, C., Carlomagno, Y., Duong, D., Kundinger, S., Wang, K., et al. (2020). Posttranslational modifications mediate the structural diversity of tauopathy strains. *Cell* 180, 633–44.e12. doi: 10.1016/j.cell.2020.01.027

Ashton, N., Benedet, A., Pascoal, T., Karikari, T., Lantero-Rodriguez, J., Brum, W., et al. (2022). Cerebrospinal fluid p-tau231 as an early indicator of emerging pathology in Alzheimer's disease. *EBioMedicine* 76:103836. doi: 10.1016/j.ebiom.2022.103836

Ashton, N., Pascoal, T., Karikari, T., Benedet, A., Lantero-Rodriguez, J., Brinkmalm, G., et al. (2021). Plasma p-tau231: a new biomarker for incipient Alzheimer's disease pathology. *Acta Neuropathol.* 141, 709–724. doi: 10.1007/s00401-021-02275-6

Blennow, K., Dubois, B., Fagan, A., Lewczuk, P., de Leon, M., and Hampel, H. (2015). Clinical utility of cerebrospinal fluid biomarkers in the diagnosis of early Alzheimer's disease. *Alzheimers Dement.* 11, 58–69. doi: 10.1016/j.jalz.2014.02.004

Braak, H., and Braak, E. (1991). Neuropathological staging of Alzheimer-related changes. *Acta Neuropathol.* 82, 239–259. doi: 10.1007/BF00308809

Chen, L., Niu, X., Wang, Y., Lv, S., Zhou, X., Yang, Z., et al. (2022). Plasma tau proteins for the diagnosis of mild cognitive impairment and Alzheimer's disease: A systematic review and meta-analysis. *Front. Aging Neurosci.* 14:942629. doi: 10.3389/fnagi.2022.942629

DeTure, M., and Dickson, D. (2019). The neuropathological diagnosis of Alzheimer's disease. *Mol. Neurodegener.* 14:32. doi: 10.1186/s13024-019-0333-5

Dujardin, S., Commins, C., Lathuiliere, A., Beerepoot, P., Fernandes, A., Kamath, T., et al. (2020). Tau molecular diversity contributes to clinical heterogeneity in Alzheimer's disease. *Nat. Med.* 26, 1256–1263. doi: 10.1038/s41591-020-0938-9

Ebenau, J., Timmers, T., Wesselman, L., Verberk, I., Verfaillie, S., Slot, R., et al. (2020). ATN classification and clinical progression in subjective cognitive decline: The SCIENCe project. *Neurology* 95, e46–e58. doi: 10.1212/WNL.0000000000009724

Ferman, T., Smith, G., Kantarci, K., Boeve, B., Pankratz, V., Dickson, D., et al. (2013). Nonamnestic mild cognitive impairment progresses to dementia with Lewy bodies. *Neurology* 81, 2032–2038. doi: 10.1212/01.wnl.0000436942.55281.47

Grundman, M. (2004). Mild cognitive impairment can be distinguished from alzheimer disease and normal aging for clinical trials. *Arch Neurol.* 61, 59–66. doi: 10.1001/archneur.61.1.59

Gustaw-Rothenberg, K., Lerner, A., Bonda, D., Lee, H., Zhu, X., Perry, G., et al. (2010). Biomarkers in Alzheimer's disease: past, present and future. *Biomark Med.* 4, 15–26. doi: 10.2217/bmm.09.86

Hansson, O., Seibyl, J., Stomrud, E., Zetterberg, H., Trojanowski, J., Bittner, T., et al. (2018). CSF biomarkers of Alzheimer's disease concord with amyloid-β PET and predict clinical progression: A study of fully automated immunoassays in BioFINDER and ADNI cohorts. *Alzheimers Dement.* 14, 1470–1481. doi: 10.1016/j.jalz.2018.01.010

Jack, C. Jr., Bennett, D., Blennow, K., Carrillo, M., Dunn, B., Haeberlein, S., et al. (2018). NIA-AA Research Framework: Toward a biological definition of Alzheimer's disease. *Alzheimers Dement.* 14, 535–562. doi: 10.1016/j.jalz.2018.02.018

Janelidze, S., Bali, D., Ashton, N., Barthélemy, N., Vanbrabant, J., Stoops, E., et al. (2023). Head-to-head comparison of 10 plasma phospho-tau assays in prodromal Alzheimer's disease. *Brain* 146, 1592–1601. doi: 10.1093/brain/awac333

Janelidze, S., Mattsson, N., Palmqvist, S., Smith, R., Beach, T., Serrano, G., et al. (2020). Plasma P-tau181 in Alzheimer's disease: relationship to other biomarkers, differential diagnosis, neuropathology and longitudinal progression to Alzheimer's dementia. *Nat. Med.* 26, 379–386. doi: 10.1038/s41591-020-0755-1

Karikari, T., Pascoal, T., Ashton, N., Janelidze, S., Benedet, A., Rodriguez, J., et al. (2020). Blood phosphorylated tau 181 as a biomarker for Alzheimer's disease: a diagnostic performance and prediction modelling study using data from four prospective cohorts. *Lancet Neurol.* 19, 422–433. doi: 10.1016/S1474-4422(20)30071-5

Kwon, H., Kim, J., Koh, S., Choi, S., Lee, E., Jeong, J., et al. (2023). Predicting cognitive stage transition using p-tau181, Centiloid, and other measures. *Alzheimers Dement.* doi: 10.1002/alz.13054 [Epub ahead of print].

Lantero-Rodriguez, J., Snellman, A., Benedet, A., Milà-Alomà, M., Camporesi, E., Montoliu-Gaya, L., et al. (2021). P-tau235: a novel biomarker for staging preclinical Alzheimer's disease. *EMBO Mol. Med.* 13, e15098. doi: 10.15252/emmm.202115098

Lee, V., Goedert, M., and Trojanowski, J. (2001). Neurodegenerative tauopathies. *Annu. Rev. Neurosci.* 24, 1121–1159. doi: 10.1146/annurev.neuro.24.1.1121

Mattsson-Carlgren, N., Salvadó, G., Ashton, N., Tideman, P., Stomrud, E., Zetterberg, H., et al. (2023). Prediction of longitudinal cognitive decline in preclinical alzheimer disease using plasma biomarkers. *JAMA Neurol.* 80, 360–369. doi: 10.1001/jamaneurol.2022.5272

Mielke, M., Hagen, C., Xu, J., Chai, X., Vemuri, P., Lowe, V., et al. (2018). Plasma phospho-tau181 increases with Alzheimer's disease clinical severity and is associated with tau- and amyloid-positron emission tomography. *Alzheimers Dement.* 14, 989–997. doi: 10.1016/j.jalz.2018.02.013

Nasreddine, Z., Phillips, N., Bédirian, V., Charbonneau, S., Whitehead, V., Collin, I., et al. (2005). The Montreal Cognitive Assessment, MoCA: a brief screening tool for mild cognitive impairment. *J. Am. Geriatr. Soc.* 53, 695–699. doi: 10.1111/j.1532-5415.2005.53221.x

Palmqvist, S., Janelidze, S., Stomrud, E., Zetterberg, H., Karl, J., Zink, K., et al. (2019). Performance of fully automated plasma assays as screening tests for Alzheimer disease-related β-amyloid status. *JAMA Neurol.* 76, 1060–1069. doi: 10.1001/jamaneurol.2019.1632

Petersen, R., Parisi, J., Dickson, D., Johnson, K., Knopman, D., Boeve, B., et al. (2006). Neuropathologic features of amnestic mild cognitive impairment. *Arch. Neurol.* 63, 665–672. doi: 10.1001/archneur.63.5.665

Rissin, D., Kan, C., Campbell, T., Howes, S., Fournier, D., Song, L., et al. (2010). Single-molecule enzyme-linked immunosorbent assay detects serum proteins at subfemtomolar concentrations. *Nat. Biotechnol.* 28, 595–599. doi: 10.1038/nbt.1641

Salvadores, N., Shahnawaz, M., Scarpini, E., Tagliavini, F., and Soto, C. (2014). Detection of misfolded Aβ oligomers for sensitive biochemical diagnosis of Alzheimer's disease. *Cell Rep.* 7, 261–268. doi: 10.1016/j.celrep.2014.02.031

Selkoe, D. (2001). Alzheimer's disease: genes, proteins, and therapy. *Physiol. Rev.* 81, 741–766. doi: 10.1152/physrev.2001.81.2.741

Thijssen, E., La Joie, R., Strom, A., Fonseca, C., Laccarino, L., Wolf, A., et al. (2021). Plasma phosphorylated tau 217 and phosphorylated tau 181 as biomarkers in Alzheimer's disease and frontotemporal lobar degeneration: a retrospective diagnostic performance study. *Lancet Neurol.* 20, 739–752. doi: 10.1016/S1474-4422(21)00214-3

Vermunt, L., Sikkes, S., van den Hout, A., Handels, R., Bos, I., van der Flier, W., et al. (2019). Duration of preclinical, prodromal, and dementia stages of Alzheimer's disease in relation to age, sex, and APOE genotype. *Alzheimers Dement.* 15, 888–898. doi: 10.1016/j.jalz.2019.04.001

Wang, W., Orru, C., Foutz, A., Ding, M., Yuan, J., Ali Shah, S., et al. (2023). Large-scale validation of skin prion seeding activity as a biomarker for diagnosis of prion diseases. *Acta Neuropathol.* in press.

Wang, Z., Manca, M., Foutz, A., Camacho, M., Raymond, G., Race, B., et al. (2019). Early preclinical detection of prions in the skin of prion-infected animals. *Nat. Commun.* 10:247. doi: 10.1038/s41467-018-08130-9

Wesseling, H., Mair, W., Kumar, M., Schlaffner, C., Tang, S., Beerepoot, P., et al. (2020). Tau PTM profiles identify patient heterogeneity and stages of Alzheimer's disease. *Cell* 183, 1699–1713. doi: 10.1016/j.cell.2020.10.029

Wu, L., Gilyazova, N., Ervin, J., Wang, S., and Xu, B. (2022a). Site-specific phospho-tau aggregation-based biomarker discovery for AD diagnosis and differentiation. *ACS Chem. Neurosci.* 13, 3281–3290. doi: 10.1021/acschemneuro.2c00342

Wu, L., Wang, Z., Lad, S., Gilyazova, N., Dougharty, D., Marcus, M., et al. (2022b). Selective detection of misfolded tau from postmortem Alzheimer's disease brains. *Front. Aging Neurosci.* 14:945875. doi: 10.3389/fnagi.2022.945875

Xia, Y., Prokop, S., and Giasson, B. (2021). "Don't Phos Over Tau": recent developments in clinical biomarkers and therapies targeting tau phosphorylation in Alzheimer's disease and other tauopathies. *Mol. Neurodegener.* 16:37. doi: 10.1186/s13024-021-00460-5

frontiers | Frontiers in Neuroscience

TYPE Study Protocol
PUBLISHED 05 March 2024
DOI 10.3389/fnins.2024.1365598

OPEN ACCESS

EDITED BY
Hai Sun,
The State University of New Jersey, United States

REVIEWED BY
Pamela Cappelletti,
Casa di Cura Privata del Policlinico Milano SpA, Italy
Fang Liu,
Fujian University of Traditional Chinese Medicine, China

*CORRESPONDENCE
Yuanhao Du
jpjs_cn@sina.com

RECEIVED 04 January 2024
ACCEPTED 08 February 2024
PUBLISHED 05 March 2024

CITATION
Cao JP, Du YH, Yin XM, Zheng N, Han JW, Chen LL and Jia LY (2024) Understanding the mechanism of acupuncture in acute cerebral infraction through a proteomic analysis: protocol for a prospective randomized controlled trial.
Front. Neurosci. 18:1365598.
doi: 10.3389/fnins.2024.1365598

Understanding the mechanism of acupuncture in acute cerebral infraction through a proteomic analysis: protocol for a prospective randomized controlled trial

Jiangpeng Cao[1,2,3], Yuanhao Du[1,3]*, Xiumei Yin[1,2,3], Na Zheng[4], Jiawei Han[5], Linling Chen[6] and Lanyu Jia[7]

[1]National Clinical Research Center for Chinese Medicine Acupuncture and Moxibustion, Tianjin, China, [2]Graduate School, Tianjin University of Traditional Chinese Medicine, Tianjin, China, [3]Department of Acupuncture and Moxibustion, First Teaching Hospital of Tianjin University of Traditional Chinese Medicine, Tianjin, China, [4]Department of Traditional Chinese medicine, Tianjin Huanhu hospital, Tianjin, China, [5]Department of Traditional Chinese Medicine, First Hospital of Jilin University, Changchun, China, [6]Department of Traditional Chinese Medicine, Huzhou Central Hospital, Zhejiang, China, [7]Department of Geriatric Medicine, Tianjin Academy of Traditional Chinese Medicine Affiliated Hospital, Tianjin, China

Background: Acute cerebral infarction (ACI), being the predominant form of stroke, presents challenges in terms of the limited effectiveness of various treatments in improving the neurological function. Although acupuncture shows promise in addressing ACI, the availability of high-quality evidence regarding its efficacy, safety, and underlying mechanism remains insufficient. In this study, we design a multicenter, prospective, single-blind, randomized controlled trial with the aim of evaluating the efficacy and safety of acupuncture for ACI, making an attempt to unveil the molecular mechanisms by proteomic.

Methods: A total of 132 patients involving four hospitals will be randomized at a 1:1:1 ratio in the acupuncture group, control group, and sham acupuncture group. All the patients will receive basic treatment, and the patients in the acupuncture and sham acupuncture groups will also receive either acupuncture or sham acupuncture treatment, respectively, at six sessions each week for a 2weeks period, followed by 3months of follow-up. The primary outcome will be the change in the National Institute of Health Stroke Scale (NIHSS) scores after treatment. The secondary outcomes will include the Fugl-Meyer Assessment (FMA) scale scores and the Barthel Index (BI). Adverse events that occur during the trial will be documented. To discover differentially expressed proteins (DEPs) and their roles between the ACI subjects and healthy controls, we will also perform 4D-DIA quantitative proteomics analysis, and the DEPs will be confirmed by enzyme-linked immunosorbent assay (ELISA). This study was approved by the institutional review board of the First Teaching Hospital of Tianjin University of Traditional Chinese Medicine (TYLL2023043). Written informed consent from patients is required. This trial is registered in the Chinese Clinical Trial Registry (ChiCTR2300079204). Trial results will be published in a peer-reviewed academic journal.

Discussion: The results of this study will determine the preliminary efficacy and safety of acupuncture in ACI patients and whether the mechanism of this form

of non-pharmacologic stimulation is mediated by a novel therapeutic target for neurorehabilitation through our proteomic analysis.

Clinical trial registration: https://www.chictr.org.cn, identifier ChiCTR2300079204.

KEYWORDS

acute cerebral infraction, acupuncture, proteomic analysis, randomized controlled trial, protocol

1 Introduction

Acute cerebral infarction (ACI) is the predominant form of stroke, comprising 60–80% of all stroke cases. It is also recognized as the second leading cause of death and the major cause of disability worldwide (Naghavi et al., 2017). The Global Burden of Disease Study has revealed an upward trend in the incidence of ischemic stroke in China, with rates escalating from 117 per 100,000 individuals in 2005 to 145 per 100,000 individuals in 2019 (GBD 2019 Stroke Collaborators, 2021). In addition, the American Heart Association's report on Heart Disease and Stroke Statistics in 2020 indicates that the prevalence of stroke in the United States was 2.5% in 2016 (Virani et al., 2020). Patients with ACI experience alterations in their lifestyle, which subsequently impacts their overall quality of life (Pan et al., 2008; Wu et al., 2014). These alterations encompass various aspects such as physical wellbeing, psychological state, social interactions, and personal beliefs (Sainsbury and Heatley, 2005). It is widely recognized that neuroprotection holds promise as a therapeutic strategy for individuals affected by ACI. The occurrence and progression of ACI involve multiple pathological and physiological mechanisms, including excitotoxicity, oxidative and nitrosative stress, cellular apoptosis, and inflammation (Lipton, 1999; Chamorro et al., 2016). Acupuncture, a significant component of traditional Chinese medicine, has emerged as a potentially efficacious non-pharmacological intervention for the management of ACI. Acupuncture has exhibited diverse neuroprotective and reparative properties that contribute to its anti-inflammatory (Cao et al., 2021) and anti-apoptotic effects (Tian and Wang, 2019) and its ability to promote angiogenesis (Zhang et al., 2020). The findings from a robust randomized controlled trial involving 862 participants in the early stage of stroke have demonstrated that the addition of acupuncture to standard care leads to a reduction in mortality compared with standard care alone (Zhang et al., 2015a). Numerous reviews have demonstrated the prospective effectiveness and safety of acupuncture in addressing ACI and its subsequent complications. According to a comprehensive examination of literature and perspectives (Qin et al., 2022), it has been observed that acupuncture facilitates the regeneration of nerve cells, thereby promoting the replacement of non-functional cells after a stroke. This process ultimately leads to the restructuring of neural connections and the restoration of functional abilities. Furthermore, a systematic review (Sang et al., 2022) has indicated that acupuncture therapy administered during the sub-acute phase of ischemic stroke may improve language function in individuals with aphasia. Moreover, another systematic review (Wang et al., 2012) has demonstrated that scalp acupuncture exhibits superior efficacy in terms of improving neurological deficit scores and clinical effectiveness compared with western conventional medicine in patients with ACI. Nevertheless, it remains challenging to derive definitive conclusions based on the currently accessible evidence. Further large-scale, well-designed randomized clinical trials on this topic are still warranted (Wong et al., 2012; Zhang et al., 2013a; Li et al., 2014a).

Since "time is brain," the prompt identification of cerebral ischemia is crucial in the acute phase of onset. Biomarkers serve as objective indicators for evaluating normal or pathological processes, assessing responses to medical interventions, and predicting outcomes (Atkinson et al., 2001). There are already few studies that analyze variations of blood biomarkers after treatment with acupuncture in patients affected by ACI. A recent study (Cui and Jia, 2022) demonstrated that acupuncture in patients with ACI cause an increase in the serum levels of malondialdehyde, superoxide dismutase, and glutathione peroxidase, and another clinical trial (Zhang et al., 2013b) reported a decrease in the levels of serum neuron-specific enolase, soluble protein-100β, and endothelin in ACI patients treated with electroacupuncture. Based on these findings, we hypothesized that alterations in the proteomic profile of blood following acupuncture interventions may potentially mirror neural modifications in individuals diagnosed with ACI.

In light of the ambiguous mechanism and uncertain effectiveness of acupuncture in treating ACI, this randomized clinical trial was devised to assess the safety and efficacy of acupuncture. Additionally, the proteomic analysis will be employed to investigate the potential underlying mechanism. Considering the potential variations in protein expression levels that may arise from acupuncture intervention, the initial set of differentially expressed proteins (DEPs) will be classified based on their associations with specific pathways and then confirmed by the enzyme-linked immunosorbent assay (ELISA) techniques. The validation procedure will be predicated upon the "threshold" of variation of the expression levels, taking into account the findings of previous studies of our team (Du et al., 2011; Li et al., 2014b, 2017, 2022, 2023) and the available relevant literature.

Abbreviations: ACI, acute cerebral infarction; AG, acupuncture group; BI, Barthel index; DDA, data-dependent acquisition; DEPs, differentially expressed proteins; DIA, data-independent acquisition; ELISA, Enzyme-linked immunosorbent assay; FMA, Fugl–Meyer assessment; HG, health group; LE, lower extremity; mRS, modified Rankin scale; NIHSS, National Institute of Health stroke scale; UE, upper extremity.

2 Methods

2.1 Study design

This is a multicenter, prospective, single-blind, randomized controlled trial that will be conducted in four centers in China. The

trial design was approved by the Institutional Review Board of the First Teaching Hospital of Tianjin University of Traditional Chinese Medicine (Tianjin, China) and registered at www.chictr.org.cn (ChiCTR2300079204) in December 2023. This study will be conducted in accordance with the latest version of the Declaration of Helsinki, the Consolidated Standards of Reporting Trials (Schulz et al., 2010), and the Standards for Reporting Interventions in Controlled Trials of Acupuncture guidelines (Macpherson et al., 2010) in trial designing and reporting.

2.2 Participant recruitment

The eligible consecutive participants will be enrolled in the First Teaching Hospital of Tianjin University of Traditional Chinese Medicine, Tianjin Huanhu Hospital, First Hospital of Jilin University, and Huzhou Central Hospital. This trial will include an enrollment and allocation period of 6 days every week over a 2 weeks intervention period followed by a 3 months follow-up period. The gender- and age-matched healthy people will also be enrolled as the health group that will be analyzed by proteomic analysis investigations. We will obtain the informed consent from each participant or an appointed legal representative if the participant lacks the decision-making capacity. The flowchart of the study is shown in Figure 1, and the mechanism exploration procedure is shown in Figure 2.

2.2.1 The diagnostic criteria

The diagnostic criteria will be designed in accordance with the Chinese guidelines for the diagnosis and treatment of acute ischemic stroke 2018 (Chinese Society of Neurology, & Chinese Stroke Society, 2018).

2.2.2 The inclusion criteria

The inclusion criteria are as follows: (1) individuals who satisfy the established diagnostic criteria for the ailment may be considered for inclusion in the therapeutic intervention; (2) an initial manifestation of the ailment; (3) progression of the ailment within a time frame of 72 h; (4) an age range of 40–75 years with no restrictions based on gender; (5) an NIHSS score ranging from 5 to less than 15; and (6) willingness to participate voluntarily and provision of a duly signed informed consent.

2.2.3 The exclusion criteria

The exclusion criteria are as follows: (1) individuals failing to meet the established inclusion criteria; (2) impairment of the Vesta channel's functionality resulting from craniocerebral trauma, tumors, and other etiologies; (3) assessment of the impact of acupuncture treatment or other therapeutic medications administered within a 3 months period prior to admission; (4) presence of consciousness disorders, deafness, severe depression, schizophrenia, and inability to cooperate; (5) coexistence of severe primary diseases affecting the cardiovascular, neurological, respiratory, hepatic, and renal systems; (6) severe dermatological conditions or hypersensitivity to the investigational treatment; (7) pregnant, lactating, or expecting women; and (8) patients concurrently participating in other research studies.

2.3 Randomization and blinding

The eligible participants will be enrolled and divided randomly in the acupuncture group (received acupuncture), the control group (received no acupuncture), or the sham acupuncture group (received sham acupuncture) at a ratio of 1:1:1 ($n = 132$) using a computer-generated randomization method. Random numbers were put into an opaque envelope and sealed, and the corresponding serial numbers were affixed to the surface of the envelope for random grouping and concealing. The envelopes were opened according to the order in which the subjects were enrolled for grouping and treatment. The patients will be informed whether they will receive acupuncture treatment or not.

The participants in the acupuncture group and sham acupuncture group will be blinded, while those in the control group will not be. Due to the particularity of acupuncture treatment, it is impossible to blind the acupuncturists in this study. All study personnel including the outcome assessors and data analysts will be blinded to the treatment allocation.

2.4 Estimation of sample size

In this study, we aim to compare the difference in the NIHSS score between the acupuncture group and sham acupuncture group after the treatment. Sample size calculations were performed for a simple comparison of the two groups. According to a previous study (Sun and Wu, 2019), the NIHSS scores of mean ± SD between the two groups were 6.2 ± 2.1 and 4.9 ± 1.8, respectively, after the treatment. A total of 36 participants per treatment group (108 in total) were required when setting a one-sided test with $\alpha = 0.025$, $\beta = 0.20$. To compensate for a 20% loss to follow-up, the sample size was increased to 44 participants in each group.

2.5 Sample collection and classification

The peripheral blood will be collected in the morning. Blood samples will be taken from the acupuncture and the control groups before and after treatment; then, the participants from both groups will be asked to wait for 30 min after the blood clotted at room temperature; serum will be collected after centrifuging at 3,000 g for 10 min at 4°C and will be stored at −80°C for proteomic analysis and ELISA validation. In total, 10 blood samples will also be taken from 10 gender- and age-matched healthy people for proteomic analysis.

2.6 Interventions

All groups will receive the basic treatment of ACI according to the Chinese guidelines for the diagnosis and treatment of acute ischemic stroke 2018, including monitoring and controlling for high blood pressure, sugar metabolic disorder, high cholesterol, and risk factors such as diabetes. The acupuncture and sham acupuncture groups will also receive an additional 30 min of acupuncture therapy as bedside treatment by three acupuncturists who had been trained for at least 3 years and have a master's degree with more than 5 years of clinical experience, 6 days per week for 2 weeks (12 sessions in total).

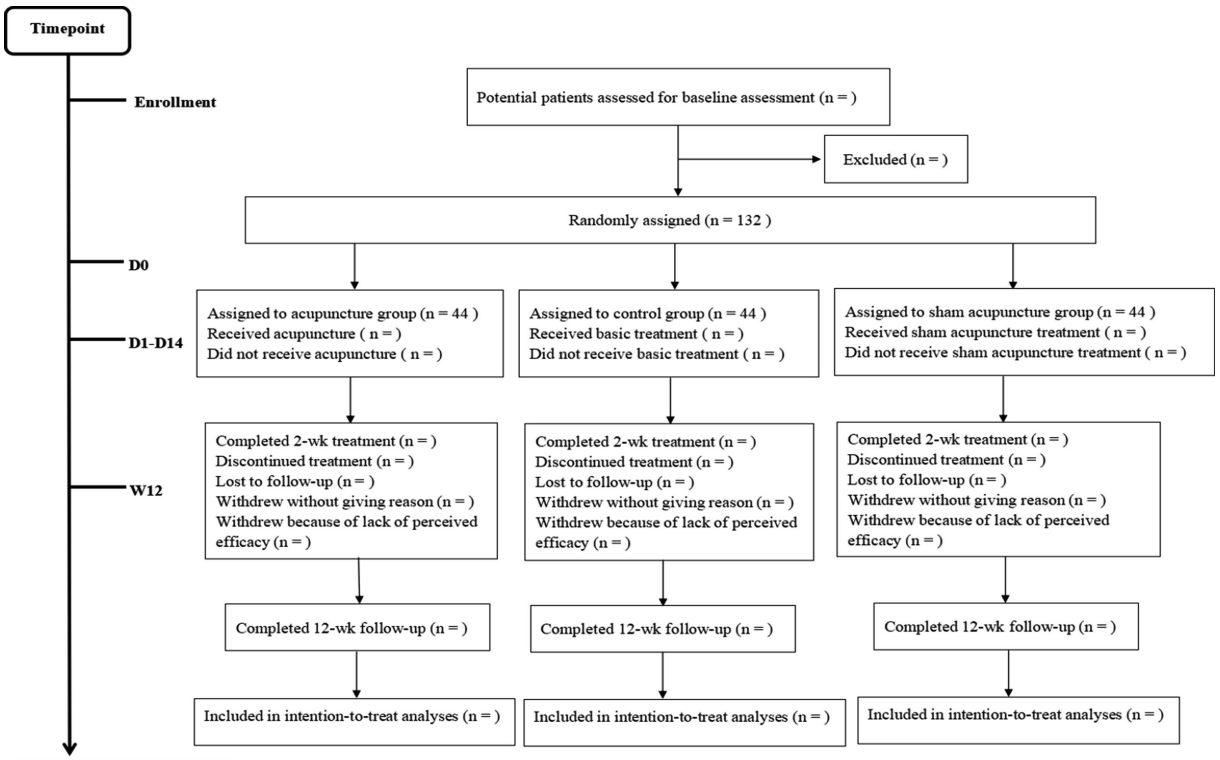

FIGURE 1
A flowchart of the study.

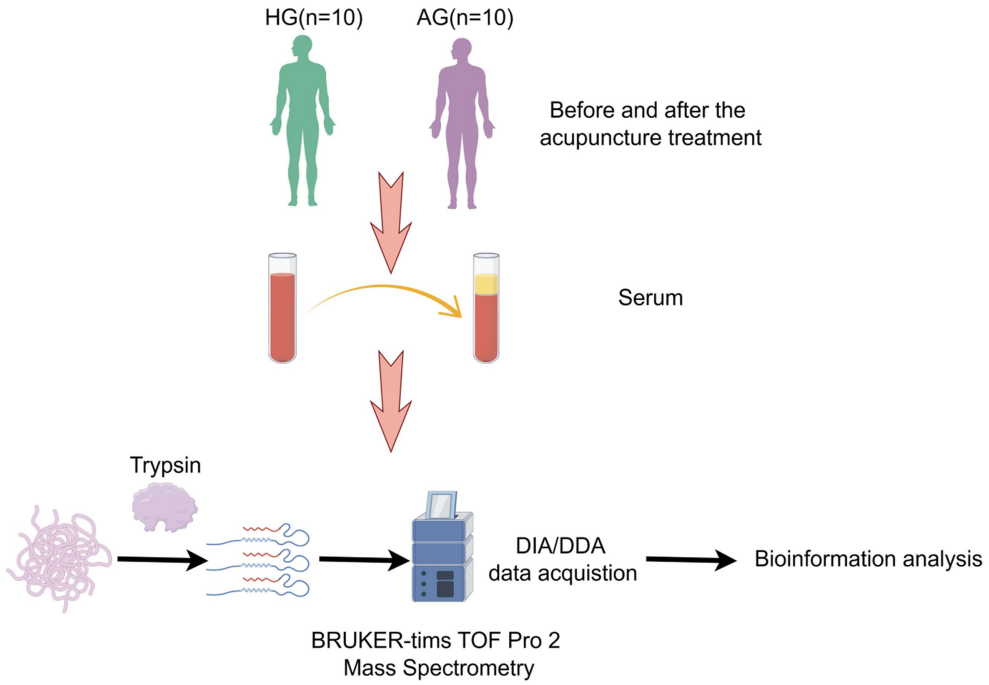

FIGURE 2
Study design and workflow. AG, acupuncture group; HG, health group; DDA, data-dependent acquisition; DIA, data-independent acquisition.

2.6.1 Acupuncture points

ACI belongs to the "apoplexy" category of traditional Chinese medicine. Traditional Chinese medicine theory believes that the brain is the capital of the *gods*, and the imbalance of *yin* and *yang* and the disorder of *qi* and *blood* lead to the occurrence of apoplexy. Therefore, we choose *dumai* as the main meridian for the treatment of apoplexy concerning its pathway and indications. *Renzhong* (DU26), *Baihui* (DU20), and *Fengfu* (DU16) are three acupoints that are located on the *dumai* and used commonly for the treatment of apoplexy. In addition, *Jingbi* (Ex-HN-21) is also chosen for improving the motor function of the trouble side. The position of acupoints is in accordance with the name and location of Acupoints (a standard of The People's Republic of China, GB/T12346-2006, 2006). Details of selected acupoints are shown in Table 1.

TABLE 1 Location of the acupoints.

Points	Location
DU16	On the posterior midline, directly below the external occipital protuberance, in the depression between the origins of the trapezius muscle
DU20	At the junction of a line connecting the apices of the ears and the midline, 5 cun (≈100 mm) from the anterior or 7 cun (≈140 mm) from the posterior hairline
DU26	At the junction of the upper 1/3 and middle 1/3 of the philtrum
Ex-HN-21	1 cun (≈20 mm) superior to the junction of the proximal and middle third of the clavicle

2.6.2 Manipulations

Participants in the acupuncture group will be asked to adopt a supine position, breathe normally, and relax their whole body for 2 min, and then, the acupuncture needle will be swiftly inserted into DU26 toward the nasal septum at a depth of 0.3–0.5 cun (≈6–10 mm) with bird-pecking needling until the eyes become wet or developed tears. After this, DU20 will be punctured at an approximately 15^0 angle to a depth of 0.8–1.2 cun (≈16–24 mm), with the needle rotated for at least 200 revolutions per minute for 1 min. For the DU16, needles will be punctured to a depth of 0.8–1.0 cun (≈16–20 mm), with the lifting, thrusting, and twirling manipulation to attain deqi (a sensation of soreness, aching, heaviness, swelling, or numbness) (MacPherson and Asghar, 2006; Zhou et al., 2011). Finally, the acupuncture needle will be vertically inserted into Ex-HN-21 at a depth of 0.3–0.5 cun (≈6–10 mm) with the lifting-manipulation on a small scale and then removed the needle if the sensation obtained (an electric sensation from the arm to the finger). Sterile, single-use filiform needles will be used in the treatment, with a length of 25 to 40 mm and a diameter of 0.25 mm, manufactured by Suzhou Medical Appliance in Jiangsu Province of China.

The number of needles and duration of treatment in the sham acupuncture group will identical in the acupuncture group, except for any manipulations (without retaining the needle to activate the *qi*). The sham DU26 point was 1 cun (≈20 mm) lateral to DU26, the sham DU20 point was 1 cun (≈20 mm) lateral to DU20, the sham DU16 point was 1 cun (≈20 mm) lateral to DU16, and the sham Ex-HN-21 point was 1 cun (≈20 mm) lateral to Ex-HN-21.

Participants in the sham acupuncture group will also probably choose the same acupoints as the acupuncture group, and participants will not be encouraged to use other therapies for management of ACI throughout the trial. Details will be documented if other therapies used.

2.7 Outcomes and assessment procedures

Three independent research assistants will take charge of their data from baseline to 2 weeks and 3 months of follow-up and for evaluating their outcomes.

2.7.1 Primary outcomes

The primary outcome we chose in this study is the NIHSS score that will be measured before and after treatment to evaluate the neurological deficit. There are 15 items in the scale including consciousness, best gaze, motor arm, facia palsy, motor leg, limb ataxia, sensation ability, dysphagia, and neglect. The score of each item scores range from 0 to 4, and the total scores range from 0 to 42. A higher score indicate a more severe neurological deficit.

2.7.2 Secondary outcomes

Secondary outcomes included the FMA scale scores and BI. The FMA scale comprises assessments of the upper extremity (UE, 66 points) and lower extremity (LE, 34 points). The BI scale includes 10 items: continence of the bowels and bladder, dressing, entering and leaving a toilet, bathing, ascending and descending stairs, etc. We select the FMA scale to evaluate the motor function and BI to evaluate the self-care and mobility before and after treatment. In addition, the modified Rankin Scale (mRS), a scale used to evaluate the state of neurological function recovery in ACI patients, will also be assessed when the follow-up period ended (at 3 months).

2.7.3 Safety assessment

Acupuncture-associated adverse events will be documented by outcome assessors throughout the trial, including bleeding, subcutaneous hemorrhage, serious pain, and fainting. All adverse events will be followed up until the adverse events will be resolved.

2.7.4 Mechanism exploration

2.7.4.1 Proteomic analysis

A quantitative proteomics analysis will be performed based on a 4D-DIA method. The samples were mixed with 1%SDC/100 mM Tris-HCL/10 mM TCEP/40 mM CAA (pH = 8.5) and incubated for 1 h at 60°C for one-step reduction and alkylation. LC–MS/MS data acquisition was carried out on a Q Exactive Plus mass spectrometer coupled with an Easy-nLC 1,200 system. The raw MS data were processed by DIA-NN software (V1.7.16) using the library free method. The general function databases that provide annotations (GO, KEGG, etc.) are used to annotate the identified proteins to understand the functional characteristics of different proteins. Data will be filtered by half the number of actual values in either group and conducted logarithmic transformation and imputation with the

random value method. The filled data will be used for subsequent analysis.

2.7.4.2 Protein validation

ELISA kits will be applied to detect differences in the DEP levels of serum in patients in the acupuncture group and the control group before and after treatment. Samples will be diluted appropriately, and the data will be analyzed in duplicate according to the manufacturer's instructions.

2.8 Statistical analyses

Quantitative variables will be presented with mean ± SD. The Shapiro–Wilk test and box plots will be used to assess the homogeneity of the quantitative variables. All continuous and independent variables in the groups will be performed by Student's *t*-test at baseline. The Mann–Whitney U test will be selected if the variance was not homogeneous between two groups. Stata software will be used to analyze the data according to the intention-to-treat principle, and a two-sided *p*-value less than 0.05 was considered significant.

3 Discussion

Cerebral infraction, which is a fundamental manifestation of ischemic stroke, initially results in a transient impairment of tissue function due to insufficient blood supply to the cerebral tissue, but over time, it leads to irreversible damage to neurons and supporting structures. Ischemia triggers a cascade of events, including increased extracellular glutamate concentration, increased intracellular calcium levels, and oxidative stress (Straus et al., 2002). Significant progress has been achieved in combating ACI over the past few decades, resulting in a transformative shift in ACI management. This shift has given rise to the emergence of efficacious thrombolytic and endovascular therapies since 1995. Given the criticality of time in preserving brain function, prompt and accurate diagnosis of ACI within the initial hours of symptom onset is imperative. Regrettably, the accessibility of neuroimaging facilities remains limited in many developing nations, while the time-sensitive nature of revascularization therapies further compounds the challenge.

The incidence of ACI is on the rise as the aging population continues to grow (Ye et al., 2015). The complement system, systemic immune responses, and inflammation play crucial roles in the progression of ischemic lesions and overall outcomes, resulting in permanent disability for 15–30% of stroke patients (Macrez et al., 2011; Zhang et al., 2015b). Therefore, there is an urgent need for effective management and diagnosis of ACI patients.

Biomarkers serve as objective indicators for evaluating physiological or pathological processes, monitoring responses to medical interventions, and predicting outcomes. These indicators encompass various molecules, including proteins, metabolites, lipids, and ribonucleic acids, among others, present in body fluids such as blood, cerebrospinal fluid, and urine. Additionally, biomarkers can also be derived from physical measurements of tissues, such as imaging and electrophysiology. Despite the identification of B-type natriuretic peptide, matrix metalloproteinase-9, D-dimer, and glial fibrillary acidic protein as potential diagnostic biomarkers for stroke within 24 h in a recent systematic review (Misra et al., 2020), the currently available biomarkers lack the desired sensitivity, specificity, rapidity, and precision. Consequently, there is a need to investigate a more accurate and sensitive biomarker to assist in the diagnosis and management of ACI. Significant advancements have been accomplished through the collaborative endeavors of scientists worldwide subsequent to the initiation of the Human Genome Project in the early 1990s. Undoubtedly, proteins serve as the agents responsible for physiological functionality and the tangible manifestation of vital phenomena. Clinical proteomics is a discipline that applies proteomic techniques to clinical diagnosis, treatment, prognosis, and etiology. By combining proteomics technology with clinical epidemiology, medical statistics, bioinformatics, artificial intelligence, molecular biology, and other technologies, we can explore the molecular effects and mechanisms of proteins related to diseases so as to prevent diseases, improve diagnosis and treatment level, accelerate disease improvement, and promote human health. Consequently, the investigation of protein structure and function will directly elucidate the mechanisms underlying alterations in life processes, whether occurring within physiological or pathological contexts.

Over the course of approximately 2,500 years, acupuncture has amassed a wealth of experience and is widely recognized as a valuable therapeutic approach for addressing ACI. Based on the traditional Chinese medicine theory, acupuncture can regulate *qi* and *blood*, warm meridians, and activate collaterals, providing some benefits for promoting the recovery of neurological function in patients with ACI. It is also suggested to select acupuncture for the treatment of ACI during the acute and early recovery phases based on the current evidence. Nevertheless, the ongoing discourse surrounding the methodology of acupuncture clinical research persists due to the challenge of employing universally accepted measures to evaluate its efficacy. In light of the need to evaluate the efficacy and safety of acupuncture for ACI and explore its probable mechanisms through a proteomic approach, we designed this study.

The purpose of this study is to evaluate the efficacy and safety of acupuncture as a therapeutic intervention for ACI and identify the possible mechanisms. Herein, a prospective randomized controlled trial will be conducted to investigate the effectiveness of acupuncture in combating ACI. Then, a 4D-DIA quantitative proteomics analysis will be used to clarify the underlying mechanism of acupuncture. Furthermore, the DEPs will be verified by ELISA. For the acupoint selection, we have chosen DU16, DU20, and DU26 from the *du mai*, of which DU16 and DU20 are the Sea of Marrow according to the Gao Wu command point. DU16 act as a function of nourishing the Sea of Marrow and lightening the *shen* and use calming internal *wind*. DU20 can exert functions of calming *wind* and *shen*, pacifying *yang*, benefiting the *brain* and sensory organs, and nourishing the Sea of Marrow. DU26 is an important emergency point, which, together with DU16, consist of the Sun Si Miao Ghost point, which can revive consciousness, benefit the face and nose, and eliminate *wind*. Ex-HN-21 is the extra point on the head and neck, which is located in the supraclavicular fossa above the brachial plexus and act with the

function of paraesthesia and paralysis of the upper extremity. We selected three acupoints located in the brain (DU16, DU20, and DU26) from the *dumai*, known for their ability to awake the brain, calm the *shen*, and alleviate *wind*-induced blockages. Furthermore, Ex-HN-21 was also chosen to improve the motor function of patients with ACI. Consequently, this study was undertaken to furnish evidence regarding the effectiveness of acupuncture intervention at the three acupoints located in the brain (DU16, DU20, and DU26) in ACI patients and investigate its underlying mechanism.

Ethics statement

The studies involving humans were approved by the Institutional Review Board of the First Teaching Hospital of Tianjin University of Traditional Chinese Medicine. The studies were conducted in accordance with the local legislation and institutional requirements. The participants provided their written informed consent to participate in this study.

Author contributions

JC: Conceptualization, Writing – original draft, Writing – review & editing. YD: Writing – review & editing. XY: Methodology, Writing – review & editing. NZ: Formal analysis, Writing – review & editing. JH: Formal analysis, Writing – review & editing. LC: Validation, Writing – review & editing. LJ: Software, Writing – review & editing.

Funding

The author(s) declare financial support was received for the research, authorship, and/or publication of this article. This study were funded by the National Natural Science Foundation of China (grant numbers: 82074543 and 82105007) and the Construction Project of Famous Traditional Chinese Medicine Du Yuanhao Inheritance Studio.

Acknowledgments

The authors would like to show their deepest gratitude to Qiuhan Cai, PhD from the First Teaching Hospital of Tianjin University of Traditional Chinese Medicine for assistance with the "Sample size" and "Statistical analysis" sections.

Conflict of interest

The authors declare that the research was conducted in the absence of any commercial or financial relationships that could be construed as a potential conflict of interest.

Publisher's note

References

Atkinson, A. J., Colburn, W. A., DeGruttola, A. G., DeMets, D. L., Downing, G. J., Hoth, J. F., et al. (2001). Biomarkers and surrogate endpoints: preferred definitions and conceptual framework. *Clin. Pharmacol. Therapeutics* 69, 89–95. doi: 10.1067/mcp.2001.113989

Cao, B. Q., Tan, F., Zhan, J., and Lai, P. H. (2021). Mechanism underlying treatment of ischemic stroke using acupuncture: transmission and regulation. *Neural Regen. Res.* 16, 944–954. doi: 10.4103/1673-5374.297061

Chamorro, Á., Dirnagl, U., Urra, X., and Planas, A. M. (2016). Neuroprotection in acute stroke: targeting excitotoxicity, oxidative and nitrosative stress, and inflammation. *Lancet Neurol.* 15, 869–881. doi: 10.1016/S1474-4422(16)00114-9

Chinese Society of Neurology, & Chinese Stroke Society (2018). Chinese guidelines for diagnosis and treatment of acute ischemic stroke 2018. *Chin. J. Neurol.* 51:e4. doi: 10.3760/cma.j.issn.1006-7876.2018.09.004

Costa, V., Angelini, C., de Feis, I., and Ciccodicola, A. (2010). Uncovering the complexity of transcriptomes with RNA-Seq. *J. Biomed. Biotechnol.* 2010, 1–19. doi: 10.1155/2010/853916

Cui, J. Y., and Jia, H. D. (2022). Xingnao Kaiqiao acupuncture combined with butylphthalide sodium chloride injection in the treatment of acute cerebral infarction and its effect on the levels of serum malondialdehyde, superoxide dismutase, and glutathione peroxidase. *Evid. Based Complement. Alternat. Med.* 2022:5990203. doi: 10.1155/2022/5990203

Du, Y. H., Shi, L., Li, J., Xiong, J., Li, O., and Fan, X. N. (2011). Angiogenesis and improved cerebral blood flow in the ischemic boundary area were detected after electroacupuncture treatment to rats with ischemic stroke. *Neurol. Res.* 33, 101–107. doi: 10.1179/016164110X12714125204317

GB/T12346-2006. (2006). *The nomenclature and location of acupuncture points, Beijing, China:* General Administration of Quality Supervision, Inspection and Quarantine of the People's Republic of China & the Standardization Administration of China.

GBD 2019 Stroke Collaborators (2021). Global, regional, and national burden of stroke and its risk factors, 1990–2019: a systematic analysis for the global burden of disease study 2019. *Lancet Neurol.* 20, 795–820. doi: 10.1016/S1474-4422(21)00252-0

Li, J., Du, Y. H., Zhang, X. Z., Bai, Z. L., Pang, B., Zhang, J. J., et al. (2017). Effects of electroacupuncture on expression of Ang/Tie-2 mRNA and protein in rats with acute cerebral infarction. *J. Tradit. Chin. Med.* 37, 659–666. doi: 10.1016/S0254-6272(17)30320-5

Li, J., He, J. J., Du, Y. H., Cui, J. J., Ma, Y., and Zhang, X. Z. (2014a). Electroacupuncture improves cerebral blood flow and attenuates moderate ischemic injury via angiotensin II its receptors-mediated mechanism in rats. *BMC Complement. Altern. Med.* 14:441. doi: 10.1186/1472-6882-14-441

Li, J., He, Y., Du, Y. H., Zhang, M., Georgi, R., Kolberg, B., et al. (2022). Effect of electro-acupuncture on vasomotor symptoms in rats with acute cerebral infarction based on phosphatidylinositol system. *Chin. J. Integr. Med.* 28, 145–152. doi: 10.1007/s11655-021-3341-6

Li, J., Zhang, M., He, Y., Du, Y. H., Zhang, X. Z., Georgi, R., et al. (2023). Molecular mechanism of electroacupuncture regulating cerebral arterial contractile protein in rats with cerebral infarction based on MLCK pathway. *Chin. J. Integr. Med.* 29, 61–68. doi: 10.1007/s11655-022-3468-0

Li, L., Zhang, H., Meng, S. Q., and Qian, H. Z. (2014b). An updated meta-analysis of the efficacy and safety of acupuncture treatment for cerebral infarction. *PLoS One* 9:114057. doi: 10.1371/journal.pone.0114057

Lipton, P. (1999). Ischemic cell death in brain neurons. *Physiol. Rev.* 79, 1431–1568. doi: 10.1152/physrev.1999.79.4.1431

Macpherson, H., Altman, D. G., Hammerschlag, R., Youping, L., Taixiang, W., White, A., et al. (2010). Revised standards for reporting interventions in clinical trials of acupuncture (stricta): extending the consort statement. *PLoS Med.* 7:e1000261. doi: 10.1371/journal.pmed.1000261

MacPherson, H., and Asghar, A. (2006). Acupuncture needle sensations associated with De qi: a classification based on experts' ratings. *J. Altern. Complement. Med.* 12, 633–637. doi: 10.1089/acm.2006.12.633

Macrez, R., Ali, C., Toutirais, O., le Mauff, B., Defer, G., Dirnagl, U., et al. (2011). Stroke and the immune system: from pathophysiology to new therapeutic strategies. *Lancet Neurol.* 10, 471–480. doi: 10.1016/S1474-4422(11)70066-7

Misra, S., Montaner, J., Ramiro, L., Arora, R., Talwar, P., Nath, M., et al. (2020). Blood biomarkers for the diagnosis and differentiation of stroke: a systematic review and meta-analysis. *Int. J. Stroke* 15, 704–721. doi: 10.1177/1747493020946157

Naghavi, M., Abajobir, A. A., Abbafati, C., Abbas, K. M., Abd-Allah, F., and Abera, S. F. (2017). Global, regional, and national age-sex specifc mortality for 264 causes of death, 1980-2016: a systematic analysis for the global burden of disease study 2016. *Lancet* 390, 1151–1210. doi: 10.1016/S0140-6736(17)32152-9

Pan, J. H., Song, X. Y., Lee, S. Y., and Kwok, T. (2008). Longitudinal analysis of quality of life for stroke survivors using latent curve models. *Stroke* 39, 2795–2802. doi: 10.1161/STROKEAHA.108.515460

Qin, S., Zhang, Z., Zhao, Y., Liu, J., Qiu, J., Gong, Y., et al. (2022). The impact of acupuncture on neuroplasticity after ischemic stroke: a literature review and perspectives. *Front. Cell. Neurosci.* 16:817732. doi: 10.3389/fncel.2022.817732

Sainsbury, A., and Heatley, R. V. (2005). Review article: psychosocial factors in the quality of life of patients with inflammatory bowel disease. *Aliment. Pharmacol. Ther.* 21, 499–508. doi: 10.1111/j.1365-2036.2005.02380.x

Sang, B., Deng, S., Zhai, J., Hao, T., Zhuo, B., Qin, C., et al. (2022). Does acupuncture therapy improve language function of patients with aphasia following ischemic stroke? A systematic review and meta-analysis. *NeuroRehabilitation* 51, 231–245. doi: 10.3233/NRE-220007

Schulz, K. F., Altman, D. C., and Moher, D. (2010). CONSORT 2010 statement: updated guidelines for reporting parallel group randomised trials. Italian. *J. Public Health* 36:e2014029. doi: 10.4178/epih/e2014029

Straus, S. E., Majumdar, S. R., and FA, M. A. (2002). New evidence for stroke prevention: scientific review. *JAMA* 288, 1388–1395. doi: 10.1001/jama.288.11.1388

Sun, H., and Wu, C. (2019). Acupuncture combined with Buyang Huanwu decoction in treatment of patients with ischemic stroke. *J. Int. Med. Res.* 47:1312. doi: 10.1177/0300060518822923

Tian, R., and Wang, S. (2019). Electroacupuncture reduced apoptosis of hippocampal neurons in mice with cerebral infarction by regulating the Notch3 signaling pathway. *J. Mol. Neurosci.* 67, 456–466. doi: 10.1007/s12031-018-1253-5

Virani, S. S., Alvaro, A., Benjamin, E. J., Bittencourt, M. S., Callaway, C. W., Carson, A. P., et al. (2020). Heart disease and stroke Statistics-2020 update: a report from the American Heart Association. *Circulation* 141, e139–e596. doi: 10.1161/CIR.0000000000000757

Wang, Y., Shen, J., Wang, X. M., Fu, D. L., Chen, C. Y., Lu, L. Y., et al. (2012). Scalp acupuncture for acute ischemic stroke: a meta-analysis of randomized controlled trials. *Evid. Based Complement. Alternat. Med.* 2012:480950. doi: 10.1155/2012/480950

Wong, I. S. Y., Ng, K. F., and Tsang, H. W. H. (2012). Acupuncture for dysphagia following stroke: a systematic review. In. *Eur. J. Integr. Med.* 4, e141–e150. doi: 10.1016/j.eujim.2012.02.001

Wu, X., Min, L., Cong, L., Jia, Y., Liu, C., Zhao, H., et al. (2014). Sex differences in health-related quality of life among adult stroke patients in northeastern China. *J. Clin. Neurosci.* 21, 957–961. doi: 10.1016/j.jocn.2013.08.030

Ye, H., Wang, L., Yang, X. K., Fan, L. P., Wang, Y. G., and Guo, L. (2015). Serum S100B levels may be associated with cerebral infarction: a meta-analysis. *J. Neurol. Sci.* 348, 81–88. doi: 10.1016/j.jns.2014.11.010

Zhang, S., Jin, T., Wang, L., Liu, W., Zhang, Y., Zheng, Y., et al. (2020). Electro-acupuncture promotes the differentiation of endogenous neural stem cells via Exosomal microRNA 146b after ischemic stroke. *Front. Cell. Neurosci.* 14:223. doi: 10.3389/fncel.2020.00223

Zhang, H., Kang, T., Li, L., and Zhang, J. J. (2013a). Electroacupuncture reduces hemiplegia following acute middle cerebral artery infarction with alteration of serum NSE, S-100B and endothelin. *Curr. Neurovasc. Res.* 10, 216–221. doi: 10.2174/15672026113109990005

Zhang, J. H., Wang, D., and Liu, M. (2013b). Overview of systematic reviews and meta-analyses of acupuncture for stroke. *Neuroepidemiology* 42, 50–58. doi: 10.1159/000355435

Zhang, Z. G., Wang, C., Wang, J., Zhang, Z., Yang, Y. L., Gao, L., et al. (2015b). Prognostic value of mannose-binding lectin: 90-day outcome in patients with acute ischemic stroke. *Mol. Neurobiol.* 51, 230–239. doi: 10.1007/s12035-014-8682-0

Zhang, S., Wu, B., Liu, M., Li, N., Zeng, X., Liu, H., et al. (2015a). Acupuncture efficacy on ischemic stroke recovery. *Stroke* 46, 1301–1306. doi: 10.1161/STROKEAHA.114.007659

Zhou, K., Fang, J., Wang, X., Wang, Y., Hong, Y., Liu, J., et al. (2011). Characterization of De qi with electroacupuncture at acupoints with different properties. *J. Altern. Complement. Med.* 17, 1007–1013. doi: 10.1089/acm.2010.0652

frontiers | Frontiers in Molecular Neuroscience

TYPE Review
PUBLISHED 23 May 2024
DOI 10.3389/fnmol.2024.1375973

OPEN ACCESS

EDITED BY
Hai Sun,
The State University of New Jersey, United States

REVIEWED BY
Venkat Venkataraman,
Rowan University School of Osteopathic Medicine, United States
Cristhian Mendoza,
San Sebastian University, Chile

*CORRESPONDENCE
Dingqun Bai
✉ baidingqun2014@163.com
Lining Yang
✉ yangln1990@163.com

RECEIVED 24 January 2024
ACCEPTED 08 May 2024
PUBLISHED 23 May 2024

CITATION
Lu Q, Yu A, Pu J, Chen D, Zhong Y, Bai D and Yang L (2024) Post-stroke cognitive impairment: exploring molecular mechanisms and omics biomarkers for early identification and intervention.
Front. Mol. Neurosci. 17:1375973.
doi: 10.3389/fnmol.2024.1375973

Post-stroke cognitive impairment: exploring molecular mechanisms and omics biomarkers for early identification and intervention

Qiuyi Lu[1], Anqi Yu[1], Juncai Pu[2], Dawei Chen[1], Yujie Zhong[1], Dingqun Bai[1]* and Lining Yang[1]*

[1]Department of Rehabilitation, The First Affiliated Hospital of Chongqing Medical University, Chonging, China, [2]Department of Neurology, The First Affiliated Hospital of Chongqing Medical University, Chonging, China

Post-stroke cognitive impairment (PSCI) is a major stroke consequence that has a severe impact on patients' quality of life and survival rate. For this reason, it is especially crucial to identify and intervene early in high-risk groups during the acute phase of stroke. Currently, there are no reliable and efficient techniques for the early diagnosis, appropriate evaluation, or prognostication of PSCI. Instead, plenty of biomarkers in stroke patients have progressively been linked to cognitive impairment in recent years. High-throughput omics techniques that generate large amounts of data and process it to a high quality have been used to screen and identify biomarkers of PSCI in order to investigate the molecular mechanisms of the disease. These techniques include metabolomics, which explores dynamic changes in the organism, gut microbiomics, which studies host–microbe interactions, genomics, which elucidates deeper disease mechanisms, transcriptomics and proteomics, which describe gene expression and regulation. We looked through electronic databases like PubMed, the Cochrane Library, Embase, Web of Science, and common databases for each omics to find biomarkers that might be connected to the pathophysiology of PSCI. As all, we found 34 studies: 14 in the field of metabolomics, 5 in the field of gut microbiomics, 5 in the field of genomics, 4 in the field of transcriptomics, and 7 in the field of proteomics. We discovered that neuroinflammation, oxidative stress, and atherosclerosis may be the primary causes of PSCI development, and that metabolomics may play a role in the molecular mechanisms of PSCI. In this study, we summarized the existing issues across omics technologies and discuss the latest discoveries of PSCI biomarkers in the context of omics, with the goal of investigating the molecular causes of post-stroke cognitive impairment. We also discuss the potential therapeutic utility of omics platforms for PSCI mechanisms, diagnosis, and intervention in order to promote the area's advancement towards precision PSCI treatment.

KEYWORDS

post-stroke cognitive impairment, omics, biomarkers, metabolomics, proteomics

1 Introduction

Post-stroke cognitive impairment (PSCI) is defined as a clinical syndrome characterized by cognitive damage that occurs after a stroke and persists for up to 6 months (Mijajlović et al., 2017). Large cohort studies show that between 24 and 53.4% of people have PSCI (Douiri et al., 2013; Lo et al., 2019), yet there are still no accurate billable codes in ICD-11. Compared to stroke survivors without cognitive impairment, individuals with cognitive impairment had significantly greater rates of disability and mortality (Gaynor et al., 2018). PSCI has numerous negative effects on stroke survivors' functional recovery, including executive function, attention (Aam et al., 2020), spatial ability, language, and executive ability (Srikanth et al., 2003). Furthermore, little is known about the pathophysiology of PSCI, which can be brought on by a number of factors such as cerebral small blood vessel disease (Teng et al., 2017), neuroanatomical lesions (Sun et al., 2014), neuroinflammation, and oxidative stress (Zhang X. et al., 2021). In clinical settings, doctors typically use imaging and scale assessments to diagnose patients (Potter et al., 2021), which the accuracy and objectivity are easily affected by the patient's education and age (Kim et al., 2022), so it is critical since to find objective biomarkers. On top of that, there is still much to learn about the disease's molecular mechanisms. A thorough understanding of the molecular mechanisms behind PSCI will facilitate the identification of reliable biomarkers to aid in disease prognosis, therapy, and prevention as well as to diagnose and track the progression of illnesses.

Given the complexity of PSCI's pathophysiology and the limitations of current diagnostic methods, there is a pressing need to explore innovative approaches. Omics is defined as the probing and analysis of large amounts of data on the entire constitutive structure and function of a given biological system at a specific level (Dai and Shen, 2022). As significant fields of omics, metabolomics, microbiomics, genomics, transcriptomics, and proteomics have made irreversible contributions to the hunt for biomarkers and underlying molecular mechanisms of diseases throughout the past few decades (Fu et al., 2010; Chen and Wu, 2012). Each omics approach delivers biological insights at distinct phases (Bjerrum et al., 2008), enhancing PSCI comprehension. Metabolomics helps identify neurological biomarkers (Zhang et al., 2013) by linking metabolic activity to genetic and environmental variables (Fiehn, 2002).Similarly, microbiomics helps analyze the interactions between microbial communities and the human body, offering insights into neurological dysfunctions (Layeghifard et al., 2017; Sorboni et al., 2022). Genomics and transcriptomics, studying genetic variants and gene expression patterns respectively, have identified key molecular alterations associated with stroke and its cognitive aftermath (Lockhart and Winzeler, 2000; Tan et al., 2021; Li W. et al., 2022; Tsimberidou et al., 2022; Ya et al., 2023). Lastly, proteomics, by mapping protein interactions and functions, supports the diagnosis and development of targeted therapies for neurological disorder (Rohlff, 2001; Sancesario and Bernardini, 2018). Although omics approaches are crucial for deepening our understanding of PSCI, the proliferation of omics research in neurological disorders is impeded by technical difficulties, limited clinical applicability, and a lack of comprehensive reviews specifically focusing on post-stroke cognitive impairment.

This study aimed to identify multi-omics alterations in patients with PSCI. In order to assist in characterizing possible biomarkers with prospective applications such as early diagnosis and tracking disease progression, we offer an overview of the multi-omics attributed with post-stroke cognitive impairment. Additionally, the obstacles inherent in biomarker research in PSCI are brought to light so that we can work towards advancing precision medicine in PSCI. We also illustrate the therapeutic relevance of the omics platform for the pathogenesis, diagnosis, and treatment of PSCI, as a means to establish the groundwork for an extensive investigation of PSCI.

2 Materials and methods

2.1 Diagnostic biomarker

All published articles from database inception to October 2023 were searched using our listed term combinations (Supplementary Tables S1–S5) in electronic databases such as PubMed, Cochrane Library, Embase, Web of Science, and common databases for each omics. We then used a snowballing strategy to expand the search. We adopted standard inclusion criteria for the selection of studies: (1) all tissue types belonging to PSCI patients; (2) differential biomarker detection using omics techniques; (3) clinical trial studies assessing changes in levels of various types of biomarkers in patients with PSCI; and (4) peer-reviewed full-text papers published in English. These were the conditions for exclusion: (1) interventional studies; (2) non-human studies; (3) non-original research (reviews, case reports, etc.). Two authors (QL and AY) independently performed screening based on inclusion and exclusion criteria. All disagreements experienced were resolved through ongoing discussions with all authors.

2.2 Data extraction and processing

Excel software was implemented to manually organize the data and perform statistical analysis (Microsoft, Ver. 2019). We separately retrieved data from publications that qualified using a pre-designed table. Elected information consisted of three sections: (1) article information including title, first author, year of publication, and region of recruitment; (2) patient information including sample size, sex ratio, mean age, stroke type, and cognitive function assessment tool; and (3) biomarker information included sample type and selected metabolites that were statistically significant ($p < 0.05$ was considered statistically significant). The pictures for this article were drawn in Adobe Photoshop and Adobe Illustrator.

3 Results

3.1 Literature search results

We systematically retrieved a total of 19,112 records in PubMed, Cochrane Library, Embase, and Web of Science databases (Figure 1A; the outcomes of each omics search are shown in Supplementary Tables S6–S10). After a first screening of titles and abstracts, a second assessment of the entire text, and additional resources, 34 papers were retained based on our predetermined inclusion and exclusion criteria. Out of the results we kept, 14 publications described metabolomics (one of which also discussed

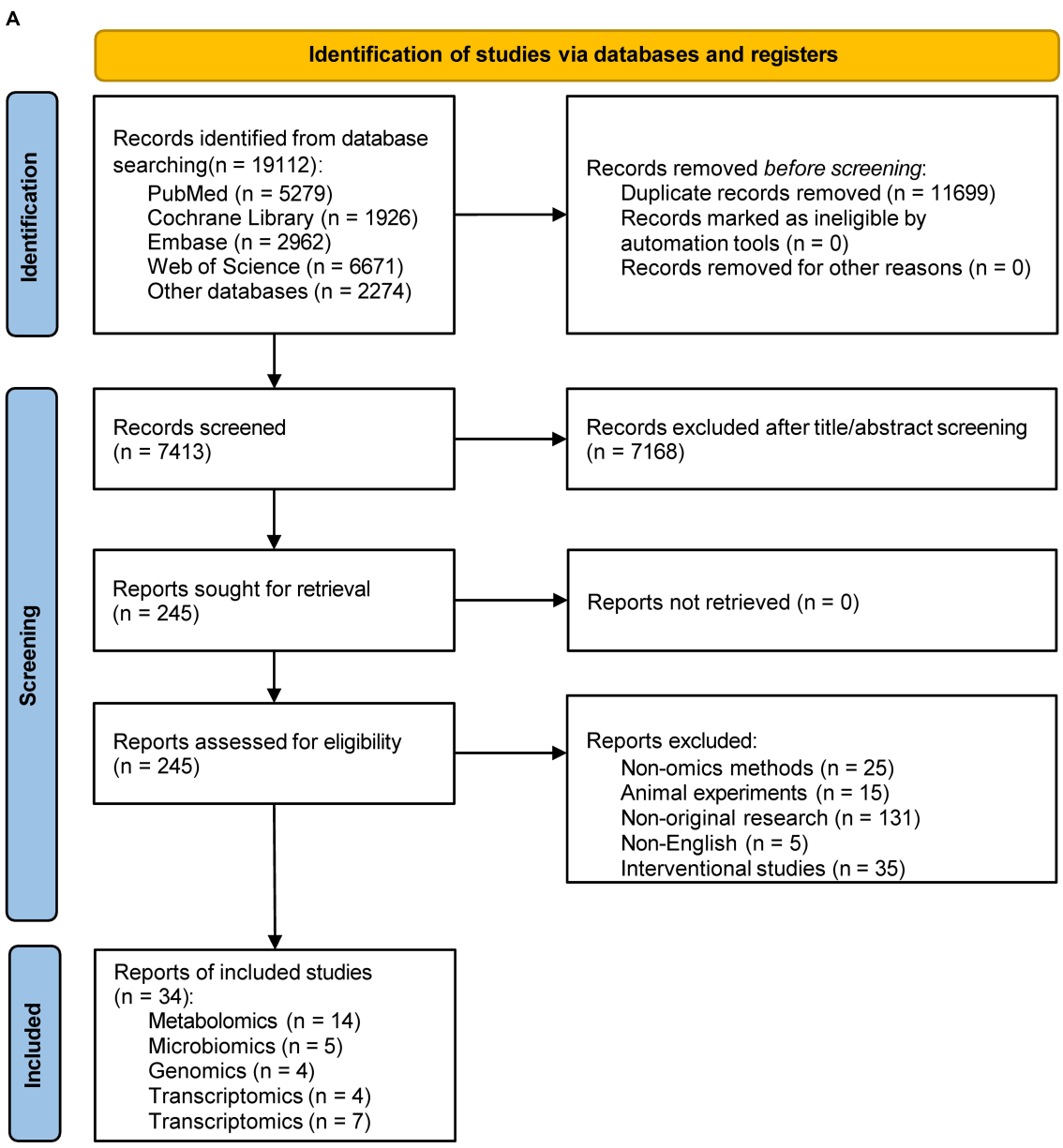

FIGURE 1 (Continued)

microbiomics), 5 articles covered microbiomics, 4 papers concerned genomics, 4 articles concerned transcriptomics, and 7 studies described proteomics (Figure 1B).

3.2 Characteristics of the included studies

Ultimately, 34 articles were included in our study, with publication years between 2011 and 2023. The features of the included studies are displayed in Table 1. Of these articles meeting the criteria, 23 (67.65%) were undertaken in China, the rest in Poland (2, 5.88%), the United States (2, 5.88%), France, Switzerland, Canada, Iran, Korea, Indonesia, Singapore, and other countries. We only counted the sample size once in the following research since two Polish studies that analyzed the same sample of subjects produced different results. A total of 4,223 stroke patients and 702 healthy controls were involved in the 34 included studies, with sample size ranging from 10 to 617. Of these, the patient source for 26 research was solely ischemic stroke, 1 study was hemorrhagic stroke, and 7 studies were not defined. Subjects were assessed neuropsychologically primarily using the Montreal Cognitive Assessment (MoCA) scale or Mini-Mental State Examination (MMSE) scale, but the study from Poland also used the California Verbal Learning Test 2nd (CVLT2) to assess specific abilities.

3.3 Metabolomics in PSCI

Metabolomics demonstrates the qualitative and quantitative analysis of the dynamic metabolic responses of the human body in

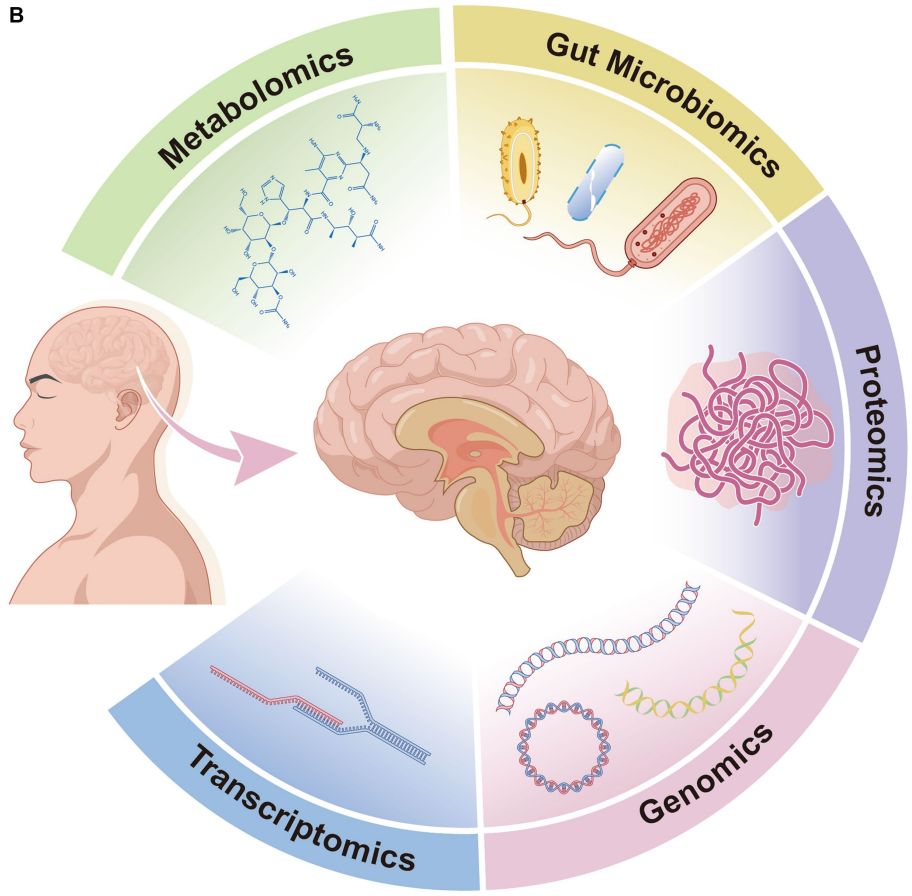

FIGURE 1
(A) Flow diagram of literature search and study selection. **(B)** Overview of multi-omics of post-stroke cognitive impairment.

response to multifactorial stimuli (Nicholson et al., 1999). Researchers typically isolate small molecules using gas chromatography (Xiayan and Legido-Quigley, 2008), liquid chromatography, or capillary electrophoresis and quantify potential biomarkers using nuclear magnetic resonance spectroscopy or mass spectrometry.

Of the research that we looked into, 14 publications described differential metabolites, with serum (50.0%) and plasma (41.7%) accounting for the majority of biological samples and one (8.3%) for feces. We extracted 54 metabolites from these studies (shown in Table 2), and 51 metabolites in total were selected once duplicates were eliminated.

There is now more evidence linking B vitamins to PSCI. For example, in patients with cerebral infarction, thiamine deficiency is predictive with early cognitive impairment (Feng et al., 2020). It has also been demonstrated that folic acid, together with its serum-specific marker methylmalonic acid (MMA), can predict (Pascoe and Linden, 2016) and help diagnose (Durga et al., 2007) cognitive function in patients with post-stroke. Following a stroke, it was discovered that folic acid metabolism products, choline and betaine (Ueland, 2011), had a negative correlation with cognitive performance (Zhong et al., 2021).

One of the possible pathologic mechanisms of PSCI is the generation of inflammation after stroke (Zhang X. et al., 2021), which activates indoleamine 2,3-dioxygenase (IDO), whose activity is associated with cognitive impairment (Gold et al., 2011; Cogo et al., 2021). IDO leads to increased production of kynurenine, while kynurenine (Sapko et al., 2006) and quinolinic acid (Santamaría et al., 2001; Stone and Darlington, 2002) are involved in the induction of synaptic plasticity, and changes in these two substances' concentrations and ratios have been considered accurate indicators of PSCI (Cogo et al., 2021). Serum glutamate levels in PSCI patients further support the idea (Wang X. et al., 2022) that although glutamate is an excitatory neurotransmitter linked to cognitive function, excessive quantities might cause severe excitotoxicity that can aggravate ROS and inflammation (Liu et al., 2020b). Meng et al. (2016) found that PSCI patients had a considerably lower N-acetylaspartic acid/creatine ratio in their hippocampal regions, whereas Liu et al. (2015) also discovered an increase in serum creatine. Several other alterations in amino acid levels have likewise been suggested to be associated with PSCI (Liu et al., 2015), including glutamine, proline, tyrosine, phenylalanine, isoleucine, tryptophan, valine, and N-acetylneuraminic acid. Notably, PSCI was negatively correlated with L-carnitine (Liu et al., 2015; Che et al., 2022), which is produced naturally from two necessary amino acids (Tein et al., 1993). This is probably because L-carnitine has a greater ability to cross the blood–brain barrier and shields neuronal cells from ischemia injury (Zhang R. et al., 2012; Ribas et al., 2014).

PSCI pathophysiology involves the metabolic cascade of polyunsaturated fatty acids (Baierle et al., 2014). Whereas alpha-linolenic acid acts as a substrate for gamma-linolenic acid, which then

TABLE 1 Basic information for omics studies.

Post-stroke cognitive impairment		Non-post-stroke cognitive impairment		Healthy control		Issue type	Patience source	Stroke type	Reference
Sample size (F/M)	Average age (year)[a]	Sample size (F/M)	Average age (year)[a]	Sample size (F/M)	Average age (year)[a]				
72 (40/32)	60.70	NA	NA	30 (18/12)	63.1	Serum	Poland	IS	Kotlęga et al. (2021b)
617 (184/433)	60.0 ± 10.5	NA	NA	NA	NA	Plasma	China	IS	Che et al. (2022)
73 (40/33)	63.40	NA	NA	30 (18/12)	63.1	Plasma	Poland	IS	Kotlęga et al. (2021a)
86 (36/50)	71.10 ± 10.40	170 (81/89)	65.00 ± 10.80	100 (NA)	NA	Plasma	China	IS	Zhu et al. (2020)
20 (10/10)	66.10 ± 6.50	20 (10/10)	67.50 ± 8.64	20 (10/10)	67.30 ± 6.81	Serum	China	IS	Liu et al. (2015)
30 (5/25)	64.90 ± 8.13	35 (11/24)	64.06 ± 8.67	NA	NA	Fecal	China	IS	Liu et al. (2020a)
617 (184/433)	60.00 ± 10.50	NA	NA	NA	NA	Plasma	China	IS	Zhong et al. (2021)
99 (46/53)	65.30 ± 9.03	83 (24/59)	61.27 ± 10.17	NA	NA	Serum	China	IS	Feng et al. (2020)
122 (42/80)	64.32 ± 9.82	106 (25/81)	60.55 ± 11.03	NA	NA	Plasma	China	IS	Gong et al. (2021)
40 (21/19)	61.32	NA	NA	20 (9/11)	61.03	Serum	China	IS	Wang X. et al. (2022)
13 (5/8)	69.40 ± 17.80	10 (4/6)	64.70 ± 13.30	NA	NA	Serum	France	IS	Cogo et al. (2021)
149 (97/52)	81.04 ± 5.30	NA	NA	NA	NA	Serum	Sweden	IS	Pascoe and Linden (2016)
36 (16/20)	59.00 ± 9.3	36 (17/19)	59.300 ± 8.20	NA	NA	Brain	China	IS	Meng et al. (2016)
41 (19/22)	72.30 ± 12.20	NA	NA	NA	NA	Plasma	Canada	IS	Gold et al. (2011)
34 (24/10)	61.50	49 (44/5)	54.00	NA	NA	Fecal	China	IS, HS	Wang H. et al. (2022)
53 (18/35)	72.20 ± 10.30	40 (13/27)	66.00 ± 10.80	NA	NA	Fecal	China	IS	Ling et al. (2020a)
41 (24/17)	69.63 ± 9.35	25 (11/14)	68.92 ± 8.46	NA	NA	Fecal	China	IS	Ling et al. (2020b)
29 (9/20)	NA	27 (13/14)	NA	19	NA	Fecal	China	IS	Huang et al. (2021)
86 (36/50)	63.12 ± 12.47	NA	NA	NA	NA	Blood	America	IS, HS	Han Z. et al. (2020)
48 (34/14)	74.52 ± 8.80	158 (93/65)	61.49 ± 10.78	NA	NA	Blood	Iran	IS, HS	Rezaei et al. (2016)
81 (20/61)	71.40 ± 11.32	NA	NA	NA	NA	Serum	China	IS	Zeng et al. (2019)
361 (123/238)	63.80 ± 9.60	NA	NA	346 (155/191)	60.6 ± 10.6	Blood	China	IS	Han Y. et al. (2020)
36 (20/16)	68.00	38 (23/15)	67.00	NA	NA	Plasma	China	IS, HS	Wang et al. (2020)
45 (NA)	NA	32	NA	NA	NA	Serum	China	IS, HS	Yuan et al. (2022)
108 (41/67)	53.78 ± 11.32	NA	NA	72 (37/39)	54.07 ± 11.18	Blood	China	IS, HS	Zhai et al. (2020)
39 (19/20)	66.20 ± 8.80	37 (17/20)	65.80 ± 9.20	38 (18/20)	65.6 ± 7.4	Serum	China	IS, HS	Huang et al. (2016)
35 (11/24)	61.63 ± 8.47	21 (10/11)	58.67 ± 9.01	NA	NA	Serum	Indonesia	IS	Prodjohardjono et al. (2020)
23 (NA)	NA	NA	NA	17 (13/4)	56	Plasma	Singapore	IS	Datta et al. (2022)
61 (NA)	NA				NA	Plasma	America	IS	Hazelwood et al. (2022)
80 (39/41)	64.50 ± 10.20	118 (44/74)	67.60 ± 9.10	NA	NA	Serum	China	IS	Zhang Y. et al. (2021)
192 (72/120)	65.70 ± 7.80	124 (49/75)	65.30 ± 8.20	NA	NA	Serum	China	HS	Gao et al. (2022)
37 (NA)	NA	43 (NA)	NA	NA	NA	Serum	China	IS	Li Z. et al. (2022)
286 (117/189)	NA	NA	NA	NA	NA	Blood	Korea	IS	Kim et al. (2012)
10 (5/5)	60.30 ± 9.17	NA	NA	10 (4/6)	55.80 ± 6.92	Plasma	China	IS	Qi et al. (2023)

[a]Continuous variables are presented as mean ± SD; NA means not available.

produces arachidonic acid through a sequence of reactions (Kotlega et al., 2020), it has been demonstrated that this inflammatory cascade is linked to cognitive impairment in stroke survivors (Kotlęga et al., 2021b). Arachidonic acid may also serve as a bridge between lipid metabolism, neuroinflammation, and cognitive function in the pathophysiology of ischemic stroke (Szczuko et al., 2020). Prostaglandins formed from arachidonic acid are key mediators of neuroinflammation, among which prostaglandin E2, 9S-HODE, and

13S-HODE were found to be significantly correlated with PSCI (Kotlęga et al., 2021a).

Apart from the metabolites present in blood samples of patients, the metabolomics of PSCI are also influenced by differential metabolites that are broken down by gut microbes. These metabolites include butyrate (Wang H. et al., 2022), lipopolysaccharide, trimethylamine-n-oxide (TMAO) (Zhu et al., 2020; Gong et al., 2021), and seven major short-chain fatty acids (Liu et al., 2020a), which are acetic acid, propionic acid, isobutyric acid, butyric acid, isovaleric acid, valeric acid, and caproic acid.

Heterogeneity in current metabolomics research on PSCI is challenging to avoid because of variations in areas, sample sizes, and analytical techniques. Secondly, most of the selected studies are blood studies, and there are no metabolomics studies of brain tissue and other organs yet. Thirdly, there is a wide variety of metabolites and a lack of replicability. Fourthly, there aren't many viable biomarkers for PSCI research in nuclear magnetic resonance spectroscopy, one of the potent metabolomics techniques. We believe that future research directions for study could focus on enhancing these elements and delving deeper into PSCI therapy that targets lipid level alterations.

3.4 Gut microbiomics in PSCI

Microbiomics is an emerging field of research aimed at identifying the components of the microbiome, characterizing the interactions between the microbiome and the host, and determining its impact on disease (Barko et al., 2018). The most used techniques are bacterial 16s ribosomal RNA genome sequencing (Wang and Qian, 2009) and shotgun sequencing (Quince et al., 2017).

Among the five studies on gut microbiomics that were considered, we found divergent microbiota in two phyla, one class, two orders, three families, and six genera. The emergence of the gut-brain axis (GBA) has enhanced our understanding of neurological disease progression. The gut microbiota may interact with GBA through autonomic, endocrine, and immune crosstalk (Zhao et al., 2021). Therefore, researchers also paid attention to the gut microbiome of PSCI patients. *Bacillota* (Liu et al., 2020a), *Proteobacteria* (Ling et al., 2020a,b) and *Bacteroidetes* (Liu et al., 2020a) at the phylum level in PSCI patients. *Gammaproteobacteria* was negatively correlated with MoCA scores in patients with post-stroke comorbid cognitive impairment and depression (Ling et al., 2020a,b). Patients with PSCI exhibited notable visual changes in *Enterobacterales* and *Lactobacillales*, which were linked to inflammation (Ling et al., 2020a). Whereas the abundance of *Enterobacteriaceae* (Huang et al., 2021; Wang H. et al., 2022), *Streptococcaceae*, and *Lactobacillaceae* increased significantly in PSCI patients (Ling et al., 2020a). At the genus level, *Fusobacterium* (Liu et al., 2020a), *Streptococcus*, *Klebsiella*, *Lactobacillus* (Ling et al., 2020a) and *Enterococcus*, *Bacteroides* (Huang et al., 2021) were significantly altered in post-stroke patients. Patients with PSCI exhibited a specific deficiency in microorganisms that produce short-chain fatty acids (SCFAs), including *Oscillibacter*, *Ruminococcus*, *Gemmiger*, *Coprococcus*, and *Barnesiella* (Liu et al., 2020a). SCFAs can cross the blood-brain barrier into the brain and act in the central nervous system (Kekuda et al., 2013), which also confirms the gut-brain axis of bidirectional communication.

TABLE 2 Metabolites in PSCI.

Metabolite	Tissue type	Expression	Reference
Arachidonic acid	Serum	Down	Kotlęga et al. (2021b)
Eicosapentaenoic acid	Serum	Down	
Alpha-linolenic acid	Serum	Up	
Stearidonic acid	Serum	Up	
Tricosanoic acid	Serum	Up	
Pentadecanoid acid	Serum	Down	
Gamma-linolenic acid	Serum	Down	
Myristic acid	Serum	Up	
Myristoleic acid	Serum	Up	
Vaccenic acid	Serum	Up	
Arachidic acid	Serum	Up	
L-carnitine[a]	Plasma	Down	Che et al. (2022)
Prostaglandin E2	Plasma	Up	Kotlęga et al. (2021a)
9-hydroxyoctadecadienoic acid	Plasma	Up	
13-hydroxyoctadecadienoic acid	Plasma	Up	
5-hydroxyeicosatetraenoic acid	Plasma	Up	
12-hydroxyeicosatetraenoic acid	Plasma	Up	
Maresin 1	Plasma	Up	
Leukotriene B4	Plasma	Up	
Resolvin D1	Plasma	Down	
Trimethylamine N-oxide[a]	Plasma	Up	Zhu et al. (2020)
L-carnitine[a]	Serum	Up	Liu et al. (2015)
Creatine	Serum	Up	
L-glutamine	Serum	Up	
L-proline	Serum	Up	
N-acetylneuraminic acid	Serum	Up	
Hypoxanthine	Serum	Up	
Uric acid	Serum	Up	
L-tyrosine	Serum	Up	
L-kynurenine[a]	Serum	Up	
L-phenylalanine	Serum	Up	
Sphingosine-1-phosphate	Serum	Up	
L-palmitoylcarnitine	Serum	Up	
Citric acid	Serum	Down	
L-valine	Serum	Down	
L-isoleucine	Serum	Down	
L-tryptophan	Serum	Down	
LysoPCs	Serum	Down	
Stearoylcarnitine	Serum	Down	

(Continued)

TABLE 2 (Continued)

Metabolite	Tissue type	Expression	Reference
Acetic acid	Plasma	Up	Liu et al. (2020a)
Acetic acid	Fecal	Down	
Propionic acid	Fecal	Down	
Isobutyric acid	Fecal	Down	
Butyric acid	Fecal	Down	
Isovaleric acid	Fecal	Down	
Valeric acid	Fecal	Down	
Caproic acid	Fecal	Down	
Choline	Plasma	Down	Zhong et al. (2021)
Betaine	Plasma	Down	
Thiamine	Serum	Down	Feng et al. (2020)
Trimethylamine N-oxide[a]	Plasma	Up	Gong et al. (2021)
L-glutamate	Serum	Up	Wang X. et al. (2022)
L-kynurenine[a]	Serum	Up	
Quinolinic acid	Serum	Up	Cogo et al. (2021)
Methylmalonic acid	Serum	Up	Pascoe and Linden (2016)

[a]For the duplicate metabolites.

The results of changed biodiversity in the PSCI microbiome varied, depending on a number of variables including age, antibiotic use, and diet (Lozupone et al., 2012). The present study did not exclude the influence of the aforementioned factors, and the cross-sectional study design made it impossible to establish a causal link between PSCI and changes in the microbiota. We further propose that, upon the present flaws have been addressed, future research should concentrate on delving deeper into the connections between PSCI and the gut microbiota in combination with other omics analyses.

3.5 Genomics in PSCI

High-throughput sequencing technology has made human diseases easier to investigate in recent years by giving researchers a deeper and more comprehensive platform to examine disease processes and underlying mechanisms. Genetic linkage analysis, candidate gene studies, genome-wide association studies (GWAS), and next-generation sequencing techniques (NGS) have become the main means to study disease etiology and risk genes (Giri et al., 2016).

Out of the 5 genomics studies we found, 4 genes were described to be significantly associated with PSCI. Brain-derived neurotrophic factor (BDNF) promotes neurology and angiogenesis (Kurozumi et al., 2004; Schäbitz et al., 2007) and influences post-stroke recovery through its neuroplastic effects (Lu, 2003). BDNF Val is considered a risk allele for patients with poststroke dementia, and it was found that ischemic stroke patients with a heterozygous Val/Met genotype developed cognitive impairment earlier than those with a Met/Met homozygous genotype and had significantly reduced survival (Kim et al., 2012; Rezaei et al., 2016). The BDNF val66Met single nucleotide polymorphism (SNP) leads to intracellular packaging of proBNDF and secretion of mature BDNF (Chen et al., 2004; Yoshida et al., 2012) and is considered a key predictor of cognitive outcome and functional recovery after stroke in hospitalized patients (Rezaei et al., 2016; Han Z. et al., 2020). The reason may be that BNDF val66Met is associated with the prefrontal cortex, anterior cingulate cortex, and hippocampus volume (Niendam et al., 2012; Balconi, 2013), affecting the neural circuits that control cognition (Schweiger et al., 2019). Serum cystatin C is similarly thought to prevent cognitive impairment by inhibiting amyloid Aβ (Sastre et al., 2004; Kaeser et al., 2007), a protein encoded by the CST3 gene. Zeng et al. (2019) claimed that the CST3B allele or CST3 gene polymorphism could be one of the early diagnostic indicators of PSCI. In addition, apolipoprotein E (APOE), one of the major members of very low-density lipoproteins (Levy et al., 2001), was found to have three alleles (ε2, ε3, and ε4), and APOE ε4 carriers and ε4 alleles are more susceptible to PSCI than healthy populations (Han Y. et al., 2020). APOE ε4 allele has also been suggested to be a biologically active factor for β-amyloid peptide deposition in the brain, which ultimately leads to the narrowing of blood vessels and altered cerebral perfusion (Gurol et al., 2006; Godin et al., 2009).

There are currently no genome-wide investigations of PSCI, and research is restricted to potential genes at this time. Genome-wide data from PSCI patients must be gathered and processed immediately in order to identify all loci of variations linked with PSCI risk and any potential regulatory mechanisms. Finding all degrees of association responses and PSCI mechanisms will be made easier by connecting genetic variations to the development of the disease. In addition, we advocate further exploration of the clinical and pharmacological applications of BDNF for stroke and PSCI, which we believe is a powerful way forward.

3.6 Transcriptomics in PSCI

Not only is transcription the initial stage of gene expression, but it is also a crucial regulatory stage. The post-genome age has seen a rise in interest in transcriptomics. These days, techniques for analyzing gene expression include RNA sequencing, microarray screening, and real-time PCR (Bagyinszky et al., 2020). Not only that, for microRNA detection, other methods based on nucleic acid amplification have been developed (Ye et al., 2019), including rolling loop amplification (RLA), double-stranded specific nuclease (DSN)-based amplification, loop-mediated isothermal amplification (LAMP), etc.

Six distinct miRNAs were proposed as PSCI biomarkers from a total of 4 transcription-related studies that were deemed relevant to patients with PSCI. MicroRNA (miRNA) is increasingly being recognized as a novel biomarker and therapeutic target for a variety of diseases, including ischemic stroke (Yang S. et al., 2020). MiRNA dysregulation provides early warning signals of brain disease outwardly by causing changes in mRNA through exosomes in concert with proteins (Zhang et al., 2015). MiRNA-132 interferes with neuronal maturation by affecting dendritic arborization and spinogenesis and has been demonstrated to exist as a key activity-dependent regulator of cognition (Hansen et al., 2013). The predictive effect of miRNA-132 on PSCI has been found (Huang et al., 2016; Yuan et al., 2022). Clinical studies have shown that miRNA-21 attenuates brain injury and

neurological dysfunction through neurogenesis and angiogenesis (Lopez et al., 2017), and its upregulation is significantly associated with an increased risk of PSCI (Yuan et al., 2022). Moreover, miRNA-200b was found to be associated with the vascular endothelial growth factor A gene (Li et al., 2017), which can enhance vascular permeability, and its expression level was also found to be up-regulated in PSCI patients (Yuan et al., 2022). Also capable of regulating VEGF expression was miRNA-195 (Wang et al., 2013), which was also found to be associated with PSCI by Zhai et al. (2020). There are also miRNAs such as miRNA-497 (Zhai et al., 2020) and miRNA-let-7i (Wang et al., 2020) that were found to be significantly associated with post-stroke cognitive function in PSCI patients.

Both non-protein-coding and protein-coding RNA are included in the entire gene expression profile linked to PSCI. Unfortunately, the present study was limited to miRNA. The supremacy of transcriptome development must be understood in order to facilitate the deciphering of PSCI molecular networks. To provide a more thorough understanding, we propose that future efforts be directed towards investigating the entire range of gene expression in PSCI.

3.7 Proteomics in PSCI

Proteomics is the characterization of the proteome, including the expression, structure, function, interactions, and modifications of proteins at any stage (Domon and Aebersold, 2006). Proteomics plays a key role in early diagnosis, prevention, and tracking of the progress of diseases. Proteomics assay techniques are complex and numerous, such as chromatography-based purification, electrophoresis-based separation, and high-throughput technologies.

Seven research on PSCI proteomics have been reported to date. One of the main roles that inflammation appears to have in the pathophysiology of PSCI. Serum amyloid A is involved in the chemotactic recruitment of inflammatory cells (Sack, 2018) and has been shown to play a role in various central nervous system diseases (Kisilevsky and Manley, 2012), including PSCI (Zhang Y. et al., 2021). The upregulation of the inflammatory protein GP1BA, which binds to the von Willebrand factor and is involved in platelet adhesion and activation (Kroll et al., 1991), indicates a pro-inflammatory response of the immune system to ischemic injury and promotes the occurrence of PSCI (Hazelwood et al., 2022). The proteins ARTN, HGF (Gallo et al., 2015), and VEGF (Lee et al., 2010) are associated with angiogenesis and neuroprotection, and their early predictive role in PSCI patients was identified (Prodjohardjono et al., 2020; Hazelwood et al., 2022). Both neuroglobin and hemoglobin, which are subtypes of pearl proteins (Lopez et al., 2010; Baez et al., 2016), play an important role in oxidative stress and protect brain tissue from hypoxic and ischemic damage, so their reduced levels increase the risk of developing PSCI (Gao et al., 2022; Li Z. et al., 2022).

According to Qi et al. (2023), 31 proteins that were up-regulated in PSCI patients compared to controls may be connected to platelet aggregation and coagulation, whereas 128 proteins that were down-regulated may be connected to pathways such complement activation, fibrin clotting, and cell adhesion protein binding. However, a quantitative proteomics study of plasma in patients with lacunar infarction identified 112 proteins associated with cognitive decline (Datta et al., 2022), most of which were not associated with inflammation, complement activation, coagulation, fibrinolysis, or endothelium. We hypothesize that this variability exists because of geographic differences, sample selection time, and subject individualization differences.

Based on current research findings, proteins are powerful biomarkers for the diagnosis and prognosis of PSCI. However, the majority of research conducted thus far has utilised blood samples, with only a small number examining additional samples such urine, saliva, brain tissue, and cerebrospinal fluid. We look forward to improving the differential expression analysis and co-expression network analysis of different samples of PSCI patients in the future to further explore the mechanism behind PSCI.

4 The clinical application prospect of multi-omics in PSCI

A variety of omics platforms have been developed to detect biomarkers at different levels, enabling us to delve into previously uncharted territories of understanding, such as diagnosis, mechanism exploration and targeted therapy for PSCI (Figure 2).

4.1 Potential diagnostic biomarker

Based on the current metabolomics of PSCI, amino acids such as glutamine, kynurenine, and its metabolite quinolinic acid may be employed as PSCI diagnostic indicators. Glutamate has been implicated in the pathophysiology of cerebral ischemia in earlier research (Dirnagl et al., 1999), and it has also been suggested that glutamate may be a biomarker for stroke (Castellanos et al., 2008), Parkinson's disease (Vascellari et al., 2020), Huntington's disease, and other neurodegenerative diseases that cause early cognitive dysfunction (Unschuld et al., 2012) due to the excitotoxicity of glutamate (Estrada Sánchez et al., 2008). One of the necessary amino acids, L-tryptophan, can be metabolized to quinolinic acid and kynurenine via the kynurenine pathway. It has been discovered that these metabolites have the ability to distinguish between atherosclerotic and cardiac cerebral infarcts (Lee et al., 2023). Moreover, a number of processes by which the kynurenine pathway causes neurotoxicity and neuronal death (Guillemin, 2012) can contribute to cognitive impairments (Heisler and O'Connor, 2015). Also, folate has been proposed for the diagnosis of PSCI and has previously been found to have potential as a biomarker for ischemic stroke (Sidorov et al., 2019).

Gut microbiomics at PSCI identified microbiota that could equally serve as non-invasive diagnostic biomarkers, including *Firmicutes*, *Bacteroidetes*, *Enterobacteriaceae*, and *Bacteroides*. Current ideas suggest that dysregulation of *Firmicutes/Bacteroidetes* ratio can be used as a potential biomarker of cognitive impairment (Ticinesi et al., 2019) and is also highly associated with obesity (Sze and Schloss, 2016). *Bacteroides*, one of the *Bacteroidetes*, can also be used as a biomarker for the recanalization of ischemic stroke (Chou et al., 2023) and the worsening of multiple sclerosis (Devolder et al., 2023), possibly because of the pathogenicity and pro-inflammatory neurotoxins it produces (Sears, 2009). *Enterobacteriaceae*, mostly considered as pro-inflammatory bacteria, have been shown to serve as noninvasive diagnostic biomarkers for Alzheimer's disease (Chen et al., 2023) and epilepsy (Cui et al., 2021).

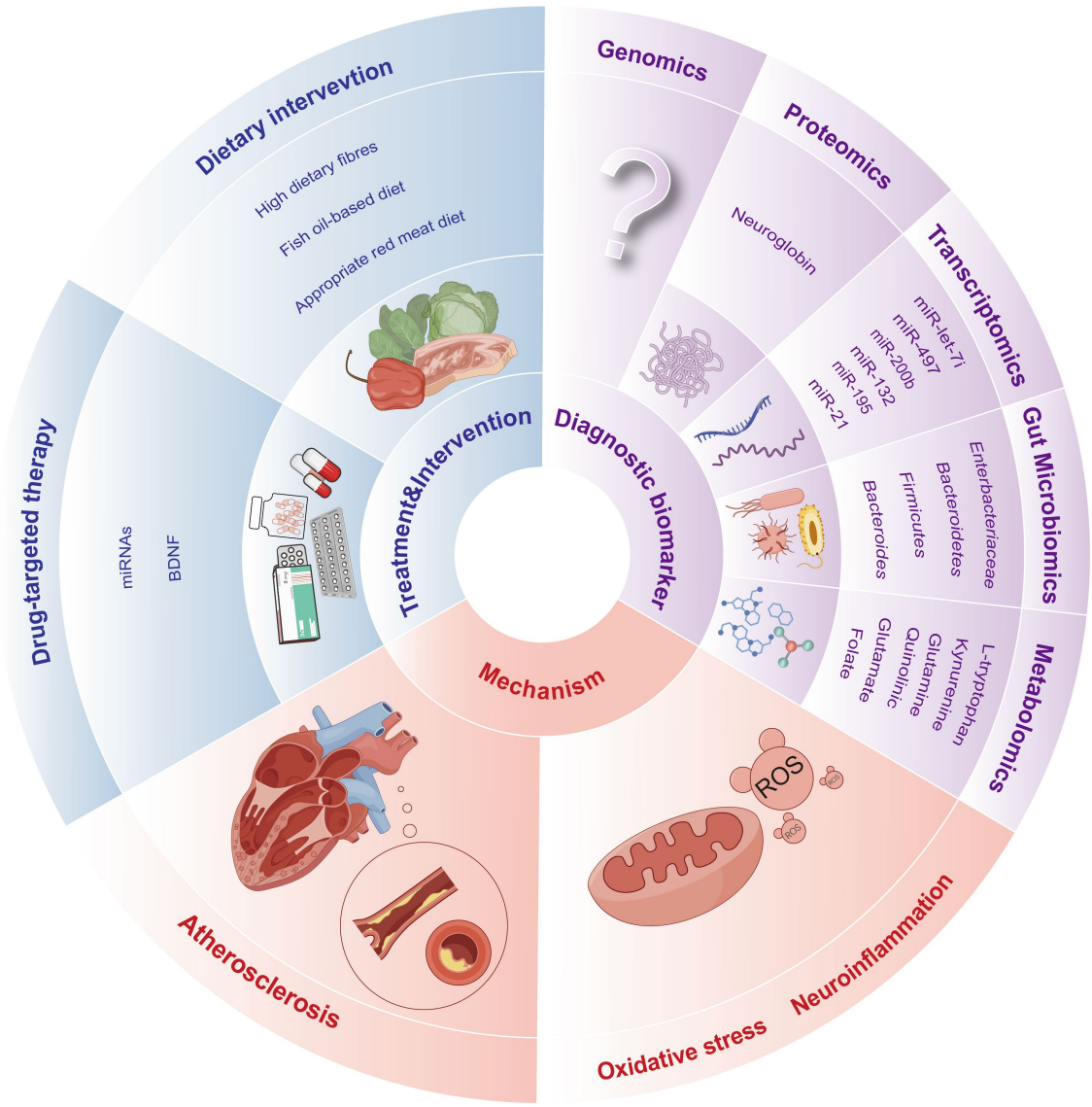

FIGURE 2
Prospects for clinical applications of the multi-omics of PSCI.

The transcriptomics of PSCI has also highlighted the effectiveness of certain miRNAs in terms of diagnosis, including miR-21, miR-132, miR-195, miR-200b, miR-497, and miR-let-7i. Thus far, research has validated the molecular diagnostic capability of miR-21 in several diseases such as acute cerebral infarction (Mohammed et al., 2022), atherosclerosis (Fontanella et al., 2021), and glioma (Zhou et al., 2018). Other studies have identified the diagnostic properties of miR-132 in mild cognitive impairment (Sheinerman et al., 2012; Xie et al., 2015) due to its modulation of glutamate receptor levels. Not only that, miR-132 also plays the role of a biomarker in the diagnosis of major depression and a variety of central nervous system disorders (van den Berg et al., 2020). The researchers also found miR-195 and miR-497 in acute stroke (Zhai et al., 2020) and cognitive impairment in schizophrenia (Huang et al., 2020). For miR-200b, current research has only identified its diagnostic possibilities in Alzheimer's disease or mild cognitive impairment (Liu et al., 2014). And more study is still needed to fully understand the precise diagnostic performance of miR-let-7i.

Only neuroglobin, which has also been utilized in the diagnosis of delayed cerebral ischemia after craniocerebral injury (Chen et al., 2015) and subarachnoid hemorrhage (Ding et al., 2020), has been asserted as a diagnostic biomarker by the proteomics of PSCI. In contrast, the genomics of PSCI is limited to the study of candidate genes without biomarker discovery.

It is worth noting that only a small number of studies have demonstrated the diagnostic performance of these markers and their causal relationship with PSCI, such as neuroglobin (Gao et al., 2022), serum amyloid A (Zhang Y. et al., 2021), L-carnitine (Che et al., 2022) and TMAO (Zhu et al., 2020). The rest of the biomarkers have only shown associations with PSCI at a statistical level, and these changes may be related to multiple pathways including inflammation, so subsequent studies need to be approached with caution. But there is not enough evidence to show how these pathways interact with each other. Also, the studies that are already out there are still in the experimental stage and absence of any multicenter or large-sample

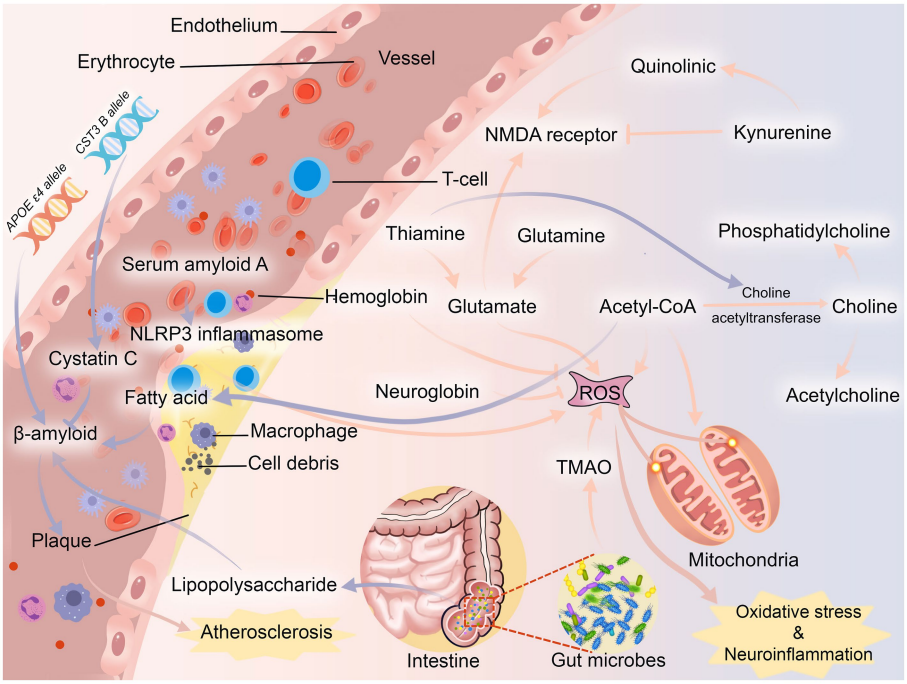

FIGURE 3
Possible pathogenesis of PSCI. NMDA receptor, N-methyl-D-aspartic acid receptor; NLRP3 inflammasome, NOD-like receptor thermal protein domain associated protein 3 inflammasome; TMAO, trimethylamine-n-oxide.

cohort studies. This needs to be fixed in the future, which means that researchers will have to deal with results that aren't identical because of different technologies, groups, or causes. Still, we prefer more study to be done on the omics of PSCI and how the results can be used in the clinic. More importantly, we need to come up with consistent diagnostic standards for these possible biomarkers so that we can quickly find the best ways to treat PSCI.

4.2 Possible mechanism

Inflammation and oxidative stress appear to play important roles in PSCI (Figure 3). It is well known that cognitive function is based on synaptic plasticity (Sloley et al., 2021). Thiamine, an antioxidant, binds to several mitochondrial enzymes and alters mitochondrial interactions (Marcé-Grau et al., 2019), and its deficiency reduces the level of the neurotransmitter acetylcholine by decreasing the activity of choline acetyltransferase (Jankowska-Kulawy et al., 2010) and induces excessive glutamate release (Mkrtchyan et al., 2016). Glutamine is a precursor of excitatory neurotransmitter glutamate, which plays an important role in synaptic plasticity (Reiner and Levitz, 2018). Overconsumption of glutamine can lead to mitochondrial damage and produce a large number of reactive oxygen species (ROS) (Verma et al., 2022), which induces neurotoxicity. Choline, a precursor of acetylcholine, is implicated in cholinergic transmission and signaling, whereas reduced or absent levels of choline in the brain lead to impaired cognitive function (de Medeiros et al., 2019). It is worth noting that choline is likewise recognized as a precursor to phosphatidylcholine, which slows cognitive decline (Blusztajn et al., 2017). An imbalance in the ratio of quinolinic acid, an NMDA (N-methyl-D-aspartic acid) receptor agonist, to kynurenine, an NMDA receptor antagonist, which is a kynurenine pathway metabolite of tryptophan and induces synaptic plasticity (Hestad et al., 2022), also contributes to neuroinflammation (Forrest et al., 2015). Also, hemoglobin and neuroglobin are neuroprotective, scavenging and detoxifying reactive oxygen species (Agyemang et al., 2021; Gorabi et al., 2021), so deficiencies in hemoglobin and neuroglobin predispose the body to cognitive dysfunction. In addition to these two proteins, serum amyloid A is involved in the chemotactic recruitment of inflammatory cells (Lee et al., 2020), and after stroke activates NLRP3 (NOD-like receptor thermal protein domain associated protein 3) inflammasome through oxidative stress to impair neuronal cells and cognitive function (Shridas and Tannock, 2019). The gut microbiota plays an important role in regulating the body's metabolism, so ecological imbalances after stroke often cause activation of pro-inflammatory microglia leading to cognition-related neuroinflammation (Liu et al., 2022). Trimethylamine-n-oxide (TMAO) produced through gut microbial metabolism can lead to neuronal cell senescence by affecting mitochondrial energy metabolism, further exacerbating neuroinflammation and oxidative stress, ultimately leading to degeneration of brain function and cognitive impairment (Brunt et al., 2021).

Another important mechanism of PSCI may be atherosclerosis (Figure 3). After stroke, changes in the body's fatty acid levels may lead to plaque formation by inducing the production of β-amyloid (Díaz et al., 2022). In turn, β-amyloid has neurotoxic effects on neurons (Fukuchi et al., 1993) and can be deposited in blood vessel walls leading to atherosclerosis (Stakos et al., 2020). The APOE ε4 allele was found to be a biologically active factor in β-amyloid deposition, (Rasmussen, 2016) and it is more likely to be found in post-stroke patients (Abboud et al., 2008). Even though β-amyloid may be initially eliminated by cystatin C, the neuroprotective effect of cystatin C decreases rapidly once the demand increases (Sheikh et al., 2021). In

contrast, CST3 B, an allele of cystatin C, often leads to a decrease in cystatin C secretion, which ultimately leads to the development of atherosclerosis (Zeng et al., 2019). In addition, *Enterobacteriaceae*, one of the microorganisms, metabolizes lipopolysaccharide, which not only leads to the release of pro-inflammatory factors, but also leads to the deposition of β-amyloid (Płóciennikowska et al., 2015). Most animal studies have shown that β-amyloid is often deposited in the thalamus after stroke (van Groen et al., 2005; Mäkinen et al., 2008; Zhang J. et al., 2012), while other studies have found that β-amyloid is deposited in the hippocampus (Dietrich et al., 1998; Basak et al., 2023). It is well known that the thalamic nuclei play an important role in cognitive function (Dalrymple-Alford et al., 2015), and the hippocampus is closely related to the thalamic nuclei (Braak et al., 1996).

The main causes of PSCI tend to be neuroinflammation, oxidative stress, and atherosclerosis. Similar to Alzheimer's disease (Acharya et al., 2024) and post-traumatic encephalopathy dementia (Kornblith et al., 2022), the pathophysiology of this disease remains complex and poorly understood. Existing research have primarily demonstrated a statistical link rather than a definitive causal relationship between specific mechanisms and the disease. Studies discovered that the accumulation of amyloid β might trigger an inflammatory reaction, and subsequent processes resulting from these inflammatory changes may be the underlying cause of the disease in PSCI (Lalancette-Hébert et al., 2012; Ott et al., 2018; Izzy et al., 2021). Likewise, oxidative stress can impact the integrity of neurons and the expression of genes, which in turn affects cognitive performance by causing changes in the structure of hippocampal dendrites (Chi et al., 2023). There is also data suggesting that atherosclerosis may be a separate yet collaborative disease phase of PSCI (Yang Z. et al., 2020). Thus far, ongoing research has not been able to conclusively establish the individual contribution of a specific mechanism in PSCI. Neuroinflammation, oxidative stress, and atherosclerosis are potential factors that could potentially contribute to the disease and/or its progression. However, the specific impact of these factors is still unknown. To fully comprehend the precise mechanisms and causal pathways underlying PSCI, more study is undoubtedly required in the future.

In addition, this paper focuses solely on the potential involvement of biomarkers in the pathogenesis within the omics context, without conducting a thorough assessment of current research findings. This limitation significantly hinders our understanding of the mechanism, which is a key drawback of the paper. Apart from these two possible mechanisms, cerebral small blood vessel disease (Teng et al., 2017), neuroanatomical lesions (Sun et al., 2014), and lymphatic pathway damage (Back et al., 2017) are also on the radar, but most of them are secondary to various levels of brain damage and lack a specific association with cognitive function. Based on this, we encourage scholars to comprehensively and further explore the pathogenesis of PSCI in order to solve the current clinical difficulties.

4.3 Feasible treatment and intervention

On the basis of existing omics research, we suggest treating PSCI with a combination of dietary intervention and drug-targeted therapy.

The main intervention for PSCI should be dietary changes since they are more widely accessible. ALA, EPA, and DHA are examples of *n*-3 unsaturated fatty acids, which are necessary fats that are exclusively found in food. *n*-3 unsaturated fatty acids (including ALA, EPA, and DHA) are essential fatty acids that can only be obtained through food. It has been found that *n*-3 fatty acids can produce specialized pro-resolving mediators through the cyclooxygenase and lipoxygenase pathways (Artiach et al., 2020; Christie and Harwood, 2020), while ALA and EPA have been shown to reduce the risk of neurological disorders such as stroke and mild cognitive impairment (Abdelhamid et al., 2020), and supplementation with ALA protects hippocampal neurons after a stroke and can also improve memory and spatial learning ability (Crupi et al., 2013). More than that, DHA has been found to reduce β-amyloid deposition and oxidative stress after stroke (Cardoso et al., 2016). Choline and its derivative betaine are involved in the irreversible cycling of methionine and homocysteine (Veskovic et al., 2019), and their addition to the diet may improve hyperhomocysteinemia to a certain extent (Rosas-Rodríguez and Valenzuela-Soto, 2021), thereby preventing stroke and cognitive impairment. L-carnitine supplementation has been found to not only improve cerebral blood flow supply in stroke patients (Endo et al., 2018) but also regulate mitochondrial energy metabolism and promote neurotransmitter release (Ferreira and McKenna, 2017), and about 3/4 of the body's L-carnitine is obtained from the diet. Gut microbes can break down dietary fiber into a variety of short-chain fatty acids (SCFAs), which not only promote cognitive function but also provide synaptic plasticity and play an important role in the gut-brain axis (Dalile et al., 2019). Some studies have found that administration of SCFAs improved cognitive function and inhibited β-amyloid aggregation (Ho et al., 2018).

Pharmacological treatment is also required for PSCI. miRNAs exist in a stable form in human plasma and are not affected by endogenous RNase activity (Eisenberg et al., 2015). miRNAs in the blood of PSCI patients suffer from an imbalance in the miRNA cycle due to tissue damage (Pascual et al., 2021). Several studies have shown that miR-21 is not only an anti-apoptotic factor (Seike et al., 2009), but also has neuroprotective effects against cerebral ischemia/reperfusion injury, and moreover alleviates neuroinflammation (Yan et al., 2021). Whereas miR-132 has been found to be a key regulator of cognition (Walgrave et al., 2021), and overexpression inhibits learning ability (Cong et al., 2021). Drug therapy for PSCI can be targeted to regulate miRNA balance in the body, thereby regulating neuronal activity and maintaining synaptic plasticity. BDNF is also believed to regulate synaptic plasticity and enhance learning ability (Lu et al., 2014), and studies have shown that BDNF can promote the recovery of movement and sensation in stroke patients (Schäbitz et al., 2007). The treatment of BDNF can also be used as a new therapeutic target to improve PSCI in the future.

In order to implement targeted interventions at various stages of the disease's incidence, we advise researchers to keep investigating the use of these biomarkers in PSCI intervention and therapy in the future and to provide constructive recommendations. However, looking at the future of PSCI intervention and treatment only from the perspective of omics is one of the limitations of this paper, because the current intervention and treatment initiatives for PSCI are numerous. The underlying method of 'hierarchical prevention' is more appropriate when discussing PSCI treatment and prevention from a non-omics standpoint. According to research, most dementia cases and strokes can be avoided (Casolla et al., 2019). We propose that primary preventive methods should take into account both stroke and cognitive impairment, since the pathophysiology of PSCI remains

uncertain. Given the current body of data, early multi-target intervention based on lifestyle or vascular problems is imperative to reduce the occurrence of PSCI. High-risk factors for PSCI include genetic predisposition, vascular risk factors, and population variables (Huang et al., 2022), so treatment in the acute stage following a cerebrovascular injury is crucial. During secondary prevention phase, it is frequently essential to actively investigate the underlying cause and administer focused care, such as thrombus removal, hyperlipidemia control, education enhancement, and improved motor function training, to prevent stroke and early cognitive damage. Postponing the additional deterioration of cognitive function and enhancing daily living skills are the primary goals of tertiary prevention of PSCI. However, PSCI is now treated mostly with other cognitive dysfunction disorders, including drug therapy and non-drug therapy, as there are no large-scale, randomized, double-blind, controlled clinical trials available. Though further clinical research is required to validate their effectiveness in PSCI, recent studies have suggested that medications such as Actovegin (Guekht et al., 2017), *Ginkgo biloba* extract (Berthier et al., 2009), and Acetylcholinesterase inhibitors (Donepezil) (Kim et al., 2020) may be able to improve cognitive performance. Acupuncture (Wang et al., 2016), transcranial magnetic stimulation, transcranial direct current stimulation (Begemann et al., 2020), adaptive cognitive training (Tang et al., 2019), and other sophisticated non-pharmacological treatments for post-stroke cognitive impairment have all demonstrated some promise in enhancing cognitive function. Therefore, we are still looking forward to advances in the treatment of PSCI, whether based on omics or traditional hierarchical prevention, which may greatly improve patient outcomes.

5 Conclusion

All things considered, the use of biomarkers in mechanism mining, early diagnostic support, illness progression tracking, and therapeutic target investigations has been eye-opening. In the context of omics, uncovering potential biomarkers of disease, exploring molecular pathways of disease, and testing drug efficacy are no longer limited to the single analyses of the past, and advances in high-throughput technologies have made PSCI research less slow. It is also the demand for disease research that in return promotes the development of omics technology, and new technologies and new platforms continue to help PSCI research. However, omics studies of PSCI are in their infancy, and there are currently no approved biomarkers for the diagnosis and prediction of PSCI. Translating initial research into clinical applications requires a more rigorous validation process involving the use of expertise, the development of predictive models, and ethical and market regulation.

We believe that future omics-based studies will help to understand the specific interactions of these biomarkers, help to determine the meaning of changes at each time node and advance the study of PSCI-specific drugs. Omics will surely show a greater light in the future market, and its other potential applications are yet to be explored.

Author contributions

QL: Writing – original draft, Investigation. AY: Writing – original draft. JP: Writing – review & editing, Data curation. DC: Writing – review & editing, Validation, Supervision. YZ: Writing – review & editing, Validation, Supervision. DB: Writing – review & editing, Supervision, Project administration, Funding acquisition. LY: Writing – review & editing, Conceptualization.

Funding

The author(s) declare financial support was received for the research, authorship, and/or publication of this article. This research was funded by Program for Youth Innovation in Future Medicine, Chongqing Medical University, Grant number W0076 and Chongqing Municipal Key Laboratory of Institutions of Higher Education, Grant number CXQT21018.

Conflict of interest

The authors declare that the research was conducted in the absence of any commercial or financial relationships that could be construed as a potential conflict of interest.

Publisher's note

Supplementary material

The Supplementary material for this article can be found online at: https://www.frontiersin.org/articles/10.3389/fnmol.2024.1375973/full#supplementary-material

References

Aam, S., Einstad, M. S., Munthe-Kaas, R., Lydersen, S., Ihle-Hansen, H., Knapskog, A. B., et al. (2020). Post-stroke cognitive impairment-impact of follow-up time and stroke subtype on severity and cognitive profile: the nor-COAST study. *Front. Neurol.* 11:699. doi: 10.3389/fneur.2020.00699

Abboud, S., Viiri, L. E., Lütjohann, D., Goebeler, S., Luoto, T., Friedrichs, S., et al. (2008). Associations of apolipoprotein E gene with ischemic stroke and intracranial atherosclerosis. *Eur. J. Hum. Genet.* 16, 955–960. doi: 10.1038/ejhg.2008.27

Abdelhamid, A. S., Brown, T. J., Brainard, J. S., Biswas, P., Thorpe, G. C., Moore, H. J., et al. (2020). Omega-3 fatty acids for the primary and secondary prevention of cardiovascular disease. *Cochrane Database Syst. Rev.* 3:Cd003177. doi: 10.1002/14651858.CD003177.pub5

Acharya, N. K., Grossman, H. C., Clifford, P. M., Levin, E. C., Light, K. R., Choi, H., et al. (2024). A chronic increase in blood-brain barrier permeability facilitates intraneuronal deposition of exogenous bloodborne amyloid-beta1-42 peptide in the brain and leads to Alzheimer's disease-relevant cognitive changes in a mouse model. *J. Alzheimers Dis.* 98, 163–186. doi: 10.3233/JAD-231028

Agyemang, A. A., Kvist, S. V., Brinkman, N., Gentinetta, T., Illa, M., Ortenlöf, N., et al. (2021). Cell-free oxidized hemoglobin drives reactive oxygen species production and pro-inflammation in an immature primary rat mixed glial cell culture. *J. Neuroinflammation* 18:42. doi: 10.1186/s12974-020-02052-4

Artiach, G., Carracedo, M., Plunde, O., Wheelock, C. E., Thul, S., Sjövall, P., et al. (2020). Omega-3 polyunsaturated fatty acids decrease aortic valve disease through the Resolvin E1 and ChemR23 axis. *Circulation* 142, 776–789. doi: 10.1161/CIRCULATIONAHA.119.041868

Back, D. B., Kwon, K. J., Choi, D. H., Shin, C. Y., Lee, J., Han, S. H., et al. (2017). Chronic cerebral hypoperfusion induces post-stroke dementia following acute ischemic stroke in rats. *J. Neuroinflammation* 14:216. doi: 10.1186/s12974-017-0992-5

Baez, E., Echeverria, V., Cabezas, R., Ávila-Rodriguez, M., Garcia-Segura, L. M., and Barreto, G. E. (2016). Protection by neuroglobin expression in brain pathologies. *Front. Neurol.* 7:146. doi: 10.3389/fneur.2016.00146

Bagyinszky, E., Giau, V. V., and An, S. A. (2020). Transcriptomics in Alzheimer's disease: aspects and challenges. *Int. J. Mol. Sci.* 21:3517. doi: 10.3390/ijms21103517

Baierle, M., Vencato, P. H., Oldenburg, L., Bordignon, S., Zibetti, M., Trentini, C. M., et al. (2014). Fatty acid status and its relationship to cognitive decline and homocysteine levels in the elderly. *Nutrients* 6, 3624–3640. doi: 10.3390/nu6093624

Balconi, M. (2013). Dorsolateral prefrontal cortex, working memory and episodic memory processes: insight through transcranial magnetic stimulation techniques. *Neurosci. Bull.* 29, 381–389. doi: 10.1007/s12264-013-1309-z

Barko, P. C., McMichael, M. A., Swanson, K. S., and Williams, D. A. (2018). The gastrointestinal microbiome: a review. *J. Vet. Intern. Med.* 32, 9–25. doi: 10.1111/jvim.14875

Basak, J. M., Falk, M., Mitchell, D. N., Coakley, K. A., Quillinan, N., Orfila, J. E., et al. (2023). Targeting BACE1-mediated production of amyloid beta improves hippocampal synaptic function in an experimental model of ischemic stroke. *J. Cereb. Blood Flow Metab.*:66:77. doi: 10.1177/0271678X231159597

Begemann, M. J., Brand, B. A., Ćurčić-Blake, B., Aleman, A., and Sommer, I. E. (2020). Efficacy of non-invasive brain stimulation on cognitive functioning in brain disorders: a meta-analysis. *Psychol. Med.* 50, 2465–2486. doi: 10.1017/S0033291720003670

Berthier, M. L., Green, C., Lara, J. P., Higueras, C., Barbancho, M. A., Dávila, G., et al. (2009). Memantine and constraint-induced aphasia therapy in chronic poststroke aphasia. *Ann. Neurol.* 65, 577–585. doi: 10.1002/ana.21597

Bjerrum, J. T., Nielsen, O. H., Wang, Y. L., and Olsen, J. (2008). Technology insight: metabonomics in gastroenterology-basic principles and potential clinical applications. *Nat. Clin. Pract. Gastroenterol. Hepatol.* 5, 332–343. doi: 10.1038/ncpgasthep1125

Blusztajn, J. K., Slack, B. E., and Mellott, T. J. (2017). Neuroprotective actions of dietary choline. *Nutrients* 9:8. doi: 10.3390/nu9080815

Braak, H., Braak, E., Yilmazer, D., and Bohl, J. (1996). Functional anatomy of human hippocampal formation and related structures. *J. Child Neurol.* 11, 265–275. doi: 10.1177/088307389601100402

Brunt, V. E., LaRocca, T. J., Bazzoni, A. E., Sapinsley, Z. J., Miyamoto-Ditmon, J., Gioscia-Ryan, R. A., et al. (2021). The gut microbiome-derived metabolite trimethylamine N-oxide modulates neuroinflammation and cognitive function with aging. *Geroscience* 43, 377–394. doi: 10.1007/s11357-020-00257-2

Cardoso, C., Afonso, C., and Bandarra, N. M. (2016). Dietary DHA and health: cognitive function ageing. *Nutr. Res. Rev.* 29, 281–294. doi: 10.1017/S0954422416000184

Casolla, B., Caparros, F., Cordonnier, C., Bombois, S., Hénon, H., Bordet, R., et al. (2019). Biological and imaging predictors of cognitive impairment after stroke: a systematic review. *J. Neurol.* 266, 2593–2604. doi: 10.1007/s00415-018-9089-z

Castellanos, M., Sobrino, T., Pedraza, S., Moldes, O., Pumar, J. M., Silva, Y., et al. (2008). High plasma glutamate concentrations are associated with infarct growth in acute ischemic stroke. *Neurology* 71, 1862–1868. doi: 10.1212/01.wnl.0000326064.42186.7e

Che, B., Chen, H., Wang, A., Peng, H., Bu, X., Zhang, J., et al. (2022). Association between plasma L-carnitine and cognitive impairment in patients with acute ischemic stroke. *J. Alzheimers Dis.* 86, 259–270. doi: 10.3233/JAD-215376

Chen, H., Cao, H. L., Chen, S. W., Guo, Y., Gao, W. W., Tian, H. L., et al. (2015). Neuroglobin and Nogo-a as biomarkers for the severity and prognosis of traumatic brain injury. *Biomarkers* 20, 495–501. doi: 10.3109/1354750X.2015.1094138

Chen, Z. Y., Patel, P. D., Sant, G., Meng, C. X., Teng, K. K., Hempstead, B. L., et al. (2004). Variant brain-derived neurotrophic factor (BDNF) (Met66) alters the intracellular trafficking and activity-dependent secretion of wild-type BDNF in neurosecretory cells and cortical neurons. *J. Neurosci.* 24, 4401–4411. doi: 10.1523/JNEUROSCI.0348-04.2004

Chen, L., and Wu, J. (2012). Systems biology for complex diseases. *J. Mol. Cell Biol.* 4, 125–126. doi: 10.1093/jmcb/mjs022

Chen, G., Zhou, X., Zhu, Y., Shi, W., and Kong, L. (2023). Gut microbiome characteristics in subjective cognitive decline, mild cognitive impairment and Alzheimer's disease: a systematic review and meta-analysis. *Eur. J. Neurol.* 30, 3568–3580. doi: 10.1111/ene.15961

Chi, X., Wang, L., Liu, H., Zhang, Y., and Shen, W. (2023). Post-stroke cognitive impairment and synaptic plasticity: a review about the mechanisms and Chinese herbal drugs strategies. *Front. Neurosci.* 17:1123817. doi: 10.3389/fnins.2023.1123817

Chou, P. S., Hung, W. C., Yang, I. H., Kuo, C. M., Wu, M. N., Lin, T. C., et al. (2023). Predicting adverse recanalization therapy outcomes in acute ischemic stroke patients using characteristic gut microbiota. *Microorganisms* 11:2016. doi: 10.3390/microorganisms11082016

Christie, W. W., and Harwood, J. L. (2020). Oxidation of polyunsaturated fatty acids to produce lipid mediators. *Essays Biochem.* 64, 401–421. doi: 10.1042/EBC20190082

Cogo, A., Mangin, G., Maïer, B., Callebert, J., Mazighi, M., Chabriat, H., et al. (2021). Increased serum QUIN/KYNA is a reliable biomarker of post-stroke cognitive decline. *Mol. Neurodegener.* 16:7. doi: 10.1186/s13024-020-00421-4

Cong, L., Cong, Y., Feng, N., Liang, W., and Wu, Y. (2021). Up-regulated microRNA-132 reduces the cognition-damaging effect of sevoflurane on Alzheimer's disease rats by inhibiting FOXA1. *Genomics* 113, 3644–3652. doi: 10.1016/j.ygeno.2021.08.011

Crupi, R., Marino, A., and Cuzzocrea, S. (2013). *n*-3 fatty acids: role in neurogenesis and neuroplasticity. *Curr. Med. Chem.* 20, 2953–2963. doi: 10.2174/09298673113209990140

Cui, G., Liu, S., Liu, Z., Chen, Y., Wu, T., Lou, J., et al. (2021). Gut microbiome distinguishes patients with epilepsy from healthy individuals. *Front. Microbiol.* 12:696632. doi: 10.3389/fmicb.2021.696632

Dai, X., and Shen, L. (2022). Advances and trends in omics technology development. *Front. Med.* 9:911861. doi: 10.3389/fmed.2022.911861

Dalile, B., Van Oudenhove, L., Vervliet, B., and Verbeke, K. (2019). The role of short-chain fatty acids in microbiota-gut-brain communication. *Nat. Rev. Gastroenterol. Hepatol.* 16, 461–478. doi: 10.1038/s41575-019-0157-3

Dalrymple-Alford, J. C., Harland, B., Loukavenko, E. A., Perry, B., Mercer, S., Collings, D. A., et al. (2015). Anterior thalamic nuclei lesions and recovery of function: relevance to cognitive thalamus. *Neurosci. Biobehav. Rev.* 54, 145–160. doi: 10.1016/j.neubiorev.2014.12.007

Datta, A., Chen, C., Gao, Y. G., and Sze, S. K. (2022). Quantitative proteomics of medium-sized extracellular vesicle-enriched plasma of lacunar infarction for the discovery of prognostic biomarkers. *Int. J. Mol. Sci.* 23:11670. doi: 10.3390/ijms231911670

de Medeiros, L. M., De Bastiani, M. A., Rico, E. P., Schonhofen, P., Pfaffenseller, B., Wollenhaupt-Aguiar, B., et al. (2019). Cholinergic differentiation of human neuroblastoma SH-SY5Y cell line and its potential use as an in vitro model for Alzheimer's disease studies. *Mol. Neurobiol.* 56, 7355–7367. doi: 10.1007/s12035-019-1605-3

Devolder, L., Pauwels, A., Van Remoortel, A., Falony, G., Vieira-Silva, S., Nagels, G., et al. (2023). Gut microbiome composition is associated with long-term disability worsening in multiple sclerosis. *Gut Microbes* 15:2180316. doi: 10.1080/19490976.2023.2180316

Díaz, G., Lengele, L., Sourdet, S., Soriano, G., and de Souto Barreto, P. (2022). Nutrients and amyloid β status in the brain: a narrative review. *Ageing Res. Rev.* 81:101728. doi: 10.1016/j.arr.2022.101728

Dietrich, W. D., Kraydieh, S., Prado, R., and Stagliano, N. E. (1998). White matter alterations following thromboembolic stroke: a beta-amyloid precursor protein immunocytochemical study in rats. *Acta Neuropathol.* 95, 524–531. doi: 10.1007/s004010050833

Ding, C., Kang, D., Chen, P., Wang, Z., Lin, Y., Wang, D., et al. (2020). Early stage neuroglobin level as a predictor of delayed cerebral ischemia in patients with aneurysmal subarachnoid hemorrhage. *Brain Behav.* 10:e01547. doi: 10.1002/brb3.1547

Dirnagl, U., Iadecola, C., and Moskowitz, M. A. (1999). Pathobiology of ischaemic stroke: an integrated view. *Trends Neurosci.* 22, 391–397. doi: 10.1016/S0166-2236(99)01401-0

Domon, B., and Aebersold, R. (2006). Mass spectrometry and protein analysis. *Science* 312, 212–217. doi: 10.1126/science.1124619

Douiri, A., Rudd, A. G., and Wolfe, C. D. (2013). Prevalence of poststroke cognitive impairment: South London stroke register 1995–2010. *Stroke* 44, 138–145. doi: 10.1161/STROKEAHA.112.670844

Durga, J., van Boxtel, M. P., Schouten, E. G., Kok, F. J., Jolles, J., Katan, M. B., et al. (2007). Effect of 3-year folic acid supplementation on cognitive function in older adults in the FACIT trial: a randomised, double blind, controlled trial. *Lancet* 369, 208–216. doi: 10.1016/S0140-6736(07)60109-3

Eisenberg, I., Kotaja, N., Goldman-Wohl, D., and Imbar, T. (2015). microRNA in human reproduction. *Adv. Exp. Med. Biol.* 888, 353–387. doi: 10.1007/978-3-319-22671-2_18

Endo, S., Takahashi, T., Sato, M., Noya, Y., and Obana, M. (2018). Effects of l-carnitine supplementation, botulinum neurotoxin injection, and rehabilitation for a chronic stroke patient. *J. Stroke Cerebrovasc. Dis.* 27, 3342–3344. doi: 10.1016/j.jstrokecerebrovasdis.2018.07.033

Estrada Sánchez, A. M., Mejía-Toiber, J., and Massieu, L. (2008). Excitotoxic neuronal death and the pathogenesis of Huntington's disease. *Arch. Med. Res.* 39, 265–276. doi: 10.1016/j.arcmed.2007.11.011

Feng, L., He, W., Huang, G., Lin, S., Yuan, C., Cheng, H., et al. (2020). Reduced thiamine is a predictor for cognitive impairment of cerebral infarction. *Brain Behav.* 10:e01709. doi: 10.1002/brb3.1709

Ferreira, G. C., and McKenna, M. C. (2017). L-carnitine and acetyl-L-carnitine roles and neuroprotection in developing brain. *Neurochem. Res.* 42, 1661–1675. doi: 10.1007/s11064-017-2288-7

Fiehn, O. (2002). Metabolomics—the link between genotypes and phenotypes. *Plant Mol. Biol.* 48, 155–171. doi: 10.1023/A:1013713905833

Fontanella, R. A., Scisciola, L., Rizzo, M. R., Surina, S., Sardu, C., Marfella, R., et al. (2021). Adiponectin related vascular and cardiac benefits in obesity: is there a role for an epigenetically regulated mechanism? *Front. Cardiovasc. Med.* 8:768026. doi: 10.3389/fcvm.2021.768026

Forrest, C. M., McNair, K., Pisar, M., Khalil, O. S., Darlington, L. G., and Stone, T. W. (2015). Altered hippocampal plasticity by prenatal kynurenine administration, kynurenine-3-monoxygenase (KMO) deletion or galantamine. *Neuroscience* 310, 91–105. doi: 10.1016/j.neuroscience.2015.09.022

Fu, W. J., Stromberg, A. J., Viele, K., Carroll, R. J., and Wu, G. (2010). Statistics and bioinformatics in nutritional sciences: analysis of complex data in the era of systems biology. *J. Nutr. Biochem.* 21, 561–572. doi: 10.1016/j.jnutbio.2009.11.007

Fukuchi, K., Sopher, B., and Martin, G. M. (1993). Neurotoxicity of beta-amyloid. *Nature* 361, 122–123. doi: 10.1038/361122a0

Gallo, S., Sala, V., Gatti, S., and Crepaldi, T. (2015). Cellular and molecular mechanisms of HGF/met in the cardiovascular system. *Clin. Sci.* 129, 1173–1193. doi: 10.1042/CS20150502

Gao, Y., Wang, B., Miao, Y., and Han, Y. (2022). Serum Neuroglobin as a potential prognostic biomarker for cognitive impairment after intracerebral hemorrhage. *Front. Neurol.* 13:885323. doi: 10.3389/fneur.2022.885323

Gaynor, E., Rohde, D., Large, M., Mellon, L., Hall, P., Brewer, L., et al. (2018). Cognitive impairment, vulnerability, and mortality post ischemic stroke: a five-year follow-up of the action on secondary prevention interventions and rehabilitation in stroke (ASPIRE-S) cohort. *J. Stroke Cerebrovasc. Dis.* 27, 2466–2473. doi: 10.1016/j.jstrokecerebrovasdis.2018.05.002

Giri, M., Zhang, M., and Lü, Y. (2016). Genes associated with Alzheimer's disease: an overview and current status. *Clin. Interv. Aging* 11, 665–681. doi: 10.2147/CIA.S105769

Godin, O., Tzourio, C., Maillard, P., Alpérovitch, A., Mazoyer, B., and Dufouil, C. (2009). Apolipoprotein E genotype is related to progression of white matter lesion load. *Stroke* 40, 3186–3190. doi: 10.1161/STROKEAHA.109.555839

Gold, A. B., Herrmann, N., Swardfager, W., Black, S. E., Aviv, R. I., Tennen, G., et al. (2011). The relationship between indoleamine 2,3-dioxygenase activity and post-stroke cognitive impairment. *J. Neuroinflammation* 8:17. doi: 10.1186/1742-2094-8-17

Gong, L., Wang, H., Zhu, X., Dong, Q., Yu, Q., Mao, B., et al. (2021). Nomogram to predict cognitive dysfunction after a minor ischemic stroke in hospitalized-population. *Front. Aging Neurosci.* 13:637363. doi: 10.3389/fnagi.2021.637363

Gorabi, A. M., Aslani, S., Barreto, G. E., Báez-Jurado, E., Kiaie, N., Jamialahmadi, T., et al. (2021). The potential of mitochondrial modulation by neuroglobin in treatment of neurological disorders. *Free Radic. Biol. Med.* 162, 471–477. doi: 10.1016/j.freeradbiomed.2020.11.002

Guekht, A., Skoog, I., Edmundson, S., Zakharov, V., and Korczyn, A. D. (2017). ARTEMIDA trial (a randomized trial of efficacy, 12 months international double-blind actovegin): a randomized controlled trial to assess the efficacy of actovegin in poststroke cognitive impairment. *Stroke* 48, 1262–1270. doi: 10.1161/STROKEAHA.116.014321

Guillemin, G. J. (2012). Quinolinic acid, the inescapable neurotoxin. *FEBS J.* 279, 1356–1365. doi: 10.1111/j.1742-4658.2012.08485.x

Gurol, M. E., Irizarry, M. C., Smith, E. E., Raju, S., Diaz-Arrastia, R., Bottiglieri, T., et al. (2006). Plasma beta-amyloid and white matter lesions in AD, MCI, and cerebral amyloid angiopathy. *Neurology* 66, 23–29. doi: 10.1212/01.wnl.0000191403.95453.6a

Han, Z., Qi, L., Xu, Q., Xu, M., Cai, L., Wong, J., et al. (2020). BDNF met allele is associated with lower cognitive function in poststroke rehabilitation. *Neurorehabil. Neural Repair* 34, 247–259. doi: 10.1177/1545968320902127

Han, Y., Zhou, A., Li, F., Wang, Q., Xu, L., and Jia, J. (2020). Apolipoprotein E epsilon4 allele is associated with vascular cognitive impairment no dementia in Chinese population. *J. Neurol. Sci.* 409:116606. doi: 10.1016/j.jns.2019.116606

Hansen, K. F., Karelina, K., Sakamoto, K., Wayman, G. A., Impey, S., and Obrietan, K. (2013). miRNA-132: a dynamic regulator of cognitive capacity. *Brain Struct. Funct.* 218, 817–831. doi: 10.1007/s00429-012-0431-4

Hazelwood, H. S., Frank, J. A., Maglinger, B., McLouth, C. J., Trout, A. L., Turchan-Cholewo, J., et al. (2022). Plasma protein alterations during human large vessel stroke: a controlled comparison study. *Neurochem. Int.* 160:105421. doi: 10.1016/j.neuint.2022.105421

Heisler, J. M., and O'Connor, J. C. (2015). Indoleamine 2,3-dioxygenase-dependent neurotoxic kynurenine metabolism mediates inflammation-induced deficit in recognition memory. *Brain Behav. Immun.* 50, 115–124. doi: 10.1016/j.bbi.2015.06.022

Hestad, K., Alexander, J., Rootwelt, H., and Aaseth, J. O. (2022). The role of tryptophan dysmetabolism and quinolinic acid in depressive and neurodegenerative diseases. *Biomolecules* 12:998. doi: 10.3390/biom12070998

Ho, L., Ono, K., Tsuji, M., Mazzola, P., Singh, R., and Pasinetti, G. M. (2018). Protective roles of intestinal microbiota derived short chain fatty acids in Alzheimer's disease-type beta-amyloid neuropathological mechanisms. *Expert. Rev. Neurother.* 18, 83–90. doi: 10.1080/14737175.2018.1400909

Huang, X., Bao, C., Lv, Q., Zhao, J., Wang, Y., Lang, X., et al. (2020). Sex difference in cognitive impairment in drug-free schizophrenia: association with miR-195 levels. *Psychoneuroendocrinology* 119:104748. doi: 10.1016/j.psyneuen.2020.104748

Huang, Y. Y., Chen, S. D., Leng, X. Y., Kuo, K., Wang, Z. T., Cui, M., et al. (2022). Post-stroke cognitive impairment: epidemiology, risk factors, and management. *J. Alzheimers Dis.* 86, 983–999. doi: 10.3233/JAD-215644

Huang, Y., Shen, Z., and He, W. (2021). Identification of gut microbiome signatures in patients with post-stroke cognitive impairment and affective disorder. *Front. Aging Neurosci.* 13:706765. doi: 10.3389/fnagi.2021.706765

Huang, S., Zhao, J., Huang, D., Zhuo, L., Liao, S., and Jiang, Z. (2016). Serum miR-132 is a risk marker of post-stroke cognitive impairment. *Neurosci. Lett.* 615, 102–106. doi: 10.1016/j.neulet.2016.01.028

Izzy, S., Brown-Whalen, A., Yahya, T., Sarro-Schwartz, A., Jin, G., Chung, J. Y., et al. (2021). Repetitive traumatic brain injury causes neuroinflammation before tau pathology in adolescent P301S mice. *Int. J. Mol. Sci.* 22:907. doi: 10.3390/ijms22020907

Jankowska-Kulawy, A., Bielarczyk, H., Pawełczyk, T., Wróblewska, M., and Szutowicz, A. (2010). Acetyl-CoA and acetylcholine metabolism in nerve terminal compartment of thiamine deficient rat brain. *J. Neurochem.* 115, 333–342. doi: 10.1111/j.1471-4159.2010.06919.x

Kaeser, S. A., Herzig, M. C., Coomaraswamy, J., Kilger, E., Selenica, M. L., Winkler, D. T., et al. (2007). Cystatin C modulates cerebral beta-amyloidosis. *Nat. Genet.* 39, 1437–1439. doi: 10.1038/ng.2007.23

Kekuda, R., Manoharan, P., Baseler, W., and Sundaram, U. (2013). Monocarboxylate 4 mediated butyrate transport in a rat intestinal epithelial cell line. *Dig. Dis. Sci.* 58, 660–667. doi: 10.1007/s10620-012-2407-x

Kim, J. O., Lee, S. J., and Pyo, J. S. (2020). Effect of acetylcholinesterase inhibitors on post-stroke cognitive impairment and vascular dementia: a meta-analysis. *PLoS One* 15:e0227820. doi: 10.1371/journal.pone.0227820

Kim, K. Y., Shin, K. Y., and Chang, K. A. (2022). Potential biomarkers for post-stroke cognitive impairment: a systematic review and meta-analysis. *Int. J. Mol. Sci.* 23:602. doi: 10.3390/ijms23020602

Kim, J. M., Stewart, R., Park, M. S., Kang, H. J., Kim, S. W., Shin, I. S., et al. (2012). Associations of BDNF genotype and promoter methylation with acute and long-term stroke outcomes in an east Asian cohort. *PLoS One* 7:e51280. doi: 10.1371/journal.pone.0051280

Kisilevsky, R., and Manley, P. N. (2012). Acute-phase serum amyloid a: perspectives on its physiological and pathological roles. *Amyloid* 19, 5–14. doi: 10.3109/13506129.2011.654294

Kornblith, E., Bahorik, A., Li, Y., Peltz, C. B., Barnes, D. E., and Yaffe, K. (2022). Traumatic brain injury, cardiovascular disease, and risk of dementia among older US veterans. *Brain Inj.* 36, 628–632. doi: 10.1080/02699052.2022.2033842

Kotlęga, D., Peda, B., Drozd, A., Zembroń-Łacny, A., Stachowska, E., Gramacki, J., et al. (2021a). Prostaglandin E2, 9S-, 13S-HODE and resolvin D1 are strongly associated with the post-stroke cognitive impairment. *Prostaglandins Other Lipid Mediat.* 156:106576. doi: 10.1016/j.prostaglandins.2021.106576

Kotlęga, D., Peda, B., Palma, J., Zembroń-Łacny, A., Gołąb-Janowska, M., Masztalewicz, M., et al. (2021b). Free fatty acids are associated with the cognitive functions in stroke survivors. *Int. J. Environ. Res. Public Health* 18:12. doi: 10.3390/ijerph18126500

Kotlega, D., Zembron-Lacny, A., Morawin, B., Golab-Janowska, M., Nowacki, P., and Szczuko, M. (2020). Free fatty acids and their inflammatory derivatives affect BDNF in stroke patients. *Mediat. Inflamm.* 2020, 1–12. doi: 10.1155/2020/6676247

Kroll, M. H., Harris, T. S., Moake, J. L., Handin, R. I., and Schafer, A. I. (1991). von Willebrand factor binding to platelet GpIb initiates signals for platelet activation. *J. Clin. Invest.* 88, 1568–1573. doi: 10.1172/JCI115468

Kurozumi, K., Nakamura, K., Tamiya, T., Kawano, Y., Kobune, M., Hirai, S., et al. (2004). BDNF gene-modified mesenchymal stem cells promote functional recovery and reduce infarct size in the rat middle cerebral artery occlusion model. *Mol. Ther.* 9, 189–197. doi: 10.1016/j.ymthe.2003.10.012

Lalancette-Hébert, M., Swarup, V., Beaulieu, J. M., Bohacek, I., Abdelhamid, E., Weng, Y. C., et al. (2012). Galectin-3 is required for resident microglia activation and proliferation in response to ischemic injury. *J. Neurosci.* 32, 10383–10395. doi: 10.1523/JNEUROSCI.1498-12.2012

Layeghifard, M., Hwang, D. M., and Guttman, D. S. (2017). Disentangling interactions in the microbiome: a network perspective. *Trends Microbiol.* 25, 217–228. doi: 10.1016/j.tim.2016.11.008

Lee, J. Y., Hall, J. A., Kroehling, L., Wu, L., Najar, T., Nguyen, H. H., et al. (2020). Serum amyloid a proteins induce pathogenic Th17 cells and promote inflammatory disease. *Cell* 180, 79–91.e16. doi: 10.1016/j.cell.2019.11.026

Lee, E. J., Kim, D. J., Kang, D. W., Yang, W., Jeong, H. Y., Kim, J. M., et al. (2023). Targeted Metabolomic biomarkers for stroke subtyping. *Transl. Stroke Res.* 15, 422–432. doi: 10.1007/s12975-023-01137-5

Lee, S. C., Lee, K. Y., Kim, Y. J., Kim, S. H., Koh, S. H., and Lee, Y. J. (2010). Serum VEGF levels in acute ischaemic strokes are correlated with long-term prognosis. *Eur. J. Neurol.* 17, 45–51. doi: 10.1111/j.1468-1331.2009.02731.x

Levy, E., Sastre, M., Kumar, A., Gallo, G., Piccardo, P., Ghetti, B., et al. (2001). Codeposition of cystatin C with amyloid-beta protein in the brain of Alzheimer disease patients. *J. Neuropathol. Exp. Neurol.* 60, 94–104. doi: 10.1093/jnen/60.1.94

Li, E. H., Huang, Q. Z., Li, G. C., Xiang, Z. Y., and Zhang, X. (2017). Effects of miRNA-200b on the development of diabetic retinopathy by targeting *VEGFA* gene. *Biosci. Rep.* 37:BSR20160572. doi: 10.1042/BSR20160572

Li, W., Shao, C., Zhou, H., Du, H., Chen, H., Wan, H., et al. (2022). Multi-omics research strategies in ischemic stroke: a multidimensional perspective. *Ageing Res. Rev.* 81:101730. doi: 10.1016/j.arr.2022.101730

Li, Z., Zhu, M., Meng, C., Lin, H., and Huang, L. (2022). Predictive value of serum adiponectin and hemoglobin levels for vascular cognitive impairment in ischemic stroke patients. *Pak. J. Med. Sci.* 38, 705–710. doi: 10.12669/pjms.38.3.5204

Ling, Y., Gong, T., Zhang, J., Gu, Q., Gao, X., Weng, X., et al. (2020a). Gut microbiome signatures are biomarkers for cognitive impairment in patients with ischemic stroke. *Front. Aging Neurosci.* 12:511562. doi: 10.3389/fnagi.2020.511562

Ling, Y., Gu, Q., Zhang, J., Gong, T., Weng, X., Liu, J., et al. (2020b). Structural change of gut microbiota in patients with post-stroke comorbid cognitive impairment and depression and its correlation with clinical features. *J. Alzheimers Dis.* 77, 1595–1608. doi: 10.3233/JAD-200315

Liu, T. W., Chen, C. M., and Chang, K. H. (2022). Biomarker of neuroinflammation in Parkinson's disease. *Int. J. Mol. Sci.* 23:4148. doi: 10.3390/ijms23084148

Liu, Y., Kong, C., Gong, L., Zhang, X., Zhu, Y., Wang, H., et al. (2020a). The association of post-stroke cognitive impairment and gut microbiota and its corresponding metabolites. *J. Alzheimers Dis.* 73, 1455–1466. doi: 10.3233/JAD-191066

Liu, Y., Wang, S., Kan, J., Zhang, J., Zhou, L., Huang, Y., et al. (2020b). Chinese herbal medicine interventions in neurological disorder therapeutics by regulating glutamate signaling. *Curr. Neuropharmacol.* 18, 260–276. doi: 10.2174/1570159X17666191101125530

Liu, C. G., Wang, J. L., Li, L., Xue, L. X., Zhang, Y. Q., and Wang, P. C. (2014). MicroRNA-135a and -200b, potential biomarkers for Alzheimer's disease, regulate β secretase and amyloid precursor protein. *Brain Res.* 1583, 55–64. doi: 10.1016/j.brainres.2014.04.026

Liu, M., Zhou, K., Li, H., Dong, X., Tan, G., Chai, Y., et al. (2015). Potential of serum metabolites for diagnosing post-stroke cognitive impairment. *Mol. Biosyst.* 11, 3287–3296. doi: 10.1039/C5MB00470E

Lo, J. W., Crawford, J. D., Desmond, D. W., Godefroy, O., Jokinen, H., Mahinrad, S., et al. (2019). Profile of and risk factors for poststroke cognitive impairment in diverse ethnoregional groups. *Neurology* 93, e2257–e2271. doi: 10.1212/WNL.0000000000008612

Lockhart, D. J., and Winzeler, E. A. (2000). Genomics, gene expression and DNA arrays. *Nature* 405, 827–836. doi: 10.1038/35015701

Lopez, I. A., Acuna, D., Shahram, Y., Mowlds, D., Ngan, A. M., Rungvivatjarus, T., et al. (2010). Neuroglobin expression in the cochlea of rat pups exposed to chronic very mild carbon monoxide (25 ppm) in air during and after the prenatal period. *Brain Res.* 1327, 56–68. doi: 10.1016/j.brainres.2010.02.078

Lopez, M. S., Dempsey, R. J., and Vemuganti, R. (2017). The microRNA miR-21 conditions the brain to protect against ischemic and traumatic injuries. *Cond. Med.* 1, 35–46

Lozupone, C. A., Stombaugh, J. I., Gordon, J. I., Jansson, J. K., and Knight, R. (2012). Diversity, stability and resilience of the human gut microbiota. *Nature* 489, 220–230. doi: 10.1038/nature11550

Lu, B. (2003). BDNF and activity-dependent synaptic modulation. *Learn. Mem.* 10, 86–98. doi: 10.1101/lm.54603

Lu, B., Nagappan, G., and Lu, Y. (2014). BDNF and synaptic plasticity, cognitive function, and dysfunction. *Handb. Exp. Pharmacol.* 220, 223–250. doi: 10.1007/978-3-642-45106-5_9

Mäkinen, S., van Groen, T., Clarke, J., Thornell, A., Corbett, D., Hiltunen, M., et al. (2008). Coaccumulation of calcium and beta-amyloid in the thalamus after transient middle cerebral artery occlusion in rats. *J. Cereb. Blood Flow Metab.* 28, 263–268. doi: 10.1038/sj.jcbfm.9600529

Marcé-Grau, A., Martí-Sánchez, L., Baide-Mairena, H., Ortigoza-Escobar, J. D., and Pérez-Dueñas, B. (2019). Genetic defects of thiamine transport and metabolism: a review of clinical phenotypes, genetics, and functional studies. *J. Inherit. Metab. Dis.* 42, 581–597. doi: 10.1002/jimd.12125

Meng, N., Shi, S., and Su, Y. (2016). Proton magnetic resonance spectroscopy as a diagnostic biomarker in mild cognitive impairment following stroke in acute phase. *Neuroreport* 27, 559–563. doi: 10.1097/WNR.0000000000000555

Mijajlović, M. D., Pavlović, A., Brainin, M., Heiss, W. D., Quinn, T. J., Ihle-Hansen, H. B., et al. (2017). Post-stroke dementia—a comprehensive review. *BMC Med.* 15:11. doi: 10.1186/s12916-017-0779-7

Mkrtchyan, G., Graf, A., Bettendorff, L., and Bunik, V. (2016). Cellular thiamine status is coupled to function of mitochondrial 2-oxoglutarate dehydrogenase. *Neurochem. Int.* 101, 66–75. doi: 10.1016/j.neuint.2016.10.009

Mohammed, A., Shaker, O. G., Khalil, M. A. F., Gomaa, M., Fathy, S. A., Abu-El-Azayem, A. K., et al. (2022). Long non-coding RNA NBAT1, TUG1, miRNA-335, and miRNA-21 as potential biomarkers for acute ischemic stroke and their possible correlation to thyroid hormones. *Front. Mol. Biosci.* 9:914506. doi: 10.3389/fmolb.2022.914506

Nicholson, J. K., Lindon, J. C., and Holmes, E. (1999). 'Metabonomics': understanding the metabolic responses of living systems to pathophysiological stimuli via multivariate statistical analysis of biological NMR spectroscopic data. *Xenobiotica* 29, 1181–1189. doi: 10.1080/004982599238047

Niendam, T. A., Laird, A. R., Ray, K. L., Dean, Y. M., Glahn, D. C., and Carter, C. S. (2012). Meta-analytic evidence for a superordinate cognitive control network subserving diverse executive functions. *Cogn. Affect. Behav. Neurosci.* 12, 241–268. doi: 10.3758/s13415-011-0083-5

Ott, B. R., Jones, R. N., Daiello, L. A., de la Monte, S. M., Stopa, E. G., Johanson, C. E., et al. (2018). Blood-cerebrospinal fluid barrier gradients in mild cognitive impairment and Alzheimer's disease: relationship to inflammatory cytokines and chemokines. *Front. Aging Neurosci.* 10:245. doi: 10.3389/fnagi.2018.00245

Pascoe, M. C., and Linden, T. (2016). Folate and MMA predict cognitive impairment in elderly stroke survivors: a cross sectional study. *Psychiatry Res.* 243, 49–52. doi: 10.1016/j.psychres.2016.06.008

Pascual, M., Calvo-Rodriguez, M., Núñez, L., Villalobos, C., Ureña, J., and Guerri, C. (2021). Toll-like receptors in neuroinflammation, neurodegeneration, and alcohol-induced brain damage. *IUBMB Life* 73, 900–915. doi: 10.1002/iub.2510

Płóciennikowska, A., Hromada-Judycka, A., Borzęcka, K., and Kwiatkowska, K. (2015). Co-operation of TLR4 and raft proteins in LPS-induced pro-inflammatory signaling. *Cell. Mol. Life Sci.* 72, 557–581. doi: 10.1007/s00018-014-1762-5

Potter, T., Lioutas, V. A., Tano, M., Pan, A., Meeks, J., Woo, D., et al. (2021). Cognitive impairment after intracerebral hemorrhage: a systematic review of current evidence and knowledge gaps. *Front. Neurol.* 12:716632. doi: 10.3389/fneur.2021.716632

Prodjohardjono, A., Vidyanti, A. N., Susianti, N. A., Sudarmanta Sutarni, S., and Setyopranoto, I. (2020). Higher level of acute serum VEGF and larger infarct volume are more frequently associated with post-stroke cognitive impairment. *PLoS One* 15:e0239370. doi: 10.1371/journal.pone.0239370

Qi, B., Kong, L., Lai, X., Wang, L., Liu, F., Ji, W., et al. (2023). Plasma exosome proteomics reveals the pathogenesis mechanism of post-stroke cognitive impairment. *Aging* 15, 4334–4362. doi: 10.18632/aging.204738

Quince, C., Walker, A. W., Simpson, J. T., Loman, N. J., and Segata, N. (2017). Shotgun metagenomics, from sampling to analysis. *Nat. Biotechnol.* 35, 833–844. doi: 10.1038/nbt.3935

Rasmussen, K. L. (2016). Plasma levels of apolipoprotein E, APOE genotype and risk of dementia and ischemic heart disease: a review. *Atherosclerosis* 255, 145–155. doi: 10.1016/j.atherosclerosis.2016.10.037

Reiner, A., and Levitz, J. (2018). Glutamatergic signaling in the central nervous system: ionotropic and metabotropic receptors in concert. *Neuron* 98, 1080–1098. doi: 10.1016/j.neuron.2018.05.018

Rezaei, S., Asgari Mobarake, K., Saberi, A., Keshavarz, P., and Leili, E. K. (2016). Brain-derived neurotrophic factor (BDNF) Val66Met polymorphism and post-stroke dementia: a hospital-based study from northern Iran. *Neurol. Sci.* 37, 935–942. doi: 10.1007/s10072-016-2520-2

Ribas, G. S., Vargas, C. R., and Wajner, M. (2014). L-carnitine supplementation as a potential antioxidant therapy for inherited neurometabolic disorders. *Gene* 533, 469–476. doi: 10.1016/j.gene.2013.10.017

Rohlff, C. (2001). Proteomics in neuropsychiatric disorders. *Int. J. Neuropsychopharmacol.* 4, 93–102. doi: 10.1017/S1461145701002267

Rosas-Rodríguez, J. A., and Valenzuela-Soto, E. M. (2021). The glycine betaine role in neurodegenerative, cardiovascular, hepatic, and renal diseases: insights into disease and dysfunction networks. *Life Sci.* 285:119943. doi: 10.1016/j.lfs.2021.119943

Sack, G. H. Jr. (2018). Serum amyloid A—a review. *Mol. Med.* 24:46. doi: 10.1186/s10020-018-0047-0

Sancesario, G. M., and Bernardini, S. (2018). Alzheimer's disease in the omics era. *Clin. Biochem.* 59, 9–16. doi: 10.1016/j.clinbiochem.2018.06.011

Santamaría, A., Galván-Arzate, S., Lisý, V., Ali, S. F., Duhart, H. M., Osorio-Rico, L., et al. (2001). Quinolinic acid induces oxidative stress in rat brain synaptosomes. *Neuroreport* 12, 871–874. doi: 10.1097/00001756-200103260-00049

Sapko, M. T., Guidetti, P., Yu, P., Tagle, D. A., Pellicciari, R., and Schwarcz, R. (2006). Endogenous kynurenate controls the vulnerability of striatal neurons to quinolinate: implications for Huntington's disease. *Exp. Neurol.* 197, 31–40. doi: 10.1016/j.expneurol.2005.07.004

Sastre, M., Calero, M., Pawlik, M., Mathews, P. M., Kumar, A., Danilov, V., et al. (2004). Binding of cystatin C to Alzheimer's amyloid beta inhibits in vitro amyloid fibril formation. *Neurobiol. Aging* 25, 1033–1043. doi: 10.1016/j.neurobiolaging.2003.11.006

Schäbitz, W. R., Steigleder, T., Cooper-Kuhn, C. M., Schwab, S., Sommer, C., Schneider, A., et al. (2007). Intravenous brain-derived neurotrophic factor enhances poststroke sensorimotor recovery and stimulates neurogenesis. *Stroke* 38, 2165–2172. doi: 10.1161/STROKEAHA.106.477331

Schweiger, J. I., Bilek, E., Schäfer, A., Braun, U., Moessnang, C., Harneit, A., et al. (2019). Effects of BDNF Val^{66}Met genotype and schizophrenia familial risk on a neural

functional network for cognitive control in humans. *Neuropsychopharmacology* 44, 590–597. doi: 10.1038/s41386-018-0248-9

Sears, C. L. (2009). Enterotoxigenic *Bacteroides fragilis*: a rogue among symbiotes. *Clin. Microbiol. Rev.* 22, 349–369. doi: 10.1128/CMR.00053-08

Seike, M., Goto, A., Okano, T., Bowman, E. D., Schetter, A. J., Horikawa, I., et al. (2009). MiR-21 is an EGFR-regulated anti-apoptotic factor in lung cancer in never-smokers. *Proc. Natl. Acad. Sci. U.S.A.* 106, 12085–12090. doi: 10.1073/pnas.0905234106

Sheikh, A. M., Wada, Y., Tabassum, S., Inagaki, S., Mitaki, S., Yano, S., et al. (2021). Aggregation of cystatin C changes its inhibitory functions on protease activities and amyloid β fibril formation. *Int. J. Mol. Sci.* 22:9682. doi: 10.3390/ijms22189682

Sheinerman, K. S., Tsivinsky, V. G., Crawford, F., Mullan, M. J., Abdullah, L., and Umansky, S. R. (2012). Plasma microRNA biomarkers for detection of mild cognitive impairment. *Aging* 4, 590–605. doi: 10.18632/aging.100486

Shridas, P., and Tannock, L. R. (2019). Role of serum amyloid a in atherosclerosis. *Curr. Opin. Lipidol.* 30, 320–325. doi: 10.1097/MOL.0000000000000616

Sidorov, E., Sanghera, D. K., and Vanamala, J. K. P. (2019). Biomarker for ischemic stroke using metabolome: a clinician perspective. *J. Stroke* 21, 31–41. doi: 10.5853/jos.2018.03454

Sloley, S. S., Main, B. S., Winston, C. N., Harvey, A. C., Kaganovich, A., Korthas, H. T., et al. (2021). High-frequency head impact causes chronic synaptic adaptation and long-term cognitive impairment in mice. *Nat. Commun.* 12:2613. doi: 10.1038/s41467-021-22744-6

Sorboni, S. G., Moghaddam, H. S., Jafarzadeh-Esfehani, R., and Soleimanpour, S. (2022). A comprehensive review on the role of the gut microbiome in human neurological disorders. *Clin. Microbiol. Rev.* 35:e0033820. doi: 10.1128/CMR.00338-20

Srikanth, V. K., Thrift, A. G., Saling, M. M., Anderson, J. F., Dewey, H. M., Macdonell, R. A., et al. (2003). Increased risk of cognitive impairment 3 months after mild to moderate first-ever stroke: a community-based prospective study of nonaphasic English-speaking survivors. *Stroke* 34, 1136–1143. doi: 10.1161/01.STR.0000069161.35736.39

Stakos, D. A., Stamatelopoulos, K., Bampatsias, D., Sachse, M., Zormpas, E., Vlachogiannis, N. I., et al. (2020). The Alzheimer's disease amyloid-beta hypothesis in cardiovascular aging and disease: JACC focus seminar. *J. Am. Coll. Cardiol.* 75, 952–967. doi: 10.1016/j.jacc.2019.12.033

Stone, T. W., and Darlington, L. G. (2002). Endogenous kynurenines as targets for drug discovery and development. *Nat. Rev. Drug Discov.* 1, 609–620. doi: 10.1038/nrd870

Sun, J. H., Tan, L., and Yu, J. T. (2014). Post-stroke cognitive impairment: epidemiology, mechanisms and management. *Ann. Transl. Med.* 2:80. doi: 10.3978/j.issn.2305-5839.2014.08.05

Szczuko, M., Kotlęga, D., Palma, J., Zembroń-Łacny, A., Tylutka, A., Gołąb-Janowska, M., et al. (2020). Lipoxins, RevD1 and 9, 13 HODE as the most important derivatives after an early incident of ischemic stroke. *Sci. Rep.* 10:12849. doi: 10.1038/s41598-020-69831-0

Sze, M. A., and Schloss, P. D. (2016). Looking for a signal in the noise: revisiting obesity and the microbiome. *mBio* 7:4. doi: 10.1128/mBio.01018-16

Tan, M. S., Cheah, P. L., Chin, A. V., Looi, L. M., and Chang, S. W. (2021). A review on omics-based biomarkers discovery for Alzheimer's disease from the bioinformatics perspectives: statistical approach vs machine learning approach. *Comput. Biol. Med.* 139:104947. doi: 10.1016/j.compbiomed.2021.104947

Tang, Y., Xing, Y., Zhu, Z., He, Y., Li, F., Yang, J., et al. (2019). The effects of 7-week cognitive training in patients with vascular cognitive impairment, no dementia (the Cog-VACCINE study): a randomized controlled trial. *Alzheimers Dement.* 15, 605–614. doi: 10.1016/j.jalz.2019.01.009

Tein, I., De Vivo, D. C., Ranucci, D., and DiMauro, S. (1993). Skin fibroblast carnitine uptake in secondary carnitine deficiency disorders. *J. Inherit. Metab. Dis.* 16, 135–146. doi: 10.1007/BF00711327

Teng, Z., Dong, Y., Zhang, D., An, J., and Lv, P. (2017). Cerebral small vessel disease and post-stroke cognitive impairment. *Int. J. Neurosci.* 127, 824–830. doi: 10.1080/00207454.2016.1261291

Ticinesi, A., Nouvenne, A., Tana, C., Prati, B., and Meschi, T. (2019). Gut microbiota and microbiota-related metabolites as possible biomarkers of cognitive aging. *Adv. Exp. Med. Biol.* 1178, 129–154. doi: 10.1007/978-3-030-25650-0_8

Tsimberidou, A. M., Fountzilas, E., Bleris, L., and Kurzrock, R. (2022). Transcriptomics and solid tumors: the next frontier in precision cancer medicine. *Semin. Cancer Biol.* 84, 50–59. doi: 10.1016/j.semcancer.2020.09.007

Ueland, P. M. (2011). Choline and betaine in health and disease. *J. Inherit. Metab. Dis.* 34, 3–15. doi: 10.1007/s10545-010-9088-4

Unschuld, P. G., Edden, R. A., Carass, A., Liu, X., Shanahan, M., Wang, X., et al. (2012). Brain metabolite alterations and cognitive dysfunction in early Huntington's disease. *Mov. Disord.* 27, 895–902. doi: 10.1002/mds.25010

van den Berg, M. M. J., Krauskopf, J., Ramaekers, J. G., Kleinjans, J. C. S., Prickaerts, J., and Briedé, J. J. (2020). Circulating microRNAs as potential biomarkers for psychiatric and neurodegenerative disorders. *Prog. Neurobiol.* 185:101732. doi: 10.1016/j.pneurobio.2019.101732

van Groen, T., Puurunen, K., Mäki, H. M., Sivenius, J., and Jolkkonen, J. (2005). Transformation of diffuse beta-amyloid precursor protein and beta-amyloid deposits to plaques in the thalamus after transient occlusion of the middle cerebral artery in rats. *Stroke* 36, 1551–1556. doi: 10.1161/01.STR.0000169933.88903.cf

Vascellari, S., Palmas, V., Melis, M., Pisanu, S., Cusano, R., Uva, P., et al. (2020). Gut microbiota and metabolome alterations associated with Parkinson's disease. *mSystems* 5:5. doi: 10.1128/mSystems.00561-20

Verma, M., Lizama, B. N., and Chu, C. T. (2022). Excitotoxicity, calcium and mitochondria: a triad in synaptic neurodegeneration. *Transl. Neurodegener.* 11:3. doi: 10.1186/s40035-021-00278-7

Veskovic, M., Mladenovic, D., Milenkovic, M., Tosic, J., Borozan, S., Gopcevic, K., et al. (2019). Betaine modulates oxidative stress, inflammation, apoptosis, autophagy, and Akt/mTOR signaling in methionine-choline deficiency-induced fatty liver disease. *Eur. J. Pharmacol.* 848, 39–48. doi: 10.1016/j.ejphar.2019.01.043

Walgrave, H., Balusu, S., Snoeck, S., Vanden Eynden, E., Craessaerts, K., Thrupp, N., et al. (2021). Restoring miR-132 expression rescues adult hippocampal neurogenesis and memory deficits in Alzheimer's disease. *Cell Stem Cell* 28, 1805–1821.e8. doi: 10.1016/j.stem.2021.05.001

Wang, Z. Q., Li, K., Huang, J., Huo, T. T., and Lv, P. Y. (2020). MicroRNA let-7i is a promising serum biomarker for post-stroke cognitive impairment and alleviated OGD-induced cell damage in vitro by regulating Bcl-2. *Front. Neurosci.* 14:215. doi: 10.3389/fnins.2020.00215

Wang, X., Peng, Y., Zhou, H., Du, W., Wang, J., Wang, J., et al. (2022). The effects of enriched rehabilitation on cognitive function and serum glutamate levels Post-stroke. *Front. Neurol.* 13:829090. doi: 10.3389/fneur.2022.829090

Wang, Y., and Qian, P. Y. (2009). Conservative fragments in bacterial 16S rRNA genes and primer design for 16S ribosomal DNA amplicons in metagenomic studies. *PLoS One* 4:e7401. doi: 10.1371/journal.pone.0007401

Wang, S., Yang, H., Zhang, J., Zhang, B., Liu, T., Gan, L., et al. (2016). Efficacy and safety assessment of acupuncture and nimodipine to treat mild cognitive impairment after cerebral infarction: a randomized controlled trial. *BMC Complement. Altern. Med.* 16:361. doi: 10.1186/s12906-016-1337-0

Wang, H., Zhang, M., Li, J., Liang, J., Yang, M., Xia, G., et al. (2022). Gut microbiota is causally associated with poststroke cognitive impairment through lipopolysaccharide and butyrate. *J. Neuroinflammation* 19:76. doi: 10.1186/s12974-022-02435-9

Wang, R., Zhao, N., Li, S., Fang, J. H., Chen, M. X., Yang, J., et al. (2013). MicroRNA-195 suppresses angiogenesis and metastasis of hepatocellular carcinoma by inhibiting the expression of VEGF, VAV2, and CDC42. *Hepatology* 58, 642–653. doi: 10.1002/hep.26373

Xiayan, L., and Legido-Quigley, C. (2008). Advances in separation science applied to metabonomics. *Electrophoresis* 29, 3724–3736. doi: 10.1002/elps.200700851

Xie, B., Zhou, H., Zhang, R., Song, M., Yu, L., Wang, L., et al. (2015). Serum miR-206 and miR-132 as potential circulating biomarkers for mild cognitive impairment. *J. Alzheimers Dis.* 45, 721–731. doi: 10.3233/JAD-142847

Ya, D., Zhang, Y., Cui, Q., Jiang, Y., Yang, J., Tian, N., et al. (2023). Application of spatial transcriptome technologies to neurological diseases. *Front. Cell Dev. Biol.* 11:1142923. doi: 10.3389/fcell.2023.1142923

Yan, H., Huang, W., Rao, J., and Yuan, J. (2021). miR-21 regulates ischemic neuronal injury via the p53/Bcl-2/Bax signaling pathway. *Aging* 13, 22242–22255. doi: 10.18632/aging.203530

Yang, Z., Wang, H., Edwards, D., Ding, C., Yan, L., Brayne, C., et al. (2020). Association of blood lipids, atherosclerosis and statin use with dementia and cognitive impairment after stroke: a systematic review and meta-analysis. *Ageing Res. Rev.* 57:100962. doi: 10.1016/j.arr.2019.100962

Yang, S., Zhan, X., He, M., Wang, J., and Qiu, X. (2020). miR-135b levels in the peripheral blood serve as a marker associated with acute ischemic stroke. *Exp. Ther. Med.* 19, 3551–3558. doi: 10.3892/etm.2020.8628

Ye, J., Xu, M., Tian, X., Cai, S., and Zeng, S. (2019). Research advances in the detection of miRNA. *J. Pharm. Anal.* 9, 217–226. doi: 10.1016/j.jpha.2019.05.004

Yoshida, T., Ishikawa, M., Niitsu, T., Nakazato, M., Watanabe, H., Shiraishi, T., et al. (2012). Decreased serum levels of mature brain-derived neurotrophic factor (BDNF), but not its precursor proBDNF, in patients with major depressive disorder. *PLoS One* 7:e42676. doi: 10.1371/journal.pone.0042676

Yuan, M., Guo, Y. S., Zhang, X. X., Gao, Z. K., Shen, X. Y., Han, Y., et al. (2022). Diagnostic performance of miR-21, miR-124, miR-132, and miR-200b serums in post-stroke cognitive impairment patients. *Folia Neuropathol.* 60, 228–236. doi: 10.5114/fn.2022.118187

Zeng, Q., Huang, Z., Wei, L., Fang, J., and Lin, K. (2019). Correlations of serum cystatin C level and gene polymorphism with vascular cognitive impairment after acute cerebral infarction. *Neurol. Sci.* 40, 1049–1054. doi: 10.1007/s10072-019-03777-8

Zhai, Y., Zhu, Z., Li, H., Zhao, C., Huang, Y., and Wang, P. (2020). miR-195 and miR-497 in acute stroke and their correlations with post-stroke cognitive impairment. *Int. J. Clin. Exp. Pathol.* 13, 3092–3099

Zhang, Y., Feng, Y., Zuo, J., Shi, J., Zhang, S., Yang, Y., et al. (2021). Elevated serum amyloid a is associated with cognitive impairment in ischemic stroke patients. *Front. Neurol.* 12:789204. doi: 10.3389/fneur.2021.789204

Zhang, J., Li, S., Li, L., Li, M., Guo, C., Yao, J., et al. (2015). Exosome and exosomal microRNA: trafficking, sorting, and function. *Genomics Proteomics Bioinformatics* 13, 17–24. doi: 10.1016/j.gpb.2015.02.001

Zhang, A. H., Sun, H., and Wang, X. J. (2013). Recent advances in metabolomics in neurological disease, and future perspectives. *Anal. Bioanal. Chem.* 405, 8143–8150. doi: 10.1007/s00216-013-7061-4

Zhang, X., Yuan, M., Yang, S., Chen, X., Wu, J., Wen, M., et al. (2021). Enriched environment improves post-stroke cognitive impairment and inhibits neuroinflammation and oxidative stress by activating Nrf2-ARE pathway. *Int. J. Neurosci.* 131, 641–649. doi: 10.1080/00207454.2020.1797722

Zhang, J., Zhang, Y., Li, J., Xing, S., Li, C., Li, Y., et al. (2012). Autophagosomes accumulation is associated with β-amyloid deposits and secondary damage in the thalamus after focal cortical infarction in hypertensive rats. *J. Neurochem.* 120, 564–573. doi: 10.1111/j.1471-4159.2011.07496.x

Zhang, R., Zhang, H., Zhang, Z., Wang, T., Niu, J., Cui, D., et al. (2012). Neuroprotective effects of pre-treatment with l-carnitine and acetyl-L-carnitine on ischemic injury *in vivo* and *in vitro*. *Int. J. Mol. Sci.* 13, 2078–2090. doi: 10.3390/ijms13022078

Zhao, J., Liu, S., Yan, J., and Zhu, X. (2021). The impact of gut microbiota on post-stroke management. *Front. Cell. Infect. Microbiol.* 11:724376. doi: 10.3389/fcimb.2021.724376

Zhong, C., Lu, Z., Che, B., Qian, S., Zheng, X., Wang, A., et al. (2021). Choline pathway nutrients and metabolites and cognitive impairment after acute ischemic stroke. *Stroke* 52, 887–895. doi: 10.1161/STROKEAHA.120.031903

Zhou, Q., Liu, J., Quan, J., Liu, W., Tan, H., and Li, W. (2018). MicroRNAs as potential biomarkers for the diagnosis of glioma: a systematic review and meta-analysis. *Cancer Sci.* 109, 2651–2659. doi: 10.1111/cas.13714

Zhu, C., Li, G., Lv, Z., Li, J., Wang, X., Kang, J., et al. (2020). Association of plasma trimethylamine-N-oxide levels with post-stroke cognitive impairment: a 1-year longitudinal study. *Neurol. Sci.* 41, 57–63. doi: 10.1007/s10072-019-04040-w

frontiers | Frontiers in Neuroscience

TYPE Original Research
PUBLISHED 09 September 2024
DOI 10.3389/fnins.2024.1411016

OPEN ACCESS

EDITED BY
Hai Sun,
The State University of New Jersey,
United States

REVIEWED BY
Andreas Wree,
University of Rostock, Germany
Jack Jiaqi Zhang,
Hong Kong Polytechnic University,
Hong Kong SAR, China

*CORRESPONDENCE
Yong Hu
yhud@hku.hk
Weitao Guo
guoweitao2000@sina.com

†These authors have contributed equally to this work

RECEIVED 02 April 2024
ACCEPTED 20 August 2024
PUBLISHED 09 September 2024

CITATION
Li K, Yang J, Wang H, Chang X, Liu G, Xue R, Guo W and Hu Y (2024) Time varying characteristic in somatosensory evoked potentials as a biomarker of spinal cord ischemic-reperfusion injury in rat. *Front. Neurosci.* 18:1411016. doi: 10.3389/fnins.2024.1411016

Time varying characteristic in somatosensory evoked potentials as a biomarker of spinal cord ischemic-reperfusion injury in rat

Kai Li[1†], Jianwei Yang[1†], Huaibo Wang[1], Xuejing Chang[1], Guanjun Liu[1], Ruiyang Xue[1], Weitao Guo[1*] and Yong Hu[1,2*]

[1]Department of Spine Surgery, The Second Hospital Affiliated to Guangdong Medical University, Zhanjiang, Guangdong, China, [2]Department of Orthopedics and Traumatology, The University of Hong Kong, Hong Kong, Hong Kong SAR, China

Spinal cord ischemic-reperfusion injury (SCIRI) could occurs during surgical procedures without detection, presenting a complex course and an unfavorable prognosis. This may lead to postoperative sensory or motor dysfunction in areas innervated by the spinal cord, and in some cases, permanent paralysis. Timely detection of SCIRI and immediate waring can help surgeons implement remedial intervention to prevent irreversible spinal cord injury. Therefore, it is crucial to develop a precise and effective method for early detection of SCIRI. This study utilized rat models to simulate intraoperative SCIRI and employed somatosensory evoked potentials (SEP) for continuous monitoring during surgery. In this study, SEP signal changes were examined in six groups with varying severities of SCIRI and one normal control group. SEP signal changes were examined during operations in different groups and correlated with postoperative behavioral and histopathological data. The result demonstrated specific changes in SEP signals during SCIRI, termed as time-varying characteristics, which are associated with the duration of ischemia and subsequent reperfusion. Time-varying characteristics in SEP could potentially serve as a new biomarker for the intraoperative detection of SCIRI. This finding is significant for clinical surgeons to identify and guide early intervention of SCIRI timely. Additionally, this measurement is easily translatable to clinical application.

KEYWORDS

spinal cord ischemia–reperfusion injury, somatosensory evoked potential, time-varying characteristic, biomarker, intraoperative monitoring, rat model

1 Introduction

Spinal cord ischemic-reperfusion injury (SCIRI) refers to the exacerbated damage to the spinal cord structure and neural function caused by blood reperfusion after a period of ischemia in spinal cord tissue (Vidal et al., 2017; Hasan et al., 2022; Algahtani et al., 2022). This complication is not rare in clinical, primarily occurring during major thoracic and abdominal vascular surgeries, as well as spinal surgeries (Kato et al., 2015; Mathkour et al., 2020; Gerardi et al., 2022).

SCIRI is a complex process involving multiple cellular and molecular-level changes. It encompasses mechanisms such as oxidative stress, inflammatory response, vascular damage, cellular apoptosis, and necrosis, which collectively lead to tissue damage and functional impairment in the spinal cord (Na et al., 2019; Han et al., 2022; Rong et al.,

2022). Therefore, several remedial interventions have been proposed to alleviate SCIRI in clinical practice (Behem et al., 2022; Mukai et al., 2022; Hou et al., 2022; Zheng et al., 2023; Chen et al., 2023). However, due to the irreversible nature of spinal nerve damage, these treatments are only effective when SCIRI is detected at an early stage. For patients who do not receive a timely detection, the lack of immediate treatment can lead to sensory or motor dysfunction in areas innervated by the spinal cord, or even permanent paralysis (Huang et al., 2022; Guo et al., 2023). Therefore, it is crucial to develop an intraoperative monitoring method capable of promptly detecting the occurrence of SCIRI.

Intraoperative monitoring using somatosensory-evoked potentials (SEP) has become an indispensable tool in surgical procedures, providing real-time monitoring of spinal cord function and potential spinal cord injury during operation procedure (Hu et al., 2001; Hu et al., 2003; Hattori et al., 2019; Park et al., 2021). However, SEP monitoring usually assesses the overall integrity of spinal cord neural function and does not clearly indicate the specific causes of potential injury. Recent research has confirmed the feasibility of using SEP for indicating localization in spinal cord injuries caused by various mechanical forces. In spinal cord injuries resulting from different mechanical mechanisms, SEP parameters exhibit distinct distribution patterns, suggesting a new method for rapidly identifying the causes of mechanical spinal cord injuries intraoperatively (Li et al., 2021; Li et al., 2023). This new measurement method also inspired our research to apply SEP for the detection of SCIRI.

SCIRI is a serious complication following surgical procedures, which is a great challenge in clinical practice because of its unpredictability, delayed onset, and severity. If SEP monitoring can detect the occurrence of intraoperative SCIRI and promptly alert the surgeon to take the appropriate intervention, it could effectively prevent postoperative neurological dysfunction. This study utilizes a rat model of SCIRI to explore this possibility. Our objective is to develop a SEP measurement as a biomarker that can accurately detect the occurrence of SCIRI, thereby providing crucial assistance in preventing and timely treating SCIRI during surgical procedures.

2 Materials and methods

2.1 Animals and study groups

All procedures were conducted in accordance with the guidelines of the Care and Use of Laboratory Animals (Institute of Laboratory Animal Resources, National Research Council, 1996). The study received approval from the Ethics Review Committee of Guangdong Medical University (GDY2302124) on March 1, 2023. Forty-two male Sprague–Dawley rats (specific-pathogen-free level), aged 8 to 9 weeks and weighing 280 to 320 g, were obtained (Liaoning Changsheng Biotech Co., Ltd., license No. SCXK (liao) 2020–0001). The rats were housed under suitable environmental conditions (temperature 20–25°C) and provided with food and water *ad libitum*.

Forty-two rats were randomly divided into seven groups: one normal control group and six experimental groups (10-min ischemia group, 20-min group, 30-min group, 40-min group, 50-min group, and 60-min group, with reperfusion time consistent at 20 min for each group), with six rats in each group (Figure 1).

2.2 Establishment of animal model

To induce SCIRI, all rats were anesthetized using isoflurane (Zuoba, Guangzhou, China) and administered via a mask connected to an anesthesia machine (Ruivode, Shenzhen, China). Once successfully anesthetized, the rats were placed on a warm pad and their limbs were secured. The surgical area was cleansed and sterilized, and electrodes for SEP recording were applied. The abdominal aorta and left renal artery were exposed. The abdominal aorta was clamped at the level of the left renal artery, and reperfusion occurred upon releasing the arterial clamp, established the SCIRI rat model (Gokce et al., 2016; Zhao et al., 2019; Li et al., 2020). Each group had different ischemia durations (10–60 min) while maintaining the same reperfusion time (20 min). We standardized the duration of abdominal closure for each group of rats to 80 min. For instance, in the rats subjected to 10 min of ischemia, after 20 min of reperfusion, we did not immediately close the abdomen but waited for 50 min instead. This ensured consistency in the duration of surgical manipulation between the rats subjected to 10 min of ischemia and those subjected to 60 min of ischemia. The objective was to minimize bias and eliminate the influence of variations in surgical procedure duration. Subsequently, the rats were returned to their cages with unrestricted access to food and water.

2.3 Measurement of somatosensory evoked potentials

SEP was continuously measured during the surgery using a neural electrophysiology test system (Yirui Technology Co., Ltd., Zhuhai, China). To elicit SEP in the cranial sensory cortex, stimulating electrodes were inserted into the toes and tibialis anterior muscles of both lower limbs, applying a constant current stimulation to the tibial nerve at a frequency of 5.3 Hz and a pulse duration of 0.2 ms. The filtering range was set at 30-2000 Hz, and the signal was averaged over 300 trials. SEP latency and amplitude were recorded for each experimental group at normal values (baseline), at the ischemic time point (Ocl values), and at 5, 10, 15, and 20 min after reperfusion.

2.4 Behavioral evaluation

After completing the experiments, each group of rats was returned to their cages with unrestricted access to food and water, allowing for free movement. Behavioral assessments of the control group and the six experimental groups were conducted using the Basso, Beattie, and Bresnahan (BBB) rating scale on postoperative days 1, 2, and 3 (Basso et al., 1995). The rats were placed in an open field, and their scores ranged from 0 to 21, with 0 indicating no motor function and 21 indicating normal function. The hind limb function of the rats during ambulation was evaluated and recorded by two independent observers.

2.5 Tissue processing

After completing the behavioral assessments, the rats in the control group and the six experimental groups were euthanized by intraperitoneal injection of sodium pentobarbital. (Sigma, St. Louis, MO, USA). Cardiac perfusion was then conducted using 250 mL of

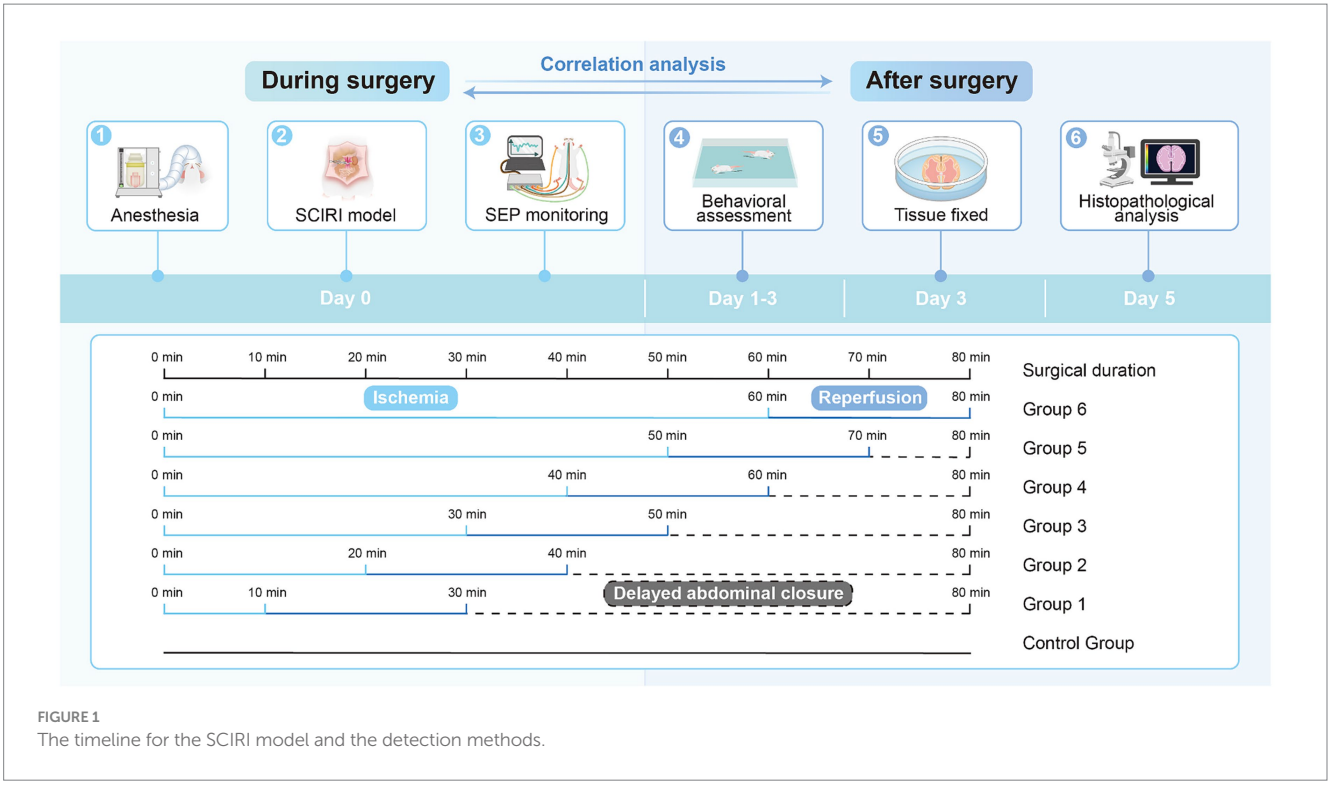

FIGURE 1
The timeline for the SCIRI model and the detection methods.

0.9% physiological saline and 250 mL of 4% paraformaldehyde. The entire lumbar spinal segment was extracted and immersed in a 4% paraformaldehyde solution. After 2 days of immersion, the spinal cord segments from the L3-L5 region were carefully and completely dissected from the vertebral canal. Each spinal cord specimen was then assigned a unique identification number, embedded in paraffin, and processed using a paraffin microtome (catalog number: RM2016, manufacturer: Leica) to obtain transverse sections with a thickness of 4 μm.

2.6 Histological staining

Histopathological examination of spinal cord tissue can more intuitively reveal the severity of spinal cord injury under a microscope. On day 3 after SCIRI, the severity of the spinal cord injury was comprehensively assessed by analyzing the expression levels of neurons, Nissl bodies within the specified region.

2.7 Hematoxylin and eosin (HE) staining

Sections were dewaxed with xylene, rehydrated in ethanol at varying concentrations, stained with hematoxylin (Servicebio, Wuhan, China), differentiated in 1% aqueous HCl, and then counterstained with eosin (Servicebio, Wuhan, China). Sections were dehydrated in ethanol and xylene and coverslipped with mounting medium.

2.8 Nissl staining

Sections were dewaxed with xylene, rehydrated in ethanol at varying concentrations, and then stained with Nissl staining solution (Boster, Wuhan, China) at 60°C for 40 min. Sections were dehydrated in ethanol and xylene and coverslipped with mounting medium.

2.9 Image acquisition and analysis

Utilizing an optical microscope, we acquired images of HE staining and Nissl staining (catalog number: HS6, manufacturer: Leica). Subsequently, we performed quantitative analysis of the spinal cord gray matter anterior horn region for HE staining and Nissl staining using ImageJ 1.47v (National Institutes of Health, USA).

2.10 Statistical analysis

Data analysis was performed using GraphPad Prism v9 software (GraphPad, USA).[1] Initially, the Shapiro–Wilk test was employed to assess the normality distribution of these groups. The SEP data were presented as percentages, while the remaining data were expressed as mean ± standard error of the mean. The statistical significance was calculated by one-way ANOVA with a Tukey's multiple comparison. Since SEP data were non-normally distributed, Spearman's correlation analysis was used to examine the relationships between SEP and behavioral data, as well as SEP and histopathological data. A p-value of <0.05 was considered statistically significant.

1 www.graphpad.com

3 Results

3.1 General situation

All rats successfully underwent SCIRI experiment without any intraoperative or post-anesthesia deaths. They regained consciousness within 2 h after anesthesia and were able to eat freely within 12 h. None of the experimental animals exhibited signs of incision infection or suture dehiscence.

3.2 The characteristic alterations of SEP in different severity of SCIRI

After the rat model was established, the SEP latency and amplitude were measured for each group. The results revealed that, with varying durations of ischemia and reperfusion, both the latency and amplitude of SEPs underwent changes. These alterations demonstrated a distinct Time-varying characteristic, being closely associated with the time of spinal cord ischemia and reperfusion (Table 1).

In the group with 10 min of ischemia, SEP exhibited a mild extension in the latency of the ischemic time point (Ocl values) compared to the normal values (baseline). Additionally, there was a slight decrease in amplitude, indicating the onset of spinal cord conduction dysfunction at this at this moment. However, following 5, 10, 15, and 20 min of reperfusion after blood reperfusion, concurrent with the gradual restoration of spinal cord blood flow, SEP latency gradually decreased, and amplitude progressively increased. The SEP signals demonstrated a trend of gradual recovery (Figure 2A), Signifying a gradual recovery of neural conduction function.

In the group with 20 min of ischemia, the latency of the ischemic time point (Ocl values) exhibited an extended duration compared to the normal values (baseline), and the amplitude decreased, indicating ischemic damage to the spinal cord at this moment. Following 5, 10, 15, and 20 min of reperfusion after blood reperfusion, SEP values did not immediately exhibit improvement or exacerbation. Instead, they fluctuated around the values of the ischemic time point (Figure 2B), indicating that SCIRI injury did not occur at this time.

However, in the 30–60 min ischemia groups, as the ischemic duration extended, SEP exhibited a gradual prolongation of latency at the ischemic time point (Ocl value) and a gradual reduction in amplitude, indicating an increasing severity of spinal cord injury with prolonged ischemia. Subsequently, upon reperfusion of spinal cord blood, the electrophysiological signals of SEP showed a different trend compared to the first two groups. Following blood reperfusion at 5, 10, 15, and 20 min, the SEP latency gradually extends on the basis of the ischemic time point (Ocl value), and the amplitude decreases, suggesting a progressive worsening of spinal cord injury with prolonged reperfusion time (Figures 2C–F), indicating the occurrence of SCIRI during this time period.

3.3 Behavioral differences among different severity of SCIRI

The BBB scoring system stands as one of the most frequently utilized methodologies for behavioral assessment in the context of spinal cord injury in rats (Basso et al., 1995; Nagarajan et al., 2021). Using this method, we assessed hindlimb behavioral

TABLE 1 Intraoperative SEP monitoring of SCIRI latency and amplitude time-varying characteristics.

Changes of SEP latency (%) in rats with SCIRI						
Group	Ischemia 10 min	Ischemia 20 min	Ischemia 30 min	Ischemia 40 min	Ischemia 50 min	Ischemia 60 min
Baseline	0	0	0	0	0	0
Occlusion	29.81	46.62	57.76	62.07	79.50	88.29
Reperfusion 5 min	21.70	36.04	62.24	63.66	82.66	95.95
Reperfusion 10 min	19.82	46.81	68.32	74.47	96.02	113.06
Reperfusion 15 min	13.51	42.66	81.61	93.02	110.59	129.73
Reperfusion 20 min	6.76	43.56	119.44	122.45	133.41	156.46

Changes of SEP amplitude (%) in rats with SCIRI						
Group	Ischemia 10 min	Ischemia 20 min	Ischemia 30 min	Ischemia 40 min	Ischemia 50 min	Ischemia 60 min
Baseline	0	0	0	0	0	0
Occlusion	−41.14	−58.53	−61.95	−67.68	−67.10	−73.36
Reperfusion 5 min	−43.70	−55.01	−64.07	−69.46	−69.03	−74.71
Reperfusion 10 min	−36.59	−54.09	−65.94	−71.92	−71.77	−76.49
Reperfusion 15 min	−29.88	−51.11	−68.79	−76.11	−74.86	−78.18
Reperfusion 20 min	−21.73	−52.12	−72.59	−77.02	−77.89	−80.88

Calculation of the changes in the latency or amplitude period of the SEP is performed as follows: (Injured latency or amplitude parameter - Baseline latency or amplitude parameter)/Baseline latency or amplitude parameter × 100%. $n = 6$.

10.3389/fnins.2024.1411016

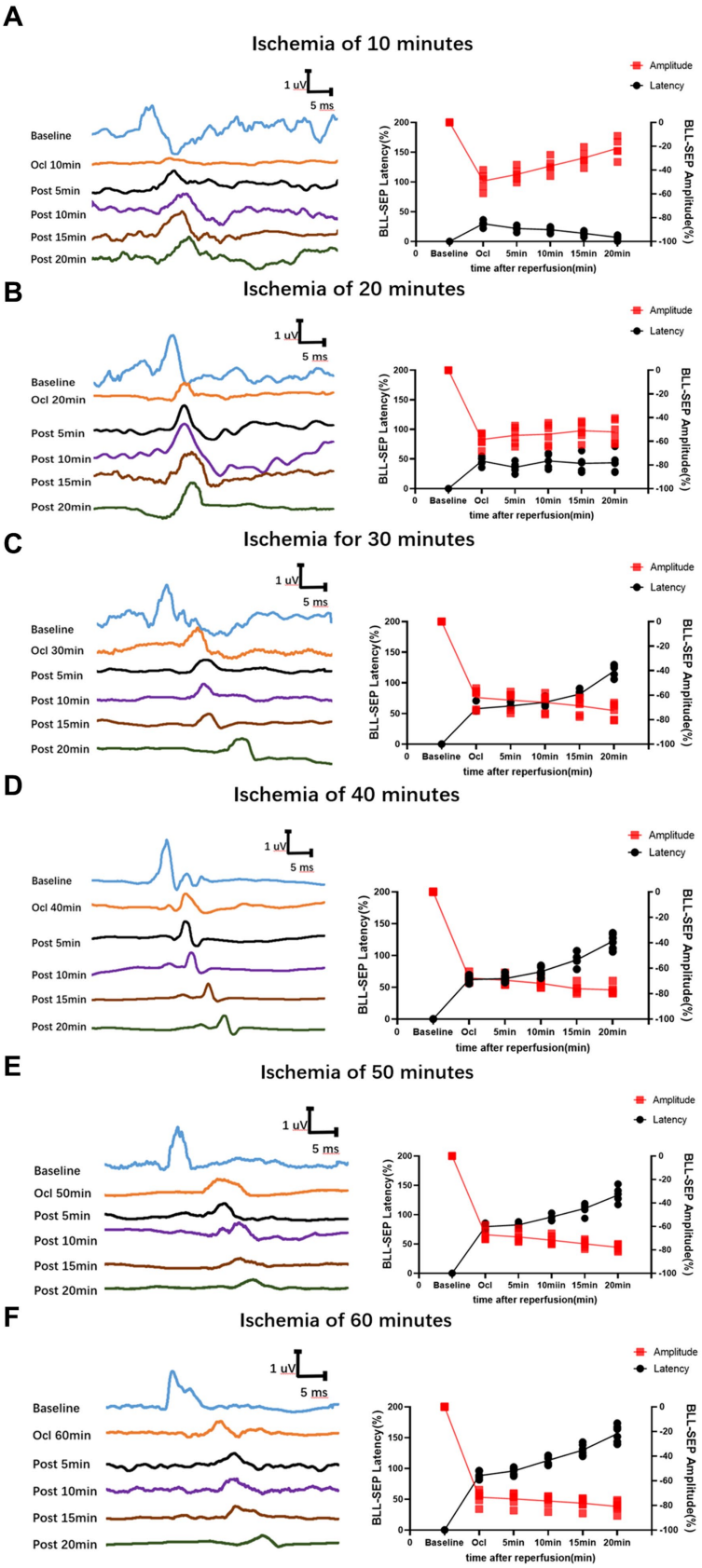

FIGURE 2
Time-varying SEP in waveform and latency/amplitude in rats with SCIRI. **(A)** 10-min ischemia group. **(B)** 20-min ischemia group. **(C)** 30 min ischemia groups. **(D)** 40 min ischemia groups. **(E)** 50 min ischemia groups. **(F)** 60 min ischemia groups. The reperfusion duration for each group is consistent at 5, 10, 15, and 20 min. Data were expressed as the percentage. (n = 6; BLL = Both lower limbs; Ocl = Occlusion).

10.3389/fnins.2024.1411016

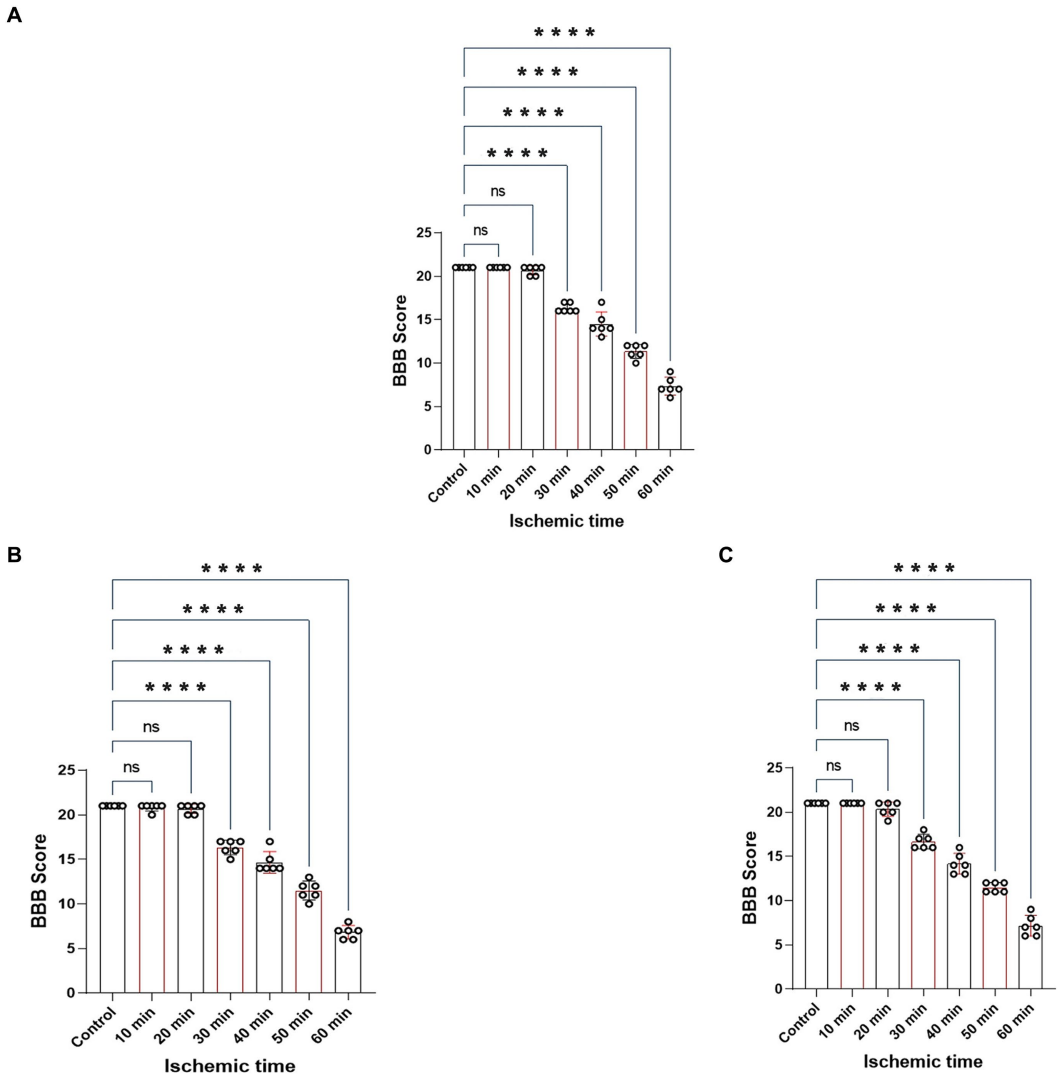

FIGURE 3
Represents the BBB scores of rats on day 1, 2 and 3 after SCIRI. **(A)** BBB score variations on day 1 after SCIRI. **(B)** BBB score changes on day 2 after SCIRI. **(C)** BBB score changes on day 3 after SCIRI. Data were presented as the mean ± SD. The statistical significance was calculated by one-way ANOVA with a Tukey's multiple comparison ($n = 6$; ns: $p > 0.05$，indicating no significance; *$p < 0.05$, signifies that there was statistical significance; *$p < 0.05$, **$p < 0.01$, ***$p < 0.001$, ****$p < 0.0001$).

changes in different groups of rats on days 1, 2, and 3 after SCIRI after SCIRI. The results showed that the behavioral scores for the 10-min and 20-min ischemia groups were similar to those of the control group, with no statistically significant differences ($p > 0.05$). However, after 30 min or more of ischemia, the behavioral scores of the rats were significantly lower than those of the control group ($p < 0.05$). Additionally, as the ischemia duration increased, the hind limb behavioral scores progressively declined, indicating a gradual deterioration of neural function (Figures 3A–C). Subsequently, we performed a correlation analysis between the behavioral changes on day 3 and SEP signal variations in the rats. The results revealed a high correlation between the trends in SEP signal changes and the severity of behavioral impairments as the ischemia and reperfusion durations varied (Figures 4A–E), confirming consistency between the two sets of results.

3.4 HE staining differences among different severity of SCIRI

The structural morphology of spinal anterior horn motor neurons in each group was assessed using HE staining within the same region (Figure 5A). In the 10-min and 20-min ischemia groups, the morphological structure of motor neurons in the anterior horn of the spinal cord appeared normal. The neuronal nuclei exhibited deep staining, maintained a complete circular shape, showed no signs of swelling, and displayed uniform cytoplasmic staining (Figures 5B–D),

10.3389/fnins.2024.1411016

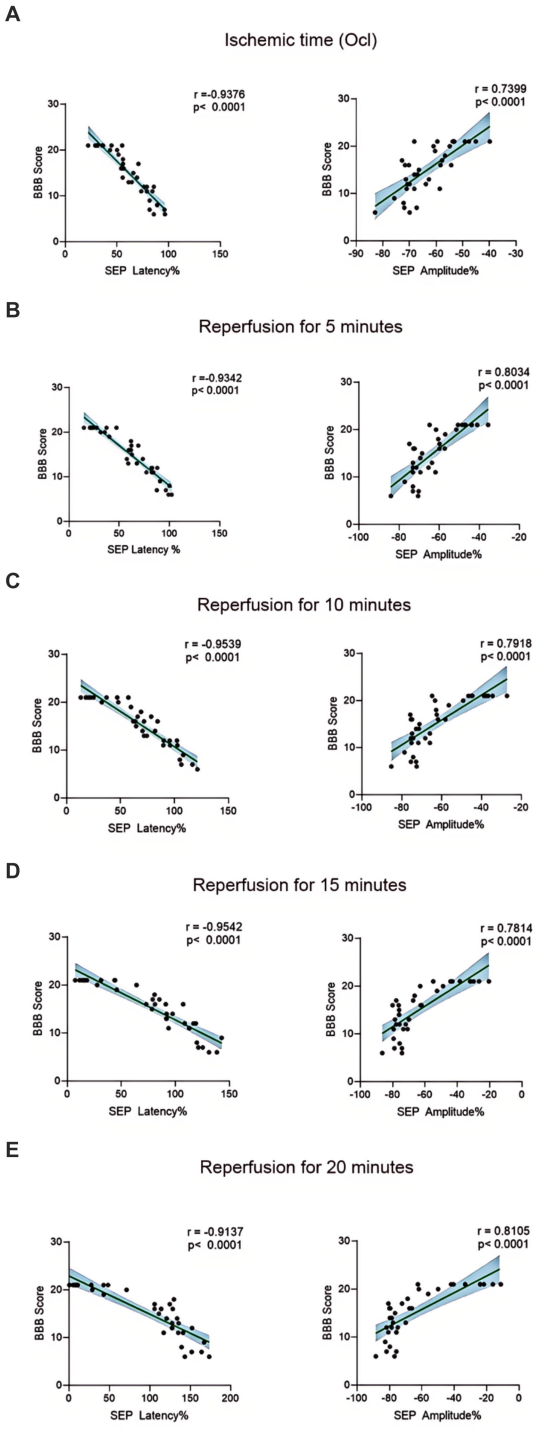

FIGURE 4
Scatterplots showing the relationship between SEP signal changes and behavioral outcomes correlation analysis in SCIRI. **(A)** Correlation analysis of SEP signal changes and behavior at different ischemia times. **(B–E)** Correlation analysis of SEP signal changes and behavior at 5, 10, 15, and 20min of reperfusion at different ischemia times. The linear regression line of the best fit is represented by a solid line. The 95% confidence interval is represented by a dotted line, were conducted using Spearman's correlation analysis (n=6; Ocl=Occlusion).

and compared to the control group, there was no statistically significant difference ($p > 0.05$). However, after 30 min or more of ischemia, there was a significant reduction in the number of neurons compared to the control group ($p < 0.05$). Additionally, as the ischemia duration increased, the neurons gradually atrophied, the cytoplasmic staining became lighter, the surrounding matrix disappeared, leading to vacuole formation, and the nuclei condensed. This indicates that with prolonged ischemia, the number of normal neurons gradually decreased (Figures 5E–H), indicating an increasing severity of spinal cord injury after SCIRI (Figure 5I). Subsequently, we conducted a correlation analysis between the pathological changes in neurons and SEP signal variations. The results revealed a high correlation between the trends in SEP signal changes and the degree of neuronal necrosis as the ischemia and reperfusion durations varied (Figures 6A–E), indicating consistency between the two sets of results.

3.5 Nissl staining differences among different severity of SCIRI

We employed Nissl staining to observe the content of Nissl bodies in the same region of the spinal cord anterior horn in each group (Figure 7A). In the 10-min and 20-min ischemia groups, the morphology of motor neurons in the anterior horn of the spinal cord appeared normal, with a rich presence of Nissl bodies (Figures 7B–D), and compared to the control group, there was no statistically significant difference ($p > 0.05$). However, after 30 min or more of ischemia, the number of Nissl bodies decreased significantly compared to the control group ($p < 0.05$). Additionally, as the ischemia duration increased, the number of Nissl bodies in this region gradually decreased, and Nissl bodies progressively vacuolated (Figures 7E–H), suggesting an increasing severity of spinal cord injury after SCIRI (Figure 7I). Subsequently, we conducted a correlation analysis between the pathological changes in Nissl bodies and SEP signal variations. The results revealed a high correlation between the trends in SEP signal changes and the decreased number of Nissl bodies as the ischemia and reperfusion durations varied (Figures 8A–E), confirming consistency between the two sets of results.

4 Discussion

In clinical practice, the prevention and treatment of SCIRI remain a big challenge. Due to the inability to obtain tissue samples from clinical patients and the difficulty in making a definitive diagnosis, some published reports only describe "suspected" cases of SCIRI following surgery, lacking sufficient evidence to support the diagnosis (Kato et al., 2015; Antwi et al., 2018; Papaioannou et al., 2019; Acharya et al., 2021; Malinovic et al., 2021; Algahtani et al., 2022; Hasan et al., 2022). The lack of effective monitoring methods is the primary reason for the failure to achieve early detection and treatment of SCIRI. This experimental study examined the intraoperative monitoring value of SEP in detecting SCIRI. A new characteristic of SEP signal changes, referred to as the "time-varying characteristic," as a novel biomarker that can specifically detect the occurrence of SCIRI. This will become an indicator for intraoperative neurophysiological monitoring, providing a novel scientific approach for the prevention, intervention, and early treatment of SCIRI.

Intraoperative SEP monitoring has become an essential tool used to assess the functional integrity of sensory pathways during surgical procedures (Hu et al., 2003; Ji et al., 2013; Li et al., 2023). The use of

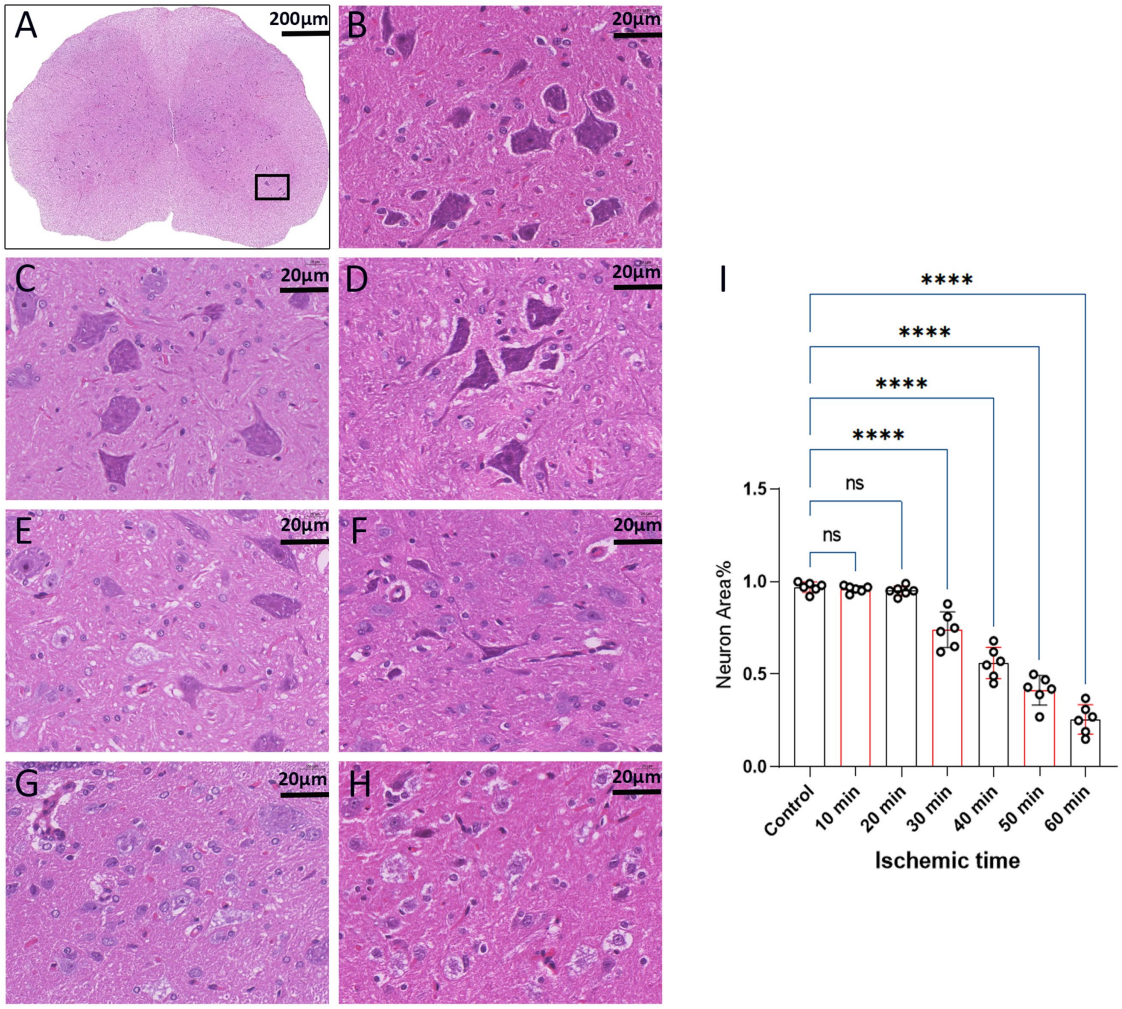

FIGURE 5
Spinal cord sections on day 3 after SCIRI (HE staining, light microscope). **(A)** Each image was selected from the anterior horn region of the spinal cord (×4, Scale bar: 200 μm). Boxes represent the magnified region. **(B)** Enumeration and morphology of motor neurons in this region for the control group (×40, scale: 20 μm). **(C–H)** Enumeration and morphology of motor neurons in this region for the 10 to 60 min ischemia groups (×40, scale: 20 μm). **(I)** Data were presented as the mean ± SD. The statistical significance was calculated by one-way ANOVA with a Tukey's multiple comparison ($n = 6$; ns: $p > 0.05$, indicating no significance; *: $p < 0.05$, signifies that there was statistical significance; *$p < 0.05$, **$p < 0.01$, ***$p < 0.001$, ****$p < 0.0001$).

SEP helps to prevent the risk of spinal cord damage by providing real-time feedback to surgeons about the patient's neurological status (Hu et al., 2003; Ji et al., 2013; Park et al., 2021; Guo et al., 2023). However, intraoperative SEP monitoring can only detect the integrity of neurological function, without detail message regarding injury mode and location (Cui et al., 2021; Li et al., 2023;). Currently, few studies elucidated the time-varying characteristics in SEP signals during the occurrence of SCIRI. Therefore, our study to explore and analyze SEP signal variations during SCIRI from a novel perspective to better understand these changes. Motor-evoked potentials (MEP) is another electrophysiological test to detect intraoperative injury to the spinal cord, which is suggested as the effective monitoring for SCIRI (Hattori et al., 2019; Li et al., 2023). However, MEP is easily disappeared when the injury happened. In SCIRI model, MEP showed too sensitive to the ischemia, so that it is not measurable during subsequent ischemia–reperfusion injury period (Li et al., 2023).

The clinical issues described above necessitate solutions derived from fundamental experimental research. In the last decade, there has been continuous exploration of SCIRI both domestically and internationally, accompanied by the refinement of animal models (Alizadeh et al., 2019). The primary approach involves inducing a rat model of SCIRI by occluding the aortic arch between the left carotid artery and the left subclavian artery (Dong Y. et al., 2023) or by clamping the abdominal aorta at the level of the left renal artery (Gokce et al., 2016; Zhao et al., 2019; Li et al., 2020). Both methods have been proven effective in inducing SCIRI. In this study, we employed the method of the abdominal aorta clamping at the level of the left renal artery to establish rat SCIRI models with varying ischemic durations. SCIRI was successfully induced in our study 30 min or more after spinal cord ischemia, aligning with previous research findings and confirming the adherence of our rat model to established standards. Intraoperative SEP monitoring was employed to dynamically observe the evolving characteristics of SEP signals

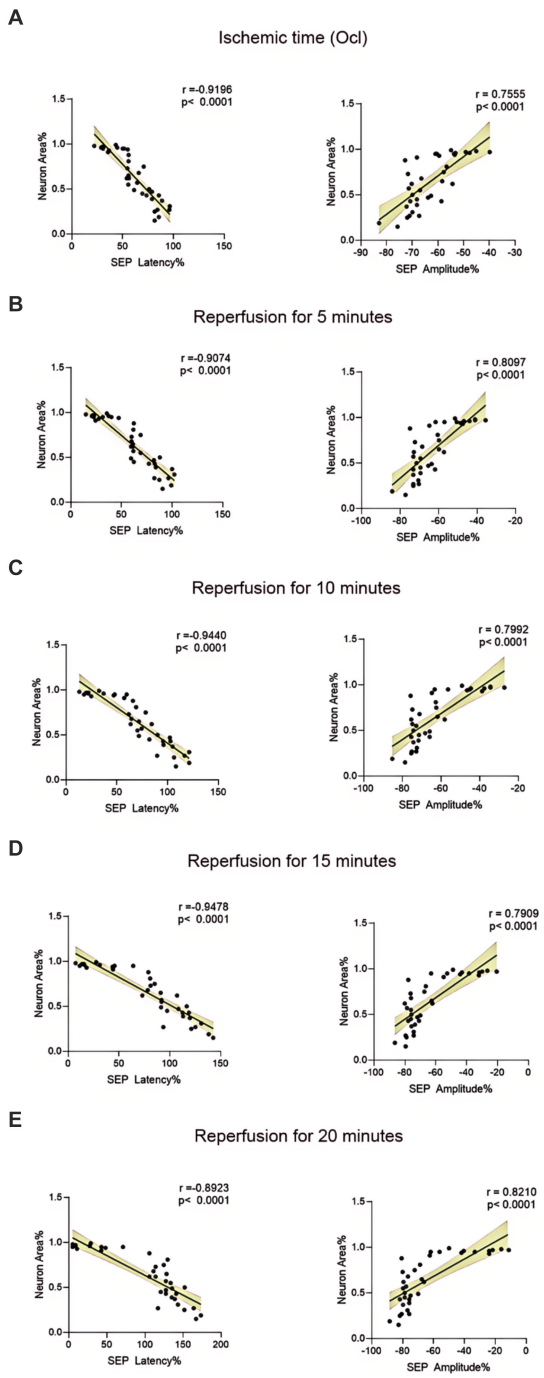

FIGURE 6
Scatterplots showing the relationship between SEP signal changes and HE staining outcomes correlation analysis in SCIRI.
(A) Correlation analysis of SEP signal changes and HE staining at different ischemia times. **(B–E)** Correlation analysis of SEP signal changes with HE staining at 5, 10, 15, and 20 min of reperfusion at different ischemia times. The linear regression line of the best fit is represented by a solid line. The 95% confidence interval is represented by a dotted line, were conducted using Spearman's correlation analysis ($n = 6$; Ocl = Occlusion).

during the SCIRI process. Correlation analyses were conducted between postoperative behavior and histopathological results with changes in SEP signals.

This study found that during a 10-min ischemic, following blood reperfusion. SEP potential signals demonstrated a trend of gradual recovery. This implies that brief periods of spinal cord ischemia do not lead to the occurrence of SCIRI. In the case of ischemia for 20 min, SEP values did not immediately exhibit improvement or exacerbation after blood reperfusion. Instead, they fluctuated around the values of the ischemic time point (Ocl values). Nevertheless, postoperative behavior and histopathological did not show any unusual changes ($p > 0.05$). We hypothesize that this phenomenon may be attributed to ischemic spinal cord injury. Due to the short ischemic duration, no SCIRI occurred upon blood reperfusion. Postoperatively, rats in this experimental group did not exhibit behavioral anomalies or histopathological changes, indicating the reversibility of this short-term ischemic spinal cord injury. In future studies, extending the monitoring time could provide insights into the long-term changes in neuroelectrical signals with this pathological condition. However, in the 30–60 min ischemia groups, after reperfusion of spinal cord blood, the signals of SEP showed a different trend compared to the first two groups. Based on the ischemia time point (Ocl value), the SEP latency gradually prolonged, and the amplitude gradually decreased, indicating a progressive deterioration in spinal cord conduction function, suggesting the occurrence of SCIRI during this time period. Moreover, the severity of spinal cord injury worsened with prolonged ischemia and reperfusion time. Postoperative behavioral and histopathological assessments similarly confirmed the monitoring results of SEP, and correlation analysis demonstrated consistency among the three outcomes. Through further extraction and analysis of SEP signals, we discovered unique alterations in SEP during SCIRI. Specifically, when SCIRI occurs, it produces specific variations depending on the duration of spinal cord ischemia and reperfusion. Importantly, these changes do not manifest in normal conditions or other types of spinal cord injuries. We term this phenomenon "the time-varying characteristic of SEP." These time-varying characteristic can dynamically reflect the severity of SCIRI. This discovery facilitates surgeons in identifying the occurrence of SCIRI during the surgical process and possesses a distinct pioneering significance.

The time-frequency analysis of SEP showed paramount significance in spinal cord research (Hu et al., 2001; Hu et al., 2003; Hattori et al., 2019; Cui et al., 2021). It elucidates the functional status of the spinal cord, facilitates the detection and localization of spinal cord injuries, monitors therapeutic efficacy and rehabilitation processes, and delves into the pathophysiological mechanisms underlying spinal cord disorders (Ji et al., 2013; Cui et al., 2021; Li et al., 2021). This methodology furnishes a wealth of information and robust tools, thereby propelling advancements in spinal cord research and clinical applications. In a previous experimental study, SEP signal changes were investigated in different mechanical spinal cord injury models (such as contusion, displacement, and traction) (Li et al., 2023). In various mechanical spinal cord injuries, SEP parameters show different distribution patterns, leading to a new method for rapid intraoperative identification of the cause of spinal cord injury (Li et al., 2023). We further conducted an analysis of the SEP datasets obtained from previous experimental studies on mechanical spinal cord injurie. In the context of

10.3389/fnins.2024.1411016

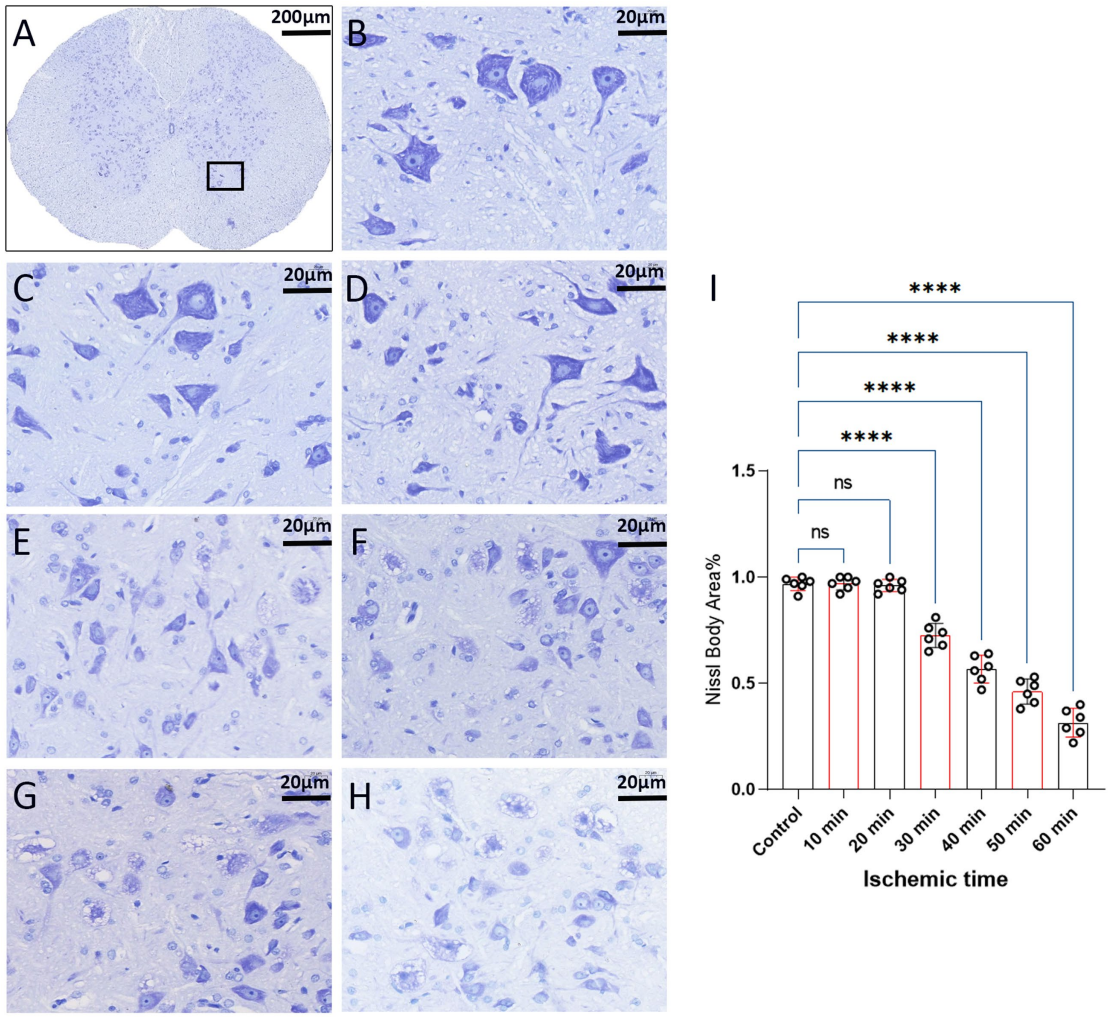

FIGURE 7
Spinal cord sections on day 3 after SCIRI (Nissl staining, light microscope). **(A)** Each image was selected from the anterior horn region of the spinal cord (×4, Scale bar: 200 μm). Boxes represent the magnified region. **(B)** Nissl body content in this region for the control group (×40, scale: 20 μm). **(C–H)** Nissl body content in this region for the 10 to 60 min ischemia groups (×40, scale: 20 μm). **(I)** Data were presented as the mean ± SD. The statistical significance was calculated by one-way ANOVA with a Tukey's multiple comparison ($n = 6$; ns: $p > 0.05$, indicating no significance; *$p < 0.05$, signifies that there was statistical significance; *$p < 0.05$, **$p < 0.01$, ***$p < 0.001$, ****$p < 0.0001$).

mechanical spinal cord injury, the latency of SEP prolongs, and the amplitude diminishes post-injury. Over a brief duration, SEP fluctuates around the injury threshold without exhibiting time-varying characteristic. However, during the occurrence of SCIRI, SEP undergoes signal alterations based on the injury threshold (Ocl value). These signal changes correlate with both ischemic and reperfusion times, showcasing distinctive time-varying characteristic (Figures 2C–F). In this study, SEP monitoring was used to investigate SCIRI induced by ischemia and revealed distinct characteristics compared to mechanical spinal cord injury (Figure 9). This demonstrated the potential use of the unique time-varying characteristics of SEP changes as a biomarker for definite detection of SCIRI during surgery.

The significance of this study lies in the unpredictability and severity of SCIRI in clinical practice. This phenomenon frequently occurs during surgical procedures, and due to the absence of effective intraoperative detection methods, the occurrence of SCIRI is often overlooked, leading to serious clinical consequences in postoperative patients. Presently, SCIRI poses a significant challenge in spinal surgery (Huang et al., 2023). If we can detect the occurrence of this phenomenon during surgery, early and effective intervention measures can be implemented to prevent irreversible spinal cord damage (Dong X. et al., 2023). Addressing these clinical needs, we utilized continuous intraoperative SEP monitoring to observe changes in electrophysiological signals during SCIRI in rats. Building upon this, we discovered a specific change in SEP during the monitoring of spinal cord ischemia–reperfusion injury, termed "time-varying characteristic." This time-varying characteristic could potentially serve as novel intraoperative biomarkers for the definitive detection of SCIRI. Simultaneously, SEP has emerged as the primary method for monitoring spinal cord function during surgical procedures, gaining widespread recognition in clinical practice (Hu

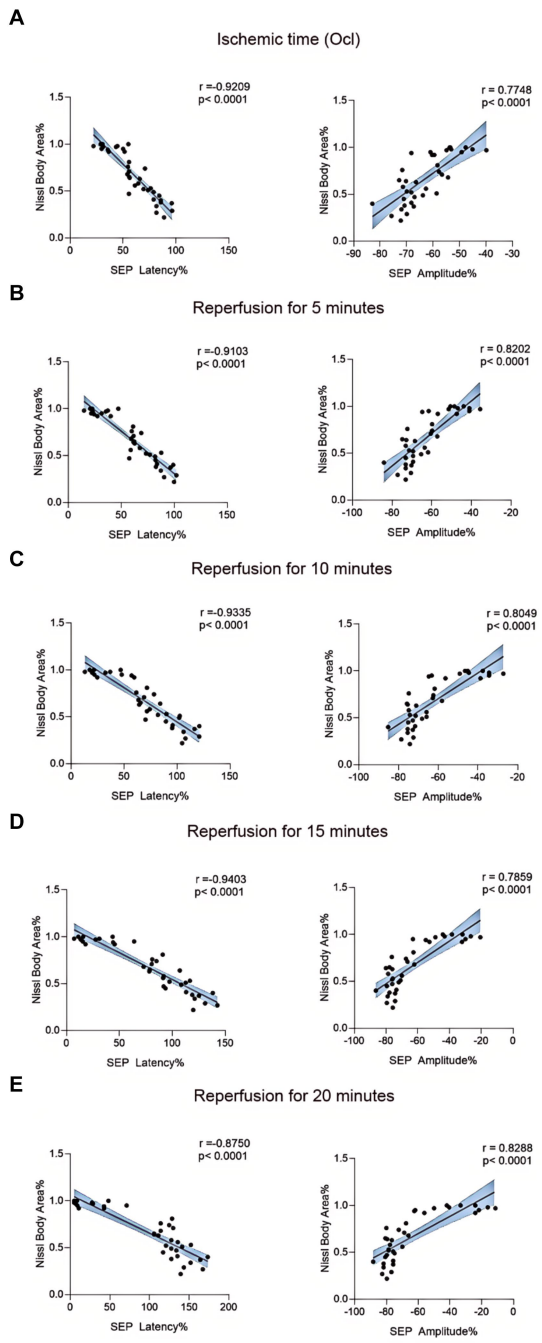

FIGURE 8
Scatterplots showing the relationship between SEP signal changes and Nissl staining outcomes correlation analysis in SCIRI. **(A)** Correlation analysis of SEP signal changes and Nissl staining at different ischemia times. **(B–E)** Correlation analysis of SEP signal changes with Nissl staining at 5, 10, 15, and 20 min of reperfusion at different ischemia times. The linear regression line of the best fit is represented by a solid line. The 95% confidence interval is represented by a dotted line, were conducted using Spearman's correlation analysis (n = 6; Ocl = Occlusion).

et al., 2001; Hu et al., 2003; Park et al., 2021). Therefore, the results of this study can be easily translated into clinical applications (Cui et al., 2021).

There are limitations to this study. Further validation of the time-varying characteristic of SEP is needed through more animal experiments. Its application in clinical surgeries also requires verification to establish its reliability as a detection criterion. Additionally, the timing and strategies for repair of neurologic injury in SCIRI need further investigation.

In summary, this study firstly introduce time-varying analysis of SEP to detect SCIRI in animal model. It provides evidence of the genuine occurrence of SCIRI, and demonstrates the capability of SEP to detect the onset of SCIRI during surgery. Furthermore, the occurrence of SCIRI is closely linked to the duration of spinal cord ischemia. Notably, when SCIRI occurs, SEP exhibits a prominent time-varying characteristic, suggesting its potential as a biomarker for definite detection of SCIRI during surgery.

Data availability statement

The raw data supporting the conclusions of this article will be made available by the authors, without undue reservation.

Ethics statement

The animal study was approved by Guangdong Medical University (GDY2302124) on March 1, 2023. The study was conducted in accordance with the local legislation and institutional requirements.

Author contributions

KL: Conceptualization, Funding acquisition, Investigation, Writing – original draft, Writing – review & editing, Data curation, Formal analysis, Methodology, Validation. JY: Data curation, Investigation, Validation, Visualization, Writing – original draft. HW: Investigation, Data curation, Supervision, Validation, Writing – review & editing. XC: Visualization, Writing – original draft, Data curation, Supervision. GL: Visualization, Writing – original draft, Investigation, Methodology. RX: Validation, Conceptualization, Methodology, Visualization, Writing – original draft. WG: Funding acquisition, Supervision, Validation, Writing – review & editing. YH: Funding acquisition, Investigation, Supervision, Writing – review & editing, Validation, Writing – original draft.

Funding

The author(s) declare that financial support was received for the research, authorship, and/or publication of this article. This work was supported by National Key Research and Development Program of China, No. 2021YFF0501600 (to YH); Disease Prevention and Control Key Program of Zhanjiang City of China, No. 2022A01146 (to YH); High Level-Hospital Research Platform Key Cultivation Program of Zhanjiang City of China, No. 2021A05087 (to WTG); Disease Prevention Program of Zhanjiang City of China, No. 2021A05103 (to HW).

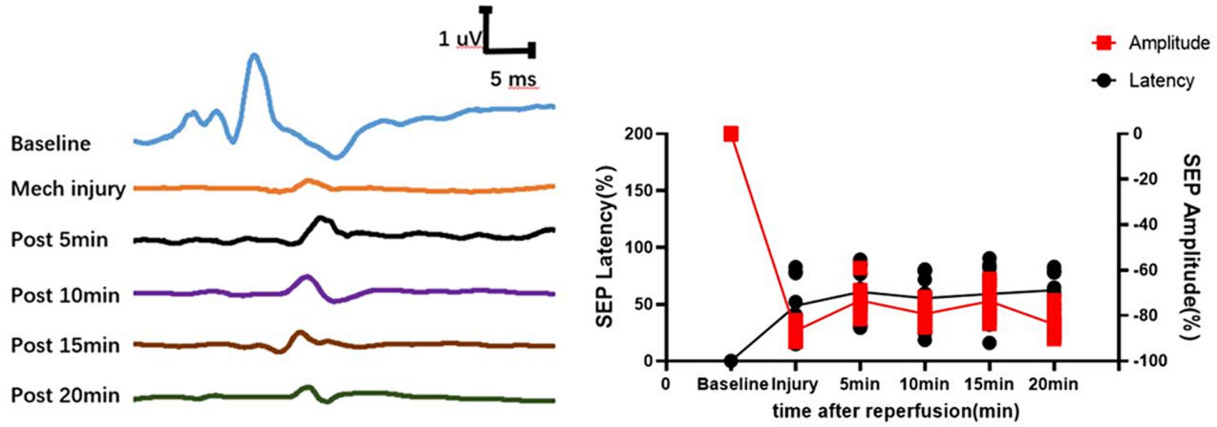

FIGURE 9
Depicts the waveform changes of SEP in mechanical spinal cord injury. Mechanical spinal cord injury (such as contusion, displacement, and traction) differs from SCIRI in that its SEP waveform remains fixed within a short period of time and does not exhibit time-varying characteristics. Data were expressed as the percentage ($n = 10$).

Acknowledgments

We would like to thank the Research Center of the Second Affiliated Hospital of Guangdong Medical University for its help and support during the study.

Conflict of interest

The authors declare that the research was conducted in the absence of any commercial or financial relationships that could be construed as a potential conflict of interest.

The author(s) declared that they were an editorial board member of Frontiers, at the time of submission. This had no impact on the peer review process and the final decision.

Publisher's note

All claims expressed in this article are solely those of the authors and do not necessarily represent those of their affiliated organizations, or those of the publisher, the editors and the reviewers. Any product that may be evaluated in this article, or claim that may be made by its manufacturer, is not guaranteed or endorsed by the publisher.

References

Acharya, S., Kaucha, D., Sandhu, A. S., Adsul, N., Chahal, R. S., and Kalra, K. L. (2021). Misdiagnosis of "white cord syndrome" following posterior cervical surgery for ossification of the posterior longitudinal ligament: a case report. *Surg. Neurol. Int.* 12:244. doi: 10.25259/SNI_268_2021

Algahtani, A. Y., Bamsallm, M., Alghamdi, K. T., Alzahrani, M., and Ahmed, J. (2022). Cervical spinal cord ischemic reperfusion injury: a comprehensive narrative review of the literature and case presentation. *Cureus* 14:e28715. doi: 10.7759/cureus.28715

Alizadeh, A., Dyck, S. M., and Karimi-Abdolrezaee, S. (2019). Traumatic spinal cord injury: an overview of pathophysiology, models and acute injury mechanisms. *Front. Neurol.* 10:282. doi: 10.3389/fneur.2019.00282

Antwi, P., Grant, R., Kuzmik, G., and Abbed, K. (2018). "white cord syndrome" of acute hemiparesis after posterior cervical decompression and fusion for chronic cervical stenosis. *World Neurosurg.* 113, 33–36. doi: 10.1016/j.wneu.2018.02.026

Basso, D. M., Beattie, M. S., and Bresnahan, J. C. (1995). A sensitive and reliable locomotor rating scale for open field testing in rats. *J. Neurotrauma* 12, 1–21. doi: 10.1089/neu.1995.12.1

Behem, C. R., Haunschild, J., Pinnschmidt, H. O., Gaeth, C., Graessler, M. F., Trepte, C. J. C., et al. (2022). Effects of fluids vs. vasopressors on spinal cord microperfusion in hemorrhagic shock induced ischemia/reperfusion. *Microvasc. Res.* 143:104383. doi: 10.1016/j.mvr.2022.104383

Chen, Y., Dong, Y., Zhang, Z. L., Han, J., Chen, F. S., Tong, X. Y., et al. (2023). Fra-1 induces apoptosis and neuroinflammation by targeting S100A8 to modulate TLR4 pathways in spinal cord ischemia/reperfusion injury. *Brain Pathol.* 33:e13113. doi: 10.1111/bpa.13113

Cui, H.-Y., Wu, Y.-X., Li, R., Li, G.-S., and Hu, Y. (2021). A translational study of somatosensory evoked potential time-frequency components in rats, goats, and humans. *Neural Regen. Res.* 16, 2269–2275. doi: 10.4103/1673-5374.310693

Dong, H., Shi, D., Bao, Y., Chen, X., Zhou, L., Lin, H., et al. (2023). Transcriptome alterations and therapeutic drugs in different organs after spinal cord injury based on integrated bioinformatic analysis. *J. Neurorestoratol.* 11:100056. doi: 10.1016/j.jnrt.2023.100056

Dong, Y., Ai, C., Chen, Y., Zhang, Z., Zhang, D., Liu, S., et al. (2023). Eph receptor A4 regulates motor neuron ferroptosis in spinal cord ischemia/reperfusion injury in rats. *Neural Regen. Res.* 18, 2219–2228. doi: 10.4103/1673-5374.369118

Gerardi, R. M., Giammalva, G. R., Basile, L., Gulì, C., Pino, M. A., Messina, D., et al. (2022). White cord syndrome after cervical or thoracic spinal cord decompression. Hemodynamic complication or mechanical damage? An Underestimated Nosographic Entity. *World Neurosurg.* 164, 243–250. doi: 10.1016/j.wneu.2022.05.012

Gokce, E. C., Kahveci, R., Gokce, A., Sargon, M. F., Kisa, U., Aksoy, N., et al. (2016). Curcumin attenuates inflammation, oxidative stress, and ultrastructural damage induced by spinal cord ischemia-reperfusion injury in rats. *J. Stroke Cerebrovasc. Dis.* 25, 1196–1207. doi: 10.1016/j.jstrokecerebrovasdis.2016.01.008

Guo, X. D., Hu, J. Z., Feng, S. Q., Gao, X. W., Sun, C. K., Ao, Q., et al. (2023). Clinical neurorestorative treatment guidelines for neurological dysfunctions of sequels from vertebral and spinal cord lesions (CANR 2023 version). *J. Neurorestoratol.* 11:100070. doi: 10.1016/j.jnrt.2023.100070

Han, B., Liang, W., Hai, Y., Liu, Y., Chen, Y., Ding, H., et al. (2022). Elucidating the potential mechanisms underlying distraction spinal cord injury-associated Neuroinflammation and apoptosis. *Front. Cell Dev. Biol.* 10:839313. doi: 10.3389/fcell.2022.839313

Hasan, W., Khan, K., and Alomani, N. (2022). Cervical cord reperfusion injury: a rare complication of spine surgery. *Int. J. Emerg. Med.* 15:39. doi: 10.1186/s12245-022-00443-3

Hattori, K., Yoshitani, K., Kato, S., Kawaguchi, M., Kawamata, M., Kakinohana, M., et al. (2019). (2019) association between motor-evoked potentials and spinal cord damage diagnosed with magnetic resonance imaging after Thoracoabdominal and descending aortic aneurysm repair. *J. Cardiothorac. Vasc. Anesth.* 33, 1835–1842. doi: 10.1053/j.jvca.2018.12.004

Hou, J., Li, H., Xue, C., and Ma, J. (2022). Lidocaine relieves spinal cord ischemia-reperfusion injury via long non-coding RNA MIAT-mediated notch 1 downregulation. *J. Biochem.* 171, 411–420. doi: 10.1093/jb/mvab150

Hu, Y., Luk, K. D., Lu, W. W., and Leong, J. C. (2003). Application of time-frequency analysis to somatosensory evoked potential for intraoperative spinal cord monitoring. *J. Neurol. Neurosurg. Psychiatry* 74, 82–87. doi: 10.1136/jnnp.74.1.82

Hu, Y., Luk, K. D. K., Lu, W. W., Holmes, A., and Leong, J. C. Y. (2001). Prevention of spinal cord injury with time-frequency analysis of evoked potentials: an experimental study. *J. Neurol. Neurosurg. Psychiatry* 71, 732–740. doi: 10.1136/jnnp.71.6.732

Huang, H., Bach, J. R., Sharma, H. S., Saberi, H., Jeon, S. R., Guo, X., et al. (2023). The 2022 yearbook of Neurorestoratology. *J Neurorestoratol* 11:100054. doi: 10.1016/j.jnrt.2023.100054

Huang, H., Sharma, H. S., Saberi, H., Chen, L., Sanberg, P. R., Xue, M., et al. (2022). Spinal cord injury or dysfunction quality of life rating scale (SCIDQLRS) (IANR 2022 version). *J. Neurorestoratol.* 10:100016. doi: 10.1016/j.jnrt.2022.100016

Ji, Y., Meng, B., Yuan, C., Yang, H., and Zou, J. (2013). Monitoring somatosensory evoked potentials in spinal cord ischemia-reperfusion injury. *Neural Regen. Res.* 8, 3087–3094. doi: 10.3969/j.issn.1673-5374.2013.33.002

Kato, M., Motoki, M., Isaji, T., Suzuki, T., Kawai, Y., and Ohkubo, N. (2015). Spinal cord injury after endovascular treatment for thoracoabdominal aneurysm or dissection. *Eur. J. Cardiothorac. Surg.* 48, 571–577. doi: 10.1093/ejcts/ezu497

Li, R., Huang, Z. C., Cui, H. Y., Huang, Z. P., Liu, J. H., Zhu, Q. A., et al. (2021). Utility of somatosensory and motor-evoked potentials in reflecting gross and fine motor functions after unilateral cervical spinal cord contusion injury. *Neural Regen. Res.* 16, 1323–1330. doi: 10.4103/1673-5374.301486

Li, R., Li, H. L., Cui, H. Y., Huang, Y. C., and Hu, Y. (2023). Identification of injury type using somatosensory and motor evoked potentials in a rat spinal cord injury model. *Neural Regen. Res.* 18, 422–427. doi: 10.4103/1673-5374.346458

Li, R., Zhao, K., Ruan, Q., Meng, C., and Yin, F. (2020). Bone marrow mesenchymal stem cell-derived exosomal micro RNA-124-3p attenuates neurological damage in spinal cord ischemia-reperfusion injury by downregulating ern 1 and promoting M2 macrophage polarization. *Arthritis Res. Ther.* 22:75. doi: 10.1186/s13075-020-2146-x

Malinovic, M., Walker, J., and Lee, F. (2021). Ischemia-reperfusion injury after posterior cervical laminectomy. *Cureus* 13:e18298. doi: 10.7759/cureus.18298

Mathkour, M., Werner, C., Riffle, J., Scullen, T., Dallapiazza, R. F., Dumont, A., et al. (2020). Reperfusion "white cord" syndrome in cervical Spondylotic myelopathy: does mean arterial pressure goal make a difference? Additional case and literature review. *World Neurosurg.* 137, 194–199. doi: 10.1016/j.wneu.2020.01.062

Mukai, A., Suehiro, K., Kimura, A., Fujimoto, Y., Funao, T., Mori, T., et al. (2022). Protective effects of remote ischemic preconditioning against spinal cord ischemia-reperfusion injury in rats. *J. Thorac. Cardiovasc. Surg.* 163, e137–e156. doi: 10.1016/j.jtcvs.2020.03.094

Na, H. S. T., Nuo, M., Meng, Q. T., and Xia, Z. Y. (2019). The pathway of let-7a-1/2-3p and HMGB1 mediated Dexmedetomidine inhibiting microglia activation in spinal cord ischemia-reperfusion injury mice. *J. Mol. Neurosci.* 69, 106–114. doi: 10.1007/s12031-019-01338-4

Nagarajan, P. P., Tora, M. S., Neill, S. G., Federici, T., Texakalidis, P., Donsante, A., et al. (2021). Lentiviral-induced spinal cord gliomas in rat model. *Int. J. Mol. Sci.* 22:12943. doi: 10.3390/ijms222312943

Papaioannou, I., Repantis, T., Baikousis, A., and Korovessis, P. (2019). Late-onset "white cord syndrome" in an elderly patient after posterior cervical decompression and fusion: a case report. *Spinal Cord Ser. Cases* 5:28. doi: 10.1038/s41394-019-0174-z

Park, J., Cho, Y. E., Park, M., Lee, J., Kim, D., and Park, Y. G. (2021). Correlation between preoperative somatosensory evoked potentials and intraoperative neurophysiological monitoring in spinal cord tumors. *J. Clin. Monit. Comput.* 35, 979–991. doi: 10.1007/s10877-020-00584-x

Rong, Y., Fan, J., Ji, C., Wang, Z., Ge, X., Wang, J., et al. (2022). USP11 regulates autophagy-dependent ferroptosis after spinal cord ischemia-reperfusion injury by deubiquitinating Beclin 1. *Cell Death Differ.* 29, 1164–1175. doi: 10.1038/s41418-021-00907-8

Vidal, P. M., Karadimas, S. K., Ulndreaj, A., Laliberte, A. M., Tetreault, L., Forner, S., et al. (2017). Delayed decompression exacerbates ischemia-reperfusion injury in cervical compressive myelopathy. *JCI Insight* 2:e92512. doi: 10.1172/jci.insight.92512

Zhao, L., Zhai, M., Yang, X., Guo, H., Cao, Y., Wang, D., et al. (2019). Dexmedetomidine attenuates neuronal injury after spinal cord ischaemia-reperfusion injury by targeting the CNPY2-endoplasmic reticulum stress signalling. *J. Cell. Mol. Med.* 23, 8173–8183. doi: 10.1111/jcmm.14688

Zheng, S. Y., Sun, F. L., Tian, X., Zhu, Z. X., Wang, Y. F., Zheng, W. R., et al. (2023, 2023). Roles of Eph/ephrin signaling pathway in repair and regeneration for ischemic cerebrovascular and cardiovascular diseases. *J Neurorestoratol.* 11:100040. doi: 10.1016/j.jnrt.2022.100040

frontiers | Frontiers in Neuroscience

TYPE Original Research
PUBLISHED 25 October 2024
DOI 10.3389/fnins.2024.1421917

OPEN ACCESS

EDITED BY
Ana Semeano,
Northeastern University, United States

REVIEWED BY
Shalini Narayana,
University of Tennessee Health Science Center (UTHSC), United States
Byung-Euk Joo,
Soonchunhyang University Hospital Seoul, Republic of Korea

*CORRESPONDENCE
Jung Bin Kim
✉ kjbin80@korea.ac.kr
Hayom Kim
✉ neurohy3@korea.ac.kr

†These authors have contributed equally to this work and share first authorship

RECEIVED 23 April 2024
ACCEPTED 07 October 2024
PUBLISHED 25 October 2024

CITATION
So M, Kong J, Kim Y-T, Kim K-T, Kim H, Kim JB (2024) Increased cerebellar vermis volume following repetitive transcranial magnetic stimulation in drug-resistant epilepsy: a voxel-based morphometry study.

Front. Neurosci. 18:1421917.
doi: 10.3389/fnins.2024.1421917

Increased cerebellar vermis volume following repetitive transcranial magnetic stimulation in drug-resistant epilepsy: a voxel-based morphometry study

Mingyeong So[1†], Jooheon Kong[1†], Young-Tak Kim[2,3], Keun-Tae Kim[4], Hayom Kim[1*] and Jung Bin Kim[1*]

[1]Department of Neurology, Korea University Anam Hospital, Korea University College of Medicine, Seoul, Republic of Korea, [2]Department of Radiology, Massachusetts General Hospital, Harvard Medical School, Boston, MA, United States, [3]Department of Biomedical Sciences, Korea University College of Medicine, Seoul, Republic of Korea, [4]Department of Convergence Medicine, Korea University College of Medicine, Seoul, Republic of Korea

Introduction: Voxel-based morphometry (VBM) was applied to explore structural changes induced by repetitive transcranial magnetic stimulation (rTMS) and the relationship with clinical outcomes. Moreover, the relationship between each segmented regional gray matter (GM) volume was investigated to identify circuits involved in the rTMS treatment process in patients with drug-resistant epilepsy (DRE).

Methods: Nineteen patients with DRE were finally included in the analysis. A session of rTMS was applied for 5 consecutive days. Participants received either 1,000 or 3,000 pulses, at a frequency of 0.5 Hz and the intensity was set at 90% of the individual's resting motor threshold. VBM analysis was performed to explore regional GM volume changes 2 months after rTMS application. The regional volume change was correlated with seizure reduction rate. Relationships between changes in GM volume in each anatomically parcellated region were analyzed using a fully-automated segmentation pipeline.

Results: Compared to the baseline, seizure frequency was reduced, and quality of life was improved after rTMS treatment. Regional volume was increased in the cerebellar vermis 2 months after rTMS application. The increased cerebellar vermis volume correlated with the reduced seizure frequency. Regional volume changes in the cerebellar vermis were correlated with changes in the subcortical and cortical GM regions including the thalamus, caudate, and frontal cortex.

Discussion: These results indicate that rTMS treatment effectively reduced seizure frequency in patients with DRE. Increased volume in the cerebellar vermis and activations of the cerebello-thalamo-cortical circuit may be a crucial mechanism underlying the effectiveness of rTMS application in patients with DRE.

KEYWORDS

repetitive transcranial magnetic stimulation, voxel-based morphometry, cerebellum, vermis, drug-resistant epilepsy

1 Introduction

Repetitive transcranial magnetic stimulation (rTMS) has been paid attention as a non-invasive treatment alternative for patients with drug-resistant epilepsy (DRE) (Carrette et al., 2016; Fregni et al., 2006; Sun et al., 2012). However, prior findings regarding its therapeutic efficacy are inconsistent (Cooper et al., 2018; Mishra et al., 2020; Tsuboyama et al., 2020), and even studies that have shown effective outcomes could not clearly elucidate the mechanisms underlying mitigating seizure activities, limiting its practical application in clinical settings for treatment of DRE. While it is widely accepted that low-frequency rTMS is beneficial for epilepsy treatment by modulating cortical excitability and reducing synaptic strength via long-term depression (LTD) at the synaptic level (Fregni et al., 2006; Kinoshita et al., 2005; Sun et al., 2012; Tergau et al., 1999; Theodore et al., 2002), the mechanisms of its effectiveness in DRE at a macroscopic neuroanatomical level remain elusive. If a sufficient understanding of the mechanism of rTMS being effective in treating DRE is achieved, clinical usability could be enhanced by optimizing the stimulation protocol, which includes intensity, the number of pulses, and especially target region.

It is well-known that the functioning of the human brain should be understood in the context of its functional connectivity (FC), rather than by the activity of specific regions (Power et al., 2011). Since epilepsy is considered as a network disorder (Spencer, 2002; van Diessen et al., 2013), in order to understand the mechanism of rTMS effect in DRE, a large-scale network approach at the whole brain level may be appropriate. Hence, exploring the anatomical correlates affected by rTMS treatment and identifying the potential circuits connected to those regions could not only help to elucidate the mechanisms involved in the effect for treatment of DRE, but also provide valuable information such as quantitatively evaluating the treatment effect and determining the stimulation target region.

Voxel-based morphometry (VBM) is a fully automated, unbiased, operator-independent magnetic resonance imaging (MRI) analysis technique that is widely used to detect subtle structural differences between groups of subjects, as well as those between before and after treatment (Ashburner and Friston, 2000; Kim et al., 2023). Several lines of evidence indicate that VBM could demonstrate the neuroplastic effects. Changes in gray matter (GM) volume were found in healthy individuals applied rTMS during cognitive tasks and patients with tinnitus following rTMS treatment (Jung and Lambon Ralph, 2016, 2021; Lehner et al., 2014; Poeppl et al., 2018). These findings revealed the potential of rTMS to induce significant structural changes, as well as VBM could be an appropriate tool for identifying the relevant brain regions in the context of neural plasticity.

To the best of our knowledge, there is currently no study investigating brain structural changes following application of rTMS in patients with DRE. In the present study, we applied VBM to explore structural changes affected by rTMS and their relationships with clinical effectiveness such as seizure reduction rate and improved quality of life. In addition, we aimed to investigate the connectivity between regional volume changes found in VBM after rTMS and those in other parcellated GM regions to explore the circuits affected by rTMS in patients with DRE. We hypothesized that the GM volume of specific regions would change after rTMS and be associated with the clinical effectiveness of rTMS in patients with DRE. Our hypothesis was based on the well-established involvement of the thalamocortical tract, as well as other areas implicated in seizure propagation—such as the cerebellum, frontal cortex, and temporal regions—would exhibit changes in GM volume following rTMS. Additionally, we anticipated that the connectivity between these regions, known to play a crucial role in epileptic networks, would reflect shared patterns of volume change.

2 Materials and methods

2.1 Participants

The eligibility criteria for study inclusion were as follows: participants aged 20–70 years, diagnosed with focal drug-resistant epilepsy (DRE) that has not responded to at least two appropriate antiseizure medications (ASMs) without changes in the ASM regimen for a duration of 6 months prior to enrollment in the study. Only DRE patients having electroclinical features and MRI findings indicative of focal cortical dysplasia (FCD) or mesial temporal lobe epilepsy (MTLE) were included. In this study, 10 DRE patients with FCD and 10 with MTLE were prospectively recruited. Within each group of 10 patients, 5 were randomly assigned to receive either 1,000 or 3,000 pulses of rTMS (**Figure 1**). The required seizure frequency for inclusion was at least one focal to generalized seizure per month and/or two focal seizures per month. The exclusion criteria were as follows: (1) contraindications for rTMS (implanted with intracranial metal devices, pacemakers, or other electrical medical devices); (2) potential for pregnancy or lactating; (3) contraindicated for neuroimaging; (4) psychiatric disorders or currently taking antipsychotic medications; (5) history of cardiovascular diseases, especially arrhythmias, neurological disorder other than epilepsy, or progressive systemic diseases; (6) skull fractures or who had undergone major brain surgery, (7) clinical dementia rating (CDR) score of more than 2 points.

The study followed the ethical guidelines of the Declaration of Helsinki and was approved by the Ministry of Food and Drug Safety of Korea (No. 1251) and the institutional review board of the Korea University Anam Hospital (No. 2021AN0584). Informed consent was obtained from all individual participants included in the study.

2.2 Clinical assessments

The primary efficacy outcome of rTMS was the seizure reduction rate at 2 months. The secondary outcomes included changes in quality of life, depressive symptom, and anxiety, which were measured by the Quality of Life in Epilepsy Inventory-10 (QOLIE-10) (Cramer et al., 1996), Beck Depression Inventory (BDI) (Beck et al., 1987), and Hospital Anxiety and Depression Scale (HADS) (Bjelland et al., 2002) at baseline and 2 months following rTMS applications.

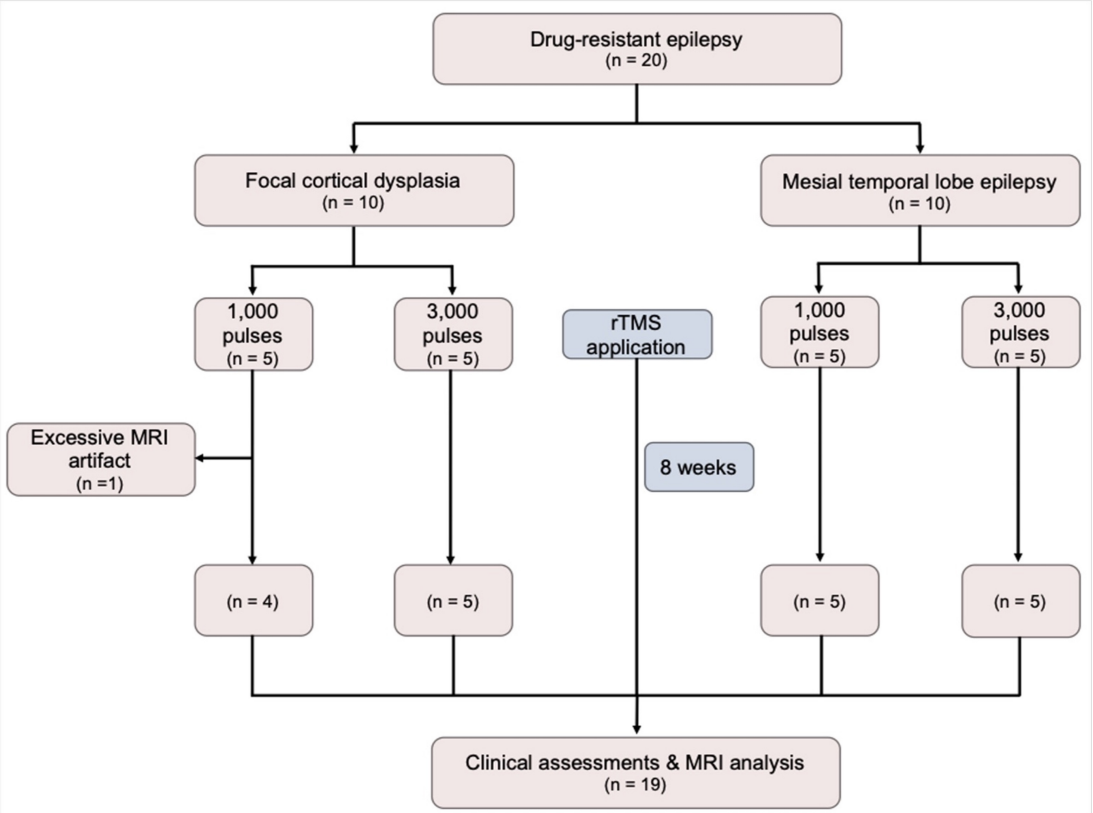

FIGURE 1
A flow diagram of the study. MRI, magnetic resonance imaging; rTMS, repetitive transcranial magnetic stimulation.

2.3 Repetitive transcranial magnetic stimulation

A session of rTMS was provided for five consecutive days. Participants were seated in specialized chair designed to minimize body movements, ensuring targeted specific stimulation area. Stimulations were delivered to the Pz electrode region following the extended international 10–20 system for electroencephalography electrode placement (Klem et al., 1999), utilizing the ALTMS® device with a figure-eight coil (REMED, Korea). The resting motor evoked potential threshold was determined as the minimum stimulus intensity required to induce contraction of the right thumb at least five times through the stimulation of the left motor cortex ten times. Participants received either 1,000 or 3,000 pulses, with a frequency of 0.5 Hz and an intensity of 90% of the individual's resting motor threshold. Participants assigned to receive 1,000 pulses were blinded to receiving 2,000 sham stimuli. For sham stimulation, no active stimulation was delivered, while providing simulated stimulator noise of the same frequency (i.e., 0.5 Hz) as for the active stimulation. The rTMS parameters (i.e., stimulation frequency, stimulation intensity, and coil type) were selected based on previous studies, with reference to the most commonly used parameters in clinical trials conducted on patients with DRE. In previous studies, the number of daily pulses ranged widely from 100 to 3,000, with randomized controlled trials typically applying a minimum of 1,000 pulses (Carrette et al., 2016). Based on this prior experience, we selected 1,000 pulses to represent a lower dose and 3,000 pulses to represent a higher dose for the purpose of this study. Additionally, Pz was chosen as the stimulation target area for several reasons. First, in the MTLE group, direct rTMS stimulation of the seizure focus was deemed unfeasible; however, indirect modulation through FC was considered possible by targeting the cortical area. Furthermore, considering the laterality of the seizure focus in MTLE, the cortical area located at the midline was determined to be appropriate for modulating the seizure focus through FC. Second, patients with FCD may have undemonstrated multiple seizure foci or dual pathology. Therefore, it was hypothesized that stimulating a common area with widespread connectivity across all participants could be more efficient than targeting a single site documented as a seizure focus. Third, Pz was selected due to its reflection of posterior cingulate cortex activity, a key node of the default mode network with strong resting-state FC, and its link to the limbic system. Consequently, it was expected that rTMS delivered to this region might be effective for both FCD and MTLE patients. A schematic overview of the study design is shown in Figure 2.

2.4 MRI acquisition

MRI scans were acquired using a 3.0 Tesla scanner (Trio whole-body imaging system, Siemens Medical Systems, Iselin, NJ). A T1-weighted magnetization-prepared rapid gradient echo sequence was used (repetition time [TR] = 2300 ms, echo time

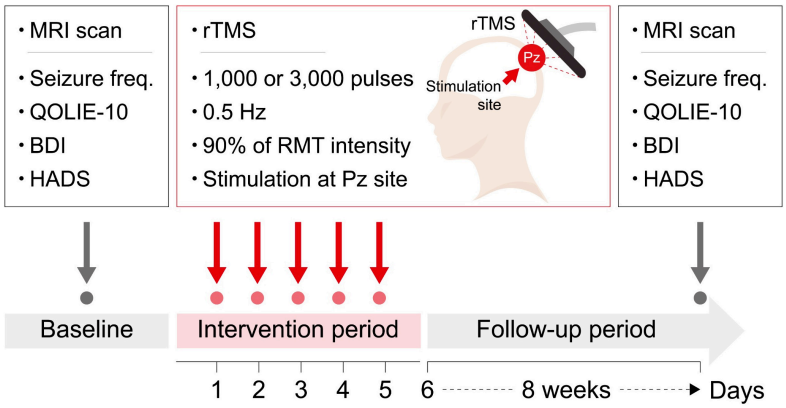

FIGURE 2
A schematic overview of the study design. Beck Depression Inventory; HADS, Hospital Anxiety and Depression Scale; Seizure freq, seizure frequency; QOLIE-10, Quality of Life in Epilepsy Inventory-10; BDI, RMT, resting motor threshold; rTMS, repetitive transcranial magnetic stimulation.

TABLE 1 Demographics and clinical characteristics.

	FCD (*n* = 9)	MTLE (*n* = 10)	*P*-value	1,000 pulses (*n* = 9)	3,000 pulses (*n* = 10)	*P*-value
Age, years (SD)	45.11 (15.81)	49.10 (11.52)	0.535	47.11 (10.89)	47.30 (16.06)	0.977
Women, *n* (%)	6 (66.7)	9 (90.0)	0.303	6 (66.7)	9 (90.0)	0.303
Education, years (SD)	11.44 (2.70)	10.90 (4.61)	0.761	12.67 (3.64)	9.80 (3.42)	0.095
Number of antiseizure medications (SD)	3.44 (1.24)	3.90 (1.37)	0.459	3.67 (0.87)	3.70 (1.64)	0.956
Mini-mental status examination (SD)	25.50 (3.50)	26.70 (3.20)	0.459	27.00 (3.28)	25.33 (3.28)	0.297
Hypertension, *n* (%)	2 (22.2)	0 (0.0)	0.211	1 (11.1)	1 (10.0)	1.000
Diabetes, *n* (%)	0 (0.0)	0 (0.0)	NA	0 (0.0)	0 (0.0)	NA
Dyslipidemia, *n* (%)	2 (22.2)	1 (10.0)	0.582	1 (11.1)	2 (20.0)	1.000
Alcohol drinking, *n* (%)	1 (11.1)	1 (10.0)	1.000	2 (22.2)	0 (0.0)	0.211
Smoking, *n* (%)	1 (11.1)	0 (0.0)	0.474	0 (0.0)	1 (10.0)	1.000

FCD, focal cortical dysplasia; MTLE, mesial temporal lobe epilepsy.

[TE] = 2.13 ms, field of view = 256 mm, matrix size = 256 × 256; voxel size = 1.0 × 1.0 × 1.0 mm3, and flip angle = 9°) for volumetric analysis.

2.5 Voxel-based morphometry

SPM12[1] was used for data preprocessing and analysis, and VBM was used with DARTEL (Ashburner, 2007). Briefly, the preprocessing included the following steps (Ashburner and Friston, 2000): (1) segmentation, (2) create a template, (3) normalization to Montreal Neurological Institute (MNI) space, and (4) smoothing the modulated GM volume. Detailed procedures are described in our previous works (Kim et al., 2014; Kim et al., 2023).

Differences in the GM volume between the baseline and 2 months after application of rTMS were examined using a paired *t*-test. An absolute GM threshold of 0.2 was used to avoid the possible edge effects around the border between the GM and white matter. Statistical significance was set at a height threshold of $P < 0.001$ and an extent threshold of cluster-level $P < 0.05$, corrected for multiple comparisons using familywise error (FWE). In addition to the overall group analysis before and after rTMS, subgroup analyses were conducted separately for the FCD and MTLE groups, and for the groups that received 1,000 and 3,000 pulses, respectively.

2.6 Regional volume connectivity analysis

Fully automated segmentation of the brain was performed using the vol2brain program[2] (Manjon et al., 2022), which implements a multi-atlas patch-based label fusion segmentation. Single anonymized compressed MRI T1-weighted Nifti files were

1 http://www.fil.ion.ucl.ac.uk/spm

2 https://www.volbrain.net/services/vol2Brain

TABLE 2 Clinical outcome following rTMS.

FCD				MTLE			
Outcome measurements	Baseline	After rTMS	*P*-value	Outcome measurements	Baseline	After rTMS	*P*-value
Seizure frequency (per month)	7.89 (3.14)	6.00 (4.92)	0.029	Seizure frequency (per month)	11.30 (9.88)	7.50 (9.85)	0.006
QOLIE-10	9.33 (4.24)	6.56 (9.08)	0.148	QOLIE-10	13.50 (6.87)	9.20 (5.45)	0.055
BDI	10.00 (8.97)	9.22 (9.50)	0.785	BDI	12.40 (10.96)	15.50 (9.38)	0.297
HADS-anxiety	5.00 (3.16)	5.33 (4.47)	0.843	HADS-anxiety	5.90 (4.46)	6.70 (3.62)	0.423
HADS-depression	6.33 (3.64)	7.11 (5.08)	0.648	HADS-depression	8.80 (4.80)	9.80 (3.33)	0.591
1,000 pulses				3,000 pulses			
Outcome measurements	Baseline	After rTMS	*P*-value	Outcome measurements	Baseline	After rTMS	*P*-value
Seizure frequency (per month)	9.44 (7.75)	6.22 (9.47)	0.024	Seizure frequency (per month)	9.90 (7.68)	7.30 (6.27)	0.048
QOLIE-10	13.89 (9.47)	9.00 (5.77)	0.014	QOLIE-10	9.40 (6.29)	7.00 (8.67)	0.388
BDI	11.33 (7.63)	15.00 (10.61)	0.246	BDI	11.20 (11.95)	10.30 (8.79)	0.738
HADS-anxiety	6.33 (3.20)	6.22 (3.23)	0.919	HADS-anxiety	4.70 (4.32)	5.90 (4.75)	0.425
HADS-depression	8.67 (2.06)	9.22 (4.26)	0.759	HADS-depression	6.70 (5.68)	7.90 (4.56)	0.499

BDI, Beck Depression Inventory; FCD, focal cortical dysplasia; HADS, Hospital Anxiety and Depression Scale; MTLE, mesial temporal lobe epilepsy; QOLIE-10, Quality of Life in Epilepsy Inventory-10; rTMS, repetitive transcranial magnetic stimulation.

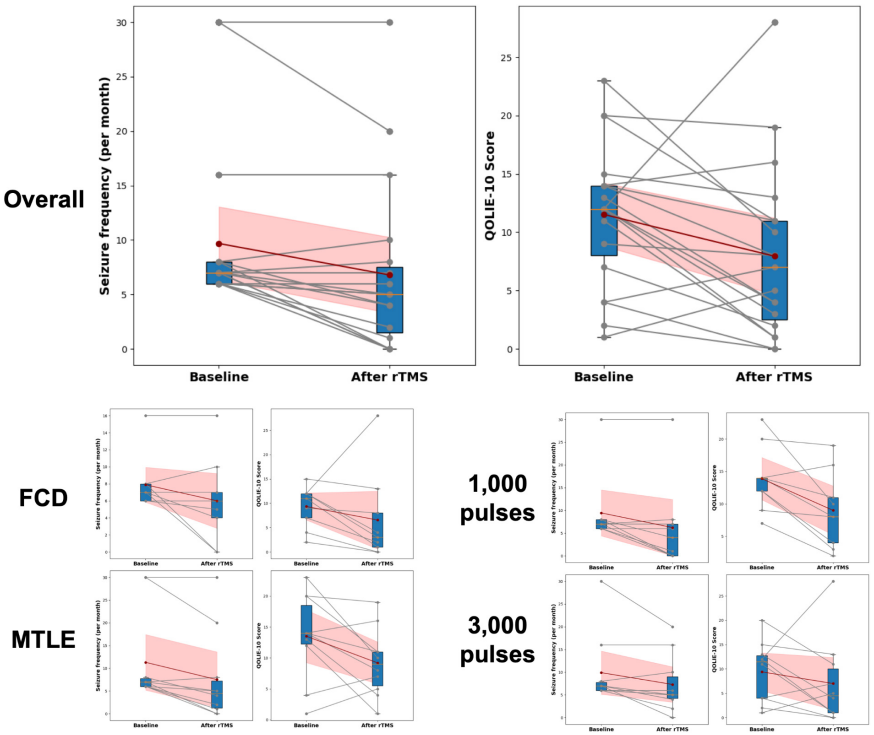

FIGURE 3
Changes in seizure frequency and Quality of Life in Epilepsy Inventory-10 (QOLIE-10) following rTMS. Changes in seizure frequency and QOLIE-10 before and after rTMS treatment are presented. The box plots summarize the distribution of scores at each time point, indicating median, interquartile ranges, and outliers. Individual changes in seizure frequency and QOLIE-10 scores for each participant are shown with gray lines connecting the baseline and post-treatment (After rTMS) values, with corresponding dots marking the actual scores. The red dots represent the mean seizure frequency and QOLIE-10 scores at baseline and after treatment, connected by a dark red line to highlight the average trend in score changes. The shaded red area indicates the 95% Confidence Interval (CI) around the mean changes. FCD, focal cortical dysplasia; MTLE, mesial temporal lobe epilepsy; QOLIE-10, Quality of Life in Epilepsy Inventory-10.

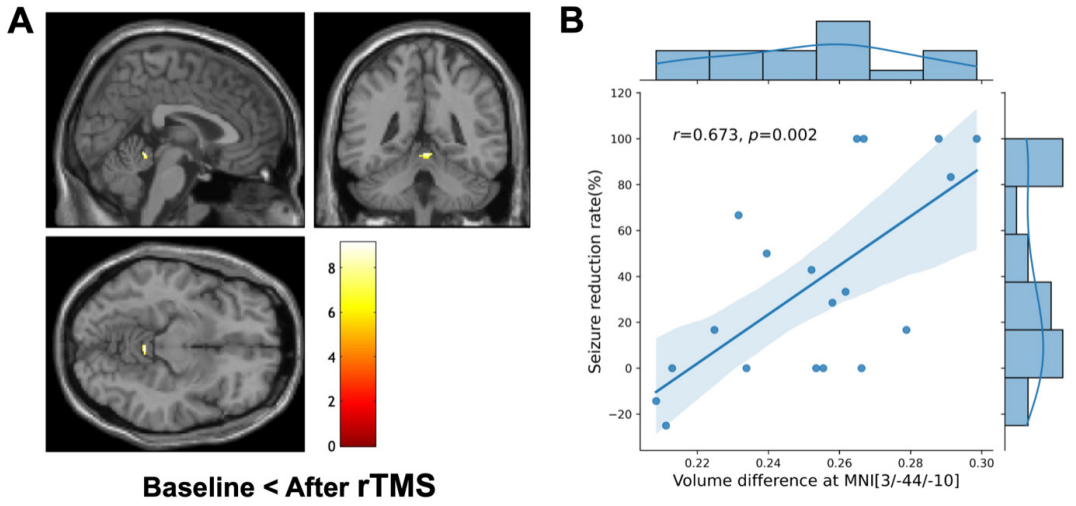

FIGURE 4
Voxel-based morphometry (VBM) and clinical correlation. **(A)** VBM shows a significant regional increase in the cerebellar vermis (MNI coordinate = 3/−44/-10, cluster-level FWE-corrected $P = 0.015$) after repetitive transcranial magnetic stimulation (rTMS) compared to the baseline. The color bar represents the *T*-value. The left side of each picture is the left side of the brain. **(B)** Combined scatterplot and boxplot depicting the relationship between volume difference at cerebellar vermis (MNI coordinates: 3/−44/−10) and the seizure reduction rate. Each data point represents an individual participant. The amount of regional volume increases in cerebellar vermis is positively correlated with seizure reduction rate (Pearson's $r = 0.673$, $P = 0.002$). The side boxplot provides a summary distribution of the seizure reduction rates corresponding to the volume differences observed.

uploaded through a web interface. Preprocessing consists of denoising, rough inhomogeneity correction, affine registration to the MNI space, fine inhomogeneity correction, and intensity normalization. To estimate the structural properties of the participants' brains, a nonlocal intracranial cavity extraction was conducted to create a brain mask. Tissue classification into white matter, GM, and cerebral spinal fluid was conducted on this mask. The pipeline segmented the brain into 116 GM regions including bilateral 9 subcortical and 49 cortical areas (17 frontal, 6 parietal, 8 temporal, 8 occipital, 5 limbic, and 5 insular). In addition, macrostructures including brainstem and cerebellar vermis were segmented. According to the purposes of this study, we were interested in 32 regions as follows: (1) 9 subcortical GM volumes in each side, (2) 6 integrated cortical GM volume, which is the sum of the volumes of each segmented region of the corresponding lobe (i.e., frontal, parietal, temporal, occipital, limbic, and insular cortices) in each side, and (3) brainstem and cerebellar vermis volumes. The connectivity between regions exhibiting volumetric changes post-rTMS, as identified by VBM, and other segmented GM regions was investigated using Pearson's correlation analysis, with a Bonferroni-corrected significance threshold of $P < 0.0016$.

2.7 Statistical analysis

Demographics and clinical characteristics were compared between FCD and MTLE groups, as well as between 1,000 and 3,000 pulses groups using independent *t*-test or χ^2 test, where appropriate ($P < 0.05$). Clinical variables were compared between the baseline and 2 months after application of rTMS using a paired *t*-test ($P < 0.05$). Voxel values were extracted from the significant cluster in the VBM analysis and were correlated with seizure reduction rate and QOLIE-10 using the Pearson's correlation ($P < 0.05$).

3 Results

Twenty patients with DRE (10 FCD and 10 MTLE) were initially included in this study. Of those, 1 FCD patient who had been received 1,000 pulses was excluded because of excessive artifact, resulting in a total of 19 patients finally included in the analysis. During the application of rTMS, no adverse effects such as headaches, scalp discomfort, seizures, muscle twitching, or burns were observed. Demographics and clinical characteristics are presented in Table 1. The FCD and MTLE groups did not differ in the age, sex, number of ASMs, MMSE, the proportion of hypertension, diabetes, dyslipidemia, alcohol drinkers, and smokers. There were no differences in all demographic and clinical characteristics between patients who received 1,000 pulses and those who received 3,000 pulses.

Clinical outcomes for rTMS application are presented in Table 2 and Figure 3. Compared with the baseline, the seizure frequency was reduced 2 months after application of rTMS ($P < 0.001$). Quality of life measured by QOLIE-10 was improved after rTMS treatment, relative to the baseline ($P = 0.033$). The BDI, HADS-anxiety, and HADS-depression scores were not changed after application of rTMS.

VBM showed a significant increase in regional GM volume in the cerebellar vermis (MNI coordinates of local maxima = 3/−44/-10, extent threshold k = 30 voxels, cluster-level FWE-corrected $P = 0.015$, Figure 4A). No area of decreased GM volume was found after rTMS at the same threshold. The amount of regional volume increases in cerebellar vermis was positively correlated with seizure reduction rate ($r = 0.673$, $P = 0.002$, Figure 4B). The volume

TABLE 3 Correlation analysis between volume changes in cerebellar vermis and other gray matter regions.

Regions	Laterality	Pearson's rho	*P*-value
Thalamus	L	0.859957	**0.000002**
Ventral diencephalon	R	0.850665	**0.000004**
Parietal cortex	R	0.847898	**0.000005**
Temporal cortex	R	0.832361	**0.000010**
Brainstem	-	0.829929	**0.000011**
Caudate	L	0.824634	**0.000014**
Accumbens	R	0.806231	**0.000031**
Frontal cortex	R	0.788191	**0.000061**
Frontal cortex	L	0.788076	**0.000061**
Caudate	R	0.770773	**0.000112**
Thalamus	R	0.687362	**0.001147**
Putamen	L	0.680551	**0.001342**
Putamen	R	0.663134	0.001969
Accumbens	L	0.659759	0.002116
Occipital cortex	L	0.615310	0.005044
Parietal cortex	L	0.610985	0.005453
Pallidum	L	0.604463	0.006119
Amygdala	L	0.593354	0.007407
Temporal cortex	L	0.569967	0.010841
Basal forebrain	R	0.548170	0.015101
Ventral diencephalon	L	0.546885	0.015388
Hippocampus	L	0.516099	0.023693
Hippocampus	R	0.454225	0.050744
Basal forebrain	L	0.442558	0.057770
Insular cortex	R	0.385516	0.103086
Occipital cortex	R	0.383489	0.105066
Insular cortex	L	0.320936	0.180337
Amygdala	R	−0.255962	0.290185
Pallidum	R	0.077314	0.753069
Limbic cortex	L	0.018814	0.939064
Limbic cortex	R	−0.005000	0.983793

Bold font denotes statistical significance (Bonferroni-corrected $P < 0.0016$). L, left; R, right.

changes in cerebellar vermis were not correlated with the QOLIE-10, BDI, HADS-anxiety, and HADS-depression scores. No GM volume changes were observed in the subgroup analyses conducted based on each etiology (i.e., FCD and MTLE) and the number of stimulation pulses (i.e., 1,000 and 3,000) at the same threshold.

The connectivity of volume changes between the 32 GM regions is presented in Figure 5. Significant correlations were found between volume changes in the cerebellar vermis and those in the bilateral thalamus, caudate, frontal cortices, right ventral diencephalon, parietal and temporal cortices, and accumbens, as well as the left putamen and brainstem ($P < 0.0016$). Results of correlation analyses are detailed in Table 3. In the subgroup analyses, the MTLE group showed volume changes in the bilateral thalamus that correlated with those in the vermis. In the FCD group, regions correlated with volume changes in the vermis included the brainstem, temporal cortex, parietal cortex, and left thalamus. When 1,000 pulses were applied, volume changes in the right ventral diencephalon correlated with those in the vermis, whereas in the group that received 3,000 pulses, volume changes in the left thalamus, right temporal cortex, brainstem, and left caudate correlated with vermis volume changes. Results of subgroup analyses are presented in Supplementary Figure 1 and Supplementary Tables 1, 2.

4 Discussion

We investigated the acute effects of rTMS on GM volumes in patients with DRE. The major findings were as follows: (1) regional volume was increased in the cerebellar vermis 2 months after rTMS application, (2) the increased volume in the cerebellar vermis was correlated with reduced seizure frequency, and (3) regional volume changes in the cerebellar vermis were correlated with those in subcortical and cortical GM regions including thalamus, caudate, and frontal cortex.

The cerebellum, traditionally known to be associated with motor functions, has been increasingly recognized for its involvement in the role in the pathophysiological mechanisms underlying epilepsy (Kim et al., 2019; Krook-Magnuson et al., 2014; Stieve et al., 2023; Streng et al., 2023; Streng and Krook-Magnuson, 2021; Wang et al., 2023; Zhou et al., 2021). The vulnerability of the cerebellum in epilepsy is a well-established phenomenon supported by a variety of studies highlighting its susceptibility to injury, neurodegeneration, excitotoxic damage, neuron loss, and oxidative stress in the context of seizure disorder (Froula et al., 2023; Kerestes et al., 2024; Lawson et al., 2000; Lomoio et al., 2011; Lores Arnaiz et al., 1998; Streng et al., 2023; Streng and Krook-Magnuson, 2021). These cerebellum's susceptibility to damage could be implicated in the mechanisms underlying seizure initiation and epileptogenesis. Moreover, the vulnerability can potentially contribute to comorbidities and negative outcomes in epilepsy, such as cognitive impairments, altered regulatory processes, and sudden unexpected death in epilepsy (SUDEP) (Hellwig et al., 2013; Wang et al., 2023), as damage to the cerebellum can further impair the neurological function in patients with epilepsy. These observations have spurred interest in the cerebellum as a potential target for novel therapeutic interventions aimed at mitigating the burdens of epilepsy. Indeed, studies employing cerebellar neuromodulation have shown promising results, including reduced seizure frequency and severity in some patients with DRE (Krook-Magnuson et al., 2014; Piper et al., 2022; Stieve et al., 2023; Streng and Krook-Magnuson, 2021). These findings not only validated the cerebellum's role in epilepsy but also highlighted the potential of cerebellar-targeted interventions to enhance treatment outcomes for patients. Taken together, the cerebellum has been implicated in the pathogenesis of seizure onset as well as a variety of complications in patients with epilepsy, making it a potential target for neuromodulations. Notably, we

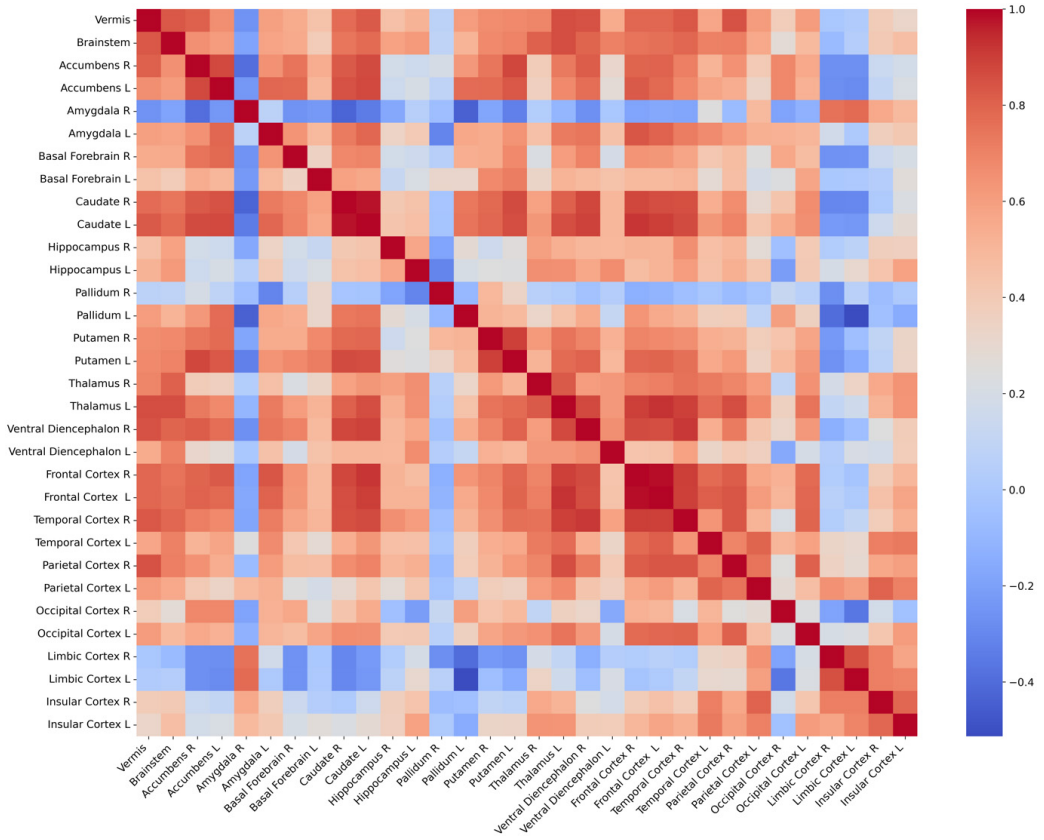

FIGURE 5
Connectivity matrix between 32 regional volume changes. Each cell in the heatmap of correlation matrix represents the Pearson's correlation coefficient between the volumes of two brain regions. Red denotes positive correlations, blue denotes negative correlations, and white denotes neutral correlations. L, left; R, right.

found that the volume changes in left thalamus exhibited significant correlations with those in vermis in most individual groups and in the overall group. These results suggest that the cerebellar vermis and thalamus are involved in the epileptic network regardless of etiology. This finding further supports our hypothesis that the cerebello-thalamo-cortical network may serve as a key target for effective rTMS treatment aimed at reducing seizures.

An increase volume found in VBM usually is usually understood as increased function in the corresponding area (Kim et al., 2023). Therefore, we speculate that our findings of increased volume in the cerebellar vermis after rTMS treatment could be interpreted as enhanced function of the cerebellar vermis area in mediating the pathological condition of DRE patients through rTMS-induced activations of inhibitory interneurons. Several lines of evidence indicate that neural plasticity could be induced by various stimulations, even by cognitive tasks (Jung and Lambon Ralph, 2016, 2021; Lehner et al., 2014; May et al., 2007; Poeppl et al., 2018). Volumetric analysis of MRI has demonstrated the structural changes in association with neural plasticity, sensitively (Jung and Lambon Ralph, 2021; Lehner et al., 2014; May et al., 2007; Poeppl et al., 2018). Given the interpretability of structural changes in the perspective of neural plasticity, our findings of volume increases in the cerebellar vermis and their relationship with reduced seizure frequency could be considered as consequences of therapeutic effects by rTMS-induced neural plasticity in patients with DRE.

It is unclear why rTMS applied to the parietal cortex at the Pz electrode attachment location in patients with DRE resulted in changes in the volume of the cerebellar vermis region away from the direct stimulation location. However, this can be explained by the knowledge that the cerebellum has multiple synapses and interconnections with a very large number of cortical and subcortical areas (Kang et al., 2021; Novello et al., 2024), suggesting that the cerebellum can be influenced through circuits connected to it, even if no direct stimulation to the cerebellum is given. Among the wide range of regions connected to the cerebellum and its circuits, our connectivity analysis of regional volume changes showed that volume changes in the cerebellar vermis following rTMS were particularly connected to those in the thalamus, caudate, frontal cortex, and brainstem. These findings are in line with previous observations that cerebellum was connected with thalamus, brainstem, and diencephalon (Novello et al., 2024), and that cerebellar stimulation could mitigate seizure activity via cerebello-thalamo-cortical pathway in patients with DRE (Eelkman Rooda et al., 2021; Piper et al., 2022). Our results suggest that stimulation of cerebellar vermis regions may be effective in the application of rTMS in patients with DRE, and that the cerebello-thalamo-cortical pathway may be the corresponding circuit that allows stimulation to produce therapeutic effects.

To the best of our knowledge, this is the first study to investigate the effect of rTMS in DRE patients in terms of neural plasticity

through VBM analysis. Our study controlled the effect of etiology and seizure focus by equally assigning the number of patients with FCD and MTLE. In addition, we evaluated the effect of rTMS and analyzed the change in GM volume after rTMS by controlling the difference between 1,000 and 3,000 pulses. Therefore, our results can be interpreted as generalizable findings that are not affected by etiology, seizure focus, or the number of pulses.

There are several limitations to our study. First, the sample size was relatively small, making our imaging findings less robust, and likely limiting our ability to detect fine structural changes in response to rTMS within each group (i.e., FCD and MTLE). With a more sufficiently powered sample size, it is plausible that distinct regions might exhibit significant structural changes in response to rTMS within each group. Future studies with larger cohorts are needed to further explore these potential differences and to confirm the findings of our study. Second, we only observed brain volume changes from baseline to 2 months later, and there is no information about serial changes and long-term effects until the rTMS effect is washed out. Additional longitudinal follow-up studies are needed to analyze long-term effects and related brain volume change patterns. Third, the interpretation of the volume connectivity results in the cerebello-thalamo-cortical region as functionally connected has an inherent limitation in the assumption. Finally, since there is no fully sham-controlled group, there are limitations in determining whether the results of VBM and regional volume change connectivity were influenced only by rTMS.

5 Conclusion

Our results indicate that rTMS treatment was effective for reducing seizure frequency in patients with DRE. Cerebellar vermis volume was increased 2 months after rTMS, and the increased volume was related to seizure reduction rate. In addition, volume changes in the cerebellar vermis were connected to those in the thalamus and frontal cortex. Our findings suggest that increased volume in the cerebellar vermis and activations of the cerebello-thalamo-cortical circuit may be a crucial mechanism underlying effectiveness of rTMS application in patients with DRE.

Data availability statement

The data analyzed in this study is subject to the following licenses/restrictions: The datasets used and/or analyzed during this study are available from the corresponding author upon reasonable request. Requests to access these datasets should be directed to Jung Bin Kim, kjbin80@korea.ac.kr.

Ethics statement

The studies involving humans were approved by the institutional review board of the Korea University Anam Hospital. The studies were conducted in accordance with the local legislation and institutional requirements. The participants provided their written informed consent to participate in this study.

Author contributions

MS: Data curation, Formal analysis, Investigation, Methodology, Validation, Visualization, Writing – original draft, Writing – review and editing. JK: Formal analysis, Investigation, Writing – review and editing. Y-TK: Data curation, Formal analysis, Investigation, Methodology, Validation, Visualization, Writing – original draft. K-TK: Investigation, Methodology, Validation, Visualization, Writing – original draft. HK: Data curation, Formal analysis, Investigation, Methodology, Validation, Visualization, Writing – original draft. JBK: Data curation, Formal analysis, Investigation, Methodology, Validation, Visualization, Writing – original draft, Writing – review and editing.

Funding

The author(s) declare financial support was received for the research, authorship, and/or publication of the article. This work was also supported by the Korea University College of Medicine and the Korea Medical Device Development Fund grant funded by the Korea government (Project Number: RS-2022-00140542). This work was also supported by a grant of the Korea Health Technology R&D Project through the Korea Health Industry Development Institute (KHIDI), funded by the Ministry of Health and Welfare, Republic of Korea (Grant Number: HI22C0946).

Acknowledgments

We would like to thank the participants themselves, all of whom contributed greatly to the successful completion of this study.

Conflict of interest

The authors declare that the research was conducted in the absence of any commercial or financial relationships that could be construed as a potential conflict of interest.

Publisher's note

Supplementary material

The Supplementary Material for this article can be found online at: https://www.frontiersin.org/articles/10.3389/fnins.2024.1421917/full#supplementary-material

References

Ashburner, J. (2007). A fast diffeomorphic image registration algorithm. *Neuroimage* 38, 95–113.

Ashburner, J., and Friston, K. J. (2000). Voxel-based morphometry–the methods. *Neuroimage* 11, 805–821.

Beck, A. T., Steer, R. A., and Brown, G. K. (1987). *Beck depression inventory*. San Antonio, TX: Psychological Corporation.

Bjelland, I., Dahl, A. A., Haug, T. T., and Neckelmann, D. (2002). The validity of the hospital anxiety and depression scale. an updated literature review. *J. Psychosom. Res.* 52, 69–77.

Carrette, S., Boon, P., Dekeyser, C., Klooster, D. C., Carrette, E., Meurs, A., et al. (2016). Repetitive transcranial magnetic stimulation for the treatment of refractory epilepsy. *Expert Rev. Neurother.* 16, 1093–1110.

Cooper, Y. A., Pianka, S. T., Alotaibi, N. M., Babayan, D., Salavati, B., Weil, A. G., et al. (2018). Repetitive transcranial magnetic stimulation for the treatment of drug-resistant epilepsy: A systematic review and individual participant data meta-analysis of real-world evidence. *Epilepsia Open* 3, 55–65. doi: 10.1002/epi4.12092

Cramer, J. A., Perrine, K., Devinsky, O., and Meador, K. (1996). A brief questionnaire to screen for quality of life in epilepsy: The QOLIE-10. *Epilepsia* 37, 577–582.

Eelkman Rooda, O. H. J., Kros, L., Faneyte, S. J., Holland, P. J., Gornati, S. V., Poelman, H. J., et al. (2021). Single-pulse stimulation of cerebellar nuclei stops epileptic thalamic activity. *Brain Stimul.* 14, 861–872. doi: 10.1016/j.brs.2021.05.002

Fregni, F., Otachi, P. T., Do Valle, A., Boggio, P. S., Thut, G., Rigonatti, S. P., et al. (2006). A randomized clinical trial of repetitive transcranial magnetic stimulation in patients with refractory epilepsy. *Ann. Neurol.* 60, 447–455.

Froula, J. M., Hastings, S. D., and Krook-Magnuson, E. (2023). The little brain and the seahorse: Cerebellar-hippocampal interactions. *Front. Syst. Neurosci.* 17:1158492. doi: 10.3389/fnsys.2023.1158492

Hellwig, S., Gutmann, V., Trimble, M. R., and van Elst, L. T. (2013). Cerebellar volume is linked to cognitive function in temporal lobe epilepsy: A quantitative MRI study. *Epilepsy Behav.* 28, 156–162. doi: 10.1016/j.yebeh.2013.04.020

Jung, J., and Lambon Ralph, M. A. (2016). Mapping the dynamic network interactions underpinning cognition: A cTBS-fMRI study of the flexible adaptive neural system for semantics. *Cereb. Cortex* 26, 3580–3590. doi: 10.1093/cercor/bhw149

Jung, J., and Lambon Ralph, M. A. (2021). The immediate impact of transcranial magnetic stimulation on brain structure: Short-term neuroplasticity following one session of cTBS. *Neuroimage* 240:118375. doi: 10.1016/j.neuroimage.2021.118375

Kang, S., Jun, S., Baek, S. J., Park, H., Yamamoto, Y., and Tanaka-Yamamoto, K. (2021). Recent advances in the understanding of specific efferent pathways emerging from the cerebellum. *Front. Neuroanat.* 15:759948. doi: 10.3389/fnana.2021.759948

Kerestes, R., Perry, A., Vivash, L., O'Brien, T. J., Alvim, M. K. M., Arienzo, D., et al. (2024). Patterns of subregional cerebellar atrophy across epilepsy syndromes: An ENIGMA-Epilepsy study. *bioRxiv* [Preprint]. doi: 10.1101/2023.10.21.562994

Kim, J. B., Suh, S. I., Seo, W. K., Oh, K., Koh, S. B., and Kim, J. H. (2014). Altered thalamocortical functional connectivity in idiopathic generalized epilepsy. *Epilepsia* 55, 592–600.

Kim, J. H., Kim, J. B., and Suh, S. I. (2019). Alteration of cerebello-thalamocortical spontaneous low-frequency oscillations in juvenile myoclonic epilepsy. *Acta Neurol. Scand.* 140, 252–258. doi: 10.1111/ane.13138

Kim, K. T., Kim, H., Kong, J., and Kim, J. B. (2023). Enhanced functional connectivity in the reward circuitry in healthy adults with weekend catch-up sleep. *Hum. Brain Mapp.* 44, 4927–4937. doi: 10.1002/hbm.26429

Kinoshita, M., Ikeda, A., Begum, T., Yamamoto, J., Hitomi, T., and Shibasaki, H. (2005). Low-frequency repetitive transcranial magnetic stimulation for seizure suppression in patients with extratemporal lobe epilepsy–a pilot study. *Seizure* 14, 387–392. doi: 10.1016/j.seizure.2005.05.002

Klem, G. H., Luders, H. O., Jasper, H. H., and Elger, C. (1999). The ten-twenty electrode system of the international federation. The international federation of clinical neurophysiology. *Electroencephalogr. Clin. Neurophysiol. Suppl.* 52, 3–6.

Krook-Magnuson, E., Szabo, G. G., Armstrong, C., Oijala, M., and Soltesz, I. (2014). Cerebellar directed optogenetic intervention inhibits spontaneous hippocampal seizures in a mouse model of temporal lobe epilepsy. *eNeuro* 1. doi: 10.1523/ENEURO.0005-14.2014

Lawson, J. A., Vogrin, S., Bleasel, A. F., Cook, M. J., and Bye, A. M. (2000). Cerebral and cerebellar volume reduction in children with intractable epilepsy. *Epilepsia* 41, 1456–1462.

Lehner, A., Langguth, B., Poeppl, T. B., Rupprecht, R., Hajak, G., Landgrebe, M., et al. (2014). Structural brain changes following left temporal low-frequency rTMS in patients with subjective tinnitus. *Neural Plast.* 2014:132058. doi: 10.1155/2014/132058

Lomoio, S., Necchi, D., Mares, V., and Scherini, E. (2011). A single episode of neonatal seizures alters the cerebellum of immature rats. *Epilepsy Res.* 93, 17–24. doi: 10.1016/j.eplepsyres.2010.10.013

Lores Arnaiz, S., Travacio, M., Llesuy, S., Rodriguez, and de Lores Arnaiz, G. (1998). Regional vulnerability to oxidative stress in a model of experimental epilepsy. *Neurochem. Res.* 23, 1477–1483. doi: 10.1007/BF03177490

Manjon, J. V., Romero, J. E., Vivo-Hernando, R., Rubio, G., Aparici, F., de la Iglesia-Vaya, M., et al. (2022). vol2Brain: A New Online Pipeline for Whole Brain MRI Analysis. *Front. Neuroinform.* 16:862805. doi: 10.3389/fninf.2022.862805

May, A., Hajak, G., Ganssbauer, S., Steffens, T., Langguth, B., Kleinjung, T., et al. (2007). Structural brain alterations following 5 days of intervention: Dynamic aspects of neuroplasticity. *Cereb. Cortex* 17, 205–210. doi: 10.1093/cercor/bhj138

Mishra, A., Maiti, R., Mishra, B. R., Jena, M., and Srinivasan, A. (2020). Effect of repetitive transcranial magnetic stimulation on seizure frequency and epileptiform discharges in drug-resistant epilepsy: A meta-analysis. *J. Clin. Neurol.* 16, 9–18.

Novello, M., Bosman, L. W. J., and De Zeeuw, C. I. (2024). A systematic review of direct outputs from the cerebellum to the brainstem and diencephalon in mammals. *Cerebellum* 23, 210–239.

Piper, R. J., Richardson, R. M., Worrell, G., Carmichael, D. W., Baldeweg, T., Litt, B., et al. (2022). Towards network-guided neuromodulation for epilepsy. *Brain* 145, 3347–3362. doi: 10.1093/brain/awac234

Poeppl, T. B., Langguth, B., Lehner, A., Frodl, T., Rupprecht, R., Kreuzer, P. M., et al. (2018). Brain stimulation-induced neuroplasticity underlying therapeutic response in phantom sounds. *Hum. Brain Mapp.* 39, 554–562. doi: 10.1002/hbm.23864

Power, J. D., Cohen, A. L., Nelson, S. M., Wig, G. S., Barnes, K. A., Church, J. A., et al. (2011). Functional network organization of the human brain. *Neuron* 72, 665–678.

Spencer, S. S. (2002). Neural networks in human epilepsy: Evidence of and implications for treatment. *Epilepsia* 43, 219–227.

Stieve, B. J., Richner, T. J., Krook-Magnuson, C., Netoff, T. I., and Krook-Magnuson, E. (2023). Optimization of closed-loop electrical stimulation enables robust cerebellar-directed seizure control. *Brain* 146, 91–108. doi: 10.1093/brain/awac051

Streng, M. L., and Krook-Magnuson, E. (2021). The cerebellum and epilepsy. *Epilepsy Behav.* 121:106909.

Streng, M. L., Froula, J. M., and Krook-Magnuson, E. (2023). The cerebellum's understated role and influences in the epilepsies. *Neurobiol. Dis.* 183:106160. doi: 10.1016/j.nbd.2023.106160

Sun, W., Mao, W., Meng, X., Wang, D., Qiao, L., Tao, W., et al. (2012). Low-frequency repetitive transcranial magnetic stimulation for the treatment of refractory partial epilepsy: A controlled clinical study. *Epilepsia* 53, 1782–1789. doi: 10.1111/j.1528-1167.2012.03626.x

Tergau, F., Naumann, U., Paulus, W., and Steinhoff, B. J. (1999). Low-frequency repetitive transcranial magnetic stimulation improves intractable epilepsy. *Lancet* 353:2209.

Theodore, W., Hunter, K., Chen, R., Vega-Bermudez, F., Boroojerdi, B., Reeves-Tyer, P., et al. (2002). Transcranial magnetic stimulation for the treatment of seizures: A controlled study. *Neurology* 59, 560–562.

Tsuboyama, M., Kaye, H. L., and Rotenberg, A. (2020). Review of transcranial magnetic stimulation in epilepsy. *Clin. Ther.* 42, 1155–1168.

van Diessen, E., Diederen, S. J., Braun, K. P., Jansen, F. E., and Stam, C. J. (2013). Functional and structural brain networks in epilepsy: What have we learned? *Epilepsia* 54, 1855–1865.

Wang, G., Liu, X., Zhang, M., Wang, K., Liu, C., Chen, Y., et al. (2023). Structural and functional changes of the cerebellum in temporal lobe epilepsy. *Front. Neurol.* 14:1213224. doi: 10.3389/fneur.2023.1213224

Zhou, X., Liu, J., Zhang, Z., Qin, L., Pang, X., Yu, L., et al. (2021). Aberrant cerebral intrinsic activity and cerebro-cerebellar functional connectivity in right temporal lobe epilepsy: A resting-state functional MRI study. *Neuroreport* 32, 1009–1016. doi: 10.1097/WNR.0000000000001681

Frontiers in
Molecular Neuroscience

Leading research into the brain's molecular structure, design and function

Part of the most cited neuroscience series, this journal explores and identifies key molecules underlying the structure, design and function of the brain across all levels.

Discover the latest Research Topics

See more →

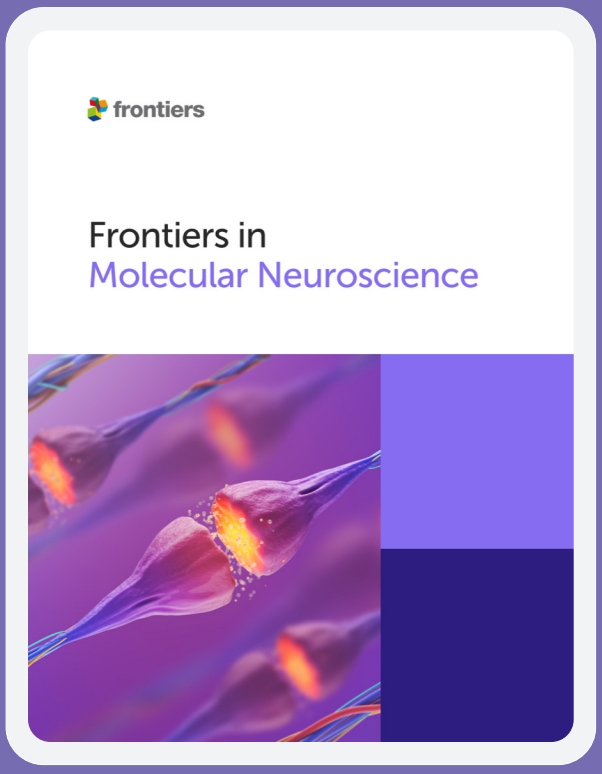

Frontiers

Avenue du Tribunal-Fédéral 34
1005 Lausanne, Switzerland
frontiersin.org

Contact us

+41 (0)21 510 17 00
frontiersin.org/about/contact